



TECHNISCHE
UNIVERSITÄT
DRESDEN

Dissertation

THERMALIZATION AND
OUT-OF-EQUILIBRIUM DYNAMICS IN
OPEN QUANTUM MANY-BODY SYSTEMS

Michael Buchhold

Supervised by:
Prof. Dr. Sebastian Diehl
Submitted on June 30th 2015

Thermalization and Out-of-Equilibrium Dynamics in Open Quantum Many-Body Systems

Dissertation

zur Erlangung des akademischen Grades

Doctor of Philosophy
(Ph. D.)

vorgelegt

der Fakultät Mathematik und Naturwissenschaften
der Technischen Universität Dresden

von

M. Sc. Michael Buchhold
geboren am 18.10.1985 in Lohr am Main

Eingereicht am 30. Juni 2015

Die Dissertation wurde in der Zeit von September 2012 bis August 2014 im Institut für Theoretische Physik der Universität Innsbruck und von September 2014 bis Juni 2015 im Institut für Theoretische Physik der Technischen Universität Dresden angefertigt.

ABSTRACT

Thermalization, the evolution of an interacting many-body system towards a thermal Gibbs ensemble after initialization in an arbitrary non-equilibrium state, is currently a phenomenon of great interest, both in theory and experiment. As the time evolution of a quantum system is unitary, the proposed mechanism of thermalization in quantum many-body systems corresponds to the so-called eigenstate thermalization hypothesis (ETH) and the typicality of eigenstates. Although this formally solves the contradiction of thermalizing but unitary dynamics in a closed quantum many-body system, it does neither make any statement on the dynamical process of thermalization itself nor in which way the coupling of the system to an environment can hinder or modify the relaxation dynamics. In this thesis, we address both the question whether or not a quantum system driven away from equilibrium is able to relax to a thermal state, which fulfills detailed balance, and if one can identify universal behavior in the non-equilibrium relaxation dynamics.

As a first realization of driven quantum systems out of equilibrium, we investigate a system of Ising spins, interacting with the quantized radiation field in an optical cavity. For multiple cavity modes, this system forms a highly entangled and frustrated state with infinite correlation times, known as a quantum spin glass. In the presence of drive and dissipation, introduced by coupling the intra-cavity radiation field to the photon vacuum outside the cavity via lossy mirrors, the quantum glass state is modified in a universal manner. For frequencies below the photon loss rate, the dissipation takes over and the system shows the universal behavior of a dissipative spin glass, with a characteristic spectral density $\mathcal{A}(\omega) \sim \sqrt{\omega}$. On the other hand, for frequencies above the loss rate, the system retains the universal behavior of a zero temperature, quantum spin glass. Remarkably, at the glass transition, the two subsystems of spins and photons thermalize to a joint effective temperature, even in the presence of photon loss. This thermalization is a consequence of the strong spin-photon interactions, which favor detailed balance in the system and detain photons from escaping the cavity. In the thermalized system, the features of the spin glass are mirrored onto the photon degrees of freedom, leading to an emergent photon glass phase. Exploiting the inherent photon loss of the cavity, we make predictions of possible measurements on the escaping photons, which contain detailed information of the state inside the cavity and allow for a precise, non-destructive measurement of the glass state.

As a further set of non-equilibrium systems, we consider one-dimensional quantum fluids driven out of equilibrium, whose universal low energy theory is formed by the so-called Luttinger Liquid description, which, due to its large degree of universality, is of intense theoretical and experimental interest. A set of recent experiments in research groups in Vienna, Innsbruck and Munich have probed the non-equilibrium time-evolution of one-dimensional quantum fluids for different experimental realizations and are pushing into a time regime, where thermalization is expected. From a theoretical point of view, one-dimensional quantum fluids are particularly interesting, as Luttinger Liquids are integrable and therefore, due to an infinite number of constants of motion, do not thermalize. The leading order correction to the quadratic theory is irrelevant in the sense of the renormalization group and does therefore not modify static correlation functions, however, it breaks integrability and will therefore, even if irrelevant, induce a completely different non-equilibrium dynamics as the quadratic Luttinger theory alone. In this thesis, we derive for the first time a kinetic equation for interacting Luttinger Liquids, which describes the time evolution of the excitation densities for arbitrary initial states. The resonant character of the interaction makes a straightforward derivation of the kinetic equation, using Fermi's golden rule, impossible and we have to develop non-perturbative techniques in the Keldysh framework. We derive a closed expression for the time evolution of the excitation densities in terms of self-energies and vertex corrections. Close to equilibrium, the kinetic equation describes the exponential decay of excitations, with a decay rate $\sigma^{\text{R}} = \text{Im}\Sigma^{\text{R}}$, determined by the self-energy at equilibrium. However, for long times τ , it also reveals the presence of dynamical slow modes, which are the consequence of exactly energy conserving dynamics and lead to an algebraic decay $\sim \tau^{-\eta_{\text{D}}}$ with $\eta_{\text{D}} = 0.58$. The presence of these dynamical slow modes is not contained in the equilibrium Matsubara formalism, while they emerge naturally in the non-equilibrium formalism developed in this thesis.

In order to initialize a one-dimensional quantum fluid out of equilibrium, we consider an interaction quench in a model of interacting, dispersive fermions in Chap. 5. In this scenario, the fermionic interaction is suddenly changed at time $t = 0$, such that for $t > 0$ the system is not in an eigenstate and therefore undergoes a non-trivial time evolution. For the quadratic theory, the stationary state in the limit $t \rightarrow \infty$ is a non-thermal, or prethermal, state, described by a generalized Gibbs ensemble (GGE). The GGE takes into account for the conservation of all integrals of motion, formed by the eigenmodes of the Hamiltonian. On the other hand, in the presence of non-linearities, the final state for $t \rightarrow \infty$ is a thermal state with a finite temperature $T > 0$. The spatio-temporal, dynamical thermalization process can be decomposed into three regimes: A prequench regime on the largest distances, which is determined by the initial state, a prethermal plateau for intermediate distances, which is determined by the metastable fixed point of the quadratic theory and a thermal region on the shortest distances. The latter spreads sub-ballistically $\sim t^\alpha$ in space with $0 < \alpha < 1$ depending on the quench. Until complete thermalization (i.e. for times $t < \infty$), the thermal region contains more energy than the prethermal and prequench region, which is expressed in a larger temperature $T_t > T_\infty$, decreasing towards its final value T_∞ . As the system has achieved local detailed balance in the thermalized region, energy transport to the non-thermal region can only be performed by the macroscopic dynamical slow modes and the decay of the temperature $T_t - T_\infty \sim t^{-\eta_D}$ again witnesses the presence of these slow modes. The very slow spreading of thermalization is consistent with recent experiments performed in Vienna, which observe a metastable, prethermal state after a quench and only observe the onset of thermalization on much larger time scales. As an immediate indication of thermalization, we determine the time evolution of the fermionic momentum distribution after a quench from non-interacting to interacting fermions. For this quench scenario, the step in the Fermi distribution at the Fermi momentum k_F decays to zero algebraically in the absence of a non-linearity but as a stretched exponential (the exponent being proportional to the non-linearity) in the presence of a finite non-linearity. This can serve as a proof for the presence or absence of the non-linearity even on time-scales for which thermalization can not yet be observed.

Finally, we consider a bosonic quantum fluid, which is driven away from equilibrium by permanent heating. The origin of the heating is atomic spontaneous emission of laser photons, which are used to create a coherent lattice potential in optical lattice experiments. This process preserves the system's $U(1)$ -invariance, i.e. conserves the global particle number, and the corresponding long-wavelength description is a heated, interacting Luttinger Liquid, for which phonon modes are continuously populated with a momentum dependent rate $\partial_t n_q \sim \gamma|q|$. In the dynamics, we identify a quasi-thermal regime for large momenta, featuring an increasing time-dependent effective temperature. In this regime, due to fast phonon-phonon scattering, detailed balance has been achieved and is expressed by a time-local, increasing temperature. The thermal region emerges locally and spreads in space sub-ballistically according to $x_t \sim t^{4/5}$. For larger distances, the system is described by a non-equilibrium phonon distribution $n_q \sim |q|$, which leads to a new, non-equilibrium behavior of large distance observables. For instance, the phonon decay rate scales universally as $\gamma_q \sim |q|^{5/3}$, with a new non-equilibrium exponent $\eta = 5/3$, which differs from equilibrium. This new, universal behavior is guaranteed by the $U(1)$ invariant dynamics of the system and is insensitive to further subleading perturbations. The non-equilibrium long-distance behavior can be determined experimentally by measuring the static and dynamic structure factor, both of which clearly indicate the exponents for phonon decay, $\eta = 5/3$ and for the spreading of thermalization $\eta_T = 4/5$. Remarkably, even in the presence of this strong external drive, the interactions and their aim to achieve detailed balance are strong enough to establish a locally emerging and spatially spreading thermal region.

The physical setups in this thesis do not only reveal interesting and new dynamical features in the out-of-equilibrium time evolution of interacting systems, but they also strongly underline the high degree of universality of thermalization for the classes of models studied here. May it be a system of coupled spins and photons, where the photons are pulled away from a thermal state by Markovian photon decay caused by a leaky cavity, a one-dimensional fermionic quantum fluid, which has been initialized in an out-of-equilibrium state by a quantum quench or a one-dimensional bosonic quantum fluid, which is driven away from equilibrium by continuous, external heating, all of these systems at the end establish a local thermal equilibrium, which spreads in space and leads to global thermalization for $t \rightarrow \infty$. This underpins the importance of thermalizing collisions and endorses the standard approach of equilibrium statistical mechanics, describing a physical system in its steady state by a thermal Gibbs ensemble.

CONTENTS

Introduction	11
1 Introduction to the Keldysh Path Integral	19
1.1 Keldysh Path Integral from the Quantum Master Equation	20
1.1.1 The Partition Function	21
1.2 Non-Equilibrium Green's functions	26
1.3 Keldysh Rotation and Fluctuation-Dissipation Relation	29
2 Dissipative Spin Glasses in Optical Cavities	33
2.1 Introduction	33
2.2 Key Results	35
2.2.1 Non-equilibrium Steady State Phase Diagram	35
2.2.2 Dissipative Spectral Properties and Universality Class	36
2.2.3 Atom-Photon Thermalization into Quantum-Critical Regime	38
2.2.4 Emergent Photon Glass Phase	40
2.2.5 Cavity Glass Microscope	40
2.3 Multimode Open Dicke Model	41
2.3.1 Hamilton Operator	41
2.3.2 Markovian Dissipation	44
2.3.3 Quenched or Quasi-static Disorder	45
2.4 Keldysh Path Integral Approach	46

2.4.1	Multimode Dicke Action	46
2.4.2	Calculation Procedure	48
2.4.3	Saddle-point Action and Self-consistency Equations	50
2.5	Results	53
2.5.1	Non-equilibrium Steady State Phase Diagram	53
2.5.2	Dissipative Spectral Properties and Universality Class	54
2.5.3	Atom-Photon Thermalization	58
2.5.4	Emergent Photon Glass	59
2.5.5	Cavity Glass Microscope	61
2.6	Conclusion	67
2.7	Photon Fields in the Superradiant Phase	68
2.8	Markovian Dissipation vs. Quenched Disorder	69
2.8.1	Non-equilibrium Fluctuation Dissipation Relation	69
2.8.2	Effective System-only Action	70
2.8.3	The Markov Approximation	71
2.8.4	The Quenched Bath	73
2.9	Linear Response in the Keldysh Formalism	74
2.9.1	Example: Laser Field Induced Polarization of Cavity Atoms	76
2.10	Distribution Function of the Photon x-Component	76
3	One-Dimensional Quantum Fluids out of Equilibrium	79
3.1	The Luttinger Formalism for One-Dimensional Interacting Bosons	80
3.1.1	Long-wavelength Action for Lieb-Lininger Type Models	81
3.1.2	Remarks on Interacting Luttinger Liquids	83
3.1.3	Keldysh Action for Interacting Luttinger Liquids	85
3.2	The Luttinger Formalism for Interacting Fermions in One Dimension	88
3.2.1	Deriving the Keldysh Action for Interacting One-Dimensional Fermions	88
3.2.2	Keldysh Path Integral for Fermionic Luttinger Liquids and Fermionic Correlation Functions	94
3.2.3	Equilibrium Fermion Green's Functions and $T = 0$ Scaling Behavior	97

4	Kinetic Theory for Interacting Luttinger Liquids	99
4.1	Introduction	99
4.2	Model	102
4.2.1	Phonon Basis	104
4.2.2	Keldysh Action	105
4.3	Self-Energies	107
4.3.1	Non-equilibrium Fluctuation-Dissipation Relation	107
4.3.2	Quasi-particle Lifetimes in Self-consistent Born Approximation	110
4.4	Kinetic Equation for the Phonon Density	114
4.4.1	Kinetic Equation for Small External Momenta	116
4.4.2	Relaxation Close to Equilibrium	117
4.5	Kinetic Equation and Diagrams in Presence of Anomalous Densities	118
4.5.1	Diagrammatics for Off-diagonal Terms	120
4.6	Relaxation of an Excited Thermal State	123
4.7	Dyson-Schwinger Equations and Vertex Corrections	125
4.8	Conclusion	129
5	Thermalization and Prethermalization in Interacting Luttinger Liquids after a Quantum Quench	133
5.1	Fermionic Interaction Quench and Initial State after the Quench	135
5.2	Quench in the Quadratic Theory	138
5.3	Quench in the Non-linear Theory	143
5.3.1	Keldysh Action and Structure of the Correlation Functions	144
5.3.2	Dynamics of the Phonon Densities	146
5.3.3	Momentum Dependent Thermalization and Emergence of Dynamical Slow Modes	149
5.3.4	Pinning of the Zero Momentum Modes due to Global Particle Number and Current Conservation	151
5.3.5	Fermion Correlations 1: Analytical Results	152
5.3.6	Fermion Correlations 2: Numerical Results	156
5.4	Conclusion	158

6	Heating Dynamics of Open, Interacting Luttinger Liquids	161
6.1	Introduction	161
6.2	Model	162
6.2.1	Master Equation in the Luttinger Description	163
6.2.2	Keldysh Action	166
6.3	Phonon Green's Functions	168
6.3.1	Non-equilibrium Fluctuation-Dissipation Relation	168
6.3.2	Self-Energies and Kinetic Equation	169
6.3.3	Validity	170
6.4	Time-Evolution and Non-equilibrium Scaling	173
6.4.1	Time-dependent Phonon Density	173
6.4.2	Quasi-particle Lifetime Scaling and Dynamical Phase Diagram . . .	174
6.4.3	Experimental Detection	176
6.4.4	Modifications for $T > 0$	177
6.5	Conclusions	179
	Bibliography	181
	Curriculum Vitae	197

INTRODUCTION

A major achievement and nowadays the foundation of classical and quantum statistical physics is the description of steady states in terms of (grand) canonical Gibbs ensembles [68, 24]. In a few words, statistical mechanics proposes that a system initialized in an arbitrary state (quantum or classical) will relax towards a statistical ensemble, which is only determined by energy (and likely) particle number conservation but, except for these macroscopic conserved quantities, has no further dependence on the initial state. The macroscopic derivation of the Gibbs ensemble relies completely on elementary statistics. It assumes that any system, whose time evolution is ergodic, will reach any point in the allowed phase space with equal probability. If the condition of ergodicity is fulfilled, the Gibbs ensemble is obtained by maximizing the entropy of the system under the constraints that are set by the allowed phase space.

Prominent examples for systems described by Gibbs ensembles are the microcanonical ensemble and the canonical ensemble. The microscopic ensemble describes systems, for which energy is exactly conserved in the dynamics, i.e. for which $\text{Var}(E) = 0$, the variance in energy E , is zero and all states with energies corresponding to the initial state are reached by the same probability. On the other hand, the canonical ensemble describes systems for which energy is only conserved on average and the probability of a state is a function of the energy and entropy difference to the initial state. In the thermodynamic limit, for a canonical ensemble the energy variance vanishes as $\text{Var}(E) \sim \frac{\sqrt{E}}{N}$ where N is the particle number and $N \rightarrow \infty$ in the thermodynamic limit. Consequently, the canonical and microcanonical ensemble coincide in the thermodynamic limit and the restriction to the canonical ensemble for a statistical description of thermodynamic systems is justified [89].

Stating the definition of ergodicity in the way it is used above, it reads, during its time evolution, a system will reach all points in phase space that are not forbidden by additional dynamical constraints with equal probability. Applying this definition of ergodicity with the inclusion of all relevant dynamical constraints, all experimentally observed long time dynamics have been proven to be ergodic. It is therefore taken as a hypothesis, that all systems fulfill ergodicity in the above sense. As a consequence, a general system initialized in an arbitrary state will evolve towards a stationary Gibbs ensemble, which has to take into account "only" the dynamical constraints set by the generator of the dynamics. The dynamical constraints, on the other hand, can be identified by conservation laws and lead to dynamically conserved quantities.

This is a very universal statement for classical and quantum dynamics, as it identifies the dynamical fixed point of the time evolution of macroscopic many-body systems in terms of conservation laws and therefore symmetries. For the special case, for which the only conserved quantity is energy, the Gibbs ensemble is also referred to as a thermal ensemble and the dynamical process of reaching the thermal ensemble is called thermalization.

Although the Gibbs ensemble has proven to correctly describe the steady state of a large class of systems and it relies on a macroscopic basis only on very simple but powerful assumptions, its emergence from the deterministic microscopic dynamical equations puzzles physicists since the last century [199, 166, 184, 21, 53]. The equations of motion for physical systems, i.e. Newton's equations, the Schrödinger equation and Maxwell's equations, are strictly reversible and the existence of a single dynamical fixed point of these equations, represented by the Gibbs ensemble, is microscopically a very unexpected result [11].

For classical systems, however, it can be explained by the non-linear structure of the equations of motion for interacting particles. The non-linearity in these equations drives the particles to explore ergodically the constant-energy manifold and quickly all particle trajectories begin to look alike [64]. Due to the non-linearity, in the classical equations of motion it is possible that the information on the initial state gets lost completely and the Gibbs ensemble is indeed the only dynamical fixed point and all classical trajectories evolve towards it in time.

For quantum mechanical systems, however, the Schrödinger equation is not only deterministic and reversible but even unitary and the energy levels are quantized to discrete values, making the time evolution invertible [199, 119]. This forbids the existence of a single dynamical fixed point in quantum dynamics in a strict sense. The fact, that even in quantum mechanics, the stationary state of almost all realistic systems is described by a Gibbs ensemble has been explained in terms of the so-called eigenstate thermalization hypothesis (ETH) [199, 184, 166, 53]. According to the eigenstate thermalization hypothesis, the off-diagonal elements of the density matrix are vanishing due to dephasing for long times, i.e. they obtain a time dependent phase factor during the time evolution, which averages out for large time spans. The resulting density matrix, after long times, is the projection of the original density matrix on its main diagonal and is called the diagonal ensemble. For typical systems, this diagonal ensemble is dominated by states that are consistent with the macroscopic initial values of the state, such as energy, particle number and other possible conserved quantities. The expectation values of local observables are not very sensitive towards quantum states with the same macroscopic properties and as a consequence, can be expressed through a typical state, consistent with the initial values. For energy and particle number as the only conserved quantities, this typical state is nothing but the Gibbs ensemble and the thermalization of quantum states can therefore be explained by the ETH [193, 70].

The effect of quantum thermalization has gained a lot of interest again [74, 122, 121, 87, 175, 171, 197, 104], when almost a decade ago, a set of cold atom experiments, starting with the quantum Newton's cradle in David Weiss' group [111], witnessed the complete absence of thermalization for certain quantum systems even at very long times. In this first experiment, Kinoshita et al. placed two one-dimensional, interacting Bose-Einstein condensates on opposite walls of a harmonic trap and let them evolve. What they observed was the macroscopic, coherent backscattering between the two Bose-Einstein condensates, similar to a Newton's cradle of two elastically colliding balls. The absence of thermalization for very long times in this experiment has been explained by the presence of an infinite number of integrals of motion in a one-dimensional gas of coherently scattering bosons [111, 167]. Although it was understood, that for this experiment the infinite number of integrals of motion restricts the dynamics to a small hyper-surface in phase space and prevents it from thermalization, it was not clear at that time, which and how many integrals of motion are necessary in order to forbid thermalization at all [166].

In subsequent theoretical works, it was understood that an infinite number of arbitrary conserved quantities is not sufficient to spoil the thermalization process. The simplest (and maybe to naive) example is an arbitrary power of the Hamiltonian, which is always an integral of motion but does not constrain the dynamics. A strict and accepted criterion for the absence of thermalization has been found to be integrability, which is defined as the presence of a macroscopic number of integrals of motion, each of which is local, i.e. does not scale extensively with the system size and does not pairwise commute with the other integrals of motion [33, 31, 157]. Although integrable systems do not thermalize, they can still reach an asymptotic steady state in the long time dynamics. This state has only lost part of the memory of the initial state but completely contains the information on the integrals of motion of the initial state for all times. Theoretically, it is described in terms of a generalized Gibbs ensemble, which is nothing but the entropy maximizing state under the constraint of all the integrals of motion [166].

At present, there exist two types of integrable systems in the literature, quadratic Hamiltonians in arbitrary dimensions and Bethe ansatz solvable, interacting models in one dimension. The former does not only include trivial, non-interacting systems but also effective Hamiltonians, which emerge as the corresponding, leading order¹ low energy theory of interacting systems, such as spin wave theory and Landau's Fermi liquid theory. Both types of integrable systems therefore play an important role in current research, as they, even though exactly solvable, feature a non-trivial dynamics and interesting asymptotic states [167, 39, 95, 96, 33, 14, 201, 142].

While the effect of thermalization, and part of its absence, in closed quantum systems has been understood in terms of the eigenstate thermalization hypothesis, the latter does not contain any statement about the dynamical process itself, which leads to thermalization. The thermalization procedure of interacting quantum many-body systems has only been solved for some exemplary models, which could be attacked with currently available numerical and semi-analytical methods and is far from being understood [186, 61, 57, 139]. On the other hand, recent experiments (both for cold atoms and condensed matter setups [38, 69]) are entering the far from equilibrium regime and observe the relaxation dynamics of strongly excited states far from equilibrium linear response [183, 74, 121, 132, 197]. In order to explain these experiments and explore the physics beyond the thermal equilibrium, it is therefore necessary to not only understand the thermalization procedure of interacting quantum many-body systems but also to better understand in which precise cases thermalization is absent even for non-integrable systems.

In dimensions larger than one, thermalizing collisions are fast and the large phase space available for such collisions indicates very fast thermalization in this case. The thermalization dynamics is therefore expected to happen on exponentially fast time scales, such that for most relevant times, the systems can be considered thermal, even if prepared in a non-thermal state. Exceptions are systems, which are almost perfectly described by an effective quasi-particle theory and which show slow relaxation towards equilibrium [186, 115]. On the other hand, in one-dimensional systems, thermalizing collisions are suppressed by small phase space volumes and the dynamics induced by the collisions is expected to be slow. This assumption is promoted by the presence of a large number of integrable models in one dimension, which feature the complete absence of effective thermalizing collisions [33, 39, 11, 117] and which evolve towards a non-thermal dynamical fixed point in their asymptotic evolution. These integrable models are expected to play an important role in the thermalization dynamics of one-dimensional systems, as many relevant one-dimensional systems can be described in terms of integrable models with small integrability breaking corrections [80, 81]. As a consequence, one expects the relaxation towards equilibrium of these models to happen in two steps. For small and transient times, the dominant dynamics is expected to be the one of the corresponding integrable model, leading to a time evolution towards the asymptotic, non-thermal dynamical fixed point of this model. This point serves as a metastable, intermediate state for the dynamics and is able to describe transient correlations in the system, which, due to the extensive number of conserved quantities of the integrable model, depend strongly on the initial state. The process of reaching the asymptotic state in the transient dynamics is called prethermalization. For much larger times, the effect of the integrability breaking terms becomes visible and leads to complete thermalization of the system [139, 33]. This scenario has been observed in recent experiments, for which, however, only the onset of thermalization has been measured at very large times [121, 172].

The prethermalization dynamics in truly thermalizing, interacting one-dimensional systems has only very recently been observed for systems of spin polarized, short-range interacting fermions with dimerized hopping amplitudes [18, 147]. In higher dimensions, prethermalization dynamics before the onset of thermalization has also been found for interacting lattice fermions in infinite dimensions [139, 186] and in the low energy description of the quark-meson model [17]. For these higher dimensional systems, the corresponding integrable theories, which describe the prethermal state, are effective, quadratic quasi-particle theories, as for instance Fermi liquid theory for the interacting fermions and Bogoliubov theory for the case of the quark-meson model.

¹Up to terms that are irrelevant in the sense of the renormalization group.

Following the results from Refs. [139, 186, 17] in higher dimensions, the thermalization dynamics (and more general, the out-of-equilibrium dynamics) of interacting many-body systems can be understood in terms of the corresponding quasi-particles. In the first step, for very short times after initializing a system in a non-equilibrium state, the corresponding quasi-particles have to be built up. While the structure of these quasi-particles depends on the form of the Hamiltonian, i.e. the microscopic particle-particle interactions and the kinetic energy, the initial distribution of quasi-particles is determined solely by the initial state. At intermediate times, scattering processes between the quasi-particles are rare and the dynamics of the system is determined essentially by the corresponding quadratic theory, initialized with a non-thermal distribution function. This corresponds to the prethermal state. At long times, scattering processes between the quasi-particles become dominant, establishing detailed balance and a thermal quasi-particle distribution, which is the final process of thermalization. Consequently, the absence of thermalization is equivalent to the absence scattering processes between the systems quasi-particles². In this picture, the GGE describes a state of non-interacting quasi-particles with a non-thermal distribution function.

Currently, cold atom experiments are pushing the limit towards observable time scales, on which the effect of quasi-particle scattering will have an impact on the dynamics and observe the corresponding relaxation dynamics. This strongly motivates the development of a kinetic theory for interacting Luttinger Liquids out of equilibrium, as we derive it in this thesis. Making use of this kinetic theory, we will explicitly demonstrate the thermalization of interacting one-dimensional quantum fluids and the importance of the prethermal state for this dynamics.

A further question of experimental relevance in the field of cold atoms, which is closely related to topic of thermalization, is whether or not a many-body system coupled to external drive and/or dissipation will be driven away from a thermal ensemble or whether interactions and their tendency to achieve detailed balance are strong enough to retain thermal (or quasi-thermal) equilibrium. Recent works have shown, that systems of exciton-polariton condensates, which are subject to drive and dissipation, can show the non-equilibrium equivalent of a Bose condensed phase and that the corresponding phase transition resembles the equilibrium Bose transition, establishing an effective low frequency temperature at the critical point in three dimensions. The corresponding universality class is the one of the equilibrium transition except for a set of new dynamical exponents, describing the relaxation towards effective equilibrium.

A similar effect may take place for other realizations of critical systems under drive and dissipation or, if the driving is strong enough, it may lead to new behavior without a corresponding equilibrium counterpart. In this thesis, additionally to the quench scenario described above, we will investigate two realistic physical setups, where a system is driven away from a thermal equilibrium by coupling it to an external bath. We analyze the question, whether the thermalizing collisions are strong enough to establish an effective thermal equilibrium in the presence of driven and/or dissipation or if the dynamics will be different from the corresponding equilibrium system.

The first realization of a driven-dissipative many-body system, which is analyzed in this thesis is a system of Ising spins coupled to the quantized radiation field inside a lossy cavity and driven by an external laser. In the absence of cavity photon losses and for strong spin-photon coupling, this system undergoes a phase transition from a disordered paramagnetic phase to an ordered ferromagnetic or superradiant phase. In the latter, all Ising spins are aligned, and the cavity field forms a coherent, standing wave. The corresponding phase transition is called the Dicke transition and features a single mode, which becomes critical at the transition. In the presence of finite cavity decay, this transition is purely classical, resembling a finite temperature transition at the critical point. However, both subsystems of spins and photons have not thermalized and show a different low energy behavior. This is due to the structure of the spin-photon interactions, which are unable to achieve detailed

²This explains the absence of thermalization for integrable models from a different perspective. As integrable models can be solved exactly on the level of quasi-particles, the corresponding excitations are non-interacting and never change their initial occupation due to the absence of collisions. As a consequence, once initialized in a non-equilibrium state, they will remain in this state forever.

balance between the two subsystems. Therefore, the photonic subsystem, which is subject to dissipation evolves towards a different equilibrium state than the spin degrees of freedom, which do not experience any external dissipation.

On the other hand, when taking into account a multi-mode optical cavity, the effective spin-photon interaction is highly frustrated and can lead, in the absence of dissipation, to a quantum spin glass transition. Furthermore, the interaction in the presence of multiple modes has a new structure, which enables the redistribution of energy between the two subsystems for a significant number of modes, leading to a joint thermalization process. While the interactions become strong enough to establish detailed balance between the two subsystems, we will see that the corresponding phase transition does not belong to the universality class of equilibrium glass transitions.

The second example of a driven system that we consider in this thesis is even more drastic. While the driven-dissipative spin glass system was evolving in time towards a stationary state and we asked the question whether this steady state resembles a thermal state or not, we will analyze in the last section of this thesis a setup of continuously heated, interacting bosons. This system does not evolve towards a steady state [25, 154, 156, 177] and features a continuously increasing energy. By definition, the only possible fixed point is the infinite temperature state. The microscopic system corresponds to interacting bosons in a one-dimensional optical lattice, where the lattice is created by a pair of counter-propagating laser beams. The atoms continuously perform stimulated absorption and emission of laser photons but there exists a finite probability of a spontaneous emission event, which localizes a single atom and leads to an energy increase of the system. These events correspond to dephasing of the local density matrix [25, 154, 192] and lead to a permanent heating of the system, which can be described by a U(1)-invariant master equation. The corresponding low energy theory is a heated, interacting Luttinger Liquid. The phonon distribution due to the heating term has a clear non-thermal structure, increasing linearly in momentum $n_q \sim |q|$ instead of a thermal, $n_q \sim \frac{1}{|q|}$ Rayleigh-Jeans divergence. While the thermalizing collisions between atoms will redistribute the energy and try to achieve detailed balance, the heating term acts diametrically opposite, which establishes a competition between the heating and collisions. As we see in chapter 6, the phonon scattering will nevertheless establish local detailed balance, starting on very short distances and spreading in space as $x_{\text{therm}} \sim t^{-4/5}$, where t is the time and $\eta_{\text{therm}} = 4/5$ is the characteristic thermalization exponent. For distances larger than the heating, however, we will find a phonon distribution dictated by the structure of the heating term, which leads to a new non-equilibrium behavior of the microscopic bosons, which has no equilibrium counterpart but nevertheless shows quite universal aspects, as we will demonstrate.

In summary, in this thesis, we investigate the effect of quantum thermalization in interacting many-body systems, which are driven away from equilibrium in experimentally relevant situations. Amongst the exemplary setups, there are closed systems, i.e. systems that are isolated from the environment, as well as open systems, which interact with their environment in a significant way. While the time evolution of the former is determined by the system Hamiltonian alone and the relaxation dynamics are a consequence of interactions, the latter contain two sources of dissipation, namely the scattering of quasi-particles and the interaction with the environment. This interaction drives the interacting system away from a thermalized state and we investigate the competition between thermalizing collisions and external drive and the resulting non-equilibrium dynamics.

The first example, is a closed, one-dimensional quantum fluid of interacting fermions, which is brought out of equilibrium by a quantum quench and which relaxes towards equilibrium, showing prethermalization and thermalization.

The second example is a quantum spin glass setup of atoms interacting with cavity photons, which is brought out of equilibrium by cavity photon dissipation. We find that the atom-photon interaction is sufficiently strong to achieve detailed balance at the glass transition and to imprint a global temperature on the combined system, while on the other hand modifying the universality class of the glass transition to a non-thermal, dissipative transition.

The third example, is a system of interacting bosons subject to permanent heating. Due to the permanently increasing energy, it is impossible for this system to reach a stationary

state. However, the interactions will establish a local detailed balance, i.e. a local quasi-equilibrium, which spreads in space and mimics on increasing length scales a thermal system with continuously increasing energy.

What we find by the examples analyzed in this thesis is, that thermalizing collisions and the corresponding process of thermalization are very strong and universal. Not only do they lead to thermalization in a closed environment, in which the system has been prepared initially in a non-thermal state. But even in the presence of drive and dissipation the interactions will lead to locally spreading, thermal quasi-equilibrium, underpinning the universality of the Gibbs ensemble for non-integrable systems. As a feature, we have identified new non-equilibrium universal behavior in the relaxation dynamics, indicating that not only the process of thermalization itself is quite universal but also its dynamics.

OUTLINE OF THIS THESIS

This thesis contains the major research of the author during the last three years. It consists of different chapters, which contain either theoretical derivations and background information or represent research projects that have been published in peer-review journals or will soon be published. From the present thesis, chapters 2 and 6 are published in Physical Review A, chapter 4 is currently under review and presented as a preprint on the arXiv, while chapter 5 will appear on the arXiv soon. Chapters 1 and 3 represent the theoretical background of the work in this thesis and consist of original work of the author as well as some necessary review of basic properties of the Keldysh field integral and Luttinger Liquids.

In Chapter 1, we start by giving a brief overview of the Keldysh path integral formalism. In this chapter, the Keldysh path integral is derived exemplary for a system, whose dynamics is described in terms of a Lindblad master equation, thereby setting the notation that will be used throughout this thesis and illustrating the reasons for which the Keldysh path integral is required for out-of-equilibrium problems and non-thermal steady states. We explain the basic properties of the Keldysh Green's function and introduce the Keldysh rotation, which transforms into the basis of retarded/advanced Green's and correlation functions.

In Chapter 2, we start with a first application of the Keldysh path integral formalism in order to describe the steady state of an open system with disorder. In this project, we analyze the steady state dynamics of an ensemble of two-level atoms, i.e. Ising spins, coupled to the quantized radiation field in an optical cavity, with multiple relevant eigenmodes. Such multi-mode cavities have been realized in cavity QED experiments [114], can introduce effective, frustrated spin-spin interaction. At equilibrium, sufficiently strong frustration leads to a quantum spin glass phase in the Ising degrees of freedom. However, as we introduce photon loss through the cavity mirrors, the photons are effectively coupled to the radiation field outside the cavity and pulled away from thermal equilibrium. This leads to a modification of the photonic and atomic degrees of freedom and the present glass transition belongs to the universality class of dissipative spin glasses. However, in the spin glass phase, due to the strong coupling of the atomic and the photonic subsystem, both systems thermalize to a joint effective low energy temperature. Making the effect of detailed balance at strong interactions dominant over the coupling to an external bath, which drives the system away from equilibrium. This highlights the universality of thermalization even in the presence of an external, non-equilibrium bath. Furthermore, we show that the information about the spin glass is mirrored onto the photons and can be detected directly from the cavity loss, transforming the lossy cavity to an effective cavity glass microscope. This project is published as

- Dicke-model quantum spin and photon glass in optical cavities: Non-equilibrium theory and experimental signatures
Michael Buchhold, Philipp Strack, Subir Sachdev, and Sebastian Diehl
Phys. Rev. A 87, 063622 (2013).

The second half of this work treats one-dimensional quantum fluids both bosonic and fermionic out-of-equilibrium. In chapter 3, we give an introduction to the effective long-wavelength description of interacting one-dimensional fermions and bosons, which is the interacting Luttinger liquid theory. We review the derivation of the Luttinger theory for both species in equilibrium and derive the corresponding Keldysh path integral description. Subsequently, we show in which way observables are transformed to the Luttinger Liquid representation in the Keldysh framework and derive formulas for the microscopic Green's functions in terms of Luttinger-Keldysh fields. This chapter is the theoretical foundation of Luttinger liquid theory out of equilibrium and contains the basic transformation formulas that are used throughout the rest of the thesis.

The interacting Luttinger liquid theory is the starting point for the derivation of the kinetic equation for interacting Luttinger liquids in chapter 4. In this chapter, we exploit the structure of the resonant, cubic phonon scattering processes in order to derive a non-equilibrium fluctuation dissipation relation for Luttinger liquids and a set of coupled equations for the phonon self-energy, the cubic vertex correction and the time evolution of the phonon densities. This set of equations can be solved self-consistently and determines the time evolution of an interacting Luttinger liquid out of equilibrium. The fact that this problem can be solved exactly relies on the structure of the cubic vertex and the nature of the resonant interactions, as we show in this chapter. As an application of the kinetic theory, we compute the relaxation of an excited state close to equilibrium. In this relaxation dynamics, we recover the linear response result of exponentially decaying excitations with a decay rate proportional to the self-energy but also an algebraic late time decay, which reveals the presence of dynamical slow modes due to exactly energy conserving dynamics. The numerical relaxation exponent for the slow modes is $z = 0.58$. This work is currently under review and can be found as a preprint

- Kinetic Theory for Interacting Luttinger Liquids
Michael Buchhold and Sebastian Diehl
arXiv:1501.01027, (2015).

In chapter 5, we investigate the relaxation dynamics of one-dimensional, dispersive fermions after a sudden interaction quench. First, we determine the time-evolution in the corresponding Luttinger liquid formalism and identify the prethermal state and the relaxation dynamics towards it, following the results by Cazalilla [39] but in the formalism presented in chapter 3, which allows us to systematically include interactions in the next step. Subsequently, we analyze the full relaxation dynamics in the presence of interaction and determine the thermalization dynamics for one-dimensional interacting fermions. We find that the relaxation happens in three different, but subsequent steps. First, for short times after the quench, the new quasi-particles have to be formed, leading to a spatio-temporal behavior, which is determined from the initial state before the quench. At intermediate times, the quasi-particles have formed but are distributed according to a non-equilibrium distribution function, leading to an intermediate time dynamics, which can be described by the prethermal state in the absence of interactions. Finally, at large times, the system starts to significantly redistribute energy between the quasi-particle modes and establishes local detailed balance. This thermal regime is described by an effective temperature, which is larger than the temperature of the corresponding equilibrium state as there are still regions in the spatio-temporal phase diagram, which have not yet reached equilibrium. The energy transport from the equilibrated, short distance modes to the thermalizing large distance modes can, due to the local detailed balance, only be performed by the dynamical slow modes, witnessing again the relaxation exponent $\eta_D = 0.58$ in the decay of the effective temperature $T_t - T_\infty \sim t^{-0.58}$ towards its final value.

Furthermore, we show, in which way the thermalization dynamics can be understood in the fermionic real space Green's function and momentum distribution and thereby, for the first time, analyze the full thermalization dynamics of interacting, dispersive fermions in one dimension.

In chapter 6, we analyze the heating dynamics of one-dimensional, interacting lattice bosons subject to permanent, particle number conserving heating. The bosons are confined to

a lattice potential created by counter-propagating lasers and heated up by subsequent stimulated absorption and spontaneous emission of laser photons. As the heating is particle number conserving, the effective low energy description for this system is an interacting Luttinger Liquid with permanent phonon production, the latter being the effect of the heating. The local nature of the spontaneous emission event induces a population rate of Luttinger phonons $\partial_t n_q \sim \gamma|q|$ in time, which does not correspond to an equilibrium distribution. However, as the interactions favors detailed balance, a redistribution of energy takes place simultaneously to the heating, starting at the shortest distances and spreading towards the longest distances as more and more phonon modes are occupied. On short distances, where collisions are fast, the system establishes detailed balance even in the presence of heating and can be described by an effective, time dependent temperature. On the other hand, for low momenta, the distribution function increases linearly in momentum. This linear increase in momentum is protected by the structure of the phonon scattering vertex, which scales to leading order linear for small momenta. On the largest distances, this non-equilibrium scaling behavior of the distribution function enters the corresponding observables and imprints a non-equilibrium behavior on large distance observables, such as for the static and dynamic structure factor at low momenta. It yields a new universal scaling law for the phonon decay rate, which scales as $\sigma_q^R \sim |q|^{5/3}$, with a non-equilibrium exponent $\eta = 5/3$. We are able to show that this scaling behavior is protected by the U(1)-invariant dynamics of the system and will even survive in the presence of initial thermal noise, which makes it a very robust observable in cold atom experiments with external heating mechanism. As a further universal feature, we show that the effective thermal regime spreads in space according to $x_{\text{therm}} \sim t^{4/5}$ and therefore ultimately erases the long distance non-equilibrium scaling regime at large times. This work is accepted for publication in Physical Review A and can be found as a preprint

- Non-equilibrium Universality in the Heating Dynamics of Interacting Luttinger Liquids
Michael Buchhold and Sebastian Diehl
arXiv:1404.3740, (2014).

1 INTRODUCTION TO THE KELDYSH PATH INTEGRAL

The Keldysh path integral formalism represents the basic theoretical foundation for this thesis. It has been developed in the 1960's in seminal works by Schwinger[178, 179], Konstantinov and Perel'[116], Kadanoff and Baym[98] and its eponymous, Leonid Keldysh[106]. Prospectively, Keldysh introduced the formalism exclusively based on real times and real frequencies and chose a convenient representation (the so-called Keldysh representation) for the variables in the path integral and thereby developed the formalism as it is used today. The Keldysh path integral formalism is a convenient formulation of the time evolution of a quantum mechanical density operator by introducing the so-called closed contour formalism. It is suited to describe both equilibrium and far from equilibrium problems and even for equilibrium problems goes beyond linear response, which can be dealt with in the imaginary time equilibrium (i.e. Matsubara) formalism.

However, in this thesis we deal with an ensemble of problems that cannot (or can only with huge difficulties) be dealt within the Matsubara technique.

First, in chapter 2, we consider systems of interacting bosonic particles subject to quenched disorder. While in the Matsubara formalism, these systems can be solved only by sophisticated replica methods (super-symmetry methods are not applicable with interactions), they are very naturally and straightforwardly approached in the Keldysh framework, which promotes the Keldysh path integral to the method of choice for these systems.

Second, in chapters 4, 5 and 6, we develop and apply a kinetic theory for the out of equilibrium dynamics of interacting one dimensional quantum fluids, theoretically described in terms of so-called interacting Luttinger Liquids. Although for a number of physical systems the corresponding kinetic equations can be derived from an equilibrium formalism by simply applying Fermi's Golden Rule, there are many exceptions for which this is impossible and a non-equilibrium formalism has to be applied. As we will see, interacting Luttinger Liquids constitute one of these exceptions as, due to the resonant character of the interactions, both the matrix elements for Fermi's Golden Rule as well as the kinetic equation will diverge without proper regularization. The latter, however, will be a functional of the excitation density and in a far from equilibrium situation can not be obtained from the Matsubara formalism.

Consequently, for the physical setups considered in this thesis, the Keldysh path integral formalism is an indispensable tool, which we will derive and explain in the following sections.

1.1 KELDYSH PATH INTEGRAL FROM THE QUANTUM MASTER EQUATION

A huge class of non-equilibrium problems are so-called open systems, where the system of interest S is coupled to a bath B via some system-bath coupling H_{SB} . This coupling is designed in such a way, that the bath can not simply be treated as a plain energy and (or) particle reservoir. As a consequence, a common thermodynamic ansatz relying on the minimization of the combined entropy functional is not easily applicable. Such systems typically have two features in common. First, the stationary state ρ_{ss} of the system alone is not described in terms of a canonical (or grand canonical) Gibbs ensemble, i.e.

$$\rho_{ss} \neq \frac{1}{Z} e^{-\beta H}, \quad (1.1.1)$$

where $\beta^{-1} = k_B T$ is the inverse temperature and H is the system Hamiltonian. Second, the dynamics of the system (even close to equilibrium) are not determined by the system Hamiltonian alone and the system-bath interaction has to be accounted for.

However, for many systems of relevance (and for all the systems considered in this thesis), the typical bath degrees of freedom equilibrate on time scales much faster than the system's degrees of freedom. If this is the case, in a stochastic wave function interpretation, between two subsequent events in which the bath interacts with the system, the bath has a sufficient amount of time to equilibrate. This means, that at each interaction event between system and bath, the system interacts with an equilibrated bath and the bath has completely lost its memory on the previous interaction event. Such a bath is referred to as memoryless or Markovian bath. For a sufficiently weak system-bath interaction, one can then perform second order perturbation theory in the system-bath coupling terms and derive an effective equation of motion for the density matrix of the system, which contains system operators only. This procedure is known as Born-Markov approximation and adiabatic elimination and the type of equation of motion, that is obtained from it as the quantum master equation¹².

The most general form for a time-local quantum master equation is the so-called Lindblad form, which reads

$$\partial_t \rho_t = \mathcal{L} \rho = \frac{1}{i} [H, \rho_t] + \sum_{\alpha} \left(2L_{\alpha} \rho_t L_{\alpha}^{\dagger} - \{L_{\alpha}^{\dagger} L_{\alpha}, \rho_t\} \right). \quad (1.1.2)$$

Here, ρ_t is the time dependent density matrix (throughout this thesis we will write temporal and spatial degrees of freedom as a subscript), H is again the system Hamiltonian, $[\cdot, \cdot]$ denotes the commutator and $\{\cdot, \cdot\}$ the anti-commutator and the operators $\{L_{\alpha}\}$ are the so-called Lindblad or quantum jump operators. The Lindblad operators are functionals, in many cases linears or bilinears, of system operators and their precise form depends on the specific system-bath coupling. The operator \mathcal{L} is called the Liouvillian and it is the generator of the dynamics of the density matrix. The Hamiltonian part of the Liouvillian represents the unitary quantum (i.e. the coherent) dynamics of the system, while the jump operators introduce a source of decoherence and therefore dissipative dynamics of the system. As a consequence of the elimination of the bath variables, the dynamics of the system and therefore the master equation in Eq. (1.1.2) is not unitary anymore.

¹The requirement of a Markovian bath is not necessary for a quantum master equation. However, for a non-Markovian bath, the quantum master equation will obtain a time non-local memory kernel, which reflects the fact, that the bath is unable to equilibrate between two subsequent system-bath interactions and retains memory of these events.

²We will not explicitly demonstrate the individual steps corresponding to the Born-Markov approximation and adiabatic elimination since it is a standard procedure in the context of open systems, but refer the reader to Refs.[27, 66]

However, the structure of the Lindblad master equation guarantees a trace (and therefore probability) conserving, positive and hermitian density matrix for all times [127, 118].

We will now take Eq. (1.1.2) as the starting point for the derivation of a path integral for the partition function and the Green's functions of a Markovian open quantum system. Of course, the steps explained above, i.e. the Born-Markov approximation and the adiabatic elimination of the bath variables, can be performed as well on the level of a path integral. For this approach, one defines the path integral for the complete system on the Keldysh contour (which displays only Hamiltonian dynamics in this case) first and subsequently integrates out the bath degrees of freedom in the Born-Markov approximation. The latter approach is demonstrated in Sec. 2.8.

1.1.1 The Partition Function

The central object in a path integral approach to many body physics is the partition function $Z(t)$, defined as

$$Z(t) = \text{Tr}(\rho_t), \quad (1.1.3)$$

as it is the starting point for any field theoretical approach, as for instance the derivation of the effective action. The time evolution of the density matrix ρ_t is described in terms of the Lindblad master equation (1.1.2), which has the formal solution

$$\rho_t = e^{t\mathcal{L}}\rho_0. \quad (1.1.4)$$

As already explained above, the Lindblad type dynamics preserve the norm of the density matrix. Considering an initial density matrix ρ_0 normalized to unity, $\text{Tr}(\rho_0) = 1$, we therefore have

$$Z(t) = \text{Tr}(\rho_t) = \text{Tr}(e^{t\mathcal{L}}\rho_0) \equiv 1_t. \quad (1.1.5)$$

Here, the artificial index t in 1_t indicates, that this expression is unity at time t . Commonly, at this point one introduces source fields, which couple linearly or bilinearly to the fields and generate correlation functions via functional derivatives with respect to these source fields. After the performing the functional derivatives, the source fields are set to zero and the partition function equals unity.

For now, we want to find a path integral representation of the partition function and therefore we are interested in ρ_t . The formal solution for the time dependent density matrix is given by Eq. (1.1.4), where the exponential is nothing but the limit

$$e^{t\mathcal{L}} = \lim_{N \rightarrow \infty} (1 + \delta_t \mathcal{L})^N, \quad \text{with} \quad \delta_t = \frac{t}{N}, \quad N \in \mathbb{N}. \quad (1.1.6)$$

Applying this expression to the time dependent density matrix, we find

$$\rho_t = \left[\lim_{N \rightarrow \infty} \prod_{l=1}^N (1 + \delta_t^{(l)} \mathcal{L}) \right] \rho_0, \quad (1.1.7)$$

which obviously solves Eq. (1.1.2). Here, the time difference $\delta_t^{(l)} = t^{(l)} - t^{(l-1)} = t/N$ obtains the same numerical value for all l and at this point only indicates the position at

which this time difference is occurring in the product above. Combining Eqs. (1.1.7) and (1.1.3), the partition function can be rewritten as

$$Z(t) = \text{Tr}(\rho_t) = \text{Tr} \left(\left[\lim_{N \rightarrow \infty} \prod_{l=1}^N \left(1 + \delta_t^{(l)} \mathcal{L} \right) \right] \rho_0 \right). \quad (1.1.8)$$

Here, we want to point out the similarities and the differences of the partition function (1.1.8) to an equilibrium partition function, which is defined as

$$Z_{\text{eq}} = \text{Tr} \left(e^{-\beta H} \right) = \text{Tr} \left(\left[\lim_{N \rightarrow \infty} \prod_{l=1}^N \left(1 - \delta_\tau^{(l)} H \right) \right] \mathbb{1} \right), \quad (1.1.9)$$

where H is the corresponding Hamiltonian and $\delta_\tau^{(l)} = \frac{\beta}{N}$ is the imaginary time difference. In order to simplify the following discussion, we define the discrete time dependent density matrices

$$\rho_t^{(m)} = \prod_{l=1}^m \left(1 + \delta_t^{(l)} \mathcal{L} \right) \rho_0 \quad \text{and} \quad \rho_{\text{eq}}^{(m)} = \prod_{l=1}^m \left(1 - \delta_\tau^{(l)} H \right). \quad (1.1.10)$$

Comparing Eqs. (1.1.8) and (1.1.9), we immediately encounter two major differences between the real time partition function of an open system to the partition function of an equilibrium system.

First, for the equilibrium system, the Hamilton operator H in imaginary time step (l) only acts from the left on $\rho_{\text{eq}}^{(l-1)}$ ³. As a consequence, in the derivation of the equilibrium path integral, it is sufficient to insert a single unit operator in terms of coherent states at each time step between $1 - \delta_\tau^{(l)} H$ and $\rho_{\text{eq}}^{(l-1)}$ to transform all operators to the corresponding fields (either complex, real or Grassmann fields)⁴. In contrast, the operator \mathcal{L} , as by its definition (see Eq. (1.1.2)), acts at time step (l) from the left and from the right on $\rho_t^{(l-1)}$. The complete replacement of operators by fields in equation (1.1.8) is therefore only possible by inserting two unit operators in terms of coherent states at each time step, one on the left and one on the right of $\rho_t^{(l-1)}$, defining the closed time path, i.e. Keldysh, contour. Second, for the partition function at equilibrium all information is contained in the Hamiltonian H , i.e. the generator of the dynamics. This is fundamentally different for the real time partition function for open systems, where both the generator of the dynamics, i.e. the operator \mathcal{L} as well as the initial state ρ_0 determine the partition function and therefore in general more information is required than for an equilibrium setup⁵.

In order to derive a path integral for the real time partition function (1.1.8), we consider a bosonic system⁶, described by bosonic creation and annihilation operators $\{b_i^\dagger, b_i\}$. Here, the variable (i) labels a complete set of single particle quantum states in terms of which the Liouvillian \mathcal{L} is expressed. In the common way, for a set of complex variables $\{\phi_i\}$, we define bosonic coherent states

$$|\phi\rangle \equiv e^{\sum_i \phi_i b_i^\dagger} |0\rangle, \quad (1.1.11)$$

³We neglect for the moment that H , of course, commutes with itself and that for this reason there is not really an ‘‘action’’ of this operator from the left.

⁴For a detailed derivation and discussion of equilibrium path integrals and coherent states see Ref. [146].

⁵The only exception are steady states of the system ρ_{ss} , which are zeros of \mathcal{L} , i.e. $\mathcal{L}\rho_{\text{ss}} = 0$. However, for non-zero jump operators, these steady states can not be described by an equilibrium density matrix.

⁶For fermionic or spin systems, the procedure will be equivalent but one has to use Grassmann or spin coherent states instead of complex coherent states.

which are eigenstates of the annihilation operators,

$$b_i |\phi\rangle = \phi_i |\phi\rangle. \quad (1.1.12)$$

Adding a proper normalization, these coherent states fulfill an exact completeness relation

$$\mathbb{1} = \int D[\phi^*, \phi] |\phi\rangle\langle\phi|, \text{ where } \int D[\phi^*, \phi] = \prod_i \int \frac{d\phi_i^* d\phi_i}{\pi} e^{-\phi_i^* \phi_i}. \quad (1.1.13)$$

Similar to the derivation of the equilibrium path integral, at each infinitesimal time step in Eq. (1.1.8), one inserts unit operators in terms of coherent states. However, as the operator $1 + \delta_t^{(l)} \mathcal{L}$ acts both from the left and from the right of $\rho^{(l-1)}$, a pair of identities is required at each time step. One identity acts from the left and obtains an additional (+) index, while the other identity acts from the right and obtains an additional (−) index. For a fixed number of time steps N , this requires the insertion of $2(N + 1)$ unit operators according to

$$\begin{aligned} Z(t) &= \text{Tr} \left(\underbrace{\phantom{D[\phi_{N+}^*, \phi_{N+}]} }_{\mathbb{1}_{N+}} \dots \left[\left(1 + \delta_t^{(l+1)} \mathcal{L} \right) \left(\underbrace{\phantom{D[\phi_{1+}^*, \phi_{1+}]} }_{\mathbb{1}_{1+}} \rho_t^{(l)} \underbrace{\phantom{D[\phi_{1-}, \phi_{1-}]} }_{\mathbb{1}_{1-}} \right) \right] \dots \underbrace{\phantom{D[\phi_{N-}, \phi_{N-}]} }_{\mathbb{1}_{N-}} \right) \\ &= \int D[\phi_{N+}^*, \phi_{N+}] D[\phi_{N-}^*, \phi_{N-}] \dots D[\phi_{1+}^*, \phi_{1+}] D[\phi_{1-}, \phi_{1-}] \dots \\ &\quad \text{Tr} \left(|\phi_{N+}\rangle\langle\phi_{N+}| \dots \left[\left(1 + \delta_t^{(l+1)} \mathcal{L} \right) \left(|\phi_{1+}\rangle\langle\phi_{1+}| \rho_t^{(l)} |\phi_{1-}\rangle\langle\phi_{1-}| \right) \right] \dots |\phi_{N-}\rangle\langle\phi_{N-}| \right). \end{aligned} \quad (1.1.14)$$

Here, we have labeled the coherent states at time step (l) with a corresponding index and the above mentioned additional (\pm) index corresponding to an action of the coherent state from the left (right) of the initial density matrix ρ_0 . This can be seen as two independent time contours, starting from the density matrix at $t = 0$ and evolving until the trace is evaluated at time t . We will from now on refer to these different sets of coherent states as the +–contour and the ––contour.

In the next step, one has to evaluate the individual matrix elements occurring in Eq. (1.1.14). For $0 < l < N$, these matrix elements are all similar, only differing in the time index l and we will compute them in the following steps. However, two special matrix elements occur in the above expression at $l = 0$ and $l = N$. First, for $l = N$, due to the trace, one has to compute the direct overlap

$$\text{Tr} (|\phi_{N+}\rangle\langle\phi_{N+}| \dots |\phi_{N-}\rangle\langle\phi_{N-}|) = \langle\phi_{N-}|\phi_{N+}\rangle \langle\phi_{N+}| \dots |\phi_{N-}\rangle \quad (1.1.15)$$

of coherent states from different contours. On the other hand, for $l = 0$, one has to evaluate the matrix element of two coherent states with the initial density matrix

$$\text{Tr} (\dots |\phi_{0+}\rangle\langle\phi_{0+}| \rho_0 |\phi_{0-}\rangle\langle\phi_{0-}|) \dots = \langle\phi_{0+}|\rho_0|\phi_{0-}\rangle \langle\phi_{0-}| \dots |\phi_{0+}\rangle. \quad (1.1.16)$$

These two matrix elements are very important, as they not only contain the complete information on the initial state of the system, but they also provide the regularization of the path integral in the absence of dissipation. As it is common in the literature, we will not explicitly evaluate these matrix elements now but later implement them in terms of initial conditions in the path integral, which is a completely equivalent procedure [99].

For those matrix elements, for which the Liouvillian is enclosed by a set of coherent states,

we find the following expression at time step 1:

$$\begin{aligned}
& |\phi_{1+}\rangle\langle\phi_{1+}| \left[\left(1 + \delta_t^{(1)} \mathcal{L} \right) (|\phi_{1-1+}\rangle\langle\phi_{1-1+}| \dots |\phi_{1-1-}\rangle\langle\phi_{1-1-}|) \right] |\phi_{1-}\rangle\langle\phi_{1-}| \\
= & |\phi_{1+}\rangle\langle\phi_{1+}| |\phi_{1-1+}\rangle\langle\phi_{1-1+}| \dots |\phi_{1-1-}\rangle\langle\phi_{1-1-}| |\phi_{1-}\rangle\langle\phi_{1-}| \\
& + \delta_t^{(1)} |\phi_{1+}\rangle\langle\phi_{1+}| \left[\mathcal{L} (|\phi_{1-1+}\rangle\langle\phi_{1-1+}| \dots |\phi_{1-1-}\rangle\langle\phi_{1-1-}|) \right] |\phi_{1-}\rangle\langle\phi_{1-}| \\
= & |\phi_{1+}\rangle\langle\phi_{1+}| |\phi_{1-1+}\rangle\langle\phi_{1-1+}| \dots |\phi_{1-1-}\rangle\langle\phi_{1-1-}| |\phi_{1-}\rangle\langle\phi_{1-}| \tag{1.1.17}
\end{aligned}$$

$$+ \frac{\delta_t^{(1)}}{i} |\phi_{1+}\rangle\langle\phi_{1+}| \mathbf{H} |\phi_{1-1+}\rangle\langle\phi_{1-1+}| \dots |\phi_{1-1-}\rangle\langle\phi_{1-1-}| |\phi_{1-}\rangle\langle\phi_{1-}| \tag{1.1.18}$$

$$- \frac{\delta_t^{(1)}}{i} |\phi_{1+}\rangle\langle\phi_{1+}| |\phi_{1-1+}\rangle\langle\phi_{1-1+}| \dots |\phi_{1-1-}\rangle\langle\phi_{1-1-}| \mathbf{H} |\phi_{1-}\rangle\langle\phi_{1-}| \tag{1.1.19}$$

$$- \delta_t^{(1)} \sum_{\alpha} |\phi_{1+}\rangle\langle\phi_{1+}| \mathbf{L}_{\alpha}^{\dagger} \mathbf{L}_{\alpha} |\phi_{1-1+}\rangle\langle\phi_{1-1+}| \dots |\phi_{1-1-}\rangle\langle\phi_{1-1-}| |\phi_{1-}\rangle\langle\phi_{1-}| \tag{1.1.20}$$

$$- \delta_t^{(1)} \sum_{\alpha} |\phi_{1+}\rangle\langle\phi_{1+}| |\phi_{1-1+}\rangle\langle\phi_{1-1+}| \dots |\phi_{1-1-}\rangle\langle\phi_{1-1-}| \mathbf{L}_{\alpha}^{\dagger} \mathbf{L}_{\alpha} |\phi_{1-}\rangle\langle\phi_{1-}| \tag{1.1.21}$$

$$+ \delta_t^{(1)} \sum_{\alpha} 2 |\phi_{1+}\rangle\langle\phi_{1+}| \mathbf{L}_{\alpha} |\phi_{1-1+}\rangle\langle\phi_{1-1+}| \dots |\phi_{1-1-}\rangle\langle\phi_{1-1-}| \mathbf{L}_{\alpha}^{\dagger} |\phi_{1-}\rangle\langle\phi_{1-}|. \tag{1.1.22}$$

All the operators in this expression have to be normal ordered in order to evaluate the matrix elements. For the Hamiltonian this is typically the case and one finds

$$|\phi_{1+}\rangle\langle\phi_{1+}| \mathbf{H}(\mathbf{b}^{\dagger}, \mathbf{b}) |\phi_{1-1+}\rangle\langle\phi_{1-1+}| = \mathbf{H}(\phi_{1+}^*, \phi_{1-1+}) |\phi_{1+}\rangle\langle\phi_{1+}| |\phi_{1-1+}\rangle\langle\phi_{1-1+}|. \tag{1.1.23}$$

for the terms in Eq. (1.1.18). This is done equivalently for the matrix elements on the minus contour with a subtle difference however. While on the plus contour, creation operators are evaluated for an infinitesimally later time than annihilation operators, on the minus contour the exact opposite is true, as one can see from

$$|\phi_{1-1-}\rangle\langle\phi_{1-1-}| \mathbf{H}(\mathbf{b}^{\dagger}, \mathbf{b}) |\phi_{1-}\rangle\langle\phi_{1-}| = \mathbf{H}(\phi_{1-1-}^*, \phi_{1-}) |\phi_{1-1-}\rangle\langle\phi_{1-1-}| |\phi_{1-}\rangle\langle\phi_{1-}|. \tag{1.1.24}$$

For typical, relevant physical setups, the jump operators are simple polynomial functions of the creation and annihilation operators and can therefore be normal ordered in a straightforward way. However, for the jump operators one should be careful since the product of normal ordered operators is in general not normal ordered, i.e.

$$: \mathbf{L}_{\alpha}^{\dagger} \mathbf{L}_{\alpha} : \neq : \mathbf{L}_{\alpha}^{\dagger} : : \mathbf{L}_{\alpha} :, \tag{1.1.25}$$

where $: \dots :$ denotes normal ordering. This fact is most easily illustrated in the case of incoherent single particle loss, for which the jump operators are simple annihilation operators $\mathbf{L}_{\alpha}^{\dagger} = \mathbf{b}_{\alpha}$ and consequently

$$: \mathbf{L}_{\alpha}^{\dagger} : : \mathbf{L}_{\alpha} := \mathbf{b}_{\alpha} \mathbf{b}_{\alpha}^{\dagger} \neq \mathbf{b}_{\alpha}^{\dagger} \mathbf{b}_{\alpha} =: \mathbf{b}_{\alpha} \mathbf{b}_{\alpha}^{\dagger} := : \mathbf{L}_{\alpha}^{\dagger} \mathbf{L}_{\alpha} :. \tag{1.1.26}$$

For simplicity, we consider the individual jump operators to be normal ordered, i.e. $\mathbf{L}_{\alpha} =: \mathbf{L}_{\alpha} :$. Then, the matrix elements in Eq. (1.1.22) evaluate to

$$|\phi_{1+}\rangle\langle\phi_{1+}| \mathbf{L}_{\alpha}(\mathbf{b}^{\dagger}, \mathbf{b}) |\phi_{1-1+}\rangle\langle\phi_{1-1+}| = \mathbf{L}_{\alpha}(\phi_{1+}^*, \phi_{1-1+}) |\phi_{1+}\rangle\langle\phi_{1+}| |\phi_{1-1+}\rangle\langle\phi_{1-1+}| \tag{1.1.27}$$

and equivalently for $\mathbf{L}_{\alpha}^{\dagger}$ and the normal ordered form of the product $\mathbf{L}_{\alpha}^{\dagger} \mathbf{L}_{\alpha}$. After evaluating the individual matrix elements and replacing all the operators by complex field variables,

the Liouvillian enclosed by coherent states can be rewritten according to

$$\begin{aligned}
& |\phi_{1+}\rangle\langle\phi_{1+}| \left[\left(1 + \delta_t^{(1)} \mathcal{L}\right) (|\phi_{1-1+}\rangle\langle\phi_{1-1+}| \dots |\phi_{1-1-}\rangle\langle\phi_{1-1-}|) \right] |\phi_{1-}\rangle\langle\phi_{1-}| \\
&= \left(1 + \delta_t^{(1)} \mathcal{L}(\phi_{1+}^*, \phi_{1-1+}, \phi_{1-}^*, \phi_{1-1-})\right) |\phi_{1+}\rangle\langle\phi_{1+}| |\phi_{1-1+}\rangle\langle\phi_{1-1+}| \dots |\phi_{1-1-}\rangle\langle\phi_{1-1-}| |\phi_{1-}\rangle\langle\phi_{1-}| \\
&= e^{\delta_t^{(1)} \mathcal{L}(\phi_{1+}^*, \phi_{1-1+}, \phi_{1-}^*, \phi_{1-1-})} |\phi_{1+}\rangle\langle\phi_{1+}| |\phi_{1-1+}\rangle\langle\phi_{1-1+}| \dots |\phi_{1-1-}\rangle\langle\phi_{1-1-}| |\phi_{1-}\rangle\langle\phi_{1-}|. \quad (1.1.28)
\end{aligned}$$

Here, we have defined the Liouville functional of the fields

$$\begin{aligned}
\mathcal{L}(\phi_{1+}^*, \phi_{1-1+}, \phi_{1-}^*, \phi_{1-1-}) &= \frac{1}{i} \left(\mathbf{H}(\phi_{1+}^*, \phi_{1-1+}) - \mathbf{H}(\phi_{1-}^*, \phi_{1-1-}) \right) \\
&\quad - \sum_{\alpha} \left[\left(\mathbf{L}_{\alpha}^{\dagger} \mathbf{L}_{\alpha} \right) (\phi_{1+}^*, \phi_{1-1+}) + \left(\mathbf{L}_{\alpha}^{\dagger} \mathbf{L}_{\alpha} \right) (\phi_{1-}^*, \phi_{1-1-}) \right] \\
&\quad + \sum_{\alpha} 2\mathbf{L}_{\alpha}(\phi_{1+}^*, \phi_{1-1+}) \mathbf{L}_{\alpha}^{\dagger}(\phi_{1-}^*, \phi_{1-1-}). \quad (1.1.29)
\end{aligned}$$

The last term in Eq. (1.1.29) corresponds to the recycling term in the quantum master equation and mixes coherent state amplitudes from the (+) and (-) part of the contour. Therefore, it has no counterpart in an equilibrium path integral formulation, where due to the purely Hamiltonian time evolution, the contours are only connected at $l = 0$, i.e. at the initial state and at $l = N$, where the trace is evaluated.

The residual state overlap elements and the coherent state measure

$$\begin{aligned}
& e^{-\phi_{1+}^* \phi_{1+}} |\phi_{1+}\rangle\langle\phi_{1+}| |\phi_{1-1+}\rangle\langle\phi_{1-1+}| \dots |\phi_{1-1-}\rangle\langle\phi_{1-1-}| |\phi_{1-}\rangle\langle\phi_{1-}| e^{-\phi_{1-}^* \phi_{1-}} \\
&= e^{-\phi_{1+}^* (\phi_{1+} - \phi_{1-1+})} |\phi_{1+}\rangle\langle\phi_{1+}| \dots |\phi_{1-1-}\rangle\langle\phi_{1-1-}| e^{-(\phi_{1-}^* - \phi_{1-1-}^*) \phi_{1-}} \\
&= e^{i\delta_t^{(1)} \phi_{1+}^* i\partial_t \phi_{1+}} |\phi_{1+}\rangle\langle\phi_{1+}| \dots |\phi_{1-1-}\rangle\langle\phi_{1-1-}| e^{i\delta_t^{(1)} (i\partial_t \phi_{1-}^*) \phi_{1-}} \quad (1.1.30) \\
&= e^{i\delta_t^{(1)} \phi_{1+}^* i\partial_t \phi_{1+}} |\phi_{1+}\rangle\langle\phi_{1+}| \dots |\phi_{1-1-}\rangle\langle\phi_{1-1-}| e^{-i\delta_t^{(1)} \phi_{1-}^* i\partial_t \phi_{1-}}, \quad (1.1.31)
\end{aligned}$$

form an effective temporal derivative of the fields, which is well known from the equilibrium path integral. Here, we used the formula for the inner product of coherent states

$$\langle\phi|\phi'\rangle = e^{\phi^* \phi'} \quad (1.1.32)$$

and the continuum limit $\delta_t \rightarrow 0$ to derive (1.1.30). After partial integration on the minus contour, one arrives at Eq. (1.1.31). The fact that the annihilation operators on the minus contour are evaluated infinitesimally later in time is expressed by the respective minus sign in front of the temporal derivative. In the continuum limit, the partition function

$$Z(t_f) = \int \mathcal{D}[\phi^*, \phi] e^{i\mathcal{S}} \quad (1.1.33)$$

is now defined in terms of the complex action

$$\mathcal{S} = \int_{t_0}^{t_f} dt \left(\phi_+^*(t) i\partial_t \phi_+(t) - \phi_-^*(t) i\partial_t \phi_-(t) - i\mathcal{L}(\phi_+^*(t), \phi_+(t), \phi_-^*(t), \phi_-(t)) \right), \quad (1.1.34)$$

which is an integral over the Liouville functional and the time derivatives of the fields, starting from the initial time t_0 to the final time t_f , at which the partition function is

evaluated. The functional measure in the integral is defined as

$$\mathcal{D}[\phi^*, \phi] = \prod_i \int d\phi_i^* d\phi_i \quad (1.1.35)$$

Up to now, in the action in Eq. (1.1.34), there are still missing the contributions from the matrix elements at $l = N$ and $l = 0$. In the continuum limit, these contributions become infinitesimal terms at $t = t_f$ and $t = t_0$, respectively. However, as mentioned above, they are necessary in order to provide a regularization of the path integral defined in Eq. (1.1.33). For completeness, we will briefly discuss the corresponding matrix elements, which are

$$\langle \phi_-(t_f) | \phi_+(t_f) \rangle = e^{\phi_+^*(t_f) \phi_-(t_f)} \quad (1.1.36)$$

and

$$\begin{aligned} \langle \phi_+(t_0) | \rho_0 | \phi_-(t_0) \rangle &= e^{\Gamma(\phi_+^*(t_0), \phi_-(t_0))}, \\ \text{with } \Gamma(\phi_+^*(t_0), \phi_-(t_0)) &= \log(\langle \phi_+(t_0) | \rho_0 | \phi_-(t_0) \rangle). \end{aligned} \quad (1.1.37)$$

While the evaluation of Eq. (1.1.36) is quite simple, the computation of the function Γ in Eq. (1.1.37) is very demanding and will not be performed directly. It acts as an initial (or boundary) condition for the path integral, which is much simpler integrated on a physically more transparent basis, namely on the basis of the bare Green's functions. This will be performed in the subsequent chapter.

As a last step, we can enlarge the contour, ranging from $t_0 = -\infty$ to $t_f = \infty$ to recover the non-equilibrium path integral on the (+)-(-) contour for a system with dynamics described by a master equation, containing both unitary dynamics and non-unitary dynamics in terms of Lindblad type jump operators.

1.2 NON-EQUILIBRIUM GREEN'S FUNCTIONS

Green's functions are expectation values of time-nonlocal operator products and as such contain important information about a system's response and correlation properties. The simplest Green's functions in general are particle-particle Green's functions, which consist of only two atomic (creation and annihilation) operators and for many purposes, they contain already sufficient information to make valuable predictions about the system of interest. However, there exist arbitrary orders of Green's functions, the most well-known being certainly the density-density correlation function, which is nothing but a four point (consisting of four atomic operators) Green's function.

In equilibrium, there exists only a single Green's function (for each different power of operators), namely the imaginary time ordered or Matsubara Green's function. This is a consequence of the fact, that response and correlation properties at equilibrium are inextricably linked via the equilibrium fluctuation dissipation relation. This is, however, no longer the case for an out-of-equilibrium situation and more information is required, as we will see in the following.

Let's for the moment neglect multiple quantum states and consider a system described by a single quantum mechanical degree of freedom. In this situation, the complex fields

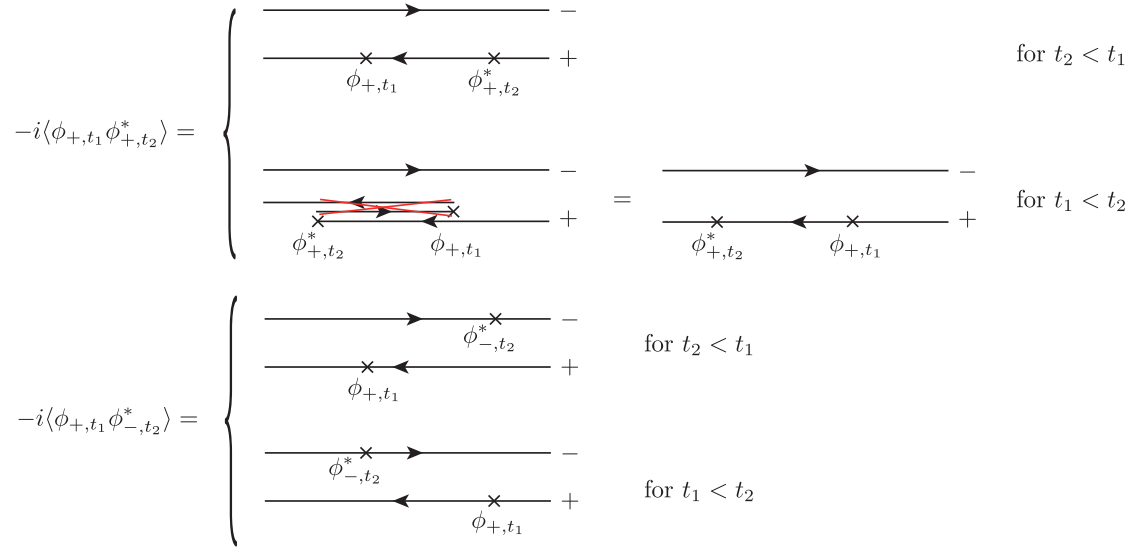


Figure 1.1: Illustration of Green's functions on equal and on distinct contours. For fields placed on equal contours (here illustrated with the $+$ -contour), either $t_2 < t_1$, then the Green's function is already time ordered, or $t_1 < t_2$. For the latter, the two overlapping contour parts, representing two identical phases in the action with opposite sign, cancel exactly and the remaining Green's function is time ordered. Therefore, equal contour Green's functions are always time ordered. For non-equal contours, there is no cancellation since both contours are represented by different, independent fields and there is no time ordering present.

$\phi_\alpha(t)$ only have a single index $\alpha = \pm$ indicating whether this field is on the plus or minus contour. The two-point Green's function on the \pm -contour is defined as⁷

$$G_{\gamma\delta}(t, t') = -i\langle\phi_\gamma(t)\phi_\delta^*(t')\rangle, \quad (1.2.1)$$

where the average in Eq. (1.2.1) is the average with respect to the functional integral over the action

$$\langle\dots\rangle = \int \mathcal{D}[\phi^*, \phi] \dots e^{iS}. \quad (1.2.2)$$

For indices $\gamma, \delta = \pm$, we have four different combinations, representing four different types of Green's functions. For $\delta = \gamma = +$, both fields are on the plus contour and located on the left of the density matrix. Since complex fields commute with each other and there is no backward time evolution in the path integral formulation (compare with Fig. 1.1), this combination represents a time ordered Green's function

$$\begin{aligned} iG_{++}(t, t') &= \langle\phi_+(t)\phi_+^*(t')\rangle \\ &= \theta(t - t')\text{Tr}\left(b(t)b^\dagger(t')\rho\right) + \theta(t' - t)\text{Tr}\left(b^\dagger(t')b(t)\rho\right) \equiv iG^T(t, t') \end{aligned} \quad (1.2.3)$$

where the operator with the larger absolute time is placed on the left of the operator with the smaller absolute time.

For $\gamma = \delta = -$, both operators are ordered in time as well, however, this time they are

⁷For simplicity, we imply U(1) invariance, i.e. strict particle number conservation for the present situation, such that off-diagonal terms $\sim \langle\phi^*\phi^*\rangle$ are exactly zero.

ordered on the minus contour, i.e. on the right of the density matrix, for which larger times are placed on the right of smaller times and correspondingly the operators are anti-time ordered

$$\begin{aligned} iG_{--}(t, t') &= \langle \phi_-(t) \phi_-^*(t') \rangle \\ &= \theta(t' - t) \text{Tr} \left(\rho b(t) b^\dagger(t') \right) + \theta(t - t') \text{Tr} \left(\rho b^\dagger(t') b(t) \right) \equiv iG^{\tilde{T}}(t, t'). \end{aligned} \quad (1.2.4)$$

For the other two possibilities, where $\gamma \neq \delta$, the operators are placed each on a distinct contour, such that no time ordering will be performed. The corresponding Green's functions are the lesser Green's function, for which the creation operator is on the left of the annihilation operator

$$\begin{aligned} iG_{+-}(t, t') &= \langle \phi_+(t) \phi_-^*(t') \rangle \\ &= \text{Tr} \left(b(t) \rho b^\dagger(t') \right) = \text{Tr} \left(b^\dagger(t') b(t) \rho \right) \equiv G^<(t, t') \end{aligned} \quad (1.2.5)$$

and the greater Green's function

$$\begin{aligned} iG_{-+}(t, t') &= \langle \phi_-(t) \phi_+^*(t') \rangle \\ &= \text{Tr} \left(b^\dagger(t') \rho b(t) \right) = \text{Tr} \left(b(t) b^\dagger(t') \rho \right) \equiv G^>(t, t'), \end{aligned} \quad (1.2.6)$$

for which the annihilation operator is on the left of the creation operator. Obviously, there is some redundancy in these four Green's functions and we can express the time ordered and anti-time ordered Green's function completely in terms of the lesser and greater Green's functions, according to

$$G^T(t, t') = \theta(t - t') G^>(t, t') + \theta(t' - t) G^<(t, t') \quad (1.2.7)$$

and

$$G^{\tilde{T}}(t, t') = \theta(t - t') G^<(t, t') + \theta(t' - t) G^>(t, t'), \quad (1.2.8)$$

which follows straightforwardly from Eqs. (1.2.3)-(1.2.6). Due to Eqs. (1.2.7) and (1.2.8), only the knowledge of two distinct Green's functions is required, such that the two missing ones can be constructed as linear combinations of known ones.

In the special case of thermal equilibrium, there is an additional relation, known as the fluctuation dissipation theorem, which reads

$$G^<(\omega) + G^>(\omega) = (2n_B(\omega) + 1) (G^<(\omega) - G^>(\omega)). \quad (1.2.9)$$

Here, we switched to frequency space and introduced the Bose distribution function⁸

$$n_B(\omega) = \frac{1}{e^{\beta\omega} - 1}. \quad (1.2.10)$$

Because of this relation, in thermal equilibrium, it is sufficient to only know a single Green's function (time-ordered, anti-time ordered, lesser or greater) such that all other Green's functions can be computed. As a consequence of this, the equilibrium path integral is situated on a single (imaginary time) contour and the Matsubara Green's function contains all relevant information on the system. However, this is no longer the case for a system out of equilibrium, where not only the dynamics have to be determined from the path integral

⁸For fermionic systems, there exists a similar fluctuation dissipation relation, where the distribution function is the Fermi-Dirac distribution.

but also the distribution function of the excitations does not longer coincide with a thermal Bose distribution. The latter point, of course, renders the fluctuation dissipation relation in its equilibrium version (i.e. Eq. (1.2.9)) invalid. As a consequence, the knowledge of at least two distinct Green's functions is required out of equilibrium.

In the previous section, we showed that it is impossible to construct a path integral based on a single contour for systems that are either driven and therefore not in thermal equilibrium or that are evolving in time, starting from a non-thermal initial state. For both of these situations, a two contour formalism is required as has been introduced in Sec. 1.1.

In this section, we illustrated that it is no longer sufficient for the dynamics to only have the knowledge on a single (imaginary time) Green's function but at least two Green's functions are required as soon as the distribution function of the system is not thermal and consequently an equilibrium fluctuation dissipation relation does not hold. These two results are of course closely related to each other and the deeper reason for them is simply that for an out of equilibrium system, both response and correlations have to be determined and described independently.

1.3 KELDYSH ROTATION AND FLUCTUATION-DISSIPATION RELATION

The Green's function in the (\pm) -basis contains a lot of redundancy and has no obvious structural properties. This implies complex diagrammatic rules and causal constraints[99]. Both of these issues can be overcome by the so-called Keldysh rotation, which we will introduce in the following. It reduces the redundancy in the Green's functions and implies a simplified fluctuation dissipation relation in a physically more appealing representation. As a further consequence, the initial conditions (1.1.37) can be implemented directly in terms of the initial correlations of the system.

The complete Green's function matrix in the (\pm) -basis reads

$$\tilde{G}(t, t') = \left\langle \begin{pmatrix} \phi_+(t) \\ \phi_-(t) \end{pmatrix} (\phi_+^*(t'), \phi_-^*(t')) \right\rangle = \begin{pmatrix} G^T(t, t') & G^<(t, t') \\ G^>(t, t') & G^{\tilde{T}}(t, t') \end{pmatrix}. \quad (1.3.1)$$

The Keldysh basis is spanned by the fields ϕ_c and ϕ_q according to the transformation

$$\begin{pmatrix} \phi_c(t) \\ \phi_q(t) \end{pmatrix} = \frac{1}{\sqrt{2}} \begin{pmatrix} 1 & 1 \\ 1 & -1 \end{pmatrix} \begin{pmatrix} \phi_+(t) \\ \phi_-(t) \end{pmatrix} = \frac{1}{\sqrt{2}} \begin{pmatrix} \phi_+(t) + \phi_-(t) \\ \phi_+(t) - \phi_-(t) \end{pmatrix}. \quad (1.3.2)$$

The field ϕ_c is referred to as the classical field and the field ϕ_q as the quantum field. The reason for this nomenclature is that the field ϕ_c can acquire a finite expectation value, while the expectation value of the field ϕ_q is always zero, by definition. In a Landau type action for phase transitions, the field ϕ_c represents the order parameter field, which goes to zero at a second order phase transition, while the field ϕ_q is the response field, which is the generator of response functions.

The Green's function in the Keldysh basis transforms to

$$\begin{aligned} G(t, t') &= \frac{1}{2} \begin{pmatrix} 1 & 1 \\ 1 & -1 \end{pmatrix} \begin{pmatrix} G^T(t, t') & G^<(t, t') \\ G^>(t, t') & G^{\tilde{T}}(t, t') \end{pmatrix} \begin{pmatrix} 1 & 1 \\ 1 & -1 \end{pmatrix} \\ &= \begin{pmatrix} G^<(t, t') + G^>(t, t') & \theta(t - t') (G^>(t, t') - G^<(t, t')) \\ \theta(t' - t) (G^<(t, t') - G^>(t, t')) & 0 \end{pmatrix} \end{aligned} \quad (1.3.3)$$

$$\equiv \begin{pmatrix} G^K(t, t') & G^R(t, t') \\ G^A(t, t') & 0 \end{pmatrix} = \left\langle \left(\begin{array}{cc} \phi_c(t)\phi_c^*(t') & \phi_c(t)\phi_q^*(t') \\ \phi_q(t)\phi_c^*(t') & \phi_q(t)\phi_q^*(t') \end{array} \right) \right\rangle. \quad (1.3.4)$$

Eq. (1.3.3) follows from a direct application of the definition of $G^{T, \tilde{T}}$ in terms of $G^{<, >}$ according to Eqs (1.2.7), (1.2.8). The elements of the Green's function (1.3.4) are the retarded/advanced Green's function $G^{R/A}$ with the property

$$G^A = (G^R)^\dagger \quad (1.3.5)$$

and an retarded, advanced structure in time. The retarded and advanced Green's function contain information on the response of the system to external perturbations and on its spectral properties. The difference is nothing but the spectral function

$$G^R(t, t') - G^A(t, t') = G^>(t, t') - G^<(t, t') \quad (1.3.6)$$

$$G^R(\omega) - G^A(\omega) = \mathcal{A}(\omega) \equiv \langle \delta(\omega - H) \rangle. \quad (1.3.7)$$

The structure of the Green's function (1.3.4) is called causal structure and it is preserved for all physical realizations, i.e. it is tridiagonal, with retarded and advanced components on the off-diagonal. For an arbitrary n-point function, a product of only quantum fields has to be zero, which is a consequence of the causality structure.

In terms of bosonic operators, the retarded Green's functions is

$$G^R(t, t') = -i\theta(t - t') \langle [b(t), b^\dagger(t')] \rangle \quad (1.3.8)$$

and the so-called Keldysh Green's function G^K , which is the expectation value of two classical operators, is

$$G^K(t, t') = -i\langle \{b(t), b^\dagger(t')\} \rangle. \quad (1.3.9)$$

It contains informations on the correlations, for instance the occupation of excitations and therefore informations on the initial state. The Keldysh Green's function is anti-hermitian, i.e.

$$G^K = - (G^K)^\dagger. \quad (1.3.10)$$

It is parametrized as

$$G^K = G^R \circ F - F \circ G^A, \quad (1.3.11)$$

where F is a hermitian function and \circ denotes the convolution in the corresponding parameter space (i.e. temporal and spatial degrees of freedom). The function F is the distribution function, which contains information on the distribution of excitations in the system. The parametrization in Eq. (1.3.11) allows the separation of spectral properties and correlation properties, which are both encoded in the Keldysh Green's function.

The inverse of the Green's function in Eq. (1.3.4) determines the quadratic part of the action (or in other words, the quadratic part of the action determines the bare Green's function) according to

$$\mathcal{S} = \int (\phi_c^*, \phi_q^*) G^{-1} \begin{pmatrix} \phi_c \\ \phi_q \end{pmatrix}. \quad (1.3.12)$$

The inverse of Eq. (1.3.4) is

$$G^{-1} = \begin{pmatrix} 0 & (G^A)^{-1} \\ (G^R)^{-1} & - (G^R)^{-1} G^K (G^A)^{-1} \end{pmatrix} \equiv \begin{pmatrix} 0 & D^A \\ D^R & D^K \end{pmatrix}. \quad (1.3.13)$$

The retarded and advanced sectors of this matrix are determined by the Liouvillian \mathcal{L} alone, while the Keldysh sector (i.e. D^K) is determined from the dissipative parts in the Liouvillian as well as from the initial state. Inserting the parametrization of the Keldysh Green's function in Eq. (1.3.11) into the definition of D^K , one finds

$$D^K = D^R \circ F - F \circ D^A. \quad (1.3.14)$$

This defines the Keldysh part of the action in terms of the Liouvillian properties (which determine $D^{R/A}$) as well as the distribution function of the particles (or excitations) F . If F is known at $t = 0$, the computation of the matrix element for the initial state in Eq. (1.1.37) is no longer required in order to determine the quadratic part of the action. Of course, this captures only the quadratic initial correlations in the system but it doesn't include higher order correlations up to this point. However, for many realizations (that we will encounter in this thesis) it is sufficient to know the quadratic initial correlations in order to describe the systems dynamics. These realizations include:

- i) quench procedures, for which the initial state is a Gaussian or thermal state and therefore fulfills an equilibrium fluctuation dissipation relation at $t = 0$.
- ii) steady states for dissipative systems, for which the initial state does not play any role for the late time dynamics in which the steady state is approached.
- iii) disordered systems, for which typically the Liouvillian alone determines the critical properties, as the disorder induced localization is a pure response property.

However, there are as well examples in the literature, which have shown cases in which the quadratic initial correlations are by far not sufficient to describe the dynamics in a reasonable way. The most prominent of these might be a fermionic Luttinger Liquid connecting two fermionic reservoirs with different chemical potential [76, 75, 77].

The intention of this chapter is to derive the Keldysh action for a system with dynamics described by a quantum master equation. These include Hamiltonian systems alone, as well as driven-dissipative systems coupled to an external bath. While for the former, the Keldysh contour is only required for disordered systems (which can again be seen as systems coupled to a quenched bath) and systems which are initialized in an out of equilibrium state, the latter will always require a path integral on the Keldysh contour because of the presence of the quantum jump operators. We introduced the basic Green's functions on the (\pm) -contour and discussed their properties and finally introduced the framework in which this thesis will be settled. Namely the Keldysh representation of the non-equilibrium path integral. In this last section, we provided basic information on the Keldysh Green's functions, fluctuation-dissipation relations and the determination of the initial correlations, which are required for an analysis of non-equilibrium systems in terms of the Keldysh path integral.

The above discussion is by far not exhaustive and for further information on the Keldysh path integral, we refer to the reviewing literature [99, 3].

2 DISSIPATIVE SPIN GLASSES IN OPTICAL CAVITIES

In the context of ultracold atoms in multimode optical cavities, the appearance of a quantum-critical glass phase of atomic spins has been predicted recently [190]. Due to the long-range nature of the cavity-mediated interactions, but also the presence of a driving laser and dissipative processes such as cavity photon loss, the quantum optical realization of glassy physics has no analog in condensed matter, and could evolve into a “cavity glass microscope” for frustrated quantum systems out-of-equilibrium. Here we develop the non-equilibrium theory of the multimode Dicke model with quenched disorder and Markovian dissipation. Using a unified Keldysh path integral approach, we show that the defining features of a low temperature glass, representing a critical phase of matter with algebraically decaying temporal correlation functions, are seen to be robust against the presence of dissipation due to cavity loss. The universality class however is modified due to the Markovian bath. The presence of strong disorder leads to an enhanced equilibration of atomic and photonic degrees of freedom, including the emergence of a common low-frequency effective temperature. The imprint of the atomic spin glass physics onto a “photon glass” makes it possible to detect the glass state by standard experimental techniques of quantum optics. We provide an unambiguous characterization of the superradiant and glassy phases in terms of fluorescence spectroscopy, homodyne detection, and the temporal photon correlation function $g^{(2)}(\tau)$.

2.1 INTRODUCTION

An emerging theme in the research on strongly correlated ultracold atoms is the creation of quantum soft matter phases ranging from nematics and smectics [71, 72], liquid crystals [123], granular materials [97, 180, 153], friction phenomena in nonlinear lattices [160, 191], to glasses [73, 190, 141, 148, 156]. Realizing glasses with strongly interacting light-matter systems bears the promise to study some of the most celebrated achievements in statistical mechanics from a new vantage point. The Parisi solution of mean-field spin glasses [20], for example, continues to trigger research more than three decades after its discovery in the early 1980’s, and may have implications for information storage [5] and “frustrated” optimization algorithms [13]. The latter is related to the inability of a glass to find its ground state; a feature that makes it inherently non-equilibrium.

Historically, quantum effects in soft matter and glasses have not played a prominent role because most soft materials are too large, too heavy and/or too hot and therefore way

outside the quantum regime. Spin and charge glass features have however been invoked in some electronic quantum materials [20, 135], mainly due to RKKY-type interactions or randomly distributed impurities providing a random potential for the electrons. However, here the glassy mechanisms occur often in combination with other more dominant (Coulomb) interactions, and it is hard to pin down which effects are truly due to glassiness. Note that the somewhat simpler Bose glass of the Bose Hubbard model [62] (see [79] for a possible realization in optical cavities), while in the quantum regime, occurs because of a short-range random potential, and does not generically exhibit some of the hallmark phenomena of frustrated glasses, such as many metastable states, aging, or replica-symmetry breaking.

It would clearly be desirable to have a tunable realization of genuinely frustrated (quantum) glasses in the laboratory. Recent work on ultracold atoms in optical cavities [73, 190, 141, 79] suggests that it may be possible to create spin- and charge glasses in these systems, which arise because of frustrated couplings of the atomic “qubits” to the dynamical potential of multiple cavity modes. It is appealing to these systems that the photons escaping the cavity can be used for in-situ detection of the atom dynamics (“cavity glass microscope”), and that the interaction mediated by cavity photons is long-ranged. The latter makes the theoretical glass models more tractable and should allow for a realistic comparison of experiment and theory.

The phases of matter achievable with cavity quantum electrodynamics (QED) systems settle into non-equilibrium steady states typically balancing a laser drive with dissipation channels such as cavity photon loss and atomic spontaneous emission. The notion of temperature is, a priori, not well defined. A line of recent research on the self-organization transition of bosonic atoms in a single-mode optical cavity (experimentally realized with a thermal gas of Cesium [23] and with a Bose-Einstein condensate of Rubidium [26, 15]), has established the basic properties of the non-equilibrium phase transition into the self-organized, superradiant phase [56, 133, 105, 143, 144, 149, 19, 49, 140, 170]. In particular it was shown that, upon approximating the atom dynamics by a single collective spin of length $N/2$ and taking the atom number N large, the dynamics can be described by classical equations of motion [105, 19], and that the phase transition becomes thermal due to the drive and dissipation [49].

In this chapter, we underpin the previous proposal [190], and show that quenched disorder from multiple cavity modes, leads to qualitatively different non-equilibrium steady states with quantum glassy properties. We develop a comprehensive non-equilibrium theory for many-body multimode cavity QED with quenched disorder and Markovian dissipation. We pay special attention to the quantum optical specifics of the pumped realization of effective spin model [55], the laser drive and the finite photon lifetimes of cavity QED. Using a field theoretic Keldysh formalism adapted to quantum optics, we compute several observables of the glass and superradiant phases, which are accessible in experiments with current technology. Our key results are summarized in the following section.

The remainder of the chapter is then organized as follows. In Sec. 2.3 we discuss the multimode open Dicke model in the simultaneous presence of quenched disorder and Markovian dissipation. Disorder and dissipative baths are contrasted more rigorously in Sec. 2.8. We switch to a unified description of both these aspects in Sec. 2.4 in the framework of a Keldysh path integral formulation, and specify the formal solution of the problem in the thermodynamic limit in terms of the partition sum, which allows to extract all atomic and photonic correlation and response functions of interest. This solution is evaluated in Sec. 2.5, with some details in Sec. 2.10. This comprises the calculation of the phase diagram in the presence of cavity loss, as well as the discussion of correlation and response functions for both atomic and photonic degrees of freedom, allowing us to uniquely characterize the simultaneous spin and photon glass phase from the theoretical perspective. We then discuss the consequences of these theoretical findings to concrete experimental observables in cavity QED experiments in Sec. 2.5.5. The combination of correlation and response measurements allows for a complete characterization of the phase diagram and in particular of the glass phase.

The relation between Keldysh path integral and quantum optics observables is elaborated on further in Sec. 2.9.

2.2 KEY RESULTS

2.2.1 Non-equilibrium Steady State Phase Diagram

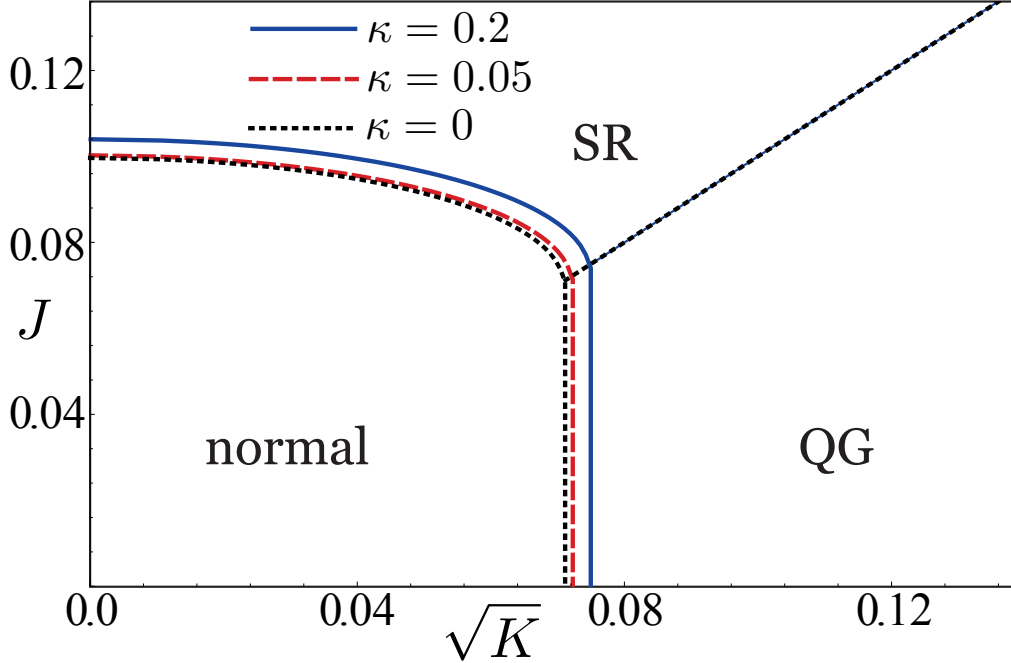


Figure 2.1: Non-equilibrium steady state phase diagram of the open multimode Dicke model, as a function of averaged atom-photon coupling J (y-axis) and disorder variance K (x-axis) and for parameters $\omega_0 = 1$ (cavity detuning) and $\omega_z = 0.5$ (effective atom detuning) for different photon decay rates κ . QG is the quantum spin and photon glass, SR the superradiant phase. The $T = 0$ equilibrium phase diagram of Ref. [190] is recovered as $\kappa \rightarrow 0$. The SR-QG transition is not affected by κ .

The shape of the phase diagram for the steady state predicted in [190], with the presence of a normal, a superradiant, and a glass phase is robust in the presence of Markovian dissipation, cf. Fig. 2.1. As to the phase diagram, the open nature of the problem only leads to quantitative modifications. In particular, the characteristic feature of a glass representing a critical phase of matter persists. The presence of photon decay overdamps the spin spectrum and changes the universality class of the glass phase, which we now discuss.

Within the glass phase, we identify a crossover scale $\omega_c \sim \kappa$ proportional to the cavity decay rate κ , above which the spectral properties of a zero temperature quantum spin glass are reproduced. Although the finite cavity decay κ introduces a finite scale “above the quantum critical point of the closed, equilibrium system”, κ acts very differently from a finite temperature. In particular, below ω_c , the spectral properties are modified due to the breaking of time reversal symmetry by the Markovian bath, while remaining critical. Due to the low frequency modification, the quantum spin glass in optical cavities formally belongs to the dynamical universality class of dissipative quantum glasses, such as glasses coupled to equilibrium ohmic baths [46, 45, 44] or metallic spin glasses [165, 141].

2.2.2 Dissipative Spectral Properties and Universality Class

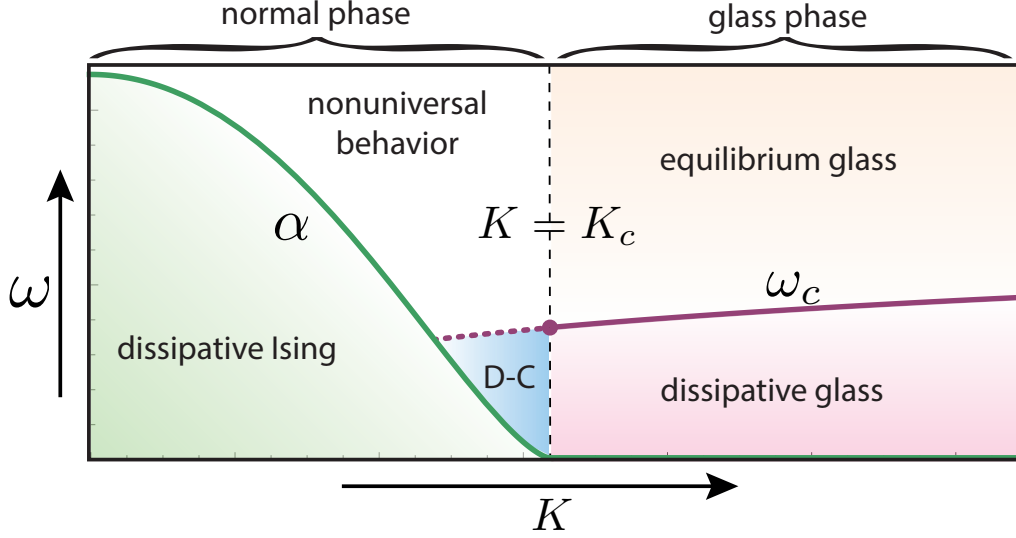


Figure 2.2: Illustration of the dissipative spectral properties and universality class. As a function of probe frequency ω (y-axis) and the disorder variance K (x-axis), we illustrate the different regimes in the phase diagram. In the normal phase, for frequencies $\omega < \alpha$ the system is represented by a dissipative Ising model, described by Eq. (2.2.2), while for frequencies $\omega > \alpha, \omega_c$ it is described by non-universal behavior of a disordered spin fluid. In the glass phase ($K > K_c$), there exist two qualitatively distinct frequency regimes, separated by the crossover scale ω_c , cf. Eq. (2.2.1). At the lowest frequencies, $\omega < \omega_c$ the system is described by the universality class of dissipative spin glasses. For $\omega > \omega_c$, we find that the system behaves quantitatively as an equilibrium spin glass. For $\alpha < \omega_c$ and $K < K_c$, there exists a dissipative crossover region (D-C in the figure), which is a precursor of the dissipative spin glass. It shows dissipative Ising behavior for smallest frequencies and resembles the dissipative glass for frequencies $\omega_c > \omega > \alpha$.

Spectral properties – The role of the crossover scale between equilibrium and dissipative spin glass is further illustrated in Fig. 2.2. It is given by

$$\omega_c = 2\kappa \left(1 + \frac{\omega_0^2}{\omega_0^2 + \kappa^2} + \frac{(\omega_0^2 + \kappa^2)^2}{\sqrt{K}\omega_z^2} \right)^{-1}. \quad (2.2.1)$$

The resulting modifications below this scale, compared to a more conventional equilibrium glass are due to the Markovian bath, introducing damping. In the normal and superradiant phases, this allows for the following form of the frequency resolved linearized Langevin equation for the atomic Ising variables,

$$\frac{1}{Z} (\omega^2 + i\gamma\omega + \alpha^2) x(\omega) = \xi(\omega), \quad (2.2.2)$$

modelling the atoms as an effective damped harmonic oscillator, with finite lifetime $\tau = \frac{1}{\gamma} < \infty$ and α the effective oscillator frequency, with the physical meaning of the gap of the atomic excitations in our case. The noise has zero mean and $\langle \xi(t')\xi(t) \rangle = \frac{2\gamma}{Z} T_{\text{eff}} \delta(t' - t)$.

At the glass transition, Z and α scale to zero simultaneously and the frequency dependence

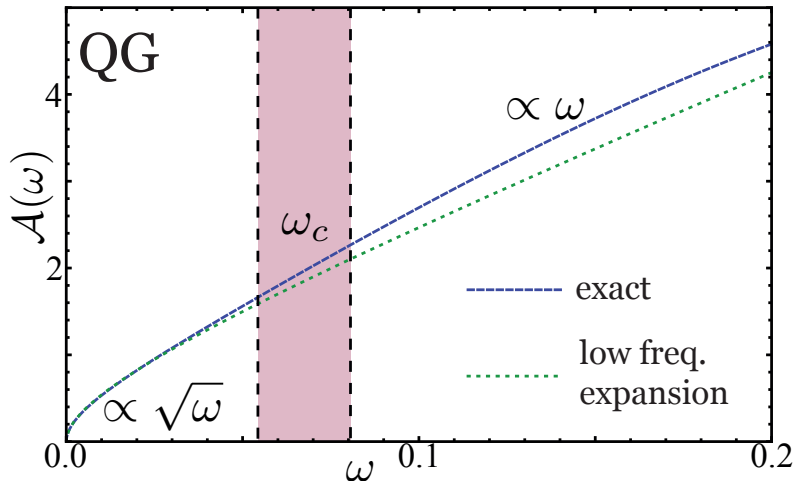


Figure 2.3: Dissipative spectral properties and universality class of the single-atom spectral density $\mathcal{A}(\omega)$ (response signal of RF spectroscopy) in the quantum glass phase for parameters $K = 0.01, J = 0.1, \omega_z = 2, \kappa = 0.1, \omega_0 = 0.7$. For frequencies $\omega < \omega_c$ below the crossover scale, the spectral density is overdamped and proportional to $\sqrt{\omega}$. For intermediate frequencies $\omega > \omega_c$, \mathcal{A} is linear in the frequency, as for the non-dissipative case [190], which is recovered in the limit $\kappa \rightarrow 0$.

becomes gapless and non-analytic. In the entire glass phase, the effective atomic low frequency dynamics is then governed by the form

$$\frac{1}{\bar{Z}} \sqrt{\omega^2 + \bar{\gamma}|\omega|} x(\omega) = \xi(\omega), \quad (2.2.3)$$

which obviously cannot be viewed as a simple damped oscillator any more. The broken time reversal symmetry manifests itself in $\gamma, \bar{\gamma} > 0$, thus modifying the scaling for $\omega \rightarrow 0$. The crossover between these different regimes is clearly visible in Fig. 2.3.

Universality class – The qualitative modification of the low-frequency dynamics below the crossover scale ω_c implies a modification of the equilibrium quantum spin glass universality class. The open system Dicke superradiance phase transition, where the Z_2 symmetry of the Dicke model is broken spontaneously due to a finite photon condensate, is enclosed by a finite parameter regime in which the dynamics is purely dissipative, or over-damped (see e.g. [49]). Together with the generation of a low frequency effective temperature (LET), for this reason the single mode Dicke phase transition can be classified within the scheme of Hohenberg and Halperin [88] in terms of the purely relaxational Model A, thereby sharing aspects of an equilibrium dynamical phase transition. This situation is different for the open system glass transition: Here, irreversible dissipative and reversible coherent dynamics rival each other at the glass transition down to the lowest frequencies. In particular, the dissipative dynamics fades out faster than the coherent dynamics as witnessed by larger critical exponents, and there is no regime in the vicinity of the critical point where either dissipative or coherent dynamics would vanish completely. This behavior is demonstrated in the inset of Fig. 2.2.5.

We note that, while these findings are unconventional from the viewpoint of equilibrium quantum glasses, they are not uniquely tied to the presence of the driven, Markovian non-equilibrium bath. In fact, such behavior is also present in the case of a system-bath setting in global thermodynamic equilibrium, where the presence of the bath variables modifies the spectral properties of the spins [45, 46, 141]. Both physical contexts share in common the time reversal breaking of the subsystem obtained after elimination of the bath modes and may be seen to belong to the same universality class.

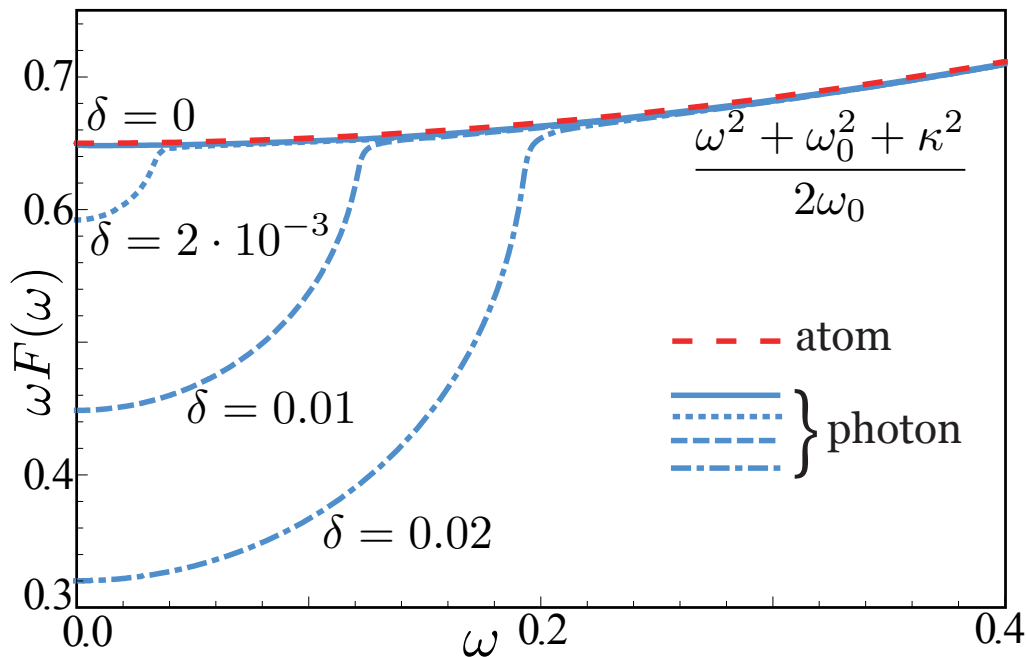


Figure 2.4: Thermalization into quantum-critical regime of the atomic (red, dashed line) and photonic (blue lines) distribution functions $F(\omega)$ when approaching the glass transition at a critical disorder variance K_c for $\omega_0 = 1.3$, $\omega_z = 0.5$, $\kappa = 0.01$, $K_c = 0.01$, $J = 0.1$ and varying parameter $\delta = K_c - K$. For larger values of J , i.e. larger distance from the glass transition, the low frequency effective temperature (LET) $2T_{\text{eff}} = \lim_{\omega \rightarrow 0} \omega F(\omega)$ of the photons is much lower than the LET of the atoms and the frequency interval for which atoms and photons are not equilibrated is larger. When the glass transition is approached, atoms and photons attain the same LET.

2.2.3 Atom-Photon Thermalization into Quantum-Critical Regime

As in the driven open Dicke model, the statistical properties of atoms and photons are governed by effective temperatures at low frequencies. The effective temperature differs in general for the two subsystems. Approaching the glass transition, these effective temperatures are found to merge. The finite cavity decay enables this mechanism but κ does not directly play the role of effective temperature. This mechanism pushes the hybrid system of atoms and photons in the glass phase into a quantum-critical regime described by a global effective temperature for a range of frequencies. This quantum critical regime retains signatures of the underlying quantum critical point.

The Markovian bath not only affects the spectral properties, but also governs the statistical properties of the system. The main statistical effect is the generation of a LET for the atomic degrees of freedom, for which we find

$$T_{\text{eff}} = \frac{\omega_0^2 + \kappa^2}{4\omega_0} \quad (2.2.4)$$

throughout the entire phase diagram, and taking the same value as in the single-mode case (in the absence of spontaneous emission for the atoms). This thermalization of the atoms happens despite the microscopic driven-dissipative nature of the dynamics, and has been observed in a variety of driven open systems theoretically [138, 54, 47, 149, 48, 51, 202, 181] and experimentally [112]. Below this scale, the occupation properties are governed by an

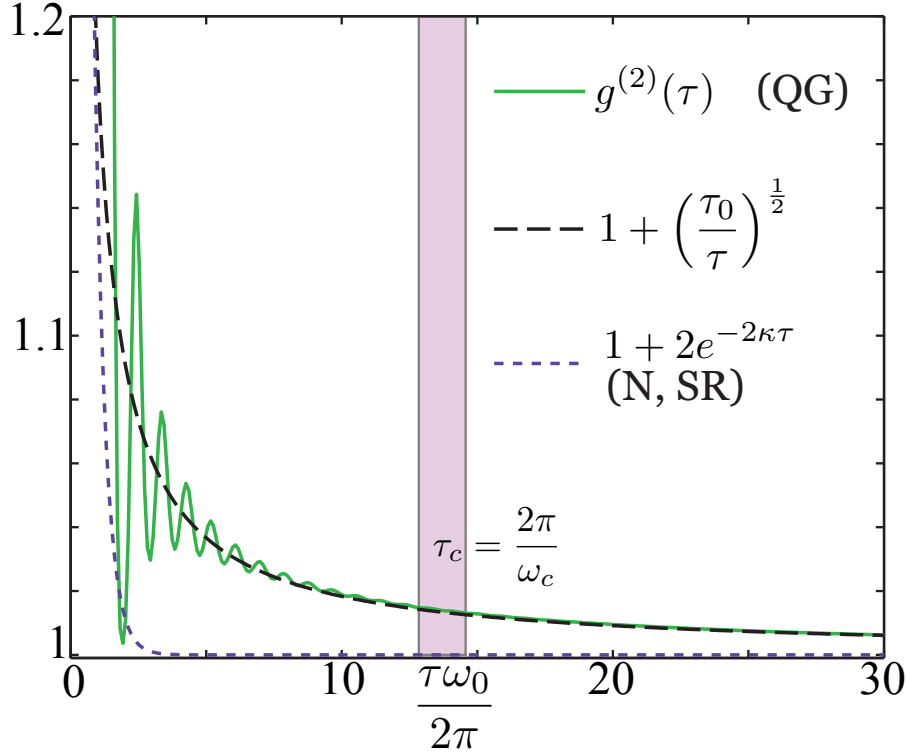


Figure 2.5: Emergent photon glass phase with algebraically decaying photon correlation function $g^{(2)}(\tau)$ at long times, for parameters $\omega_0 = 1, \kappa = 0.4, \omega_z = 6, J = 0.4, K = 0.16$. The time-scale for which algebraic decay sets in is determined by the inverse crossover frequency ω_c , given by Eq. (2.5.11). For comparison, we have also plotted the envelope of the exponential decay of the correlation function in the normal and superradiant phase. The short time behavior of the correlation function is non-universal and not shown in the figure, however, $g^{(2)}(0) = 3$ due to the effective thermal distribution for low frequencies. The parameter $\tau_0 = O(\frac{1}{\omega_0})$ was determined numerically.

effective classical thermal distribution $2T_{\text{eff}}/\omega$, while above it the physics is dominated by non-equilibrium effects [49]. For cavity decay $\kappa \ll \omega_0$, the crossover scale obeys $\omega_c \ll T_{\text{eff}}$. As a consequence, in an extended regime of frequencies between ω_c and T_{eff} , the correlations describe a finite temperature equilibrium spin glass.

In the single-mode open Dicke model, the photon degrees of freedom are also governed by an effective temperature, which however differs from the one for atoms [49], indicating the absence of equilibration between atoms and photons even at low frequencies. The increase of the disorder variance leads to an adjustment of these two effective temperatures, cf. Fig. 2.4. At the glass transition, and within the entire glass phase, the thermalization of the subsystems is complete, with common effective temperature given in Eq. (2.4.27). This effect can be understood qualitatively as a consequence of the disorder induced long ranged interactions, cf. Sec. 2.2.4. These allow to redistribute energy and enable equilibration.

We emphasize that the notion of thermalization here refers to the expression of a $1/\omega$ divergence for the system's distribution function, as well as the adjustment of the coefficients for atoms and photons. This provides an understanding for distinct scaling properties of correlations (where the distribution function enters) vs. responses (which do not depend on the statistical distribution), which can be addressed separately in different experiments (see below). Crucially, this notion of “thermalization” does not mean that the characteristics features of the glass state are washed out or overwritten.

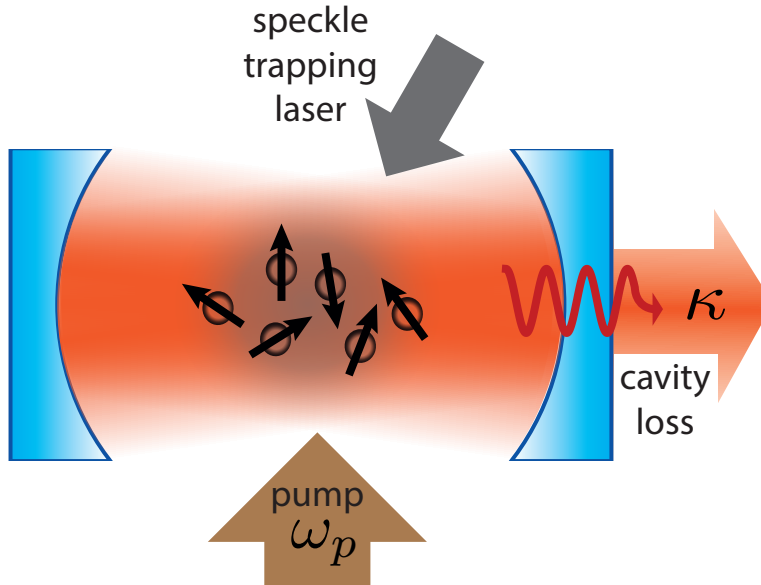


Figure 2.6: Cavity glass microscope set-up: Atoms are placed in a multimode cavity subject to a transversal laser drive with pump frequency ω_p . The atoms are fixed at random positions by an external speckle trapping potential over regions inside the cavity, wherein mode functions $g(\mathbf{k}_i, \mathbf{x}_i)$ randomly change sign as a function of the atomic positions, in order to provide frustration, as well as vary in magnitude. The more cavity modes, the better, and in particular the regime where the ratio of the number of cavity modes (M) over the number of atoms (N), $\alpha = M/N$ is kept sizable is a promising regime for glassy behavior [5, 73]. Photons leaking from the cavity with rate κ give rise to additional dissipative dynamics and allow for output detection measurements.

2.2.4 Emergent Photon Glass Phase

The strong light-matter coupling results in a complete imprint of the glass features of the atomic degrees of freedom onto the photons in the cavity. We refer to the resulting state of light as a photon glass highlighting the connection of multimode cavity QED to random lasing media [9, 7].

The photon glass is characterized by a photonic Edwards-Anderson order parameter signaling infinitely long memory in certain temporal two-point correlation function. This implies that a macroscopic number of photons is permanently present in the cavity (extensive scaling with the system size), which are however not occupying a single mode coherently, but rather a continuum of modes. The presence of a continuum of modes at low frequency is underpinned by the slow algebraic decay of the system's correlation functions as shown for the photon correlation function in Fig. 2.5. This is a consequence of the disorder-induced degeneracies. $g^{(2)}(\tau)$ is accessible by detecting the photons that escape the cavity.

2.2.5 Cavity Glass Microscope

The cavity set-up of Fig. 2.6 should allow for unprecedented access to the strongly coupled light-matter phase with disorder. Adapting the input-output formalism of quantum optics [42, 65] to the Keldysh path integral, we provide a comprehensive experimental characterization of the various phases in terms of the cavity output spectrum and the photon correlations $g^{(2)}(\tau)$ in the real time domain.

This continues and completes a program started in [49] of setting up a translation table between the language and observables of quantum optics, and the Keldysh path integral approach. The frequency and time resolved correlations can be determined via fluorescence spectroscopy, cf. Fig. 2.2.5, and the measurement of $g^{(2)}(\tau)$ follows time-resolved detection of cavity output, cf. Fig. 2.5. The fluorescence spectrum shows a characteristic $\frac{1}{\sqrt{\omega}}$ divergence for small frequencies $\omega < \omega_c$. This indicates a macroscopic but incoherent occupation of the cavity as anticipated above: The glass state is not characterized by a single-particle order parameter where a single quantum state is macroscopically occupied, and which would result in (temporal) long range order such as a superradiant condensate. Rather it is characterized by a strong and infrared divergent occupation of a continuum of modes, giving rise to temporal quasi-long range order. This phenomenology is reminiscent of a Kosterlitz-Thouless critical phase realized e.g. in low temperature weakly interacting Bose gases, with the difference that spatial correlations are replaced by temporal correlations.

Finally, the combined measurement of response and correlations enables the quantitative extraction of the effective temperature.

2.3 MULTIMODE OPEN DICKE MODEL

In this section, we explain the model for fixed atoms in an open multimode cavity subject to a transversal laser drive shown in Fig. 2.6. We first write down the explicitly time-dependent Hamilton operator for a level scheme involving two Raman transitions proposed by Dimer et al. [55]. We then transform this Hamiltonian to a frame rotating with the pump frequency. This eliminates the explicit time dependencies in the Hamiltonian at the expense of violating detailed balance between the system and the electromagnetic bath surrounding the cavity. The bath becomes effectively Markovian in accordance with standard approximations of quantum optics. Finally, we eliminate the excited state dynamics to arrive at a multimode Dicke model with tunable couplings and frequencies.

2.3.1 Hamilton Operator

The unitary time evolution of the atom-cavity system with the level scheme of Fig. 2.8 follows the Hamiltonian

$$\hat{H} = \hat{H}_{\text{cav}} + \hat{H}_{\text{at}} + \hat{H}_{\text{int}} + \hat{H}(t)_{\text{pump}}, \quad (2.3.1)$$

which we now explain one-by-one. The cavity contains M photon modes with frequencies ν_i

$$\hat{H}_{\text{cav}} = \sum_{i=1}^M \nu_i a_i^\dagger a_i, \quad (2.3.2)$$

which we later take to be in a relatively narrow frequency range $\nu_i \approx \nu_0$ such that the modes couple with comparable strengths to the detuned internal transition shown in Fig. 2.8. The atom dynamics with frequencies given relative to the lower ground state $|0\rangle$ is

$$\hat{H}_{\text{at}} = \sum_{\ell=1}^N \omega_r |r_\ell\rangle \langle r_\ell| + \omega_s |s_\ell\rangle \langle s_\ell| + \omega_1 |1_\ell\rangle \langle 1_\ell|. \quad (2.3.3)$$

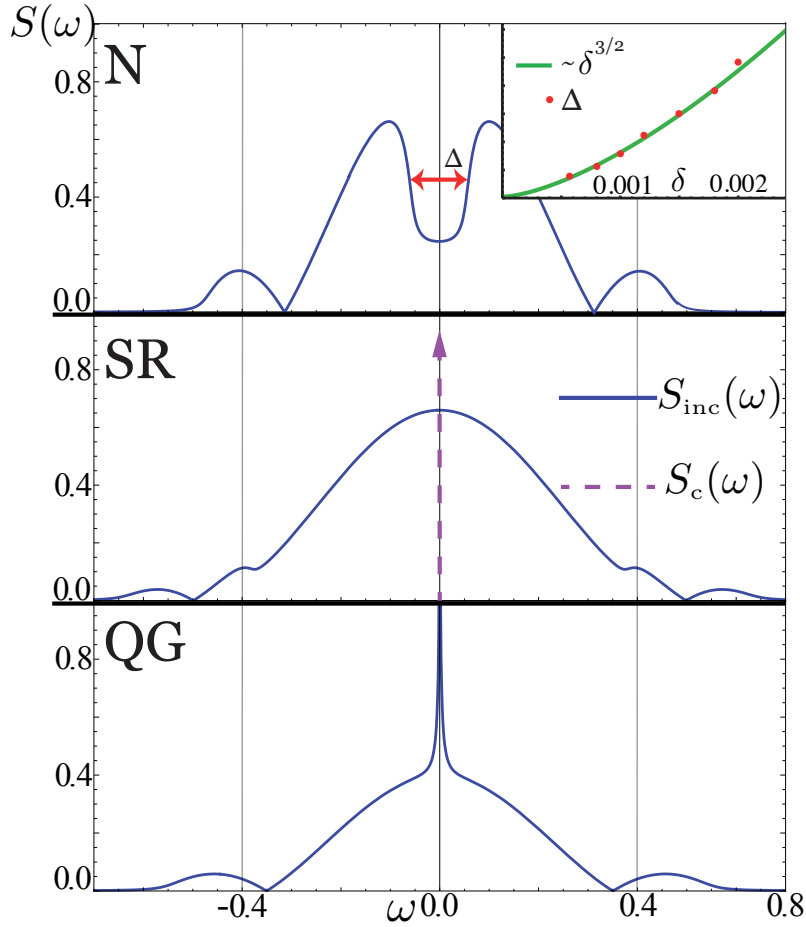


Figure 2.7: Cavity glass microscope output of a typical fluorescence spectrum $S(\omega)$ (not normalized), decomposed in coherent S_c and incoherent part S_{inc} for the three distinct phases in the multimode Dicke model. The parameters J, K are varied, while $\omega_0 = 1, \kappa = 0.1, \omega_z = 0.5$ are kept fixed for each panel. Normal phase, $(J, K) = (0.13, 0.008)$. Central and outer doublets are visible but broadened by the disorder, only the incoherent contribution is non-zero. Superradiant phase, $(J, K) = (0.4, 0.008)$. The central doublets have merged due to the presence of a critical mode at $\omega = 0$. At zero frequency there is a coherent δ -contribution indicated by the arrow (dashed). Glass phase, $(J, K) = (0.13, 0.017)$. There is a characteristic $\frac{1}{\sqrt{\omega}}$ divergence for small $\omega < \omega_c$ due to the non-classical critical modes at zero frequency. The peak at $\omega = 0$ is incoherent and can therefore easily be discriminated from the coherent peak in the middle panel. Scaling of correlations. The inset in the upper panel shows the behavior of the peak distance of $S(\omega)$ in the normal phase when approaching the glass phase. The two peaks approach each other and merge at the glass transition. The distance follows the dominant coherent exponent $\alpha_\delta \propto \delta^{\frac{3}{2}}$, cf. Sec. 2.2.2.

The interaction between the atoms and cavity modes

$$\hat{H}_{\text{int}} = \sum_{\ell=1}^N \sum_{i=1}^M \left(g_r(\mathbf{k}_i, \mathbf{x}_\ell) |r_\ell\rangle \langle 0_\ell| + g_s(\mathbf{k}_i, \mathbf{x}_\ell) |s_\ell\rangle \langle 1_\ell| \right) \hat{a}_i + \text{H.c.} \quad (2.3.4)$$

involves a set of cavity mode functions $g(\mathbf{k}_i, \mathbf{x}_\ell)$ which depend on the wave vector of the cavity mode \mathbf{k}_i and the position of the atom \mathbf{x}_ℓ . The pump term

$$\hat{H}_{\text{pump}}(t) = \sum_{\ell=1}^N \left(e^{-i\omega_{p,r}t} \frac{\Omega_r(\mathbf{k}_r, \mathbf{x}_\ell)}{2} |r_\ell\rangle\langle 1_\ell| + e^{-i\omega_{p,s}t} \frac{\Omega_s(\mathbf{k}_s, \mathbf{x}_\ell)}{2} |s_\ell\rangle\langle 0_\ell| \right) + \text{H.c.} \quad (2.3.5)$$

does not involve photon operators and induces coherent transitions between the excited and ground states as per Fig. 2.8. ω_p is the (optical) frequency of the pump laser. We assume the atoms to be homogeneously pumped from the side so that the mode function of the pump lasers are approximately constant $\Omega_{r,s}(\mathbf{k}_{r,s}, \mathbf{x}_\ell) \approx \Omega_{r,s}$.

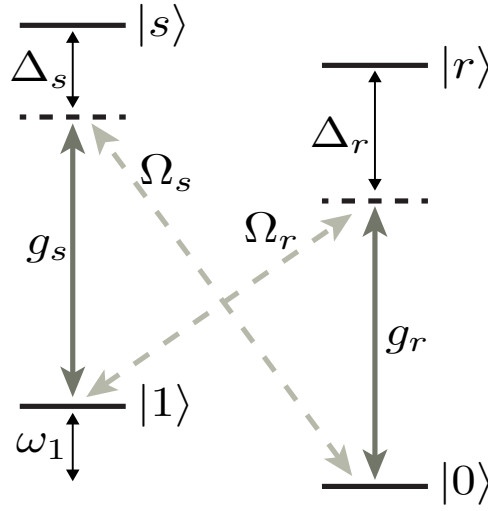


Figure 2.8: Internal level scheme to generate tunable Dicke couplings between the ground state levels $|1\rangle$, $|0\rangle$ and the cavity. Adapted from Dimer et al. [55].

We now transform Eqs. (2.3.1)-(2.3.5) to a frame rotating with the (optical) frequency of the pump laser, mainly to eliminate the explicit time dependence from the pump term Eq. (2.3.5) [55]. The unitary transformation operator is $\hat{U}(t) = \exp(-i\hat{H}_0 t)$ with $\hat{H}_0 = (\omega_{p,s} - \omega'_1) \sum_{i=1}^M \hat{a}_i^\dagger \hat{a}_i + \sum_{\ell=1}^N \left\{ (\omega_{p,r} + \omega'_1) |r_\ell\rangle\langle r_\ell| + \omega_{p,s} |s_\ell\rangle\langle s_\ell| + \omega'_1 |1_\ell\rangle\langle 1_\ell| \right\}$, with ω'_1 a frequency close to ω_1 satisfying $\omega_{p,s} - \omega_{p,r} = 2\omega'_1$ [55]. We then eliminate the excited states in the limit of large detuning Δ to finally obtain the multimode Dicke model

$$\hat{H} = \sum_{i=1}^M \omega_i \hat{a}_i^\dagger \hat{a}_i + \frac{\omega_z}{2} \sum_{l=1}^N \sigma_l^z + \sum_{i,l} \frac{g_{il}}{2} \sigma_l^x (\hat{a}_i^\dagger + \hat{a}_i), \quad (2.3.6)$$

with a correspondence of the effective spin operators in Eq. (2.3.6) to the internal atomic levels

$$\sigma_\ell^z = |1_\ell\rangle\langle 1_\ell| - |0_\ell\rangle\langle 0_\ell|, \quad \sigma_\ell^x = |1_\ell\rangle\langle 0_\ell| + |0_\ell\rangle\langle 1_\ell|. \quad (2.3.7)$$

The couplings and frequencies are tunable:

$$\begin{aligned}\omega_i &= \nu_i - (\omega_{p,s} - \omega'_1) + \frac{\tilde{g}_r^2(\mathbf{k}_i)}{\Delta_r}, & \omega_z &= 2(\omega_1 - \omega'_1), \\ g_{i\ell} &= \frac{g_r(\mathbf{k}_i, \mathbf{x}_\ell)\Omega_r}{2\Delta_r},\end{aligned}\tag{2.3.8}$$

where we assume Eq. (15) of Ref. [55] to be satisfied: $\frac{g_r^2}{\Delta_r} = \frac{g_s^2}{\Delta_s}$ and $\frac{g_r\Omega_r}{\Delta_r} = \frac{g_s\Omega_s}{\Delta_s}$. In particular the effective spin-photon coupling $g_{i\ell}$ can now be tuned sufficiently strong to reach superradiant regimes by changing the amplitude of the pump Ω_r . The effective cavity frequencies receive an additional shift from a mode mixing term $a_i a_j$ with space averaged cavity couplings $\sim \tilde{g}^2/\Delta_r$ from which we only keep the mode-diagonal contribution (for running wave cavity mode functions $\sim e^{i\mathbf{k}_i \cdot \mathbf{x}_\ell}$ this is exact; we do not expect qualitative changes to our results from this approximation).

The multimode Dicke model with internal atomic levels obeys the same Ising-type \mathbb{Z}_2 symmetry, $(a_i, \sigma_i^x) \rightarrow (-a_i, -\sigma_i^x)$, familiar from the single-mode Dicke model [84, 200, 35, 43, 59, 58]. Therefore, there exists a critical coupling strength J_c , such that the ground state of the system spontaneously breaks the \mathbb{Z}_2 symmetry as soon as the average coupling strength

$$J \equiv \frac{1}{N} \sum_{l,m=1}^N \sum_{i=1}^M \frac{g_{il}g_{im}}{4}\tag{2.3.9}$$

exceeds the critical value, $J \geq J_c$. The phase transition from the symmetric to the symmetry broken, superradiant (SR) phase has been well analyzed for the single-mode Dicke model and the essential findings, such as the universal behavior for zero and finite temperature transitions [59, 58] or in the presence of dissipation [144, 149, 49], remain valid also for the multimode case. The superradiant phase is determined by the presence of a photon condensate, i.e. the emergence of a coherent intra-cavity field [15, 16], which is described by a finite expectation value of a photon creation operator $\langle a_C^\dagger \rangle \neq 0$. The superradiant condensate $a_C^\dagger = \sum_i \alpha_i^C a_i^\dagger$, with $\sum_i |\alpha_i^C|^2 = 1$, is a superposition of many cavity modes a_i^\dagger , and its explicit structure depends on the realization of the couplings $\{g_{i\ell}\}$.

2.3.2 Markovian Dissipation

In a cavity QED experiment of the type described in Fig. 2.6, the atoms and photons governed by the Hamiltonian (2.3.6) are additionally coupled to the electromagnetic field outside the cavity. This leads to the additional processes of spontaneously emitted photons into the environment and to cavity photon loss through imperfect mirrors, accurately captured by a Markovian master equation [66, 34]) of the form

$$\partial_t \rho = -i[\hat{H}, \rho] + \mathcal{L}(\rho) \equiv \mathcal{L}_{\text{tot}}(\rho),\tag{2.3.10}$$

where ρ is the density matrix of the atom-photon system, \hat{H} is the Hamiltonian (2.3.6) and \mathcal{L} is a Liouville operator in Lindblad form

$$\mathcal{L}(\rho) = \sum_{\alpha} \kappa_{\alpha} \left(2L_{\alpha}\rho L_{\alpha}^{\dagger} - \{L_{\alpha}^{\dagger}L_{\alpha}, \rho\} \right).\tag{2.3.11}$$

Here, $\{\cdot, \cdot\}$ represents the anti-commutator and the L_α are Lindblad or quantum jump operators. The photon dissipation is described by the Liouvillian

$$\mathcal{L}_{\text{ph}}(\rho) = \sum_{i=1}^M \kappa_i \left(2\hat{a}_i \rho \hat{a}_i^\dagger - \{\hat{a}_i^\dagger \hat{a}_i, \rho\} \right), \quad (2.3.12)$$

where κ_i is the loss rate of a cavity photon from mode (i). Eq. (2.3.12) describes a Markovian loss process that, while being a standard approximation in quantum optics, violates detailed balance between the system and the bath. Formally, it can be derived by starting with a cavity-bath setup in which both are at equilibrium with each other, and performing the transformation into the rotating frame outlined above Eq. (2.3.6) also on the system-bath couplings (see Sec. 2.8.3).

In this work, we consider $\kappa_i < \omega_i, \omega_z$ but of the same order of magnitude. In contrast, the atomic dissipative dynamics are considered to happen by far on the largest time scale, which can be achieved in typical cavity experiments [15, 16]. In a recent open system realization of the single-mode Dicke model [15, 16], spontaneous individual atom-light scattering is suppressed by five orders of magnitude compared to the relevant system time-scales, such that atomic dephasing effectively plays no role [15]. As a result, only global atomic loss is influencing the dynamics, which, however, can be compensated experimentally by steadily increasing the pump intensity or chirping the pump-cavity detuning [15]. We therefore do not consider atomic spontaneous emission in this thesis.

2.3.3 Quenched or Quasi-static Disorder

The glassy physics addressed in this chapter arises when the spatial variation of cavity mode couplings

$$K = \frac{1}{N} \sum_{l,m=1}^N \left(\sum_{i=1}^M \frac{g_{il} g_{im}}{4} \right)^2 - J^2, \quad (2.3.13)$$

is sufficiently large. The specific values of the couplings g_{il} in Eq. (2.3.6) are fluctuating as a function of the atom (l) and photon (i) numbers and depend on the cavity geometry and realization of the random trapping potential (Fig. 2.6). After integrating out the photonic degrees of freedom in Eq. (2.3.6), we obtain the effective atomic Hamiltonian

$$H_{\text{eff}} = \frac{\omega_z}{2} \sum_{l=1}^N \sigma_l^z - \sum_{l,m=1}^N J_{lm} \sigma_l^x \sigma_m^x, \quad (2.3.14)$$

where we introduced the effective atom-atom couplings $J_{lm} = \sum_{i=1}^M \frac{g_{il} g_{im}}{4}$, and at this point neglected the frequency dependence in the atom-atom coupling term in Eq. (2.3.14). This is appropriate for $\omega_i \approx \omega_0$ and ω_0 large compared to other energy scales (in particular, $|(\omega_i - \omega_0)/\omega_0| \ll 1$). In order to solve the effective Hamiltonian (2.3.14), it is sufficient to know the distribution of the couplings J_{lm} , which itself is a sum over M random variables. For a large number of modes ($M \rightarrow \infty$), this distribution becomes Gaussian, according to the central limit theorem, with expectation value J and variance K, as defined in Eqs. (2.3.9), (2.3.13), respectively.

The variables J_{lm} can be seen as spatially fluctuating but temporally static variables, connecting all atoms with each other. This may be seen as a coupling to a bath with random variables J_{lm} , which vary on time scales τ_Q much larger than the typical time scales of the system τ_S only. The dynamics of the bath is then frozen on time scales of the

system, and the bath is denoted as quasi-static or quenched [20]. This type of bath is in a regime opposite to a Markovian bath, where the dynamics of the bath happens on much faster time scales τ_M than for the system, $\tau_M \ll \tau_S$ [66, 34]. We have summarized basic properties of these baths in Sec. 2.8.

2.4 KELDYSH PATH INTEGRAL APPROACH

In this section, we introduce the Keldysh formalism [100, 99, 49] and derive the set of self-consistency equations for the atoms and photons from which all our results can be extracted. We first formulate the open multimode Dicke model Eqs. (2.3.6, 2.3.12) as an equivalent Keldysh action that includes the non-unitary time evolution induced by cavity decay. In the Keldysh approach, one additionally benefits from the fact that the partition function

$$Z = \text{Tr}(\rho(t)) = 1 \quad (2.4.1)$$

is normalized to unity, independent of the specific realization of disorder, and we perform the disorder average directly on the partition function. We then integrate out the photons (carefully keeping track of their correlations, as explained below) and derive a set of saddle-point equations for frequency-dependent correlation functions which can be solved.

2.4.1 Multimode Dicke Action

To describe the photon dynamics, one starts from an action for the coupled system of cavity photons and a Markovian bath. Then the bath variables are integrated out in Born-Markov and rotating wave approximations. The resulting Markovian dissipative action for the photonic degrees of freedom on the (\pm) -contour reads

$$\begin{aligned} S_{\text{ph}} = & \sum_j \int_{-\infty}^{\infty} dt \left(a_{j+}^* (i\partial_t - \omega_j) a_{j+} - (a_{j-}^* (i\partial_t - \omega_j) a_{j-} \right. \\ & \left. - i\kappa [2a_{j+} a_{j-}^* - (a_{j+}^* a_{j+} + a_{j-}^* a_{j-})] \right). \end{aligned} \quad (2.4.2)$$

Here, the creation and annihilation operators have been replaced by time-dependent complex fields. The structure of the master equation (2.3.10) is clearly reflected in the action on the (\pm) -contour in Eq. (2.4.2). The first line corresponds to the Hamiltonian part of the dynamics, with a relative minus sign between $(+)$ and $(-)$ contour stemming from the commutator. The second line displays the characteristic form of the dissipative part in Lindblad form.

For practical calculations, it is more convenient to switch from a (\pm) -representation of the path integral to the so-called Keldysh or RAK representation. In the latter, the fields on the (\pm) -contour are transformed to “classical” $a_{j,c} = (a_{j+} + a_{j-})/\sqrt{2}$ and “quantum” fields $a_{j,q} = (a_{j+} - a_{j-})/\sqrt{2}$, where the labeling of these fields indicates that $a_{j,c}$ can acquire a finite expectation value, while the expectation value of $a_{j,q}$ is always zero. After a Fourier transformation to frequency space, $a_i(\omega) = \int dt a_i(t) e^{-i\omega t}$, the photonic action in Keldysh representation is obtained as

$$S_{\text{ph}} = \int_{j,\omega} (a_{j,c}^*, a_{j,q}^*) \begin{pmatrix} 0 & D_j^R(\omega) \\ D_j^A(\omega) & D_j^K(\omega) \end{pmatrix} \begin{pmatrix} a_{j,c} \\ a_{j,q} \end{pmatrix}, \quad (2.4.3)$$

where we used the abbreviation $\int_{j,\omega} = \sum_{j=1}^M \int \frac{d\omega}{2\pi}$. The integral kernel of Eq. (2.4.3) is the inverse Green's function in Keldysh space with the inverse retarded/advanced Green's function

$$D_j^{\text{R/A}}(\omega) = [G_j^{\text{R/A}}]^{-1}(\omega) = \omega \pm i\kappa_j - \omega_j \quad (2.4.4)$$

and the Keldysh component of the inverse Green's function

$$D_j^K(\omega) = 2i\kappa_j. \quad (2.4.5)$$

From now on, we will focus on the case where the variation in the photon parameters is much smaller than all other energy scales of this problem and consider only a single photon frequency ω_0 and photon loss rate κ , i.e. $|\kappa - \kappa_j| \ll \kappa$ and $|\omega_0 - \omega_j| \ll \omega_0$ for all photon modes (j). As a result all photon Green's functions are identical with $\kappa_j = \kappa$ and $\omega_j = \omega_0$. The Green's function in Keldysh space takes the form

$$\mathcal{G}(\omega) = \begin{pmatrix} G^K(\omega) & G^R(\omega) \\ G^A(\omega) & 0 \end{pmatrix} = \begin{pmatrix} 0 & D^R(\omega) \\ D^A(\omega) & D^K(\omega) \end{pmatrix}^{-1}, \quad (2.4.6)$$

where we already identified retarded/advanced Green's function $G^R(\omega)$ in Eq. (2.4.4). The Keldysh component of the Green's function is obtained by performing the inversion (2.4.6) as

$$G^K(\omega) = -G^R(\omega)D^K(\omega)G^A(\omega). \quad (2.4.7)$$

The retarded Green's function encodes the response of the system to external perturbations and its anti-hermitian part is proportional to the spectral density

$$\mathcal{A}(\omega) = i(G^R(\omega) - G^A(\omega)), \quad (2.4.8)$$

since $G^A(\omega) = [G^R(\omega)]^\dagger$. The retarded Green's function $G^R(\omega)$ and the Keldysh Green's function $G^K(\omega)$ constitute the basic players in a non-equilibrium path integral description, determining the system's response and correlations. For a more detailed discussion of a Keldysh path integral description of cavity photons, we refer the reader to [49].

The atomic sector of the Dicke Hamiltonian (2.3.6) can be mapped to an action in terms of real fields ϕ_l , as long as the physically relevant dynamics happens on frequencies below ω_z [174]. The ϕ_l obey the non-linear constraint

$$\delta(\phi_1^2(t) - 1) = \int \mathcal{D}\lambda_1(t) e^{i\lambda_1(t)(\phi_1^2(t)-1)}, \quad (2.4.9)$$

where $\lambda_1(t)$ are Lagrange multipliers, in order to represent Ising spin variables (see Ref. [49] for further explanation). As a result, we can apply the following mapping to Eq. (2.3.6)

$$\sigma_1^x(t) \longrightarrow \phi_1(t), \quad (2.4.10)$$

$$\sigma_1^z(t) \longrightarrow \frac{2}{\omega_z^2} (\partial_t \phi_1(t))^2 - 1, \quad (2.4.11)$$

On the (\pm) -contour, we then obtain

$$S_{\text{at}} = \frac{1}{\omega_z} \int_{1,t} (\partial_t \phi_{1+})^2 - (\partial_t \phi_{1-})^2, \quad (2.4.12)$$

subject to the non-linear constraint

$$S_{\text{const}} = \frac{1}{\omega_z} \int_{1,t} \lambda_{1+} (\phi_{1+}^2 - 1) - \lambda_{1-} (\phi_{1-}^2 - 1). \quad (2.4.13)$$

The atom-photon coupling reads

$$S_{\text{coup}} = \int_{t,i,l} \frac{g_{il}}{2} \left(\phi_{1+} (a_{i+}^* + a_{i+}) - \phi_{1-} (a_{i-}^* + a_{i-}) \right). \quad (2.4.14)$$

Transforming to the Keldysh basis and frequency space, the atomic propagator becomes

$$S_{\text{at}} = \frac{1}{\omega_z} \int_{\omega,l} (\phi_{c,l}, \phi_{q,l}) D_{\text{at}}(\omega) \begin{pmatrix} \phi_{c,l} \\ \phi_{q,l} \end{pmatrix} + \frac{1}{\omega_z} \int_{\omega,l} \lambda_{q,l}, \quad (2.4.15)$$

with

$$D_{\text{at}}(\omega) = \begin{pmatrix} \lambda_{q,l} & \lambda_{c,l} - (\omega + i\eta)^2 \\ \lambda_{c,l} - (\omega - i\eta)^2 & \lambda_{q,l} \end{pmatrix}. \quad (2.4.16)$$

Here, $\eta \rightarrow 0^+$ plays the role of a regulator that ensures causality for the retarded/advanced Green's functions. For the atom-photon coupling in the Keldysh basis, we get

$$S_{\text{coup}} = \int_{\omega,l,j} \frac{g_{il}}{2} \left((\phi_{c,l}, \phi_{q,l}) \sigma^x \begin{pmatrix} a_{c,l} \\ a_{q,l} \end{pmatrix} + (a_{c,l}^*, a_{q,l}^*) \sigma^x \begin{pmatrix} \phi_{c,l} \\ \phi_{q,l} \end{pmatrix} \right). \quad (2.4.17)$$

For the atomic fields, it is useful in the following to introduce the Keldysh vector $\Phi_1(\omega) = \begin{pmatrix} \phi_{c,l}(\omega) \\ \phi_{q,l}(\omega) \end{pmatrix}$, which will simplify the notation in the following.

The Keldysh action for the open multimode Dicke model is then obtained as the sum of Eqs. (2.4.3, 2.4.15, 2.4.17)

$$S \left[\{a^\dagger, a, \phi, \lambda\} \right] = S_{\text{ph}} + S_{\text{at}} + S_{\text{coup}}. \quad (2.4.18)$$

2.4.2 Calculation Procedure

We now explain how we solve the Keldysh field theory described by Eq. (2.4.18). The calculation proceeds in three steps:

1. Integration of the photon modes: This step can be performed exactly via Gaussian integration, since the action (2.4.18) is quadratic in the photon fields. Note that this does not mean that we discard the photon dynamics from our analysis. To also keep track of the photonic observables, we modify the bare inverse photon propagator, Eq. (2.4.3), by adding (two-particle) source fields μ according to

$$D_{\text{ph}}(\omega) \rightarrow D_{\text{ph}}(\omega) + \mu(\omega), \quad \text{with } \mu = \begin{pmatrix} \mu^{\text{cc}} & \mu^{\text{cq}} \\ \mu^{\text{qc}} & \mu^{\text{qq}} \end{pmatrix}. \quad (2.4.19)$$

Atoms		Photons
$\frac{\psi_c}{\sqrt{2}} = \overline{\langle \sigma_1^x \rangle}$ $\psi_q(t) = 0$	$Q_{cc}(t) = Q^K(t) = -i \overline{\langle \{ \sigma_1^x(t), \sigma_1^x \} \rangle}$	$G_{cc}(t) = G^K(t) = -i \overline{\langle \{ a_m(t), a_m^\dagger \} \rangle}$
	$Q_{cq}(t) = Q^R(t) = -i \Theta_t \overline{\langle [\sigma_1^x(t), \sigma_1^x] \rangle}$	$G_{cq}(t) = G^R(t) = -i \Theta_t \overline{\langle [a_m(t), a_m^\dagger] \rangle}$
	$Q_{qc}(t) = Q^A(t) = (Q^R(t))^\dagger$	$G_{qc}(t) = G^A(t) = (G^R(t))^\dagger$
	$Q_{qq}(t) = 0$	$G_{qq}(t) = 0$

Table 2.1: Translation table for the atomic order parameter and Green's functions, from now on labeled with Q, and the intra-cavity photon Green's function, labeled with G. For simplicity, we have implicitly assumed time translational invariance.

The photon Green's functions are then obtained via functional variation of the partition function with respect to the source fields

$$G^{R/A/K}(\omega) = \frac{\delta}{\delta \mu^{qc/cq/cc}(\omega)} Z \Big|_{\mu=0}. \quad (2.4.20)$$

The resulting action is a sum of the bare atomic part (2.4.15) and an effective atom-atom interaction

$$S_{\text{at-at}} = - \int_{\omega} \sum_{l,m} J_{lm} \Phi_l^T(-\omega) \Lambda(\omega) \Phi_m(\omega), \quad (2.4.21)$$

with atom-atom coupling constants J_{lm} defined in (2.3.14) and the frequency dependent coupling

$$\Lambda(\omega) = \frac{1}{2} \sigma^x (G_0(\omega) + G_0^T(-\omega)) \sigma^x, \quad (2.4.22)$$

which is the bare photon Green's function G_0 after symmetrization respecting the real nature of the Ising fields Φ_l . We note that the information of the photonic coupling to the Markovian bath is encoded in $\Lambda(\omega)$.

2. Disorder average: The coupling parameters J_{lm} are considered to be Gaussian distributed and the corresponding distribution function is determined by the expectation value and covariance of the parameters J_{lm}

$$\overline{J_{lm}} = \frac{J}{N}, \quad (2.4.23)$$

$$\overline{\delta J_{lm} \delta J_{l'm'}} = \frac{K}{N} (\delta_{ll'} \delta_{mm'} + \delta_{lm'} \delta_{ml'}) \equiv \hat{K}_{lml'm'}, \quad (2.4.24)$$

where the line denotes the disorder average and $\delta J_{lm} = J_{lm} - \overline{J_{lm}}$ represents the variation from the mean value. The disorder averaged partition function can be expressed as

$$\overline{Z} = \int \mathcal{D}(\{\Phi, \lambda, J\}) e^{i(S_{\text{at}} + S_{\text{at-at}} + S_{\text{dis}})}, \quad (2.4.25)$$

with the disorder ‘‘action’’

$$S_{\text{dis}} = \frac{i}{2} \sum_{l,m,l',m'} (J_{lm} - \overline{J_{lm}}) \hat{K}_{lml'm'}^{-1} (J_{l'm'} - \overline{J_{l'm'}}), \quad (2.4.26)$$

describing a temporally frozen bath with variables J_{lm} . Performing the disorder average, i.e. integrating out the variables J_{lm} in the action (2.4.25) replaces the parameters $J_{lm} \rightarrow J/N$ in (2.4.21) by their mean value. Furthermore, the variance K introduces a quartic interaction term for the atomic Ising variables which is long-range in space

$$S_{\text{at-4}} = \frac{iK}{N} \int_{\omega, \omega'} \sum_{l,m} (\Phi_l \Lambda \Phi_m)(\omega) (\Phi_l \Lambda \Phi_m)(\omega'), \quad (2.4.27)$$

with the shortcut $(\Phi_l \Lambda \Phi_m)(\omega) \equiv \Phi_l^T(\omega) \Lambda(\omega) \Phi_m(\omega)$.

3. Collective variables: Atomic order parameter and Green's function: To decouple the spatially non-local terms in (2.4.21) and (2.4.27), we introduce the Hubbard-Stratonovich fields ψ_α and $Q_{\alpha\alpha'}$ with $\alpha, \alpha' = c, q$, which represent the atomic order parameter

$$\psi_\alpha(\omega) = \frac{1}{N} \sum_l \langle \overline{\phi_{\alpha,l}(\omega)} \rangle \quad (2.4.28)$$

and average atomic Green's function

$$Q_{\alpha\alpha'}(\omega, \omega') = \frac{1}{N} \sum_l \langle \overline{\phi_{\alpha,l}(\omega) \phi_{\alpha',l}(\omega')} \rangle. \quad (2.4.29)$$

Now, the action is quadratic in the original atomic fields ϕ_ℓ , and so these can be integrated out. The resulting action has a global prefactor N and we will perform a saddle-point approximation which becomes exact in the thermodynamic limit and upon neglecting fluctuations of the Lagrange multiplier. We replace the fluctuating Lagrange multipliers $\lambda_l(t)$ by their saddle-point value $\lambda_l(t) = \lambda$. In the steady state, the atomic observables become time-translational invariant which restricts the frequency dependence of the fields to

$$\psi_\alpha(\omega) = 2\pi\delta(\omega)\psi_\alpha, \quad (2.4.30)$$

$$Q_{\alpha\alpha'}(\omega, \omega') = 2\pi\delta(\omega + \omega')Q_{\alpha\alpha'}(\omega). \quad (2.4.31)$$

2.4.3 Saddle-point Action and Self-consistency Equations

The saddle-point action is given by the expression

$$\begin{aligned} \mathcal{S}/N &= -\frac{2\lambda_q}{\omega_z} + \int_{\omega} \Psi^T(-\omega) \left[J\Lambda(\omega) - J^2\Lambda(\omega)\tilde{G}(\omega)\Lambda(\omega) \right] \Psi(\omega) \\ &\quad - \frac{i}{2} \text{Tr} \left[\ln \tilde{G}(\omega) \right] + iK \text{Tr} \left[\Lambda Q \Lambda Q \right](\omega), \end{aligned} \quad (2.4.32)$$

with the ‘‘Green's function’’

$$\tilde{G}(\omega) = \left(D_{\text{at}}(\omega) - 2K\Lambda(\omega)Q(\omega)\Lambda(\omega) \right) \quad (2.4.33)$$

and the field $\Psi^T = (\psi_c, \psi_q)$. The matrices Λ, \tilde{G} and Q in Eq. (2.4.32) possess Keldysh structure, i.e. they are frequency dependent triangular matrices with retarded, advanced and Keldysh components. The matrix Λ contains the photon frequencies ω_0 , the decay rate κ , and also depends on the photon Lagrange multiplier μ , so that all photon correlations can be extracted from Eq. (2.4.32).

Atomic Sector

In order to find a closed expression for the macroscopic fields $\{\Phi, Q\}$ and to determine the saddle-point value for the Lagrange multiplier λ , we have to evaluate the saddle-point equations

$$\frac{\delta S}{\delta X} \stackrel{!}{=} 0, \quad \text{with } X = Q_{\alpha\alpha'}, \psi_\alpha, \lambda_\alpha, \quad \alpha = c, q. \quad (2.4.34)$$

In stationary state, $\lambda_q = \psi_q = Q_{qq} = 0$ by causality and we set $\lambda_c = \lambda$ and $\psi_c = \psi$ for convenience.

The saddle-point equation for λ_q expresses the constraint

$$2 = \int_\omega iQ^K(\omega) = iQ^K(t=0) = 2 \frac{1}{N} \sum_{l=1}^N \langle (\sigma_l^x)^2 \rangle, \quad (2.4.35)$$

which has been reduced to a soft constraint, present on average with respect to (1), compared to the original hard constraint, $(\sigma_l^x)^2 = 1$ for each (1) individually.

In the superradiant phase and in the glass phase, the spin attain locally “frozen” configurations. The correlation time of the system becomes infinite, expressed via a non-zero value of the Edwards-Anderson order parameter

$$q_{EA} := \lim_{\tau \rightarrow \infty} \frac{1}{N} \sum_{l=1}^N \langle \sigma_l^x(\tau) \sigma_l^x(0) \rangle. \quad (2.4.36)$$

As a consequence, the correlation function $Q^K(\omega)$ is the sum of a regular part, describing the short time correlations and a δ -function at $\omega = 0$, caused by the infinite correlation time. We decompose the correlation function according to

$$Q^K(\omega) = 4i\pi q_{EA} \delta(\omega) + Q_{reg}^K(\omega), \quad (2.4.37)$$

with the Edwards-Anderson order parameter q_{EA} , being defined in Eq. (2.4.36) and a regular contribution Q_{reg}^K . In the literature [46, 108], this decomposition is referred to as modified fluctuation dissipation relation (FDR) as also discussed in Sec. 2.8. The saddle-point equations for atomic response function and the regular part of the Keldysh function are

$$Q^R(\omega) = \left(\frac{2(\lambda - \omega^2)}{\omega_z} - 4K (\Lambda^R(\omega))^2 Q^R(\omega) \right)^{-1} \quad (2.4.38)$$

and

$$Q_{reg}^K(\omega) = \frac{4K |Q^R|^2 \Lambda^K (Q^A \Lambda^A + Q^R \Lambda^R)}{1 - 4K |Q^R \Lambda^R|^2}. \quad (2.4.39)$$

Eqs. (2.4.35), (2.4.38), (2.4.39) form a closed set of non-linear equations, describing the physics of the atomic subsystem in the thermodynamic limit, which will be discussed in Sec. 2.5.

Photonic Sector

The photon response G^R and correlation function G^K are determined via functional derivatives of the partition function \mathcal{Z} with respect to the source fields μ , as described in (2.4.19) and (2.4.20). The saddle-point for the partition function is

$$\mathcal{Z} = e^{i\mathcal{S}} \times Z_{\text{ph}}^{(0)}, \quad (2.4.40)$$

with the action \mathcal{S} from Eq. (2.4.32) and the bare photon partition function $Z_{\text{ph}}^{(0)}$.

In the Dicke model, the photon occupation n_i is not a conserved quantity, such that anomalous expectation values $\langle a^2 \rangle \neq 0$ will become important. This has to be taken into account by introducing a Nambu representation, where the photon Green's functions become 2×2 matrices, see Sec. 2.7. Generalizing the source fields μ to include normal and anomalous contributions, and evaluating the functional derivatives with respect to these fields, results in the inverse photon response function

$$D_{2 \times 2}^R(\omega) = \quad (2.4.41)$$

$$\begin{pmatrix} \omega + i\kappa - \omega_0 + \Sigma^R(\omega) & \Sigma^R(\omega) \\ (\Sigma^R(-\omega))^* & -\omega - i\kappa - \omega_0 + (\Sigma^R(-\omega))^* \end{pmatrix}. \quad (2.4.42)$$

Here, the subscript 2×2 indicates Nambu representation and

$$\Sigma^R(\omega) = (\Sigma^R(-\omega))^* = \frac{1}{2\Lambda^R(\omega)} \left(\frac{\omega_z D_{\text{at}}^R(\omega)}{2(\omega^2 - \lambda)} - 1 \right) \quad (2.4.43)$$

is the self-energy, resulting from the atom-photon interaction. The Keldysh component of the inverse Green's function is

$$D_{2 \times 2}^K(\omega) = \begin{pmatrix} 2i\kappa + \Sigma^K(\omega) & \Sigma^K(\omega) \\ -(\Sigma^K(\omega))^* & 2i\kappa - (\Sigma^K(\omega))^* \end{pmatrix} \quad (2.4.44)$$

with the self-energy

$$\Sigma^K(\omega) = -(\Sigma^K(\omega))^* = \frac{Q^K(\omega)}{4\text{Re}(Q^R(\omega)\Lambda^R(\omega))}. \quad (2.4.45)$$

In the Dicke model, the natural choice of representation for the photon degrees of freedom is the x-p basis, i.e. in terms of the real fields $x = \frac{1}{\sqrt{2}}(a^* + a)$, $p = \frac{1}{\sqrt{2i}}(a^* - a)$, since the atom-photon interaction couples the photonic x-operator to the atoms. In this basis, the self-energy gives only a contribution to the x-x component of the inverse Green's function, and the inverse response function reads

$$D_{\text{xp}}^R(\omega) = \begin{pmatrix} 2\Sigma^R(\omega) - \omega_0 & \kappa - i\omega \\ -\kappa + i\omega & -\omega_0 \end{pmatrix}. \quad (2.4.46)$$

In the limit of vanishing disorder $K \rightarrow 0$, the self-energy approaches the value $\Sigma^R(\omega) = \frac{J\omega_z}{2(\omega^2 - \lambda)}$, reproducing the result for the single mode Dicke model [49, 59, 58].

2.5 RESULTS

We now present our predictions from solving the atomic saddle-point equations Eqs. (2.4.35), (2.4.38), (2.4.39) and then extracting the photonics correlations using Eqs. (2.4.42)-(2.4.46), in the same order as in the Key Results Section 2.2. In the subsection Cavity Glass Microscope, we present signatures for standard experimental observables of cavity QED by adapting the input-output formalism to the Keldysh path integral.

2.5.1 Non-equilibrium Steady State Phase Diagram

The phases in the multimode Dicke model shown in Fig. 2.1 can be distinguished by the two order parameters, namely the Edwards-Anderson order parameters q_{EA} in Eq. (2.4.36), indicating an infinite correlation time τ and the ferromagnetic order parameter ψ defined (Eq. (2.4.30)), indicating a global magnetization:

Normal	$q_{\text{EA}} = 0$	$\psi = 0$
SR	$q_{\text{EA}} \neq 0$	$\psi \neq 0$
QG	$q_{\text{EA}} \neq 0$	$\psi = 0$

In the normal phase, the Edwards-Anderson parameter q_{EA} and the ferromagnetic order parameter ψ are both zero and Eq. (2.4.35) implicitly determines the numerical value of the Lagrange parameter λ_{N} . In contrast, in the superradiant phase $\psi \neq 0$, and the Lagrange parameter can be determined analytically to be

$$\lambda_{\text{SR}} = \frac{\omega_z \omega_0}{\omega_0^2 + \kappa^2} \left(J + \frac{K}{J} \right). \quad (2.5.1)$$

In the quantum glass phase the Lagrange parameter is pinned to

$$\lambda_{\text{QG}} = \frac{\omega_z \omega_0}{\omega_0^2 + \kappa^2} \sqrt{K}. \quad (2.5.2)$$

The normal phase is characterized by a vanishing Edwards-Anderson order parameter, and the corresponding Lagrange multiplier λ_{N} is determined via the integral

$$0 = 2 - i \int_{\omega} Q_{\text{reg}}^{\text{K}}(\omega) \Big|_{\lambda=\lambda_{\text{N}}}. \quad (2.5.3)$$

The normal-SR phase border is located at the line for which $\lambda_{\text{N}} = \lambda_{\text{SR}}$, while the normal-QG transition happens at $\lambda_{\text{N}} = \lambda_{\text{QG}}$. In the same way, the transition between superradiant phase and quantum glass phase happens when ψ vanishes for finite $q_{\text{EA}} \neq 0$. This is the case for

$$\lambda_{\text{SR}} = \lambda_{\text{QG}} \Leftrightarrow K = J^2. \quad (2.5.4)$$

The phase diagram for the open system for different values of the photon dissipation κ is shown in Fig. 2.1. As can be seen from this figure, the qualitative features of the zero temperature phase diagram [190] are preserved in the presence of dissipation. However, with increasing κ , the phase boundaries between normal and SR, QG phase are shifted to larger values of J , K respectively, while the QG-SR transition is still located at the values for which $J^2 = K$ as for the zero temperature equilibrium case. Finite dissipation neither

Analytic expressions	SR to QG	Normal to QG
$Q^R(\omega) = Z_\delta \left((\omega + i\gamma_\delta)^2 - \alpha_\delta^2 \right)^{-1}$ $\alpha_\delta = \frac{\sqrt{2}(\omega_0^2 + \kappa^2)}{8\sqrt{K^3} \kappa} \times$ $\gamma_\delta = \frac{\omega_0^2 + \kappa^2}{16K^2 \kappa} \times$ $Z_\delta = \frac{\omega_0(\omega_0^2 + \kappa^2)}{8\sqrt{K^5} \kappa^2} \times$	$\delta^{\frac{3}{2}}$ δ^2 δ^3	$\left \frac{\delta}{\log(\delta)} \right ^{\frac{3}{2}}$ $\left \frac{\delta}{\log(\delta)} \right ^2$ $\left \frac{\delta}{\log(\delta)} \right ^3$

Table 2.2: Atomic spectral response and scaling behavior approaching the glass transition in two different ways. The normal to glass transition shows logarithmic corrections compared to the SR to QG transition. The logarithmic scaling correction is a typical feature of the glass transition and has also been found for $T = 0$ and finite temperature glass transitions in equilibrium [203, 134]. We see that the lifetime of the excitations γ_δ scales differently from the excitation energy α_δ , which indicates a strong competition of the reversible quantum dynamics and the classical relaxational dynamics. Although the inverse lifetime scales faster to zero than the excitation energy, there is no point before the transition, where one of these quantities becomes exactly zero as it was the case for the superradiance transition. The described behavior at the glass transition means that there is no purely relaxational low energy theory which is able to describe the dynamics close to the transition. It does not fall into the Halperin-Hohenberg classification of dissipative dynamical systems, but belongs to the universality class of dissipative spin glasses [165, 46, 45, 44].

favors the QG nor the SR phase and as a result, the competition between disorder and order is not influenced by the dissipative dynamics. The line at $K = 0$, i.e. zero disorder, describes the normal-SR transition for the single mode Dicke model, which is known to be located at $J_c = \frac{\omega_0^2 + \kappa^2}{4\omega_0} \omega_z$ [49, 59, 58]. This result is exactly reproduced within our approach.

2.5.2 Dissipative Spectral Properties and Universality Class

The atomic excitation spectrum and the influence of the system-bath coupling on the atomic dynamics are encoded in the retarded atomic Green's function, which is identical to the atomic linear susceptibility, $Q^R(\omega) = \chi^{(1)}(\omega)$. It describes the response of the atomic system to a weak perturbation as, for instance, the coupling to a weak coherent light field (see Sec. 2.9.1), and its imaginary part determines the atomic spectral response

$$\mathcal{A}(\omega) = -2\text{Im} (Q^R(\omega)), \quad (2.5.5)$$

which can be measured directly via radio-frequency spectroscopy [188, 82]. The spectral response \mathcal{A} for the normal and SR phase (the regular part for the latter) is shown in Fig. 2.9. In order to describe the low frequency behavior of the atomic spectrum, we decompose it into a regular and singular part, where the singular part captures the critical mode of the SR phase in terms of a δ -function at zero frequency, which is absent in the normal phase. The regular part of the spectrum has the same structure for the normal and superradiant

phase, and a derivative expansion of the inverse Green's function yields the low frequency response function

$$Q^R(\omega) = Z_\delta \left((\omega + i\gamma_\delta)^2 - \alpha_\delta^2 \right)^{-1} \quad (2.5.6)$$

with the analytic expressions for the coefficients given in Table 2.2. This is the Green's function of a damped harmonic oscillator with characteristic frequency $\omega = \alpha_\delta$ and damping γ_δ , which is described by classical relaxational dynamics and correctly determines the atomic spectral response for frequencies $\omega < \|\alpha_\delta - i\gamma_\delta\|$ smaller than the pole. The index δ in Eq. (2.5.6) indicates that the parameters scale with the distance to the glass transition

$$\delta = K_c - K, \quad (2.5.7)$$

which happens at $K = K_c$ ($\delta > 0$ in SR and normal phases). Transforming the response function to the time-domain,

$$Q^R(t) = Z_\delta e^{-\gamma_\delta t} \cos(\alpha_\delta t), \quad (2.5.8)$$

which describes an excitation of the system with inverse lifetime $\gamma_\delta = 1/\tau_\delta$, energy α_δ and quasi-particle residuum Z_δ . For frequencies $\omega < \alpha_\delta$, the spectral response is determined by the imaginary part of Eq. (2.5.6), yielding

$$\mathcal{A}(\omega) \approx \frac{Z_\delta \gamma_\delta \omega}{\alpha_\delta^4} = \frac{2\kappa}{\omega_0 \sqrt{K}\delta} \omega. \quad (2.5.9)$$

This linear behavior is completely determined by parameters of the quenched and the Markovian bath and vanishes for $\kappa \rightarrow 0$, resulting in a gap in the spectral weight for the zero temperature equilibrium case, as discussed in [190]. For $\omega > \alpha_\delta$, i.e. for ω larger than the gap, the atomic response function develops a non-analytic square root behavior

$$\mathcal{A}(\omega) \propto \sqrt{\omega - \alpha_\delta}, \quad (2.5.10)$$

resulting from the quadratic form in Eq. (2.4.38). The scaling of the excitation gap α_δ and the ratio $\frac{Z_\delta \gamma_\delta}{\alpha_\delta^4}$ can be obtained directly from the atomic spectral response, as illustrated in Fig. 2.9, lower panel. At the glass transition, the gap vanishes, such that the square root behavior starts from $\omega = 0$.

In Table 2.2, we compare the scaling behavior of the atomic spectral response close to the normal-QG transition versus SR-QG transition lines. At the glass transition, Z_δ , γ_δ and α_δ vanish, which for the latter two results in zero energy excitations with infinite lifetime and therefore infinite correlation times. The vanishing of the residuum Z_δ indicates that the discrete poles of the system, representing quasi-particles with weight Z , transform into a continuum represented by a branch cut in the complex plane as illustrated in Fig. 2.10. As a consequence, a derivative expansion of the inverse propagator is no longer possible in the quantum glass phase.

When approaching the glass phase, the frequency interval which is described by classical relaxational dynamics (i.e. $[0, \alpha_\delta]$) shrinks and vanishes completely at the transition, where the system becomes quantum critical. The linear scaling of $\mathcal{A}(\omega)$ in combination with the closing of the spectral gap is taken in thermal equilibrium as the defining property of a quantum glass. However, for a general non-equilibrium setting, the closing of the spectral gap is only a necessary but not a sufficient condition for the glass phase. The unique property of the glass transition in a non-equilibrium setting is the emergence of a critical continuum at zero frequency, which leads to the closing of the gap of the retarded Green's function (distinct from the spectral gap). From the structure of the low frequency response function, Eq. (2.5.6), we see that closing the spectral gap and a linear behavior of the

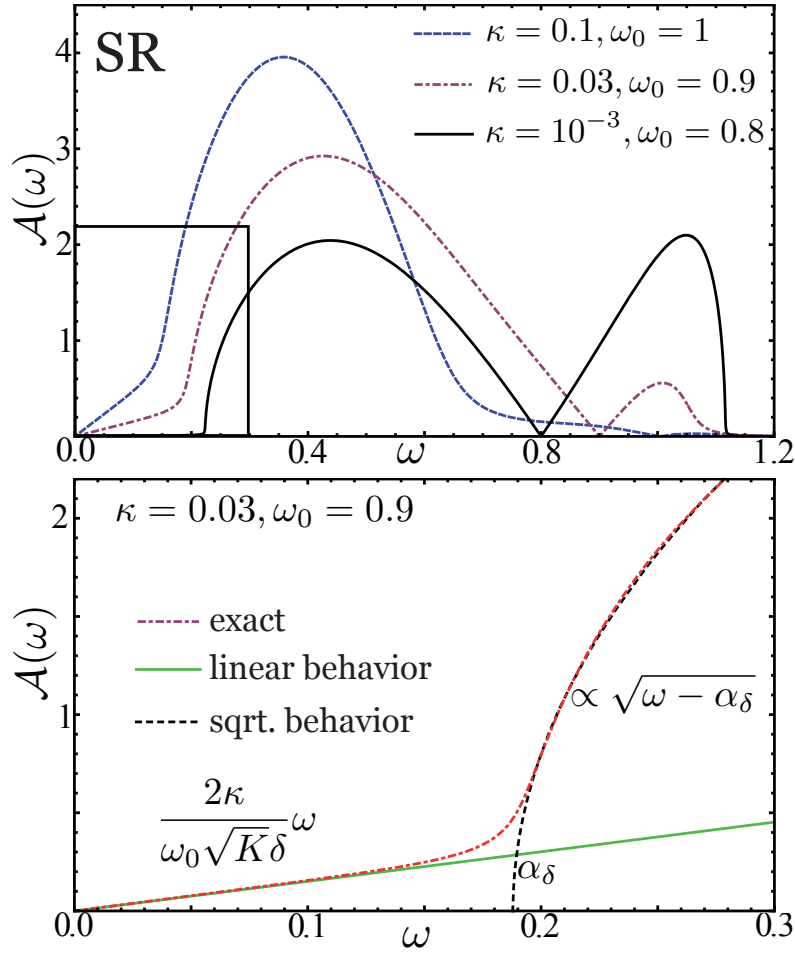


Figure 2.9: Regular part of the spectral density $\mathcal{A}(\omega)$ in the superradiant phase for parameters $K = 0.05$ and $J = 0.4$ and varying κ and ω_0 . For small frequencies $\omega < \alpha_\delta$ the spectral density is linear in ω and κ and behaves as a square root for intermediate frequencies $\omega > \alpha_\delta$. For the non-dissipative case ($\kappa \rightarrow 0$), the spectral weight develops a gap at low frequencies, which is indicated for $\kappa = 10^{-3}$ (solid line). The lower panel depicts the low frequency behavior of \mathcal{A} (red, dash-dotted line) for values $\kappa = 0.03$ and $\omega_0 = 0.9$. The green (full) and the black (dashed) line indicate the linear, square root behavior, respectively. Approaching the glass transition, α_δ scales to zero $\propto \delta^{\frac{3}{2}}$.

spectral density is a non-trivial (and glass) signature only for a system where time-reversal symmetry is preserved, i.e. $\gamma = 0$. On the other hand, the spectral gap closing is always present for broken time-reversal symmetry.

Within the glass phase, it is again possible to separate two distinct frequency regimes delimited by a cross-over frequency

$$\omega_c = 2\kappa \left(1 + \frac{\omega_0^2}{\omega_0^2 + \kappa^2} + \frac{(\omega_0^2 + \kappa^2)^2}{\sqrt{K}\omega_z^2} \right)^{-1}, \quad (2.5.11)$$

which depends on all system and bath parameters. For $\omega < \omega_c$, the atomic spectral density

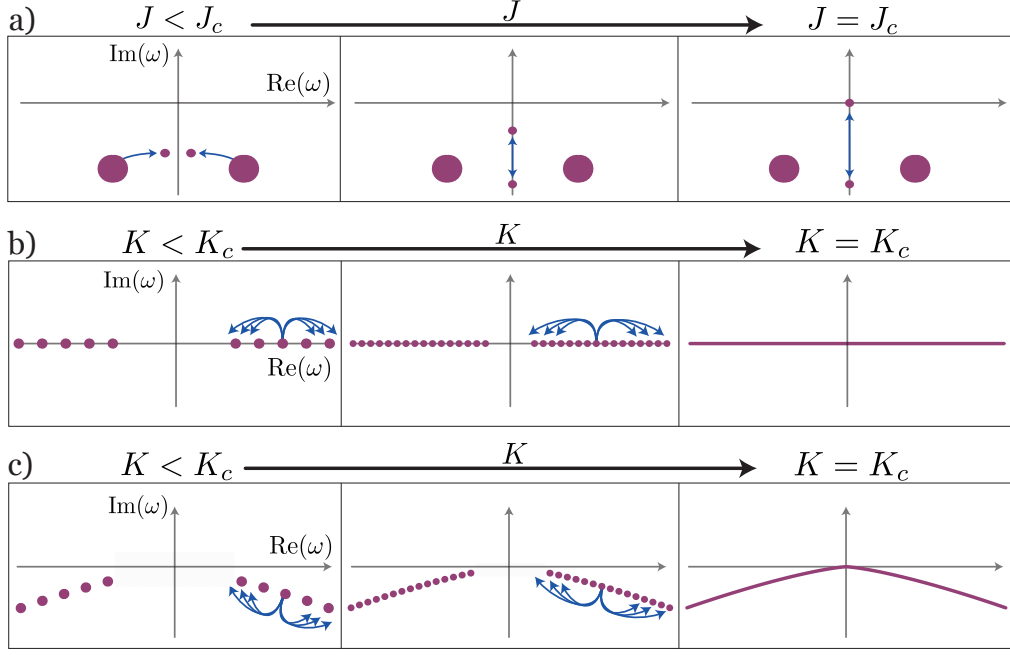


Figure 2.10: Schematic illustration of the pole structure and critical dynamics in the present model: a) the normal to superradiance transition in the dissipative Dicke model, b) the normal to glass transition in the zero temperature equilibrium model, c) the normal to glass transition in the dissipative model. a) When approaching the superradiance transition, two of the polaritonic modes advance to the imaginary axis and become purely imaginary before the transition point. This leads to the effective classical relaxational dynamics close to the transition. At the transition point, the \mathbb{Z}_2 symmetry is broken by only a single mode approaching zero and becoming critical for $J \rightarrow J_c$. b) For moderate disorder K , the poles are located on the real axis away from zero. For increasing K , the poles approach zero, with the closest pole scaling proportional to $|K - K_c|^{\frac{1}{2}}$. At $K = K_c$ the modes form a continuum which reaches zero and becomes quantum critical. No dissipative dynamics is involved. c) For moderate disorder K , the set of modes is located in the complex plane, away from zero. For increasing variance K , the modes get shifted closer to the origin, however, due to the scaling of real ($\propto |K - K_c|^{\frac{3}{2}}$) and imaginary part ($\propto |K - K_c|^2$), they neither become purely real nor purely imaginary. At $K = K_c$ a continuum of modes reaches zero.

is described by

$$\mathcal{A}(\omega) \underset{\omega < \omega_c}{=} \text{sgn}(\omega) \sqrt{\frac{2\kappa(\omega_0^2 + \kappa^2)|\omega|}{K\omega_0^2}}. \quad (2.5.12)$$

This unusual square root behavior of the spectral density in the glass phase, illustrated in Fig. 2.3 and also reflected in the pole structure Fig. 2.10, is a characteristic feature for glassy systems that are coupled to an environment [45, 141]. It has been discussed previously in the context of metallic glasses, where collective charges couple to a bath of mobile electrons [141] or for spin glasses, where the spins couple to an external ohmic bath [45]. For intermediate frequencies, $\omega > \omega_c$, the spectral density is linear, as it is known for the non-dissipative zero temperature case. In the limit $\kappa \rightarrow 0$, ω_c is shifted to smaller and smaller frequencies, vanishing for $\kappa = 0$. The cross-over frequency ω_c sets a time-scale $t_c = \frac{1}{\omega_c}$, such that for times $t < t_c$ the system behaves as if it were isolated

and one would observe the behavior of a $T = 0$ quantum glass for (relative) time scales $t < t_c$ in experiments. On the other hand, the long time behavior, $t > t_c$, of the atoms is described by overdamped dynamics, resulting from the coupling of the photons to a Markovian bath. This is a strong signature of low frequency equilibration of the atomic and photonic subsystem, which happens exactly at the glass transition (see Sec. 2.5.3).

2.5.3 Atom-Photon Thermalization

We now discuss thermalization properties. The presence of quenched disorder in our model leads to an effective quartic atom-atom interaction, shown in Eq. (2.4.27), which allows for an energy redistribution to different frequency regimes.

Atom Distribution Function

In order to determine the atomic distribution function $F_{\text{at}}(\omega)$, we make use of the FDR (see Sec. 2.8, Eq. (2.8.3)), which for the atoms described by a scalar degree of freedom simplifies to

$$Q^K(\omega) = F_{\text{at}}(\omega) (Q^R(\omega) - Q^A(\omega)). \quad (2.5.13)$$

The atomic correlation function Q^K is determined via Eq. (2.4.39). This equation contains the photonic Keldysh Green's function via $\Lambda^K(\omega)$, and it is therefore evident, that the atomic distribution function will depend on the distribution function of the bare photons. The bare photon distribution function $f_{\text{ph}}(\omega)$ is again defined via the FDR, reading

$$G_0^K(\omega) = f_{\text{ph}}(\omega) (G_0^R(\omega) - G_0^A(\omega)), \quad (2.5.14)$$

with the bare photon response and correlation functions $G_0^{R/A/K}$. Decomposing $f = f_S + f_{\text{AS}}$ into a symmetric $f_S(\omega) = f_S(-\omega)$ and an anti-symmetric $f_{\text{AS}}(\omega) = -f_{\text{AS}}(-\omega)$ contribution allows us to rewrite $\Lambda^K(\omega)$ in Eq. (2.4.39) as

$$\begin{aligned} 2\Lambda^K(\omega) &= G_0^K(\omega) + G_0^K(-\omega) \\ &= 2f_{\text{AS}}(\omega) (\Lambda^R(\omega) - \Lambda^A(\omega)) + f_S(\omega) (g^R(\omega) + g^R(-\omega) - g^A(\omega) - g^A(-\omega)) \\ &= 2 \left(f_{\text{AS}}(\omega) + \frac{\omega^2 + \kappa^2 + \omega_0^2}{2\omega\omega_0} f_S(\omega) \right) (\Lambda^R(\omega) - \Lambda^A(\omega)). \end{aligned} \quad (2.5.15)$$

Inserting this result into the expression for the correlation function (2.4.39), and making use of Eq. (2.4.40) and its complex conjugate yields

$$Q_{\text{reg}}^K = \left(f_{\text{AS}} + \frac{\omega^2 + \kappa^2 + \omega_0^2}{2\omega\omega_0} f_S \right) (Q^R - Q^A) \quad (2.5.16)$$

and thus identifies the atomic distribution function

$$F_{\text{at}}(\omega) = f_{\text{AS}}(\omega) + \frac{\omega^2 + \kappa^2 + \omega_0^2}{2\omega\omega_0} f_S(\omega). \quad (2.5.17)$$

This very general expression for the atomic distribution function incorporates the two most important examples, either a coupling to a thermal or a Markovian bath. For the coupling to a heat bath, the bare photonic distribution function is fully anti-symmetric with

$f_{\text{AS}}(\omega) = \coth\left(\frac{\omega}{2T}\right)$, $f_{\text{S}}(\omega) = 0$, which implies that the atoms will be distributed according to a thermal distribution as well and experience the same temperature T as the photons. For the case of dissipative photons, the bare distribution function of the photons is fully symmetric, with $f_{\text{S}}(\omega) = 1$, $f_{\text{AS}}(\omega) = 0$. Therefore the atomic distribution function for this system is

$$F_{\text{at}}(\omega) = \frac{\omega^2 + \kappa^2 + \omega_0^2}{2\omega\omega_0}. \quad (2.5.18)$$

For small frequencies $\omega \ll \sqrt{\omega_0^2 + \kappa^2}$, the atomic distribution function diverges as $F_{\text{at}}(\omega) \sim \frac{1}{\omega}$. This is the same asymptotic low frequency behavior as for the thermal distribution function $\coth\left(\frac{\omega}{2T}\right) \sim \frac{2T}{\omega}$, such that for low frequencies, the system is effectively described by a thermal distribution with a non-zero low frequency effective temperature (LET)

$$T_{\text{eff}} = \lim_{\omega \rightarrow 0} \frac{\omega F_{\text{at}}(\omega)}{2} = \frac{\omega_0^2 + \kappa^2}{4\omega_0}. \quad (2.5.19)$$

The atomic distribution F_{at} and low-frequency effective temperature T_{eff} in Eqs. (2.5.18), (2.5.19) is identical to the distribution function and LET of the photonic x-component, which is obtained by expressing the photonic action in terms of the x and p component, $p = \frac{i}{\sqrt{2}}(a^\dagger - a)$, and subsequently integrating out the p component. This procedure is shown in Sec. 2.10. From the resulting action, the x component is described by a distribution function $F_{\text{xx}}(\omega) = F_{\text{at}}(\omega)$, resulting from the coupling of the photons to the Markovian bath. Due to the strong atom-photon interaction, the atoms and the photonic x component equilibrate, resulting in the same distribution function and LET.

Photon Distribution Function

To compute the photon distribution function, we use the FDR

$$G^{\text{K}}(\omega) = G^{\text{R}}(\omega)F_{\text{ph}}(\omega) - F_{\text{ph}}G^{\text{A}}(\omega), \quad (2.5.20)$$

which in this case is an equation for the 2×2 matrices $G^{\text{R/A/K}}$ and F . The matrix F solving Eq. (2.5.20) is not diagonal, and the distribution of the excitations is determined by its eigenvalues f_α . These are shown in Fig. 2.4 and illustrate the thermalization process of the system. In the normal and superradiant phase, the photons have a lower LET than the atoms, resulting from the frequency regime for which the dynamics is classical relaxational. As for the spectral response, when the glass transition is approached, this classical region is shifted towards $\omega = 0$ and the photon LET approaches the atomic effective temperature. At the transition, the photons and atoms have thermalized completely in the low frequency regime.

2.5.4 Emergent Photon Glass

In the glass phase, the condensate order parameter $\langle a_i \rangle \propto \frac{1}{N} \sum_l \langle \sigma_l^x \rangle = \psi$ vanishes for all photon modes (i). However there exists a photon version of the Edwards-Anderson parameter

$$\tilde{q}_{\text{EA}} = \lim_{\tau \rightarrow \infty} \frac{1}{M} \sum_{i=1}^M \langle x_i(t + \tau)x_i(t) \rangle \propto q_{\text{EA}}, \quad (2.5.21)$$

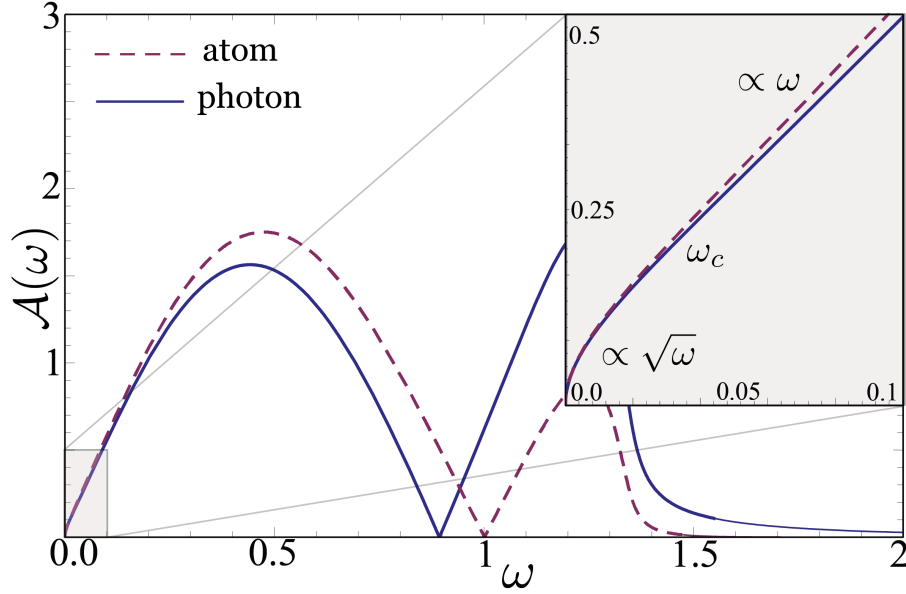


Figure 2.11: Spectral equilibration: Photon x-x spectral response $\mathcal{A}_{xx}(\omega) = -2\text{Im}(G_{xx}^R(\omega))$ in the glass phase for parameters $K = 0.04, J = 0.12, \omega_z = 2, \omega_0 = 1, \kappa = 0.02$. As for the SR phase, it shows the same low frequency behavior as the atomic spectral response $-2\text{Im}(Q^R(\omega))$ (multiplied with a constant $\frac{\omega_z \omega_0}{2\lambda}$). As for the atomic spectral density, one can clearly identify the overdamped regime with the unusual square-root behavior and the linear regime, separated by the frequency ω_c .

where $x = \frac{1}{\sqrt{2}}(a + a^\dagger)$ is the photon x operator and Eq. (2.5.21) only holds for the x-x correlations (and for those with finite contributions to x-x). A non-vanishing photon Edwards-Anderson parameter implies an infinite correlation time for the photons, analogous to the atomic q_{EA} -parameter. This is best illustrated by the correlator in the complex basis

$$\lim_{\tau \rightarrow \infty} \langle a(t + \tau) a^\dagger(t) \rangle = \frac{1}{2} \lim_{\tau \rightarrow \infty} \langle x(t + \tau) x(t) \rangle = \frac{\tilde{q}_{\text{EA}}}{2}, \quad (2.5.22)$$

where we made use of the fact that the x-p and p-p correlations vanish for $\tau \rightarrow \infty$. Eq. (2.5.22) implies that a photon which enters the cavity at time t has a non-vanishing probability to decay from the cavity at arbitrary time $t + \tau$, with $\tau \in [0, \infty)$. This highlights a connection to photon localization in disordered media [9, 7].

Close to the glass transition, the properties of the atomic system are completely mapped to the inverse photon Green's function. In the low frequency and small κ limit, i.e. $\omega, \kappa \ll \omega_0, \omega_z$, the inverse photon Green's function Eq. (2.4.46) has the expansion

$$D_{x-p}^R(\omega) = \begin{pmatrix} -\frac{\omega_0 \omega_z D_{\text{at}}^R(\omega)}{2(\omega^2 - \lambda)} & 0 \\ 0 & -\omega_0 \end{pmatrix}, \quad (2.5.23)$$

such that the atomic low frequency physics is mapped to the photon x-x component.

The determinant of D_{x-p}^R vanishes at the zeros of D_{at}^R , such that the photon propagator shows the same poles or branch cuts as the atomic propagator, and the scaling behavior at the glass transition obtained from the photons is identical to the one obtained from the

atoms. The photon response properties induced by the atom-photon coupling are most pronounced in the x-x component G_{xx}^R of the retarded photon Green's function,

$$G_{xx}^R(\omega) = \frac{\omega_0}{(\omega + i\kappa)^2 + 2\omega_0\Sigma^R(\omega) - \omega_0^2}. \quad (2.5.24)$$

For low frequencies, we can perform the same approximation as above to find

$$G_{xx}^R(\omega) = \frac{2(\lambda - \omega^2)}{\omega_0\omega_z D_{at}^R(\omega)} = \frac{2(\lambda - \omega^2)}{\omega_0\omega_z} Q^R(\omega). \quad (2.5.25)$$

Close to the glass transition and in the glass phase, the atomic retarded Green's function Q^R determines the low frequency photon x-x response function. This is reflected in Fig. 2.11. The discussion of the atomic response and scaling behavior in Sec. 2.5.2 remains valid for the photons.

2.5.5 Cavity Glass Microscope

We now describe three experimental signatures (cavity output fluorescence spectrum, photon real-time correlation function $g^{(2)}(\tau)$, and the photon response via driven homodyne detection) of the superradiant and glassy phases and their spectral properties. The cavity output is determined by the cavity input and the intra-cavity photons via the input-output relation [65, 42]

$$a_{out}(\omega) = \sqrt{2\kappa} \tilde{a}(\omega) + a_{in}(\omega), \quad (2.5.26)$$

with the cavity input annihilation operator $a_{in}(\omega)$ and the averaged intra-cavity field

$$\tilde{a}(\omega) = \frac{1}{\sqrt{M}} \sum_{i=1}^M a_i(\omega) \quad (2.5.27)$$

accounting for the M distinct cavity modes.

Cavity-output Fluorescence Spectrum

The fluorescence spectrum $S(\omega)$ describes the (unnormalized) probability of measuring a photon of frequency ω at the cavity output [55], and is defined by

$$S(\omega) = \langle a_{out}^\dagger(\omega) a_{out}(\omega) \rangle, \quad (2.5.28)$$

where $a_{out}^\dagger(\omega)$, $a_{out}(\omega)$ are creation, annihilation operators of the output field. Considering a vacuum input field, the fluorescence spectrum is expressed solely by the auto-correlation function of the intra-cavity field

$$S(\omega) = \langle \tilde{a}^\dagger(\omega) \tilde{a}(\omega) \rangle = \int_{\tau} e^{i\omega\tau} \langle \tilde{a}^\dagger(0) \tilde{a}(\tau) \rangle = iG^<(\omega), \quad (2.5.29)$$

which is the ‘‘G-lesser’’ Green’s function, occurring in the (\pm) -representation (see [99, 3]). Introducing also the ‘‘G-greater’’ Green’s function

$$iG^>(\omega) = \int_{\tau} e^{i\omega\tau} \langle \tilde{a}(\tau) \tilde{a}^{\dagger}(0) \rangle, \quad (2.5.30)$$

we can express response and correlation functions in terms of $G^{</>}$

$$G^K(\omega) = G^>(\omega) + G^<(\omega) \quad (2.5.31)$$

$$G^R(\omega) - G^A(\omega) = G^>(\omega) - G^<(\omega), \quad (2.5.32)$$

which yields

$$\begin{aligned} S(\omega) &= \frac{i}{2} (G^K(\omega) - G^R(\omega) + G^A(\omega)) \\ &= \frac{i}{2} (G^R(\omega) (F(\omega) - 1) - (F(\omega) - 1) G^A(\omega)). \end{aligned} \quad (2.5.33)$$

In thermal equilibrium ($F(\omega) = 2n_B(\omega) + 1$), where F is diagonal in Nambu space, this expression simply reads

$$S(\omega) = n_B(\omega) \mathcal{A}(\omega) \quad (2.5.34)$$

and the fluorescence spectrum reveals information about the intra-cavity spectral density \mathcal{A} .

In order to further analyze Eq. (2.5.33), we decompose the fluorescence spectrum into a regular part and a singular part as it was done for the Keldysh Green’s function in Eq. (2.4.37),

$$S(\omega) = S_{\text{reg}}(\omega) + 2\pi \tilde{q}_{\text{EA}} \delta(\omega), \quad (2.5.35)$$

with the Edwards-Anderson parameter for the photons \tilde{q}_{EA} . The regular part S_{reg} is determined by the regular contributions from the response and distribution function, $G^{R/A}$, F , which we have analyzed in the previous section. For small frequencies, $F(\omega) \propto \frac{1}{\omega}$ and in the normal and SR phase, $(G^R - G^A) \propto \omega$, which leads to a finite contribution of S_{reg} to the spectrum. In contrast, in the QG phase, $(G^R - G^A) \propto \sqrt{\omega}$, such that

$$S_{\text{reg}}(\omega) \propto \frac{1}{\sqrt{\omega}} \quad (2.5.36)$$

has a square root divergence for small frequencies $\omega < \omega_{\text{QG}}^c$ (see Eq. (2.5.11)). This divergence is indicated in Fig. 2.2.5 (c) and is a clear experimental signature of the glass phase.

A further distinction between all three phases is possible by decomposing the fluorescence spectrum into a coherent and an incoherent part, where the coherent part describes the ‘‘classical’’ solution (i.e. the part resulting from the presence of a photon condensate $\langle \tilde{a} \rangle \neq 0$) and the incoherent part describes the fluctuations. Accordingly, the coherent part is

$$S_c(\omega) = 2\pi |\langle \tilde{a} \rangle|^2 \delta(\omega) \quad (2.5.37)$$

and the incoherent part reads

$$S_{\text{inc}}(\omega) = S_{\text{reg}}(\omega) + 2\pi (\tilde{q}_{\text{EA}} - |\langle \tilde{a} \rangle|^2) \delta(\omega). \quad (2.5.38)$$

Typical fluorescence spectra characterizing the three distinct phases are plotted in Fig. 2.2.5. For the normal phase, the spectrum shows central and outer doublets associated with the hybridized atomic and photonic modes. Above the critical point for the superradiance transition, the doublets merge since a single mode becomes critical. However, compared to the single-mode transition, the central peak is much broader as a consequence of disorder. Additionally, in the superradiant phase, the fluorescence spectrum has a non-zero coherent contribution, which allows for a unique identification of this phase.

In the glass phase, the doublets have merged after the emergence of a critical continuum of modes at $\omega = 0$, and one can clearly identify the square root divergence for small frequencies, as discussed above. Additionally, the singular behavior of $S(\omega)$ in the glass phase is of incoherent nature, since $\langle a^\dagger \rangle = 0$. This combination of an incoherent zero frequency peak together with the absence of a coherent contribution uniquely defines the fluorescence spectrum in the glass phase and allows for a complete classification of the system's phases via fluorescence spectroscopy.

The coherent contribution to the spectrum can be determined via homodyne detection (see below), where $\langle \tilde{a} \rangle$ can be measured directly.

Photon Real-time Correlation Function $g^{(2)}(\tau)$

The time-resolved four-point correlation function of the output field

$$g^{(2)}(t, \tau) = \frac{\langle a_{\text{out}}^\dagger(t) a_{\text{out}}^\dagger(t + \tau) a_{\text{out}}(t + \tau) a_{\text{out}}(t) \rangle}{|\langle a_{\text{out}}^\dagger(t) a_{\text{out}}(t) \rangle|^2} \quad (2.5.39)$$

reveals how the correlations in the cavity decay with the time difference τ . In steady state, $g^{(2)}(t, \tau)$ only depends on the time difference τ and we write $g^{(2)}(\tau)$. For $\tau \rightarrow 0$, $g^{(2)}(0)$ is a measure of the underlying photon statistics in the cavity, e.g. indicates bunching or anti-bunching of the cavity photons, respectively.

In the open Dicke model, due to the effective temperature (cf. Fig. 2.4 and Ref. [49]), $g^{(2)}(0) > 1$, describing photon bunching, as expected for thermal bosons. We find $g^{(2)}(0) = 3$ for all the three phases, which stems from the off-diagonal atom-photon coupling in the Dicke model and coincides with the findings in Ref. [149] for the normal and superradiant phase.

In the normal and superradiant phase, the long time behavior is governed by the classical low frequency dynamics, leading to an exponential decay

$$g^{(2)}(\tau) \sim 1 + 2e^{-2\kappa\tau}. \quad (2.5.40)$$

This behavior is well known for the single mode Dicke model [149] and remains valid for the multimode case, away from the glass transition. In contrast, when the glass phase is approached, the modes of the system form a branch cut in the complex plane and the correlation function in the glass phase decays algebraically, according to

$$g^{(2)}(\tau) \sim 1 + \left(\frac{\tau_0}{\tau}\right)^{\frac{1}{2}}, \quad (2.5.41)$$

where $\tau_0 = O(1/\omega_0)$. This algebraic decay of the correlation function provides clearcut evidence for a critical continuum of modes around zero frequency witnessing the glass phase. In Fig. 2.5, we show $g^{(2)}(\tau)$ demonstrating this behavior.

In order to compute the four-point correlation function (2.5.39), we make use of Eq. (2.5.26) and the vacuum nature of the input field, i.e. the fact that all averages over $a_{\text{in}}, a_{\text{in}}^\dagger$ vanish. As a consequence, the operators for the output field in Eq. (2.5.39) can be replaced by the operators for the averaged cavity field \tilde{a} , see Eq. (2.5.27). The denominator in Eq. (2.5.39) is then

$$|\langle \tilde{a}^\dagger(t) \tilde{a}(t) \rangle|^2 = |\langle \tilde{a}_-^*(t) \tilde{a}_+(t) \rangle|^2 = |G^<(0)|^2. \quad (2.5.42)$$

The numerator similarly is expressed as

$$\langle \tilde{a}^\dagger(t) \tilde{a}^\dagger(t + \tau) \tilde{a}(t + \tau) \tilde{a}(t) \rangle = \langle \tilde{a}_-^*(t) \tilde{a}_-^*(t + \tau) \tilde{a}_+(t + \tau) \tilde{a}_+(t) \rangle. \quad (2.5.43)$$

Note that both expressions (Eqs. (2.5.42), (2.5.43)) preserve the correct operator ordering of Eq. (2.5.39), according to the different time-ordering on the (+), (−)-contour, respectively.

The four-point function in Eq. (2.5.43) can be expressed in terms of functional derivatives of the partition function \mathcal{Z} (Eq. (2.4.40)) with respect to the source fields μ (Eq. (2.4.19)). In the thermodynamic limit, the macroscopic action, Eq. (2.4.32), depends only on atomic and photonic two-point functions and, equivalent to Wick's theorem, the four-point function becomes the sum over all possible products of two-point functions

$$\begin{aligned} G^{(2)}(\tau) &= \langle \tilde{a}_-^*(t) \tilde{a}_-^*(t + \tau) \tilde{a}_+(t + \tau) \tilde{a}_+(t) \rangle \\ &= \langle \tilde{a}_-^*(t) \tilde{a}_+(t) \rangle \langle \tilde{a}_-^*(t + \tau) \tilde{a}_+(t + \tau) \rangle \\ &\quad + \langle \tilde{a}_-^*(t + \tau) \tilde{a}_+(t) \rangle \langle \tilde{a}_-^*(t) \tilde{a}_+(t + \tau) \rangle \\ &\quad + \langle \tilde{a}_-^*(t) \tilde{a}_-^*(t + \tau) \rangle \langle \tilde{a}_+(t + \tau) \tilde{a}_+(t) \rangle \\ &= |G^<(0)|^2 + |G^<(\tau)|^2 + |G_{\text{an}}^<(\tau)|^2, \end{aligned} \quad (2.5.44)$$

with the anomalous G-lesser function

$$G_{\text{an}}^<(\tau) = -i \langle \tilde{a}(\tau) \tilde{a}(0) \rangle. \quad (2.5.45)$$

Inserting Eq. (2.5.44) into the expression for the four-point correlation function yields

$$g^{(2)}(\tau) = 1 + |g^{(1)}(\tau)|^2 + \frac{|G_{\text{an}}^<(\tau)|^2}{|G^<(0)|^2}, \quad (2.5.46)$$

with the two-point correlation function

$$g^{(1)}(\tau) = \frac{G^<(\tau)}{G^<(0)} = \frac{\langle \tilde{a}^\dagger(\tau) \tilde{a}(0) \rangle}{\langle \tilde{a}^\dagger(0) \tilde{a}(0) \rangle}. \quad (2.5.47)$$

$G^<(\tau)$ is the Fourier transform of the fluorescence spectrum $S(\omega)$, as discussed in the previous section, and we therefore decompose it according to

$$G^<(\tau) = \tilde{q}_{\text{EA}} + G_{\text{reg}}^<(\tau), \quad (2.5.48)$$

with $G_{\text{reg}}^<(\tau)$ being the Fourier transform of $S_{\text{reg}}(\omega)$. In the infinite time limit, the regular part of $G^<(\tau)$ decays to zero, such that the infinite correlation time value becomes

$$g^{(1)}(\tau) \underset{\tau \rightarrow \infty}{=} \frac{\tilde{q}_{\text{EA}}}{\tilde{q}_{\text{EA}} + G_{\text{reg}}^<(0)} = \frac{\tilde{q}_{\text{EA}}}{\tilde{q}_{\text{EA}} + N_{\text{reg}}}. \quad (2.5.49)$$

N_{reg} denotes the occupation of the non-critical cavity modes. The way how this value of $g^{(1)}$ is reached in time is determined by the $\frac{1}{\sqrt{\omega}}$ divergence of $S_{\text{reg}}(\omega)$ for frequencies $\omega < \omega_c$ smaller than the cross-over frequency ω_c , cf. Fig. 2.2.5. This leads to

$$g^{(1)}(\tau) \xrightarrow{\tau > \tau_c} \frac{\tilde{q}_{\text{EA}}}{\tilde{q}_{\text{EA}} + N_{\text{reg}}} + \left(\frac{\tilde{\tau}_0}{\tau}\right)^{\frac{1}{2}}, \quad (2.5.50)$$

where $\tau_c = \frac{2\pi}{\omega_c}$ and $\tilde{\tau}_0$ has to be determined numerically. This algebraic decay to the infinite τ value of the correlation function with the exponent $\nu = \frac{1}{2}$ has also been found in Ref. [46] for the correlation function of a spin glass coupling to a finite temperature ohmic bath, in line with the discussion of universality in Sec. 2.5.2. The finite temperature exponent results from the non-zero effective temperature of the system, which influences the correlation function. For the case of $T_{\text{eff}} = 0$ this exponent changes to $\nu = \frac{3}{2}$ but the spectral properties are left unchanged.

The non-zero value of the two-point correlation $g^{(1)}(\tau) \rightarrow \frac{\tilde{q}_{\text{EA}}}{\tilde{q}_{\text{EA}} + N_{\text{reg}}}$ for $\tau \rightarrow \infty$ serves as a possible measure of the photonic Edwards-Anderson parameter \tilde{q}_{EA} in the glass phase: \tilde{q}_{EA} can be inferred from a correlation measurement, if the total photon number in the cavity $N_{\text{tot}} = \tilde{q}_{\text{EA}} + N_{\text{reg}}$ has been measured separately.

Taking the absolute value of $g^{(1)}(\tau)$ in Eq. (2.5.50), leads to the dominant contribution

$$|g^{(1)}(\tau)|^2 \xrightarrow{\tau > \tau_c} \left(\frac{\tilde{q}_{\text{EA}}}{\tilde{q}_{\text{EA}} + N_{\text{reg}}}\right)^2 + 2\frac{\tilde{q}_{\text{EA}}}{\tilde{q}_{\text{EA}} + N_{\text{reg}}}\left(\frac{\tilde{\tau}_0}{\tau}\right)^{\frac{1}{2}}, \quad (2.5.51)$$

as displayed in the asymptotic behavior of the four-point correlation function (Eq. (2.5.41)), where we have absorbed the prefactors in the definition of τ_0 and normalized the long-time limit to unity.

While the non-zero value of $g^{(1)}(\tau \rightarrow \infty)$ is caused by critical poles of the system, it does not include any more information about the pole structure of the system and may for instance be caused by a single critical pole, as it is the case for the superradiance transition. However, the algebraic decay to the infinite correlation time value of $g^{(1)}$, and the same for $g^{(2)}$, is a clear signature of a branch cut in the complex plane and therefore a continuum of modes reaching to zero frequency. This in turn is a strong signature of the critical glass phase in the cavity.

Photon Response via Driven Homodyne Detection

Here we relate homodyne detection measurements of the output signal to the quadrature response functions in the Keldysh formalism and calculate the corresponding signal. This gives predictions for the experimental analysis of the spectral properties and the scaling at the glass transition, which have been discussed in previous sections.

In the process of homodyne detection, the output field a_{out} is sent to a beam-splitter, where it is superimposed with a coherent light field $\beta(t) = \beta e^{-i(\omega_\beta t + \theta)}$ with frequency ω_β , amplitude β and phase θ . After passing the beam-splitter, the intensity of the two resulting light fields is measured and the difference in this measurement (the difference current) for the case of a 50/50 beam-splitter is described by

$$\begin{aligned} n_-(t) &= i \left\langle a_{\text{out}}^\dagger(t)\beta(t) - \beta^*(t)a_{\text{out}}(t) \right\rangle \\ &= \beta \left\langle e^{i(\theta - \frac{\pi}{2})} a_{\text{out}}(t) e^{i\omega_\beta t} + e^{-i(\theta - \frac{\pi}{2})} a_{\text{out}}^\dagger(t) e^{-i\omega_\beta t} \right\rangle. \end{aligned} \quad (2.5.52)$$

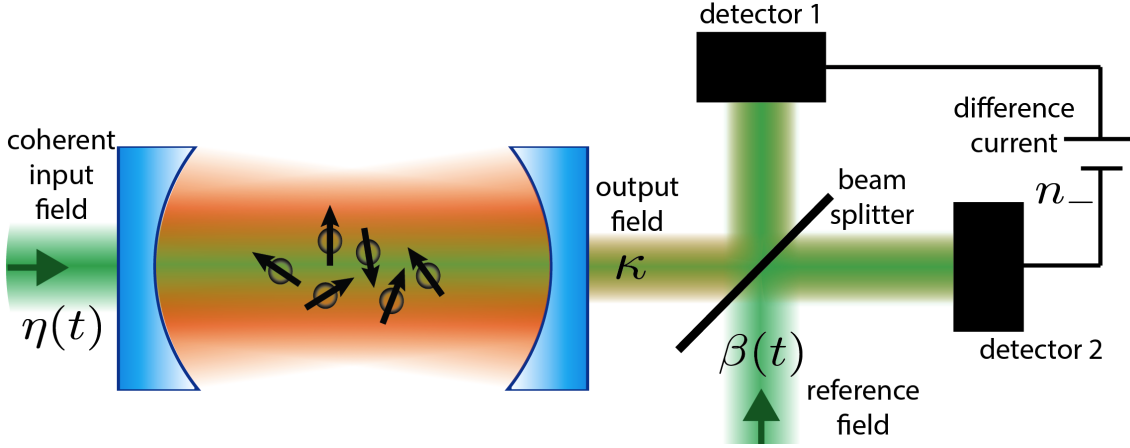


Figure 2.12: Illustration of homodyne detection of a weakly driven cavity. The cavity is driven via a weak coherent input field $\eta(t)$ entering the cavity through one of the mirrors. Then a homodyne measurement is performed on the output signal of the driven cavity. For this, the output signal is superimposed with a reference laser $\beta(t)$ via a 50/50 beam-splitter and the difference current of the two outgoing channels is measured. From this, the response function of the photons in the cavity can be measured by tuning the relative phases and frequencies of $\beta(t)$ and $\eta(t)$, as explained in the text.

Here, we added a conventional phase shift $\phi = \frac{\pi}{2}$ of the beam-splitter. For the case of a vacuum input field, Eq. (2.5.52) simply measures the steady state expectation value of the cavity quadrature components

$$X_{\theta-\frac{\pi}{2},\omega_\beta}(t) = e^{i(\theta-\frac{\pi}{2})}\tilde{a}(t)e^{i\omega_\beta t} + e^{-i(\theta-\frac{\pi}{2})}\tilde{a}^\dagger(t)e^{-i\omega_\beta t}, \quad (2.5.53)$$

with the intra-cavity operators \tilde{a} , as defined in Eqs. (2.5.26), (2.5.27). This quantity indicates a finite superradiance order parameter $\langle \tilde{a} \rangle$, but for the steady state contains no further information.

This situation changes when the input field is changed from the vacuum state to a weak coherent laser field $\eta(t)$. For this special case, the difference current in Eq. (2.5.52) is modified according to

$$\begin{aligned} n_-(t) &= i(\eta^*\beta - \beta^*\eta)(t) + i\sqrt{2\kappa} \left\langle \tilde{a}^\dagger(t)\beta(t) - \beta^*(t)\tilde{a}(t) \right\rangle \\ &= i(\eta^*\beta - \beta^*\eta)(t) + \sqrt{2\kappa}|\beta| \left\langle X_{\theta-\frac{\pi}{2},\omega_\beta}(t) \right\rangle. \end{aligned} \quad (2.5.54)$$

For the special case of the input field coming from the same signal as the reference laser, we have $\eta(t) = \beta(t)$ (which we assume from now on for simplicity) and the first term in Eq. (2.5.54) vanishes. The main difference here, is that the quadrature operator $X_{\theta,\omega_\beta}(t)$ is not evaluated for the steady state but for a state which has been perturbed by the weak laser field $\beta(t)$. For a weak laser amplitude $|\beta| \ll 1$, the system stays in the linear response regime and the difference current is proportional to the retarded Green's function for the quadrature component $X_{\theta+\frac{\pi}{2},\omega_\beta}$ as we proceed to show.

The interaction between the cavity photons and the radiation field outside the cavity is commonly described by the Hamiltonian

$$H_{\text{int}} = i\sqrt{2\kappa} \left(\tilde{a}^\dagger a_{\text{in}} - a_{\text{in}}^\dagger \tilde{a} \right), \quad (2.5.55)$$

which after a transformation to the Keldysh action and replacing the input fields by the coherent light field $\beta(t)$ enters the action as

$$S_{\text{int}} = \sqrt{2\kappa} \int_{\omega} (\tilde{a}_c^*, \tilde{a}_q^*) (\omega) i\sigma^x \begin{pmatrix} \beta_c \\ \beta_q \end{pmatrix} (\omega) + \text{h.c.}, \quad (2.5.56)$$

which is exactly the form of a source term in quantum field theory, generating all Green's functions of the system via functional derivatives with respect to the fields β . Expressing the action (2.5.56) in terms of Keldysh components of the quadrature fields $X_{\theta, \omega_{\beta}}$ yields

$$S_{\text{int}} = \sqrt{2\kappa} \int_{\omega} \left(X_{c, \theta - \frac{\pi}{2}, \omega_{\beta}}, X_{q, \theta - \frac{\pi}{2}, \omega_{\beta}} \right) (\omega) \sigma^x \begin{pmatrix} |\beta_c| \\ |\beta_q| \end{pmatrix} (\omega). \quad (2.5.57)$$

The linear response $\langle X_{\theta - \frac{\pi}{2}, \omega_{\beta}} \rangle^{(1)}(t)$ of the quadrature expectation value is expressed as (see Sec. 2.9)

$$\langle X_{\theta - \frac{\pi}{2}, \omega_{\beta}} \rangle^{(1)}(t) = -2\kappa |\beta|^2 \int_{t'} G_{X_{\theta - \frac{\pi}{2}, \omega_{\beta}}}^{\text{R}}(t - t'), \quad (2.5.58)$$

with the quadrature response function

$$G_{X_{\theta - \frac{\pi}{2}, \omega_{\beta}}}^{\text{R}}(t - t') = -i\theta(t - t') \langle [X_{\theta - \frac{\pi}{2}, \omega_{\beta}}(t), X_{\theta - \frac{\pi}{2}, \omega_{\beta}}(t')] \rangle. \quad (2.5.59)$$

For the specific choice of $\theta = \frac{\pi}{2}$,

$$X_{\theta - \frac{\pi}{2}, \omega_{\beta}} = \sqrt{2}x_{\omega_{\beta}} = \left(\tilde{a}(t)e^{i\omega_{\beta}t} + \tilde{a}^{\dagger}(t)e^{-i\omega_{\beta}t} \right), \quad (2.5.60)$$

the response function $G_{X_{\theta - \frac{\pi}{2}, \omega_{\beta}}}^{\text{R}}(t - t') = 2G_{x_{\omega_{\beta}}}^{\text{R}}(t - t')$ becomes the x-x retarded Green's function in a frame rotating with the laser frequency ω_{β} . In this case, the difference current is a direct measurement of the x-x response

$$n_-(t) = -4\kappa |\beta|^2 \int_{t'} G_{x_{\omega_{\beta}}}^{\text{R}}(t - t'), \quad (2.5.61)$$

which we have discussed in detail in Sec. 2.5.4. The frequency dependence of $x_{\omega_{\beta}}$, indicated by the subscript ω_{β} , coming from Eq. (2.5.53), can be used to scan through different frequency regimes and directly access the atom and photon x-x spectral response.

2.6 CONCLUSION

We have developed the non-equilibrium theory of the multimode Dicke model with quenched disorder and Markovian dissipation, and provided a comprehensive characterization of the resulting phases in terms of standard experimental observables. The main theoretical findings relate to the interplay of disorder and dissipation. We establish the robustness of a disorder induced glass in the presence of Markovian dissipation. This concerns, for example, the presence of an Edwards-Anderson order parameter and the algebraic decay of correlation functions in the entire glass phase. Central quantitative aspects, such as the decay exponents of the correlation functions, are strongly affected by the presence of dissipation. Disorder leads to enhanced equilibration of the atomic and photonic subsystems for

both the spectral (response) and their statistical properties. The spin glass physics of the atoms is mirrored onto the photonic degrees of freedom. We presented direct experimental signatures for the atomic and photonic dynamics that allow unambiguous characterization of the various superradiant and glassy phases.

Several directions for future work emerge from these results. In particular, the realization of disorder may not be governed by an ideal single Gaussian probability distribution in experimental realizations of multimode Dicke models. This may concern, for example, effects relating to the finite number of cavity modes (M) or effective two-level atoms (N). $1/N$ corrections contain information on the critical behavior close to the conventional Dicke transition [144, 49], with similar features expected for the glass transition. While we expect the main glassy features to be robust to such finite-size effects, it would be interesting to study a concrete cavity geometry with specific information of the cavity mode functions.

Furthermore, with our focus on the stationary state we did not touch upon the interesting questions of glassy dynamics [108, 45] in this work (for thermalization dynamics of the single mode Dicke model, see [2]). An interesting problem is a quantum quench of the open, disordered system. In particular, the non-universal short time and transient regimes should contain more system specific and non-equilibrium information. In the long time limit, the nature of aging and dependencies on the aging protocol remains to be explored.

2.7 PHOTON FIELDS IN THE SUPERRADIANT PHASE

In order to describe a system where the particle number is not conserved, as it is the case for the photons in the Dicke model, we introduce the spinor field

$$A_{\alpha,j}(t) = \begin{pmatrix} a_{\alpha,j}(t) \\ a_{\alpha,j}^*(t) \end{pmatrix}, \quad (2.7.1)$$

containing the bosonic fields $a_{\alpha,j}(t), a_{\alpha,j}^*(t)$ for a quantum state j and with index $\alpha = q, c$. The corresponding adjoint field is

$$A_{\alpha,j}^\dagger(t) = \left(a_{\alpha,j}^*(t), a_{\alpha,j}(t) \right). \quad (2.7.2)$$

The action for a quadratic problem is (for simplicity we consider only a single quantum state)

$$S = \int_{t,t'} \left(A_c^\dagger(t), A_q^\dagger(t) \right) D_{4 \times 4}(t, t') \begin{pmatrix} A_c(t') \\ A_q(t') \end{pmatrix}, \quad (2.7.3)$$

where

$$D_{4 \times 4}(t, t') = \begin{pmatrix} 0 & D_{2 \times 2}^A(t, t') \\ D_{2 \times 2}^R(t, t') & D_{2 \times 2}^K(t, t') \end{pmatrix} = (G_{4 \times 4})^{-1}(t, t') \quad (2.7.4)$$

is the inverse Green's function. The Keldysh correlation and retarded Green's function are also 2×2 matrices, which can be expressed in terms of operator averages according to

$$\begin{aligned} G_{2 \times 2}^R(t, t') &= (D_{2 \times 2}^R)^{-1}(t, t') \\ &= -i\theta(t - t') \left\langle \left(\begin{array}{cc} [a(t), a^\dagger(t')] & [a(t), a(t')] \\ [a^\dagger(t), a^\dagger(t')] & [a^\dagger(t), a(t')] \end{array} \right) \right\rangle \end{aligned} \quad (2.7.5)$$

and

$$\begin{aligned} G_{2 \times 2}^K(t, t') &= - (G_{2 \times 2}^R \circ D_{2 \times 2}^K \circ G_{2 \times 2}^A)(t, t') \\ &= -i \left\langle \left(\begin{array}{cc} \{a(t), a^\dagger(t')\} & \{a(t), a(t')\} \\ \{a^\dagger(t), a^\dagger(t')\} & \{a^\dagger(t), a(t')\} \end{array} \right) \right\rangle. \end{aligned} \quad (2.7.6)$$

In Eq. (2.7.6), the \circ -operation represents convolution with respect to time.

For the Dicke model with strong atom-photon coupling, it is reasonable to transform to the x-p representation in terms of real fields

$$x(t) = \frac{1}{\sqrt{2}} (a^*(t) + a(t)), \quad p(t) = \frac{1}{\sqrt{2}i} (a^*(t) - a(t)). \quad (2.7.7)$$

This is done via the unitary transformation for the fields

$$(x(t), p(t)) = \left(a^\dagger(t), a(t) \right) \underbrace{\frac{1}{\sqrt{2}} \begin{pmatrix} 1 & -i \\ 1 & i \end{pmatrix}}_{=V}. \quad (2.7.8)$$

and the Green's function

$$G_{x-p}^R(t, t'') = V^\dagger G_{2 \times 2}^R(t, t') V = \begin{pmatrix} G_{xx}^R(t, t') & G_{xp}^R(t, t') \\ G_{px}^R(t, t') & G_{pp}^R(t, t') \end{pmatrix}. \quad (2.7.9)$$

The same can be done for the advanced and Keldysh Green's functions, leading to the expressions for response and correlation functions as discussed in the main text.

2.8 MARKOVIAN DISSIPATION VS. QUENCHED DISORDER

As anticipated in the main text, the quenched bath, resulting from the coupling to a static distribution, is fundamentally different from the Markovian bath, represented by the fast electromagnetic field outside the cavity. While the dynamics of the quenched bath is frozen on the time scales of the system, the dynamics of the Markovian bath happens on much faster time scales than those of the system. As we will see, both types of bath inherently lead to non-equilibrium dynamics of the system since the system-bath equilibration time becomes infinite. For both cases this implies a non-equilibrium fluctuation-dissipation-relation (FDR), connecting response and correlations via a non-thermal distribution function.

2.8.1 Non-equilibrium Fluctuation Dissipation Relation

Correlation and response properties are not fully independent of each other but connected via fluctuation-dissipation relations, which we will briefly introduce in this part. In a system with multiple degrees of freedom, the response properties are encoded in the retarded (advanced) Green's function $G^{R(A)}(t, t')$, which is defined as

$$G_{ij}^R(t, t') = -i\theta(t - t') \langle [a_i(t), a_j^\dagger(t')] \rangle, \quad (2.8.1)$$

with the commutator $[\cdot, \cdot]$, the system creation and annihilation operators a_i^\dagger, a_i and $G^R(t, t') = (G^A(t', t))^\dagger$. The correlation function on the other hand

$$\mathcal{C}_{ij}(t, t') = \langle \{a_i(t), a_j^\dagger(t')\} \rangle = iG_{ij}^K(t, t') \quad (2.8.2)$$

is defined via the anti-commutator $\{\cdot, \cdot\}$ and defines the Keldysh Green's function $G^K(t, t')$ [100, 99, 3].

The fluctuation dissipation relation states

$$G^K(\omega) = G^R(\omega)F(\omega) - F(\omega)G^A(\omega) \quad (2.8.3)$$

and relates the response and correlations of the system via the distribution function $F(\omega)$. In thermal equilibrium, the distribution function is fully determined by the quantum statistics of the particles and the temperature T according to

$$F_{ij}(\omega) = \delta_{ij} (2n_B(\omega) + 1), \quad (2.8.4)$$

with the Bose distribution function n_B . As a result, in equilibrium, it is sufficient to determine either response or correlation properties in order to gain information on each of these.

2.8.2 Effective System-only Action

In this part, we present a derivation of a system-only action after elimination of the bath variables via Gaussian integration. Depending on the nature of the bath, different distribution functions will be imprinted to the system. We start with the general action of the bath, which we consider to be well described by a quadratic action and in the (\pm) -basis

$$S_B = \sum_{\mu} \int_{t, t'} (\zeta_{+\mu}^\dagger(t), \zeta_{-\mu}^\dagger(t)) \begin{pmatrix} G_{\mu}^{++} & G_{\mu}^{+-} \\ G_{\mu}^{-+} & G_{\mu}^{--} \end{pmatrix}^{-1} (t, t') \begin{pmatrix} \zeta_{+\mu}(t') \\ \zeta_{-\mu}(t') \end{pmatrix}, \quad (2.8.5)$$

with the bath variables ζ_{μ} and the bath mode index μ , which will be chosen a continuous index below. The Green's functions for the uncoupled bath variables are assumed to be in equilibrium and read

$$G_{\mu}^{+-}(t, t') \equiv G_{\mu}^<(t, t') = -i\bar{n}(\omega_{\mu}) e^{-i\omega_{\mu}(t-t')} \quad (2.8.6)$$

$$G_{\mu}^{-+}(t, t') \equiv G_{\mu}^>(t, t') = -i(\bar{n}(\omega_{\mu}) + 1) e^{-i\omega_{\mu}(t-t')} \quad (2.8.7)$$

$$G_{\mu}^{++}(t, t') \equiv G_{\mu}^T(t, t') = \theta(t-t')G_{\mu}^> + \theta(t'-t)G_{\mu}^< \quad (2.8.8)$$

$$G_{\mu}^{--}(t, t') \equiv G_{\mu}^{\tilde{T}}(t, t') = \theta(t-t')G_{\mu}^< + \theta(t'-t)G_{\mu}^>, \quad (2.8.9)$$

with the bath frequencies ω_{μ} and the familiar Green's functions G-lesser, G-greater, the time-ordered and the anti-time ordered Green's function. The linear coupling between system and bath is

$$S_I = \sum_{\mu} \sqrt{\gamma_{\mu}} \int_t (a_{+}^\dagger(t), a_{-}^\dagger(t)) \begin{pmatrix} 1 & 0 \\ 0 & -1 \end{pmatrix} \begin{pmatrix} \zeta_{+\mu}(t) \\ \zeta_{-\mu}(t) \end{pmatrix} + \text{h.c.}, \quad (2.8.10)$$

where a^\dagger, a are the system's creation and annihilation operators. For simplicity we consider only a single quantum state of the system, but a generalization to many states is straightforward. The partition function is of the general form

$$\begin{aligned} Z &= \int \mathcal{D}[a, a^\dagger, \zeta_\mu, \zeta_\mu^\dagger] e^{i(S_S + S_I + S_B)} \\ &= \int \mathcal{D}[a, a^\dagger] e^{iS_S} \underbrace{\left\{ \int \mathcal{D}[\zeta_\mu, \zeta_\mu^\dagger] e^{i(S_I + S_B)} \right\}}_{e^{iS_{\text{eff}}}}, \end{aligned} \quad (2.8.11)$$

where S_S is the bare action of the system. Now we integrate out the bath via completion of the square. The contribution $iS_{\text{eff},\mu}$ of the μ th mode to the effective action reads

$$S_{\text{eff},\mu}[a, a^\dagger] = \gamma_\mu \int_{t,t'} (a_+^\dagger(t), -a_-^\dagger(t)) \begin{pmatrix} G_\mu^{++}(t, t') & G_\mu^{-+}(t, t') \\ G_\mu^{+-}(t, t') & G_\mu^{--}(t, t') \end{pmatrix} \begin{pmatrix} a_+(t') \\ -a_-(t') \end{pmatrix} \quad (2.8.12)$$

The signs for the operators on the $-$ contour come from the backward integration in time. Thus the mixed terms will occur with an overall $-$ sign, while the $++$ and $--$ terms come with an overall $+$. Summing over all the modes μ we obtain the effective action of the bath for the field variables of the subsystem. We now take the continuum limit of densely lying bath modes, centered around some central frequency ω_0 and with bandwidth ϑ . That is, we substitute the sum over the modes with an integral in the energy Ω weighted by a (phenomenologically introduced) density of states (DOS) $\nu(\Omega)$ of the bath

$$\sum_\mu \gamma_\mu \simeq \int_{\omega_0 - \vartheta}^{\omega_0 + \vartheta} d\Omega \gamma(\Omega) \nu(\Omega) \quad (2.8.13)$$

and obtain

$$S_{\text{eff}} = - \int_{\omega_0 - \vartheta}^{\omega_0 + \vartheta} d\Omega \gamma(\Omega) \nu(\Omega) \int_{t,\tau} (a_+^\dagger(t), a_-^\dagger(t)) \begin{pmatrix} G_\Omega^{++}(\tau) & -G_\Omega^{+-}(\tau) \\ -G_\Omega^{-+}(\tau) & G_\Omega^{--}(\tau) \end{pmatrix} \begin{pmatrix} a_+(t - \tau) \\ a_-(t - \tau) \end{pmatrix} \quad (2.8.14)$$

where in addition we have used the translation invariance of the bath Green's function, $G_\Omega^{\alpha\beta}(t, t') = G_\Omega^{\alpha\beta}(t - t')$ to suitably shift the integration variables. Eq. (2.8.14) is a general expression for an effective system action resulting from a coupling of the system to a bath of harmonic oscillators with a coupling that is linear in the bath operators. In the case of a strong separation of time scales, the effective action can be further simplified. Here we consider two extreme and opposite limiting cases, namely a Markov and a quenched disorder bath.

2.8.3 The Markov Approximation

The Markov approximation is appropriate when there exists a rotating frame in which the evolution of the system is slow compared to the scales of the bath, i.e. $\omega_{\text{sys}} \ll \omega_0, \vartheta$, such that the system is considered as being static on the typical time scale of the bath. This leads to a temporally local form of the resulting effective action. As an example, we derive

the (\pm) -part of the effective action

$$\begin{aligned}
S_{\text{eff}}^{+-} &= - \int dt a_{-}^{\dagger}(t) \int d\tau \int_{\omega_0-\vartheta}^{\omega_0+\vartheta} \frac{d\Omega}{2\pi} \gamma(\Omega) \nu(\Omega) G_{\Omega}^{+-}(\tau) a_{+}(t-\tau) \\
&\stackrel{\text{Markov}}{\approx} -\gamma\nu \int dt a_{-}^{\dagger}(t) \left(\int d\tau \int_{\omega_0-\vartheta}^{\omega_0+\vartheta} \frac{d\Omega}{2\pi} G_{\Omega}^{+-}(\tau) \right) a_{+}(t-\delta) \\
&\stackrel{\text{Eq. (2.8.6)}}{=} i\gamma\nu \int dt a_{-}^{\dagger}(t) \left(\int d\tau \int_{\omega_0-\vartheta}^{\omega_0+\vartheta} \frac{d\Omega}{2\pi} n(\Omega) e^{-i(\Omega-\omega_0)\tau} \right) a_{+}(t-\delta) \\
&\approx 2i\kappa\bar{n} \int dt a_{-}^{\dagger}(t) a_{+}(t-\delta). \tag{2.8.15}
\end{aligned}$$

In the second line, we made use of the Markov approximation, i.e. the time evolution of the system is much slower than the one of the bath in the rotating frame, and the coupling and DOS are constant over the relevant frequency interval. In the third line, we replaced the Green's function by its definition (in the rotating frame). Finally, in the last line, we introduced the particle number $\bar{n} = \bar{n}(\omega_0)$ at the rotating frequency and the effective coupling $2\kappa = \gamma\nu$. Performing these steps for all the four contributions to the action in the (\pm) -basis leads to the action

$$S_{\text{eff}}[a, a^{\dagger}] = \int dt (a_{+}^{\dagger}(t), a_{-}^{\dagger}(t)) \Sigma_{\text{Mar}} \begin{pmatrix} a_{+}(t) \\ a_{-}(t) \end{pmatrix}, \tag{2.8.16}$$

which is local in time, containing the Markovian dissipative self-energies

$$\Sigma_{\text{Mar}} = i\kappa \begin{pmatrix} 2\bar{n} + 1 & -2(\bar{n} + 1) \\ -2\bar{n} & 2\bar{n} + 1 \end{pmatrix}. \tag{2.8.17}$$

Transforming this self-energy to the Keldysh representation, we finally obtain

$$\Sigma_{\text{Mar}} = i\kappa \begin{pmatrix} 0 & 1 \\ -1 & 4\bar{n} + 2 \end{pmatrix}. \tag{2.8.18}$$

The additional contribution to the distribution function $F_{\text{Mar}}(\omega)$ for the Markovian case is obtained from the FDR for the self-energies

$$\Sigma^K(\omega) = F(\omega) (\Sigma^R(\omega) - \Sigma^A(\omega)). \tag{2.8.19}$$

For the case when the system couples only to the Markovian bath or to an additional thermal bath, these contributions are infinitesimal and only those from the Markovian bath have to be taken into account, yielding

$$i\kappa(4\bar{n} + 2) = F(\omega) 2i\kappa, \tag{2.8.20}$$

i.e. the distribution function

$$F(\omega) = 2\bar{n} + 1. \tag{2.8.21}$$

In this expression, the frequency dependent particle distribution $n(\omega)$ has been replaced by the relevant particle number $n(\omega_0)$ of the bath. The interpretation of this, is that the dynamics in the bath are so fast compared to the system, that the for the full frequency regime, the system only couples to the slowest bath modes (in the rotating frame), located at $\omega = \omega_0$. This makes it impossible for the system to equilibrate with the bath and it can therefore not be described by a thermal distribution, i.e. stays out of equilibrium.

2.8.4 The Quenched Bath

The quenched bath is located in the opposite limit of the Markovian bath, i.e. it constitutes of a system bath coupling, such that there exists a rotating frame for which the system dynamics is much faster than the bath dynamics, i.e. $\omega_0, \vartheta \ll \omega_{\text{sys}}$. The corresponding approximation is to assume that the bath is static on the relevant time scale of the system and the resulting effective action for the system is infinite range in time. In this case, the contribution to the action for the $(+-)$ -component reads

$$\begin{aligned}
S_{\text{eff}}^{+-} &= - \int dt a_{-}^{\dagger}(t) \int d\tau \int_{\omega_0 - \vartheta}^{\omega_0 + \vartheta} \frac{d\Omega}{2\pi} \gamma(\Omega) \nu(\Omega) G_{\Omega}^{+-}(\tau) a_{+}(t - \tau) \\
&\stackrel{\text{quenched}}{\approx} i\gamma\nu \int dt \int d\tau a_{-}^{\dagger}(t) \left(\int_{\omega_0 - \vartheta}^{\omega_0 + \vartheta} \frac{d\Omega}{2\pi} n(\Omega) \right) a_{+}(t - \tau) \\
&= 2i\kappa\bar{N} \int \frac{d\omega}{2\pi} a_{-}^{\dagger}(\omega) \delta(\omega) a_{+}(\omega).
\end{aligned} \tag{2.8.22}$$

In the second line, we inserted the definition of the Green's function and made the approximation of a slowly varying bath as well as a constant DOS and coupling, ν, γ . In the third line, we replaced $\gamma\nu = 2\kappa$ and inserted the average particle number of the bath \bar{N} .

Repeating these steps for all contributions to the action in the (\pm) basis and subsequently transforming to the Keldysh basis, we have the self-energy

$$\Sigma_{\text{Q}}(\omega) = i\kappa\delta(\omega) \begin{pmatrix} 0 & 1 \\ -1 & 4\bar{N} + 2 \end{pmatrix}. \tag{2.8.23}$$

This contribution is structurally different from the one from integrating out the Markovian bath, since it only acts at $\omega = 0$. As a result, the distribution function for the system is only changed for $\omega = 0$ compared to the uncoupled, bare system. And therefore

$$F(\omega) = \begin{cases} 2\bar{N} + 1 & \text{if } \omega = 0 \\ F_{\text{bare}}(\omega) & \text{if } \omega \neq 0 \end{cases}, \tag{2.8.24}$$

where F_{bare} is the distribution of the bare system. In contrast to the Markovian case, where we obtain a constant distribution for all frequencies and therefore higher system frequencies are strongly pronounced, the quenched bath shifts the occupation distribution to the very slowest modes of the system, therefore implying very slow dynamics on the system. This is reflected in the modified FDR and the appearance of a glassy phase, as discussed in Sec. 2.4.2.

The picture obtained from these extreme cases of possible system bath couplings is quite transparent. For an equilibrium system, one assumes that the bath is such that for any possible frequency of the system, there exists a continuum of modes in the bath, such that thermalization of the system will happen on the whole frequency interval. In contrast, when the bath modes are located at much higher frequencies than the system, all the system modes interact the strongest with the slowest bath modes, leading to a distribution function as depicted in Eq. (2.8.21) and avoiding direct thermalization. On the other hand, for a bath that evolves on much slower time scales than the system, the picture is reversed, and only the slowest modes of the system interact with all the bath modes in an equivalent way. For the extreme case of a static bath, all the bath modes interact with the system's zero frequency mode, and the distribution function becomes the one in Eq. (2.8.24). This is again a non-equilibrium distribution, such that the system does not directly thermalize.

2.9 LINEAR RESPONSE IN THE KELDYSH FORMALISM

A common experimental procedure to probe a physical system is to apply a small external perturbation and measure the system's corresponding response. If the perturbation is sufficiently weak, the measured response will be linear in the generalized perturbing force. Here we review this construction in the Keldysh formalism in order to provide the background for the connection to the input-output formalism of quantum optics made in the text.

We consider a setup, where the hermitian operator $\hat{O} = \hat{O}^\dagger$ is measured after a perturbation of the form

$$H_{\text{per}}(t) = F(t)\hat{O} \quad (2.9.1)$$

has been switched on at $t = 0$. Here, the (unknown) real valued field $F(t) \propto \Theta(t)$ is the corresponding generalized force.

The expectation value

$$\langle \hat{O} \rangle(t) = \frac{1}{Z} \text{Tr} \left(\hat{\rho}(t) \hat{O} \right) \quad (2.9.2)$$

is evaluated by introducing a source field $h(t)$, such that

$$\langle \hat{O} \rangle(t) = \frac{1}{Z} \left. \frac{\delta Z(h)}{\delta h(t)} \right|_{h=0}, \quad (2.9.3)$$

where

$$Z(h) = \text{Tr} \left(e^{-\beta H + \int dt h(t) \hat{O}(t)} \right). \quad (2.9.4)$$

Expressing Z in a real-time Keldysh framework, we have

$$Z(h) = \int \mathcal{D}[\psi^*, \psi] e^{iS_0[\psi^*, \psi]} e^{i\delta S[h, \psi^*, \psi]}, \quad (2.9.5)$$

where S_0 is the unperturbed action and $\{\psi, \psi^*\}$ are the complex fields representing the creation and annihilation operators of the system (in the \pm -basis). The term

$$\begin{aligned} \delta S[h, \psi^*, \psi] = & \int dt \left(h_+(t) O_+(t) [\psi_+^*, \psi_+] \right. \\ & \left. - h_-(t) O_-(t) [\psi_-^*, \psi_-] \right) \end{aligned} \quad (2.9.6)$$

contains the source fields h_\pm coupling to O_\pm which are polynomials in ψ^*, ψ . The expectation value (2.9.2) transforms according to

$$\langle \hat{O}(t) \rangle = \langle O_+(t) \rangle = \langle O_-(t) \rangle = \frac{1}{2} \langle O_+(t) + O_-(t) \rangle, \quad (2.9.7)$$

whereas the averages on the right always mean averages with respect to the functional

integral. In terms of functional derivatives of the partition function, we find

$$\begin{aligned}\langle \hat{O}(t) \rangle &= -\frac{i}{2} \left(\frac{\delta}{\delta h_+(t)} - \frac{\delta}{\delta h_-(t)} \right) Z(h) \Big|_{h=0} \\ &= -\frac{i}{\sqrt{2}} \frac{\delta}{\delta h_q(t)} Z(h) \Big|_{h=0}.\end{aligned}\quad (2.9.8)$$

The second equality results from a rotation to the Keldysh representation and determines the time-dependent expectation value of $\hat{O}(t)$ for a system described by the action S_0 . In order to incorporate the perturbation (2.9.1), we add the perturbation to the bare action of Eq. (2.9.5)

$$S_0 \longrightarrow S_0 + \int dt (F_+(t)O_+(t) - F_-(t)O_-(t)). \quad (2.9.9)$$

Now we can expand the expectation value of \hat{O} to various orders in the force. The zeroth order simply is the expectation value in the absence of the perturbation:

$$\langle \hat{O}(t) \rangle^{(0)} = -\frac{i}{\sqrt{2}} \frac{\delta}{\delta h_q(t)} Z(h, F) \Big|_{F=h=0}. \quad (2.9.10)$$

The linear order term is then obtained via

$$\begin{aligned}\langle \hat{O}(t) \rangle^{(1)} &= \int_{-\infty}^t dt' F_+(t') \left(\frac{\delta}{\delta F_+(t')} \langle \hat{O}(t) \rangle \right)_{F=0} \\ &\quad + F_-(t') \left(\frac{\delta}{\delta F_-(t')} \langle \hat{O}(t) \rangle \right)_{F=0},\end{aligned}\quad (2.9.11)$$

which after a translation into the Keldysh representation reads

$$\begin{aligned}\langle \hat{O}(t) \rangle^{(1)} &= \frac{1}{2} \int_{-\infty}^t dt' \left(F_+(t') \left(\frac{\delta}{\delta F_+(t')} \langle O_+(t) + O_-(t) \rangle \right)_{F=0} \right. \\ &\quad \left. + F_-(t') \left(\frac{\delta}{\delta F_-(t')} \langle O_+(t) + O_-(t) \rangle \right)_{F=0} \right) \\ &= \frac{1}{2} \int dt' F(t') \left(\left(\frac{\delta}{\delta F_+(t')} + \frac{\delta}{\delta F_-(t')} \right) \langle O_+(t) + O_-(t) \rangle \right)_{F=0} \\ &= -\frac{i}{2} \int dt' F(t') \left(\frac{\delta}{\delta F_+(t')} + \frac{\delta}{\delta F_-(t')} \right) \left(\frac{\delta}{\delta h_+(t)} - \frac{\delta}{\delta h_-(t)} \right) Z(h, F) \Big|_{h=F=0} \\ &= -i \int dt' F(t') \frac{\delta^2}{\delta F_c(t') \delta h_q(t)} Z(h, F) \Big|_{F=h=0} = - \int dt' F(t') G_{OO}^R(t, t')\end{aligned}\quad (2.9.12)$$

where we made use of (at the point where we extract physical information) $F_+(t) = F_-(t) \equiv F(t)$, and furthermore that $t' \leq t$, such that the last equality indeed yields the retarded Green's function for the operator O . The integral in (2.9.12) runs from minus infinity to plus infinity, whereas the retarded Green's function defines the upper bound being t and the force $F(t')$ sets the lower bound to be t_0 since it vanishes for $t < t_0$ when the perturbation is switched on at $t = t_0$. Since the integral formally runs from minus infinity to plus infinity, we can switch to frequency space, where for the time-translational system (stationary state) we find

$$\langle \hat{O} \rangle^{(1)}(\omega) = -F(\omega) G_{OO}^R(\omega). \quad (2.9.13)$$

2.9.1 Example: Laser Field Induced Polarization of Cavity Atoms

The polarization of an atomic two-level system can be expressed as

$$P(t) = \langle \mu_R \sigma^x(t) + \mu_I \sigma^y(t) \rangle, \quad (2.9.14)$$

or after a rotation around the z-axis

$$P(t) = \mu \langle \sigma^x(t) \rangle. \quad (2.9.15)$$

We are interested in the response of the polarization to a perturbation of the system by a coherent monochromatic light field. Since the coupling of the light field is proportional to the polarization, the corresponding Hamiltonian reads

$$H(t) = \Omega(t) \sigma^x, \quad (2.9.16)$$

where $\Omega(t) = \theta(t) \mu E(t)$ is the generalized force and $E(t)$ is the electric field. The corresponding action for this problem is then

$$\begin{aligned} S &= S_0 + \delta S[h, \Omega, \phi] \\ &= S_0 + \int dt h_q(t) \phi_c(t) + h_c(t) \phi_q(t) \\ &\quad + \Omega_q(t) \phi_c(t) + \Omega_c(t) \phi_q(t), \end{aligned} \quad (2.9.17)$$

where we have replaced σ^x by the real fields ϕ as in Sec. 2.4.1. Applying (2.9.12), we then find

$$\begin{aligned} P^{(1)}(t) &= -i \mu \int dt' \Omega(t') \frac{\delta^2}{\delta \Omega_c(t') \delta h_q(t)} Z(h, \Omega) \Big|_{\Omega=h=0} \\ &= -\mu \int dt' \Omega(t') Q^R(t-t'), \end{aligned} \quad (2.9.18)$$

where $Q^R(t-t')$ is the retarded atomic propagator as in the previous sections. Now we again switch to frequency space and use the definition of Ω , such that we find

$$P^{(1)}(\omega) = \mu^2 E(\omega) Q^R(\omega), \quad (2.9.19)$$

where we have absorbed the θ -function into the electric field. This equation identifies the retarded atomic Green's function that we used in the previous section with the linear atomic susceptibility $\chi^{(1)}(\omega)$, which is commonly used in a quantum optics context.

2.10 DISTRIBUTION FUNCTION OF THE PHOTON X-COMPONENT

In this section, we derive the distribution function for the photonic x-component and show that it is identical to the atomic distribution function, proving that the atoms equilibrate with the photon x-component.

The Keldysh action describing the bare photon degrees of freedom is given by Eq. (2.4.3)

and we express this action directly in the Nambu basis, using the vector

$$A_4(\omega) = \begin{pmatrix} a_c(\omega) \\ a_c^*(-\omega) \\ a_q(\omega) \\ a_q^*(-\omega) \end{pmatrix}, \quad (2.10.1)$$

the photonic action reads

$$S_{\text{ph}} = \int_{\omega} A_4^\dagger(\omega) D_{4 \times 4}(\omega) A_4(\omega), \quad (2.10.2)$$

with the inverse Green's function in Nambu representation

$$D_{4 \times 4}(\omega) = \begin{pmatrix} 0_{2 \times 2} & (\omega + i\kappa) \sigma^z + \omega_0 1_{2 \times 2} \\ (\omega - i\kappa) \sigma^z + \omega_0 1_{2 \times 2} & 2i\kappa 1_{2 \times 2} \end{pmatrix}. \quad (2.10.3)$$

The action (2.10.2) can also be expressed in terms of real fields by performing the unitary transformation

$$\begin{pmatrix} x_\alpha(\omega) \\ p_\alpha(\omega) \end{pmatrix} = \frac{1}{\sqrt{2}} \begin{pmatrix} 1 & 1 \\ i & -i \end{pmatrix} \begin{pmatrix} a_\alpha(\omega) \\ a_\alpha^*(-\omega) \end{pmatrix}, \quad (2.10.4)$$

with $\alpha = c, q$. After this transformation, we express the action in terms of the real field

$$V_4(\omega) = \begin{pmatrix} x_c(\omega) \\ p_c(\omega) \\ x_q(\omega) \\ p_q(\omega) \end{pmatrix}, \quad (2.10.5)$$

such that

$$S_{\text{ph}} = \int_{\omega} V_4^T(-\omega) D_{x-p}(\omega) V_4(\omega), \quad (2.10.6)$$

with the inverse Green's function

$$D_{x-p}(\omega) = \begin{pmatrix} 0 & 0 & -\omega_0 & \kappa - i\omega \\ 0 & 0 & -\kappa + i\omega & -\omega_0 \\ -\omega_0 & -\kappa - i\omega & 2i\kappa & 0 \\ \kappa + i\omega & -\omega_0 & 0 & 2i\kappa \end{pmatrix}. \quad (2.10.7)$$

The action (2.10.6) is quadratic in the fields x_α and p_α and we can eliminate the p-fields from the action via Gaussian integration. The resulting action is

$$S_x = \frac{1}{\omega_0} \int_{\omega} X^T(\omega) D_x(\omega) X(\omega), \quad (2.10.8)$$

with the field

$$X(\omega) = \begin{pmatrix} x_c(\omega) \\ x_q(\omega) \end{pmatrix} \quad (2.10.9)$$

and the inverse Green's function

$$D_x(\omega) = \begin{pmatrix} 0 & (\omega + i\kappa)^2 - \omega_0^2 \\ (\omega - i\kappa)^2 - \omega_0^2 & \frac{2i\kappa(\kappa^2 + \omega^2 + \omega_0^2)}{\omega_0} \end{pmatrix}. \quad (2.10.10)$$

The distribution function $F_x(\omega)$ for the x-field is obtained via the fluctuation-dissipation relation

$$D_x^K(\omega) = F_x(\omega) (D_x^R(\omega) - D_x^A(\omega)), \quad (2.10.11)$$

yielding

$$F_x(\omega) = \frac{\omega^2 + \kappa^2 + \omega_0^2}{2\omega_0\omega}. \quad (2.10.12)$$

This is indeed identical to the atomic distribution function, that we have computed in Sec. 2.5.3, which proves that the atoms equilibrate with the photon x-field.

3 ONE-DIMENSIONAL QUANTUM FLUIDS OUT OF EQUILIBRIUM

One dimensional quantum fluids, both bosonic and fermionic, represent a remarkable example for universal dynamics in physical systems as in equilibrium there long wavelength behavior is described in terms of a quadratic theory, which requires only two effective parameters. They feature superfluidity at sufficiently low temperatures, algebraic real space correlation functions and, for fermions, absence of a quasi-particle residue known from Fermi Liquid theory in higher dimensions. The theoretical description of these system was derived by Luttinger, Luther and Peschel and Haldane and is based on the Luttinger Liquid Hamiltonian, which is quadratic in some effective fields ϕ and θ , which we call the Luttinger fields. While the Hamiltonian of these systems is very simple, the mapping of the microscopic bosonic and fermionic fields to the Luttinger fields is non-trivial and the reason for the specific features of one-dimensional systems. The Luttinger formalism at equilibrium has proven to be very accurate in describing the properties of one-dimensional quantum wires (both for condensed matter and cold atom experiments) for various different setups and its success and importance is at the same level as Bogoliubov theory for interacting bosons (attractively interacting fermions) and Landau's Fermi Liquid theory for interacting fermions in higher dimensions, $d > 1$.

For non-equilibrium setups, Luttinger Liquids have another remarkable properties, namely that the quadratic Luttinger theory is integrable. As a consequence, a system prepared in a non-equilibrium state will, according to the Luttinger Liquid Hamiltonian, not relax to its corresponding equilibrium state but instead reach a so-called prethermal state. The reason for reaching this state instead of a thermal one is that simply the eigenmodes of the Luttinger Hamiltonian, which are density waves, i.e. phonons, do not interact with each other and therefore the occupations of these phonons are constants of motion. Remarkably, the microscopic models, from which the Luttinger Hamiltonian is derived as the leading order description in the renormalization group sense, are in most cases not integrable and relaxation to equilibrium is expected in the long time limit.

In fact, the irrelevant corrections to the quadratic Luttinger theory break the integrability of the model and enforce thermalization for long times and consequently, they can not be neglected in a non-equilibrium setting. An interesting question is however, in which way the competition of the quadratic theory, which drives the system towards a non-equilibrium fixed point and the nonlinear correction, which enforces thermalization in the long time limit is visible in the non-equilibrium dynamics of the system in view of the fact, that the nonlinearity is irrelevant.

In this chapter, we derive the Keldysh path integral for the interacting Luttinger model, which describes one-dimensional quantum fluids out of equilibrium both for bosonic and

fermionic microscopic models and discuss the properties of Luttinger Liquids at equilibrium. In the following chapters, the dynamics of interacting Luttinger Liquids is studied for particular examples of out of equilibrium setups, namely a fermionic quantum quench and a bosonic system subject to permanent heating. The development of a theoretical description for interacting Luttinger Liquids is particularly relevant for cold atom experiments, where one dimensional systems of interacting particles have been realized experimentally and where the experiments are currently at a status, at which they reach the limit of the noninteracting Luttinger theory, observing for instance the onset of thermalization and non-trivial Bragg responses.

3.1 THE LUTTINGER FORMALISM FOR ONE-DIMENSIONAL INTERACTING BOSONS

One of the main features of bosonic particles is that the corresponding quantum statistics allows for an arbitrarily large occupation of a single quantum state. For a macroscopic system consisting of N bosonic particles it is even possible to occupy a single quantum state with a number of N_0 bosons, such that in the thermodynamic limit, the ratio $\lim_{N \rightarrow \infty} \frac{N_0}{N} > 0$ remains finite. If a single quantum state is macroscopically occupied, the system is considered to be in a so-called Bose-Einstein condensate, BEC. As Einstein has shown, for non-interacting particles, there exists a phase transition between a normal phase, which has no macroscopically occupied quantum states and a BEC. While in three dimensions, this transition happens at finite temperature, in two and one dimensions it takes place exactly at zero temperature and a true BEC can only exist in the limit $T \rightarrow \infty$.

In a field theoretical language, this BEC transition is associated with the spontaneous breaking of the continuous $U(1)$ symmetry of the system and is therefore a second order phase transition. The $U(1)$ -symmetry in turn corresponds to exact particle number conservation. While the system as a whole of course has a conserved particle number in both the normal and the BEC phase (since it is not spontaneously coupled to an external bath with particle number exchange), in the BEC the macroscopically occupied single particle state itself acts as a bath, which exchanges particles with the rest of the system. None of these two subsystems (the macroscopically occupied single particle state and the macroscopically occupied residual system) itself has exact particle number conservation and so, in the presence of a BEC, the non-condensed particles do not possess a $U(1)$ symmetry, which is spontaneously broken at the transition where the BEC state occurs.

The theoretical approach to describe the dynamics close to the ground state of interacting bosons in the presence of a BEC is typically to expand the action in terms of fluctuations around a perfectly condensed state. This state corresponds to a homogeneous and temporally fluctuationless density, where fluctuations of the density (of both thermal and quantum mechanical origin) and the phase of the system are small and one can expand around the stationary density profile. This leads to the famous and well-known Bogoliubov theory, which is very successfully applied for the physics of two- and three-dimensional systems of interacting bosons.

However, in one spatial dimension, due to the Mermin-Wagner-Hohenberg theorem, there exists no BEC phase for short-range interacting particles¹. As a consequence, there is no macroscopically occupied single particle state and no static density field around which a fluctuation expansion can be performed. This implies that both density and phase fluctuations are gapless in one dimension² and a Bogoliubov type expansion is not applicable. In contrast, the proper long wavelength description is the so-called Luttinger Liquid theory.

¹The exact statement of the theorem is that in classical systems with short range interactions, spontaneous symmetry breaking at finite temperature is forbidden. Since one-dimensional quantum systems with a linear excitation spectrum at $T = 0$ can be mapped to a two-dimensional classical system, this statement applies to one-dimensional interacting bosons.

²In contrast to higher dimensions, where due to the presence of a BEC only phase fluctuations are gapless.

In order to derive the Luttinger action, the complex bosonic fields are decomposed into a phase and amplitude representation according to

$$\psi(X) = [\rho(X)]^{\frac{1}{2}} e^{i\theta(X)}, \quad (3.1.1)$$

where ρ, θ are real fields representing the density and phase of the bosonic particles. The phase is a dimensionless field by definition, while the density has the dimension of an inverse length scale. In a sequence of seminal papers, Haldane found a representation of the density operator in terms of an additional dimensionless variables according to

$$\rho(X) = \left(\rho_0 - \frac{1}{\pi} \partial_x \phi(X) \right) \sum_{m=-\infty}^{\infty} \alpha_m e^{2im(\pi\rho_0 x - \phi(X))}. \quad (3.1.2)$$

Here, ρ_0 is the macroscopic expectation value of the particle density and the parameters α_m are real and depend non-universally on the specific theoretical generator of the dynamics, i.e. the Hamiltonian or the Liouvillian. As proven by Haldane, such a decomposition is always possible for one-dimensional bosons and the real field ϕ is the conjugate field for the phase variable in the sense that in a operator representation

$$\left[\partial_x \hat{\phi}(x), \hat{\theta}(x') \right] = i\pi \delta(x - x'). \quad (3.1.3)$$

The representation of the density operator in Eq. (3.1.2) is exact, as well as the commutation relation in Eq. (3.1.3). This leads to an exact representation of the bosonic fields in terms of the dimensionless fields

$$\psi(X) = \left(\rho_0 - \frac{1}{\pi} \partial_x \phi(X) \right)^{\frac{1}{2}} \left(\sum_{m=-\infty}^{\infty} \beta_m e^{2im(\pi\rho_0 x - \phi(X))} \right) e^{i\theta(X)} \quad (3.1.4)$$

with a new set of non-universal parameters β_m . In the long wavelength limit, the oscillations in the second parenthesis will average out and the only relevant contribution is the one for $m = 0$. As a consequence, in the long wavelength limit, the bosonic fields are approximately

$$\psi(X) \approx \left(\rho_0 - \frac{1}{\pi} \partial_x \phi(X) \right)^{\frac{1}{2}} e^{i\theta(X)}. \quad (3.1.5)$$

3.1.1 Long-wavelength Action for Lieb-Lininger Type Models

The specific action describing a system of interacting bosons depends on the model under consideration. However, the form of the action for a one-dimensional bosonic quantum fluid is quite universal and is called Luttinger Liquid action. In order to derive it exemplarily, we start with a generic model for interacting bosons, which is the so-called Lieb-Liniger model. It is an integrable model, describing bosons with a short ranged δ -type interaction³ and a quadratic dispersion. Although this model does of course not cover all bosonic systems in one dimension (as most of the models are not exactly integrable), the Luttinger formalism that is derived from it takes on the same form for a much broader class of one-dimensional models and only the corresponding effective parameters have to be adjusted

³This is the effective interaction potential for spin polarized bosons with short range interactions in the infrared limit.

to the microscopic model under consideration. The Lieb-Liniger model is described by the Hamiltonian

$$H_{\text{LiLi}} = \int_{\mathbf{x}} \left[-\hat{\psi}_{\mathbf{x}}^\dagger \frac{\partial_{\mathbf{x}}^2}{2m} \hat{\psi}_{\mathbf{x}} + g \left(\hat{\psi}_{\mathbf{x}}^\dagger \hat{\psi}_{\mathbf{x}} \right)^2 \right]. \quad (3.1.6)$$

Inserting the definition of the bosonic fields in the long-wavelength limit (3.1.5) into the Hamiltonian, the interaction part is transformed trivially, reading

$$g \int_{\mathbf{x}} \left(\hat{\psi}_{\mathbf{x}}^\dagger \hat{\psi}_{\mathbf{x}} \right)^2 = \frac{g}{\pi^2} \int_{\mathbf{x}} (\partial_{\mathbf{x}} \phi(\mathbf{X}))^2, \quad (3.1.7)$$

where we neglected irrelevant constants.

On the other hand, the kinetic term becomes more complicated, as it transforms according to

$$\int_{\mathbf{x}} \hat{\psi}_{\mathbf{x}}^\dagger \frac{\partial_{\mathbf{x}}^2}{2m} \hat{\psi}_{\mathbf{x}} = \frac{1}{4\pi m} \int_{\mathbf{x}} \left[2\pi\rho (\partial_{\mathbf{x}}\theta_{\mathbf{x}})^2 - 2\partial_{\mathbf{x}}\phi (\partial_{\mathbf{x}}\theta)^2 + \frac{(\partial_{\mathbf{x}}^2\phi)^2}{2\pi\rho - 2\partial_{\mathbf{x}}\phi} \right]. \quad (3.1.8)$$

In the long-wavelength limit, only the lowest order derivative terms in this expansion contribute to the dynamics and typically one only takes into account the quadratic terms in the derivatives. However, we will derive an intermediate action up to forth power in the derivatives, which reads

$$H_{\text{LiLi}} = \int_{\mathbf{x}} \left[\frac{\rho}{2m} (\partial_{\mathbf{x}}\theta_{\mathbf{x}})^2 - \frac{1}{2\pi m} \partial_{\mathbf{x}}\phi (\partial_{\mathbf{x}}\theta)^2 + \frac{(\partial_{\mathbf{x}}^2\phi)^2}{8\pi^2 m \rho} + \frac{g}{\pi^2} (\partial_{\mathbf{x}}\phi(\mathbf{X}))^2 \right]. \quad (3.1.9)$$

The terms of this Hamiltonian, which are quadratic in derivatives form the well-known Luttinger Liquid Hamiltonian, which is commonly described in terms of two distinct parameters according to

$$H_{\text{LL}} = \frac{1}{2\pi} \int_{\mathbf{x}} \left[uK (\partial_{\mathbf{x}}\theta_{\mathbf{x}})^2 + \frac{u}{K} (\partial_{\mathbf{x}}\phi(\mathbf{X}))^2 \right]. \quad (3.1.10)$$

Here K is the Luttinger parameter and u is the speed of sound that determines the dispersion of the excitations of the system. In terms of microscopic parameters, we find

$$K = \pi \sqrt{\frac{\rho}{2mg}} \quad \text{and} \quad u = \frac{1}{\pi} \sqrt{\frac{\rho g}{2m}}. \quad (3.1.11)$$

However, one should be careful with the microscopic parameters, since the Luttinger Hamiltonian describes an effective long-wavelength description, for which the short wavelength modes have been integrated out in the renormalization group sense. This procedure renormalizes the effective parameters of the theory, i.e. u and K strongly and Eq. (3.1.10) only holds in the limit of weak interactions.

The higher order terms in the expansion of the Lieb-Liniger Hamiltonian (3.1.9) will induce two different features. Let us start with the term proportional to the second order derivative of the field ϕ . This term is quadratic in the field but quartic in the derivatives. As a consequence, it introduces a correction to the dispersion of the fields in agreement with Bogoliubov theory, i.e. for very short distances, this term will become the dominant one and introduces a quadratic dispersion for the excitations. For this reason, we will refer to this term as the Bogoliubov term. However, since it is quadratic in ϕ , it will not lead to any coupling between the different modes of the system and will therefore not induce any non-trivial dynamics. On the other hand, the cubic term $\sim \partial_{\mathbf{x}}\phi (\partial_{\mathbf{x}}\theta)^2$ contains only three

spatial derivatives and will therefore be relevant on larger length scales than the Bogoliubov term. Therefore the cubic interaction term is more relevant than the modification of the dispersion due to the quartic term. We will also see in the following chapters, that the cubic term induces a redistribution of energy between the different modes of the Luttinger Liquid and can lead to a relaxation of an excited state into the thermal equilibrium. Therefore, even if not relevant compared to the quadratic terms, this term is non-negligible in a non-equilibrium setting, where the relaxation of the state is the major feature of the dynamics.

In order to give an estimate of the relevance of the higher order terms, we diagonalize the Luttinger Liquid Hamiltonian (3.1.10) by performing the rescaling $\phi \rightarrow \sqrt{K}\phi$ and $\theta \rightarrow \frac{1}{\sqrt{K}}\theta$. This leads to

$$H_{\text{LiLi}} = \frac{u}{2\pi} \int_{\text{x}} \left[(\partial_{\text{x}}\theta)^2 + (\partial_{\text{x}}\phi)^2 - \frac{1}{\text{mu}\sqrt{K}} \partial_{\text{x}}\phi (\partial_{\text{x}}\theta)^2 + \frac{K}{4\pi\text{mu}\rho} (\partial_{\text{x}}^2\phi)^2 \right]. \quad (3.1.12)$$

In momentum space, the Bogoliubov term becomes of the same order of magnitude as the Luttinger terms at the Luttinger cutoff Λ , which fulfills

$$1 = \frac{K\Lambda^2}{4\pi\text{mu}\rho}. \quad (3.1.13)$$

For momenta $q > \Lambda$, the influence of the Bogoliubov term is no longer negligible and the dispersion gets a quadratic correction to the linear one, which is a feature of the Luttinger Hamiltonian. Therefore, we restrict ourselves to momenta below the Luttinger cutoff, which in macroscopic parameters reads

$$\Lambda = \frac{2}{\sqrt{\pi}} \sqrt{g\text{m}\rho} \quad (3.1.14)$$

For momenta q below this cutoff (in other words, for length-scales larger than the inverse cutoff), the Bogoliubov term can be dropped and we obtain a quadratic Luttinger Liquid with a cubic interaction term. The resulting Hamiltonian and the corresponding systems are from now on referred to as interacting Luttinger Liquids. The Hamiltonian is

$$H_{\text{ILL}} = \frac{u}{2\pi} \int_{\text{x}} \left[(\partial_{\text{x}}\theta)^2 + (\partial_{\text{x}}\phi)^2 + v (\partial_{\text{x}}\phi) (\partial_{\text{x}}\theta)^2 \right] \quad (3.1.15)$$

and we have introduced the effective coupling constant v .

3.1.2 Remarks on Interacting Luttinger Liquids

For the derivation of the interacting Luttinger Liquid, Eq. (3.1.15), we have neglected several terms, including the Bogoliubov term, because of their irrelevance in the long wavelength limit. In principle, one could argue the same way in order to get rid of the cubic nonlinearity that describes the interaction in the Hamiltonian (3.1.15). Actually this is performed for most equilibrium problems, where the theoretical description is based solely on the quadratic Luttinger Liquid Hamiltonian. The justification for this is that the cubic interaction term does not modify the dispersion of the excitations but leads to a redistribution of energy and to scattering processes between the excitations. As a consequence, in an equilibrium setup, where the system has reached its stationary state, the only impact of the cubic term is the generation of a finite lifetime for the excitations (due to the scattering processes) and therefore a modification of dynamical, frequency resolved observables. Therefore it can be and is commonly neglected in equilibrium setups. However, as pointed out above, for any non-equilibrium setup, the cubic nonlinearity is the

leading order term that introduces relaxational dynamics to the system and can therefore under no circumstances be neglected, as we will see in the following sections of this thesis.

The global position and momentum operator in the Luttinger basis are

$$\hat{X} = \frac{1}{N} \int_{\mathbf{x}} \mathbf{x} \rho(\mathbf{x}) = -\frac{1}{N\pi} \int_{\mathbf{x}} \mathbf{x} \partial_{\mathbf{x}} \phi_{\mathbf{x}}, \quad (3.1.16)$$

where N is the global particle number and

$$\hat{P} = \frac{\hbar}{2mi} \int_{\mathbf{x}} \psi_{\mathbf{x}}^{\dagger} \partial_{\mathbf{x}} \psi_{\mathbf{x}} - \left(\partial_{\mathbf{x}} \psi_{\mathbf{x}}^{\dagger} \right) \psi_{\mathbf{x}} = \frac{\hbar}{m\pi} \int_{\mathbf{x}} (\pi \rho_0 - \partial_{\mathbf{x}} \phi_{\mathbf{x}}) \partial_{\mathbf{x}} \theta_{\mathbf{x}}. \quad (3.1.17)$$

Galilean invariance of the non-relativistic system requires

$$Nm\hat{P} = \partial_t \hat{X} = \frac{i}{\hbar} [\mathbf{H}, \hat{X}], \quad (3.1.18)$$

where Nm is the global mass of the system. As by the commutation relation $[\partial_{\mathbf{x}} \phi_{\mathbf{x}}, \theta_{\mathbf{x}'}] = i\pi \delta(\mathbf{x} - \mathbf{x}')$ an operator θ annihilates a derivative of ϕ , the linear contribution of the momentum operator is recovered from the quadratic part of the Hamiltonian, while the quadratic part of the momentum operator is recovered only in the presence of the cubic nonlinearity. The nonlinearity is therefore required for Galilean invariance of the system. On the other hand, operators proportional to $\partial_{\mathbf{x}} \theta (\partial_{\mathbf{x}} \phi)^2$ and $(\partial_{\mathbf{x}} \theta)^3$ in the Hamiltonian are forbidden, since they would create additional terms in Eq. (3.1.18), which are incompatible with the momentum operator in Eq. (3.1.17) and therefore with Galilean invariance.

As pointed out briefly above, the interacting Luttinger Liquid is an effective long wavelength description for interacting one-dimensional bosons. It can be seen as the resulting theoretical description after the fast, short distance degrees of freedom have been integrated out. This procedure however does not only reduce the Hamiltonian to the form of Eq. (3.1.15), which contains only the leading order terms in the sense of a derivative expansion but also renormalizes the remaining effective parameters in the Hamiltonian. As a consequence, for strong microscopic interactions, the Luttinger parameters can no longer be determined straightforwardly from the microscopic parameters and the definition of the Luttinger K and u in Eq. (3.1.11) is no longer correct and can only for very few cases be determined numerically. The same is true for the nonlinear part of the Hamiltonian, where v becomes an effective parameter as well. Furthermore, the projection onto the long wavelength modes generates an additional nonlinear term proportional to $(\partial_{\mathbf{x}} \phi)^3$, which corresponds to an effective cubic density interaction. However, although the effective parameters governing the dynamics of the interacting Luttinger Liquid are no longer easy to determine, the structure of the Hamiltonian (3.1.15) is protected. As we will see in the following sections, this leads to a non-equilibrium dynamics that is determined by only three free parameters, which can be determined from experimental measurements, which makes the non-equilibrium dynamics of the interacting Luttinger Liquid in the same sense universal as the well studied equilibrium dynamics of the non-interacting Luttinger Liquid.

The parameters $uK \equiv \nu_J$ and $\frac{u}{K} \equiv \nu_N$ for instance can be uniquely identify in terms of thermodynamic properties of the system's ground state. While ν_J is in a direct way related to Kohn's stiffness, i.e. the weight of the Drude peak ($\sim \delta(\omega)$) in the conductivity [113, 67, 80]. On the other hand, ν_N determines the inverse macroscopic compressibility of the system. The latter increases for increasing microscopic interactions and is therefore a continuous function of $1/K$.

3.1.3 Keldysh Action for Interacting Luttinger Liquids

In order to study the non-equilibrium dynamics of interacting bosons in one dimension, we have to develop the Keldysh path integral for the interacting Luttinger Liquid described by the Hamiltonian (3.1.15). In chapter 1, the partition function of a corresponding physical system has been formulated in terms of a Keldysh functional integral. This has been achieved by first deriving a path integral formulation for the time evolution of the system's density matrix on the (\pm) -contour and subsequently performing the Keldysh rotation to classical and quantum coordinates. While the Keldysh rotation is a linear and unitary transformation, this is not true for the transformation from microscopic bosonic operators to the Luttinger fields (Eqs. (3.1.1), (3.1.2)). Because of the latter, both transformation do not commute and the order in which a Luttinger Liquid is transformed to Keldysh space is important.

Complex fields on the (\pm) -contour have the same physical meaning as quantum field operators and therefore a transformation as shown in Eqs. (3.1.1) and (3.1.2) which is based on physical arguments remains valid for fields on the (\pm) -contour. On the other hand, classical and quantum fields have no clear, direct physical meaning and Haldane's arguments leading to the Luttinger transformation have no meaning in the Keldysh rotated space. Therefore, one has to perform first the transformation to the Luttinger fields in the (\pm) basis and then transform to Keldysh space, for which the action becomes simplified again. This implies however some computational effort for bosonic response and correlation functions, as we will see.

The action for the interacting Luttinger Liquid on the (\pm) -contour is derived exactly as described in (1.1.34). Starting from the Lieb-Liniger model, in terms of microscopic bosonic operators, it reads

$$\mathcal{S} = \int_{\mathbf{X}} \left[\psi_{+,X}^\dagger i \partial_t \psi_{+,X} - \psi_{-,X}^\dagger i \partial_t \psi_{-,X} \right] + H_{\text{LiLi}}^+ - H_{\text{LiLi}}^-, \quad (3.1.19)$$

where

$$H_{\text{LiLi}}^\alpha = \int_{\mathbf{X}} \psi_{\alpha,X}^\dagger \left(-\frac{\partial_x^2}{2m} \right) \psi_{\alpha,X} + g \left(\psi_{\alpha,X}^\dagger \psi_{\alpha,X} \right)^2 \quad (3.1.20)$$

is the Hamilton functional on the $\alpha = \pm$ -contour. The time derivative part in the action transforms into the Luttinger representation according to

$$\begin{aligned} \int_{\mathbf{X}} \psi_{\alpha,X}^\dagger i \partial_t \psi_{\alpha,t} &= \int_{\mathbf{X}} \left(-\frac{i}{2\pi} \partial_t \partial_x \phi_{\alpha,X} - \left(\rho_0 - \frac{1}{\pi} \partial_x \phi_{\alpha,X} \right) \partial_t \theta_{\alpha,X} \right) \\ &= \frac{1}{\pi} \int_{\mathbf{X}} \partial_x \phi_{\alpha,X} \partial_t \theta_{\alpha,X}, \end{aligned} \quad (3.1.21)$$

where we dropped all constant terms in the last equality. The Hamiltonian part transforms according to the steps described in Sec. 3.1.1, such that the action in the Luttinger basis is

$$\mathcal{S} = \frac{1}{\pi} \int_{\mathbf{X}} [\partial_x \phi_{+,X} \partial_t \theta_{+,X} - \partial_x \phi_{-,X} \partial_t \theta_{-,X}] + H_{\text{ILL}}^+ - H_{\text{ILL}}^-. \quad (3.1.22)$$

Here we have replaced the indices $(\mathbf{X}) = \mathbf{X}$ by a collective one and inserted the Hamilton functional for the interacting Luttinger Liquid

$$H_{\text{ILL}}^\alpha = \frac{u}{2\pi} \int_{\mathbf{X}} \left[(\partial_x \theta_{\alpha,X})^2 + (\partial_x \phi_{\alpha,X})^2 + v (\partial_x \phi_{\alpha,X}) (\partial_x \theta_{\alpha,X})^2 \right]. \quad (3.1.23)$$

Now, one can perform the Keldysh rotation for this action, which leads to

$$\begin{aligned} \mathcal{S} = & \frac{1}{\pi} \int_X -(\theta_{c,X}, \phi_{c,X}) \begin{pmatrix} uK\partial_x^2 & \partial_x\partial_t \\ \partial_x\partial_t & \frac{u}{K}\partial_x^2 \end{pmatrix} \begin{pmatrix} \theta_{q,X} \\ \phi_{q,X} \end{pmatrix} \\ & + \frac{v}{\sqrt{8\pi}} \int_X \left[2(\partial_x\theta_{c,X})(\partial_x\phi_{q,X})(\partial_x\theta_{q,X}) + (\partial_x\phi_{q,X}) \left((\partial_x\theta_{q,X})^2 + (\partial_x\theta_{c,X})^2 \right) \right]. \end{aligned} \quad (3.1.24)$$

Eq. (3.1.24) is the Keldysh action for the interacting Luttinger Liquid. So far, there is no regularization and no information on the initial conditions included and this will only be done in the following chapters, when explicit examples of Luttinger Liquids out of equilibrium are considered. However, from the quadratic part of the action, one can already derive non-interacting excitation spectrum, obtained by requiring

$$\det \begin{pmatrix} uK\partial_x^2 & \partial_x\partial_t \\ \partial_x\partial_t & \frac{u}{K}\partial_x^2 \end{pmatrix} = 0 \Leftrightarrow \partial_t \pm u\partial_x = 0 \Leftrightarrow \omega_q^\pm = \pm u|q|. \quad (3.1.25)$$

Describing sound waves with a linear dispersion $\omega_q^\pm = \pm u|q|$ in momentum space.

The real fields in this expression are neither representing bosonic nor fermionic statistics and lack a simple quasi-particle picture. Even further, they do not represent the eigenmodes of the system, since the quadratic part of the action is not diagonal in these fields. In order to transform to the eigenmodes, we perform a canonical Bogoliubov transformation according to

$$\phi_{\alpha,X} = \phi_{\alpha,t} - \pi\delta N_{\alpha,t}\theta(x) - \frac{i}{2} \int_q' \left(\frac{2\pi K}{|q|} \right)^{\frac{1}{2}} \text{sgn}(q) e^{-iqx} (\bar{a}_{\alpha,q,t} + a_{\alpha,-q,t}), \quad (3.1.26)$$

$$\theta_{\alpha,X} = \theta_{\alpha,t} + J_{\alpha,t}\theta(x) + \frac{i}{2} \int_q' \left(\frac{2\pi}{|q|K} \right)^{\frac{1}{2}} e^{-iqx} (\bar{a}_{\alpha,q,t} - a_{\alpha,-q,t}). \quad (3.1.27)$$

The integral \int_q' is over momentum space⁴, where the apostrophe indicates that it leaves out the value $q = 0$. The complex fields \bar{a}_α, a_α represent complex bosonic fields with the Keldysh index $\alpha = c, q$ and for momenta $q \neq 0$ are the eigenmodes of the system. the corresponding $q = 0$ modes are represented by the two real fields δN and J . The fields $\phi_{\alpha,t}, \theta_{\alpha,t}$ represent global modes, which do not appear in the Hamiltonian (since their spatial derivative is zero) but in principle can be added to the variables, i.e. a global center of mass motion and a global phase of the initial state. The corresponding spatial derivatives read

$$\partial_x\phi_{\alpha,X} = -\pi\delta N_{\alpha,t}\delta(x) - \frac{1}{2} \int_q' (2\pi|q|K)^{\frac{1}{2}} e^{-iqx} (\bar{a}_{\alpha,q,t} + a_{\alpha,-q,t}), \quad (3.1.28)$$

$$\partial_x\theta_{\alpha,X} = J_{\alpha,t}\delta(x) + \frac{1}{2} \int_q' \left(\frac{2\pi|q|}{K} \right)^{\frac{1}{2}} \text{sgn}(q) e^{-iqx} (\bar{a}_{\alpha,q,t} - a_{\alpha,-q,t}). \quad (3.1.29)$$

The global, zero momentum modes δN and J represent global density fluctuations and persistent currents in the system. The first statement becomes evident, when integrating the density (3.1.2) over the complete space for

$$\int_x \rho_X = \int_x \left(\rho_0 - \frac{1}{\pi} \partial_x\phi_X \right) = V\rho_0 - \delta N_t, \quad (3.1.30)$$

⁴We use the abbreviation $\int_q \equiv \int_{-\infty}^{\infty} \frac{dq}{2\pi}$ throughout the thesis.

where V is the volume of the system. The second is visible when considering the total momentum operator (3.1.17)

$$\hat{P} = \frac{\hbar}{m} \rho_0 \int_x \partial \theta_X = \frac{\hbar \rho_0}{m} J_t. \quad (3.1.31)$$

As we consider a system with exact particle number conservation and without any persistent currents, we will drop δN and J and do not consider them as relevant degrees of freedom. However, one must be careful with persistent currents in Luttinger Liquids in general as they turn out to be relevant for a huge class of physical setups⁵. Plugging the fields and derivatives of the fields (and neglecting all global operators) into the action (3.1.24), we obtain a quadratic part

$$\mathcal{S}^{(2)} = \frac{1}{2\pi} \int_{p,t} (\bar{a}_{c,p,t}, \bar{a}_{q,p,t}) \begin{pmatrix} 0 & i\partial_t - u|p| \\ i\partial_t - u|p| & 0 \end{pmatrix} \begin{pmatrix} a_{c,p,t} \\ a_{q,p,t} \end{pmatrix}, \quad (3.1.32)$$

reflecting that the bosonic fields represent the eigenmodes of the non-interacting Luttinger Liquid. They represent sound waves, i.e. phonons, with a dispersion $\omega_p = u|p|$ and a velocity u . The cubic part transforms to a more complicated expression, which we render here in a simplified form, without Keldysh indices

$$\begin{aligned} \mathcal{S}^{(3)} &= v \sqrt{\frac{2\pi}{K}} \int_{q,p,k,t} \sqrt{|qpk|} \text{sgn}(pk) (\bar{a}_{q,t} + a_{-q,t}) (\bar{a}_{p,t} - a_{-p,t}) (\bar{a}_{k,t} - a_{-k,t}) \delta(q + p + k) \\ &= \int_{q,p,k,t} V(q, p, k) \left(\frac{1}{3} \bar{a}_{q,t} \bar{a}_{k,t} \bar{a}_{p,t} \delta(q + k + p) + \bar{a}_{q,t} a_{k,t} a_{p,t} \delta(q - k - p) + \text{h.c.} \right) \end{aligned} \quad (3.1.33)$$

with the symmetrized vertex function

$$V(q, p, k) = 3v \sqrt{\frac{2\pi}{K}} \sqrt{|qpk|} (\text{sgn}(qp) + \text{sgn}(pk) + \text{sgn}(kq)). \quad (3.1.34)$$

The cubic interaction represents phonon scattering processes, which do not conserve the total phonon number and consist of four different processes. The term $\sim \hat{a}^3$ creates three phonons out of the vacuum, the term $\sim a^3$ annihilates three phonons, the term $\sim \hat{a}a^2$ converts two phonons into a single one and the term $\sim \hat{a}^2a$ converts a single phonon into two. While all the scattering processes are momentum conserving, only the two conversion processes can be energy conserving as there is associated a positive energy for the creation of a single phonon. Therefore the processes $\sim \hat{a}^3$ and $\sim a^3$ cannot be energy conserving and are only able to induce virtual processes, which possibly renormalizes the parameters of the action. We will analyze the impact of the interaction on the dynamics of the system for different physical setups in the following sections and now proceed with the introduction of the Luttinger Liquid action for fermions out of equilibrium.

⁵For instance it has been shown, that an impurity with a certain velocity might be slowed down in a Luttinger Liquid by inducing a persistent current to the system, which becomes the relevant degree of freedom for this setup. And therefore no external modulation of the system is needed in order to induce persistent currents.

3.2 THE LUTTINGER FORMALISM FOR INTERACTING FERMIONS IN ONE DIMENSION

3.2.1 Deriving the Keldysh Action for Interacting One-Dimensional Fermions

We consider a model of spin-polarized one-dimensional fermions with some short ranged interaction potential $g(x - x')$, which are described by the Hamiltonian

$$H_F = \int_{\mathbf{k}} \psi_{\mathbf{k}}^\dagger \epsilon_{\mathbf{k}} \psi_{\mathbf{k}} + \int_{\mathbf{x}, \mathbf{x}'} g(\mathbf{x} - \mathbf{x}') \rho(\mathbf{x}) \rho(\mathbf{x}'), \quad (3.2.1)$$

where $\epsilon_{\mathbf{k}}$ is the fermionic dispersion and $\rho(\mathbf{x}) = \psi_{\mathbf{x}}^\dagger \psi_{\mathbf{x}}$ is the fermionic real-space density. Close to the Fermi edge, the dispersion can be linearized since in the presence of interactions, the corrections to a linear dispersion in one dimension are small and irrelevant in the renormalization group sense. This leads to

$$\epsilon_{\mathbf{k}} = \epsilon_F + v_F(\mathbf{k} - \mathbf{k}_F) + \frac{(\mathbf{k} - \mathbf{k}_F)^2}{2m^*} + \mathcal{O}(k^3), \quad (3.2.2)$$

with the Fermi momentum \mathbf{k}_F , the Fermi energy $\epsilon_F = \epsilon_{\mathbf{k}}|_{\mathbf{k}=\mathbf{k}_F}$, the Fermi velocity $v_F = \partial_{\mathbf{k}} \epsilon_{\mathbf{k}}|_{\mathbf{k}=\mathbf{k}_F}$ and the effective mass $m^* = (\partial_{\mathbf{k}}^2 \epsilon_{\mathbf{k}}|_{\mathbf{k}=\mathbf{k}_F})^{-1}$. For fermions, the relevant low energy excitations are close to the Fermi edge and low momentum, i.e. long wavelength, behavior is determined by momenta close to the Fermi edge. Therefore, we introduce the notation of left and right moving fermions, where left moving fermions have a negative absolute momentum and right movers have a positive absolute momentum. Now, we can express momentum in terms of momentum relative to the left and right Fermi momentum and we label left and right movers with the index $\eta = \pm$. The energy is as well expressed relative to the Fermi energy and so we have

$$\epsilon_{\mathbf{k}}^\eta = \eta v_F \mathbf{k} + \frac{\mathbf{k}^2}{2m^*} \quad (3.2.3)$$

We will as well introduce left and right moving fermions $\psi_{\eta, \mathbf{k}}^\dagger, \psi_{\eta, \mathbf{k}}$ with the commutation relation

$$\{\psi_{\eta, \mathbf{k}}, \psi_{\eta', \mathbf{k}'}^\dagger\} = \delta_{\eta, \eta'} \delta_{\mathbf{k}, \mathbf{k}'}. \quad (3.2.4)$$

This is an exact relation for momenta $|\mathbf{k}| < \mathbf{k}_F$ as for these momenta the definition is unique⁶. The corresponding Hamiltonian transforms to

$$H_F = \int_{\mathbf{x}} \sum_{\eta=\pm} \psi_{\eta, \mathbf{x}}^\dagger \left(i\eta v_F \partial_{\mathbf{x}} - \frac{\partial_{\mathbf{x}}^2}{2m^*} \right) \psi_{\eta, \mathbf{x}} + \int_{\mathbf{x}, \mathbf{x}'} g(\mathbf{x} - \mathbf{x}') \rho(\mathbf{x}) \rho(\mathbf{x}'). \quad (3.2.5)$$

Without the band curvature term $\sim \partial_{\mathbf{x}}^2$, this system is integrable and we will now derive the Luttinger Hamiltonian for this system and add the band curvature term as an irrelevant perturbation later.

⁶A right moving fermion with momentum $\mathbf{k} < -\mathbf{k}_F$ is of course equal to a left moving fermion with momentum $\mathbf{k}' = -|\mathbf{k} - \mathbf{k}_F$.

The Hamiltonian under consideration is the linear fermion model, first considered by Luttinger, and reads

$$\mathbf{H}_{\text{FL}} = \int_{\mathbf{x}} \sum_{\eta=\pm} \psi_{\eta,\mathbf{x}}^\dagger (i\eta v_{\text{F}} \partial_{\mathbf{x}}) \psi_{\eta,\mathbf{x}} + \int_{\mathbf{x},\mathbf{x}'} g(\mathbf{x} - \mathbf{x}') \rho(\mathbf{x}) \rho(\mathbf{x}'). \quad (3.2.6)$$

This model has in principle an infinite number of negative energy states and one has to implement the constraint, that for both species $\eta = \pm$ only states with positive energy can be occupied and states with negative energy can become unoccupied. Both processes cost energy and are therefore allowed. As a consequence, we have to express all operators in normal ordered form, i.e. for states below the Fermi momentum $\eta q < \eta k_{\text{F}}$, the operator product $\psi_{\eta,\mathbf{q}}^\dagger \psi_{\eta,\mathbf{q}}$ transforms to

$$: \psi_{\eta,\mathbf{q}}^\dagger \psi_{\eta,\mathbf{q}} : := -\psi_{\eta,\mathbf{q}} \psi_{\eta,\mathbf{q}}^\dagger = \psi_{\eta,\mathbf{q}}^\dagger \psi_{\eta,\mathbf{q}} - 1 = \psi_{\eta,\mathbf{q}}^\dagger \psi_{\eta,\mathbf{q}} - \langle 0 | \psi_{\eta,\mathbf{q}}^\dagger \psi_{\eta,\mathbf{q}} | 0 \rangle, \quad (3.2.7)$$

where $|0\rangle$ denotes the vacuum state, i.e. the filled Fermi sea. On the other hand, for momenta $\eta q > \eta k_{\text{F}}$, the states are unoccupied and the energy is positive, such that normal ordering does not change the operator and we have

$$: \psi_{\eta,\mathbf{q}}^\dagger \psi_{\eta,\mathbf{q}} : := \psi_{\eta,\mathbf{q}}^\dagger \psi_{\eta,\mathbf{q}} - 0 = \psi_{\eta,\mathbf{q}}^\dagger \psi_{\eta,\mathbf{q}} - \langle 0 | \psi_{\eta,\mathbf{q}}^\dagger \psi_{\eta,\mathbf{q}} | 0 \rangle. \quad (3.2.8)$$

As a consequence, normal ordering is simply implemented by subtracting the vacuum expectation value. From now on, all bilinear operators will be considered normal ordered and we skip the explicit signature $: \dots :$ for these. The normal ordered densities of left and right movers are defined as

$$\rho_{\eta,\mathbf{x}} =: \psi_{\eta,\mathbf{x}}^\dagger \psi_{\eta,\mathbf{x}} :. \quad (3.2.9)$$

It has the Fourier transform

$$\begin{aligned} \rho_{\eta,\mathbf{q}} &= \int_{\mathbf{x}} \rho_{\eta,\mathbf{x}} e^{-i\mathbf{q}\mathbf{x}} = \int_{\mathbf{k}} \left(\psi_{\eta,\mathbf{k}+\mathbf{q}}^\dagger \psi_{\eta,\mathbf{k}} - \langle 0 | \psi_{\eta,\mathbf{k}+\mathbf{q}}^\dagger \psi_{\eta,\mathbf{k}} | 0 \rangle \right) \\ &= \begin{cases} \int_{\mathbf{k}} \psi_{\eta,\mathbf{k}+\mathbf{q}}^\dagger \psi_{\eta,\mathbf{k}} & \text{for } \mathbf{q} \neq 0 \\ \int_{\mathbf{k}} \left(\psi_{\eta,\mathbf{k}}^\dagger \psi_{\eta,\mathbf{k}} - \langle 0 | \psi_{\eta,\mathbf{k}}^\dagger \psi_{\eta,\mathbf{k}} | 0 \rangle \right) = \hat{N}_\eta & \text{for } \mathbf{q} = 0 \end{cases}, \end{aligned} \quad (3.2.10)$$

where \hat{N}_η counts the number of excitations (particles minus holes) in the direction η . Now we can take a look at the commutators of the normal ordered densities. For mixtures of left and right movers

$$[\rho_{+,\mathbf{q}}, \rho_{-,\mathbf{p}}] = 0, \quad (3.2.11)$$

these are of course always zero, since the different species anti-commute already on the level of bare fermions. For densities of the same species, we find however

$$[\rho_{\eta,\mathbf{q}}, \rho_{\eta,\mathbf{p}}] = \int_{\mathbf{k},\mathbf{k}'} : \left[\psi_{\eta,\mathbf{k}+\mathbf{q}}^\dagger \psi_{\eta,\mathbf{k}}, \psi_{\eta,\mathbf{k}'+\mathbf{p}}^\dagger \psi_{\eta,\mathbf{k}'} \right] :. \quad (3.2.12)$$

Here we have already used the fact, that the vacuum expectation values of both operators cancel each other in the commutator. However, the commutator itself has to be evaluated in a normal ordered way, which leads to

$$[\rho_{\eta,\mathbf{q}}, \rho_{\eta,\mathbf{p}}] = \int_{\mathbf{k}} \left(\langle \psi_{\eta,\mathbf{k}+\mathbf{q}+\mathbf{p}}^\dagger \psi_{\eta,\mathbf{k}} \rangle - \langle \psi_{\eta,\mathbf{k}+\mathbf{q}}^\dagger \psi_{\eta,\mathbf{k}-\mathbf{p}} \rangle \right) = -\delta(\mathbf{p} + \mathbf{q}) \eta \frac{\mathbf{p}}{2\pi}. \quad (3.2.13)$$

This commutation relation, which strictly relies on the filled Fermi sea state, is called Kac-Moody algebra and is very similar to bosonic commutation relations, if one would normalize the density operators by one over the corresponding momentum. Additionally, we instantly see that

$$\rho_+(p < 0)|0\rangle = 0, \quad (3.2.14)$$

$$\rho_-(p > 0)|0\rangle = 0, \quad (3.2.15)$$

since the corresponding states are occupied. This hints towards defining a bosonic annihilation operator according to

$$b_q = \left(\frac{2\pi}{|q|}\right)^{\frac{1}{2}} \sum_{\eta} \theta(\eta p) \rho_{\eta, -p}. \quad (3.2.16)$$

Obviously, this operator has the property

$$b_q|0\rangle = 0 \quad (3.2.17)$$

for all $q \neq 0$. In combination with the Kac-Moody algebra of the densities, this implies

$$[b_q, b_p^\dagger] = \delta(q - p), \quad (3.2.18)$$

where

$$b_q^\dagger = \left(\left(\frac{2\pi}{|q|}\right)^{\frac{1}{2}} \sum_{\eta} \theta(\eta p) \rho_{\eta, -p}\right)^\dagger = \left(\frac{2\pi}{|q|}\right)^{\frac{1}{2}} \sum_{\eta} \theta(\eta p) \rho_{\eta, p}. \quad (3.2.19)$$

The kinetic part of the Hamiltonian (3.2.6)

$$H_{\text{Kin}} = \int_x \sum_{\eta=\pm} \psi_{\eta,x}^\dagger i\eta v_F \partial_x \psi_{\eta,x} \quad (3.2.20)$$

has the following commutation relation with a bosonic annihilation operator with arbitrary (positive) momentum q

$$\begin{aligned} [b_q, H_{\text{Kin}}] &= \left(\frac{2\pi}{|q|}\right) \int_k v_F k [\rho_{+,-q}, \psi_{+,k}^\dagger \psi_{+,k}] = \left(\frac{2\pi}{|q|}\right) v_F q \int_k \psi_{+,k-q}^\dagger \psi_{+,k} \\ &= v_F q b_q. \end{aligned} \quad (3.2.21)$$

In the same way, we find for arbitrary negative momenta $q < 0$,

$$[b_q, H_{\text{Kin}}] = -v_F q b_q = v_F |q| b_q. \quad (3.2.22)$$

Combining the results from Eqs. (3.2.21) and (3.2.22), the kinetic part of the Hamiltonian takes the form

$$H_{\text{Kin}} = \int_k v_F |k| b_k^\dagger b_k, \quad (3.2.23)$$

i.e. the Hamiltonian of one-dimensional fermions with linear dispersion can be expressed in terms of bosonic operators with a linear dispersion. This result is possible only because

of the commutation relations of the fermionic density operators, which crucially rely on a filled Fermi sea. As a consequence, the elementary excitations are not single fermions but particle-hole excitations, which aren't bosons in a strict sense, but for which we found a bosonic representation.

In order to find a representation of fermionic single particle operators in terms of the densities, we evaluate the commutator

$$[\rho_{\eta,q}, \psi_{\eta',x}] = \delta_{\eta,\eta'} \int_{\mathbf{k},\mathbf{p}} e^{i\mathbf{p}\mathbf{x}} \left[\psi_{\eta,\mathbf{k}+\mathbf{q}}^\dagger \psi_{\eta,\mathbf{k}}, \psi_{\eta,\mathbf{p}} \right] = -\delta_{\eta,\eta'} e^{i\mathbf{q}\mathbf{x}} \psi_{\eta,x}. \quad (3.2.24)$$

Due to the Kac-Moody algebra of the fermionic density operators (3.2.13), we can interpret the density in an commutator in terms of a derivative, i.e.

$$[\rho_{\eta,q}, \dots] = -\eta \frac{q}{2\pi} \frac{\partial}{\partial \rho_{\eta,-q}} \dots \quad (3.2.25)$$

and with the combination of the commutation with a single particle operator (3.2.24), this yields

$$\frac{\partial}{\partial \rho_{\eta,-q}} \psi_{\eta',x} = \delta_{\eta,\eta'} \frac{2\pi\eta}{q} e^{i\mathbf{q}\mathbf{x}} \psi_{\eta,x}. \quad (3.2.26)$$

This differential equation is solved straightforwardly by

$$\psi_{\eta,x} = U_\eta e^{-\int_{\mathbf{q}} \left(\frac{2\pi\eta}{q} e^{-i\mathbf{q}\mathbf{x}} \rho_{\eta,q} \right)}, \quad (3.2.27)$$

where the undetermined operator U cannot be a function of any fermionic operator, neither single particle nor density operators, i.e. its commutation relation with all possible fermionic densities is zero. It is, however, very simple to determine the operator U_η . The only density operator that is not contained in the right side of Eq. (3.2.27) is the global number operator $N_\eta = \rho_{\eta,0}$. On the other hand, in the present form, the right hand side of Eq. (3.2.27) does not change the global particle number of the system, while the left hand side does lower the global particle number. Since the removal of a particle from a specific state of the system would lead to additional commutation relations in Eq. (3.2.24), U_η can only change the global particle number uniformly and fulfills the relation

$$U_\eta^\dagger U_\eta = N_\eta. \quad (3.2.28)$$

A rigorous derivation of the prefactor U_η can be found in Refs. [83, 67, 80] but the discussion presented here is sufficient to understand its meaning and sufficient for the following sections.

So far we have found a simple expression for the kinetic part of the Hamiltonian in terms of bosonic operators and an expression for the single fermion operators in terms of fermion densities. In order to relate the two in a simple and straightforward way, we now introduce, very similar as for the bosonic case, the real operators ϕ and θ according to

$$\phi_x = -(N_+ + N_-)\pi x - i\pi \int_{\mathbf{q}}' \frac{1}{q} e^{-i\mathbf{q}\mathbf{x}} (\rho_{+,\mathbf{q}} + \rho_{-,\mathbf{q}}) e^{-\frac{\mathbf{q}}{\Lambda}} \quad (3.2.29)$$

$$\theta_x = (N_+ - N_-)\pi x + i\pi \int_{\mathbf{q}}' \frac{1}{q} e^{-i\mathbf{q}\mathbf{x}} (\rho_{+,\mathbf{q}} - \rho_{-,\mathbf{q}}) e^{-\frac{\mathbf{q}}{\Lambda}}. \quad (3.2.30)$$

We will now briefly discuss these operators. First, as for the bosonic case, $\frac{1}{\pi} \partial_x \phi_x$ can be seen as the density fluctuation operator, describing the global density fluctuations of left

and right moving particles in the zero momentum term $\sim (N_+ + N_-)$ and momentum dependent density fluctuation in the sum term. On the other hand $\partial_x \theta$ is proportional to a current in the system, the term $\sim (N_+ - N_-)$ describing a global current through the system, while the momentum dependent terms describe local current fluctuations. We also added a cutoff Λ in this description, which was not present in the previous formulas. This cutoff fulfills actually two requirements. For a perfectly linear fermionic dispersion, the presented derivations are exact on all length scales and there exists no physical cutoff in the system, however, the theory must be regularized at some point and this is the task of the cutoff. For a fermionic system on a lattice, or for fermions with band curvature, the cutoff represents the microscopic cutoff for the Luttinger theory and is implemented here in a smooth way.

In terms of the real fields, the fermionic single particle operators can be expressed as

$$\psi_{\eta,x} = U_\eta \frac{1}{\sqrt{2\pi}} e^{i\eta k_F x} e^{-i(\eta\phi_x - \theta_x)}. \quad (3.2.31)$$

Using the commutation relations for the bosons, b_q^\dagger, b_q and the fermionic densities $\rho_{\eta,q}$, it is simple (cf. Ref. [67]) to derive the following commutation relation

$$[\partial_x \phi_x, \theta_{x'}] = -i\pi \delta(x - x'), \quad (3.2.32)$$

which are again the ones known from the bosonic Luttinger Liquid theory (Eq. (3.1.3)). The kinetic part of the Hamiltonian is

$$H_{\text{Kin}} = \frac{1}{2\pi} \int_x v_F \left[(\partial_x \theta_x)^2 + (\partial_x \phi_x)^2 \right]. \quad (3.2.33)$$

The interactions can be formulated in terms of left and right movers according to

$$H_{\text{Int}} = \int_{x,x'} g(x-x') [\rho_{+,x} + \rho_{-,x}] [\rho_{+,x'} + \rho_{-,x'}]. \quad (3.2.34)$$

Terms proportional to $\psi_{+,q_1}^\dagger \psi_{-,q_2}^\dagger \psi_{-,q_3} \psi_{-,q_4}$ are energetically strongly suppressed since the momentum conservation of this process requires $q_1 + q_2 + 2k_F = q_3 + q_4$ and so the energy difference between the state before the collision and after is $\approx 2v_F k_F = 2\epsilon_F$.

From Eq. (3.2.29), we see that

$$\rho_{+,x} + \rho_{-,x} = \frac{1}{\pi} \partial_x \phi_x \quad (3.2.35)$$

and thus

$$H_{\text{Int}} = \int_{x,x'} \frac{g(x-x')}{\pi^2} (\partial_x \phi_x) (\partial_x \phi_{x'}). \quad (3.2.36)$$

As the interaction is supposed to be short ranged, we can perform a derivative expansion up to second order of the interaction, leading to

$$H_{\text{Int}} = \int_{x,x'} \frac{g_0}{\pi^2} (\partial_x \phi_x)^2 + \frac{g_0 \lambda^2}{\pi^2} (\partial_x^2 \phi_x)^2, \quad (3.2.37)$$

where λ is the effective range of the interaction. Putting interactions and the kinetic term

together, we obtain the Hamiltonian

$$H_{\text{FL}} = \frac{1}{2\pi} \int_{\text{x}} \left[v_{\text{F}} (\partial_{\text{x}} \theta_{\text{x}})^2 + \left(v_{\text{F}} + \frac{2g_0}{\pi} \right) (\partial_{\text{x}} \phi_{\text{x}})^2 + \frac{2g_0 \lambda^2}{\pi} (\partial_{\text{x}}^2 \phi_{\text{x}})^2 \right]. \quad (3.2.38)$$

This Hamiltonian, which is only quadratic in the fields ϕ and θ is very similar to the Hamiltonian that we obtained earlier from the bosonic theory. Again, we have a term that is quadratic in the derivatives, which will finally lead to a linear dispersion of the elementary excitations.

So far, we have completely neglected the band curvature terms in the original fermionic Hamiltonian (3.2.5). From their canonical scaling behavior (a one-dimensional density times a second order derivative), it is clear that they will be proportional to a cubic derivative term in the Luttinger variables ϕ and θ . The band curvature term is

$$\begin{aligned} H_{\text{BC}} &= - \int_{\text{x}} \sum_{\eta=\pm} \psi_{\eta,\text{x}}^\dagger \partial_{\text{x}}^2 \psi_{\eta,\text{x}} = - \int_{\text{x}} \sum_{\eta=\pm} \psi_{\eta,\text{x}}^\dagger U_{\eta} \partial_{\text{x}}^2 e^{-i(\eta\phi_{\text{x}} - \theta_{\text{x}})} \\ &= \int_{\text{x}} \sum_{\eta=\pm} \rho_{\eta,\text{x}} \left[(\eta \partial_{\text{x}} \phi_{\text{x}} - \partial_{\text{x}} \theta_{\text{x}})^2 + i (\eta \partial_{\text{x}}^2 \phi_{\text{x}} - \partial_{\text{x}}^2 \theta) \right] \\ &= \pi \int_{\text{x}} \left[(\partial_{\text{x}} \phi_{\text{x}}) (\partial_{\text{x}} \theta_{\text{x}})^2 + i (\partial_{\text{x}} \phi_{\text{x}} \partial_{\text{x}}^2 \theta_{\text{x}} + \partial_{\text{x}} \theta_{\text{x}} \partial_{\text{x}}^2 \phi_{\text{x}}) \right]. \end{aligned} \quad (3.2.39)$$

The second term, proportional to i cancels exactly by partial integration and the only term left is the one that is cubic in the fields. As a consequence, we can write down the Hamiltonian of the system including band curvature terms, which reads

$$\begin{aligned} H_{\text{FL}} &= \frac{1}{2\pi} \int_{\text{x}} \left[v_{\text{F}} (\partial_{\text{x}} \theta_{\text{x}})^2 + \left(v_{\text{F}} + \frac{2g_0}{\pi} \right) (\partial_{\text{x}} \phi_{\text{x}})^2 + \frac{1}{\text{m}} (\partial_{\text{x}} \phi_{\text{x}}) (\partial_{\text{x}} \theta_{\text{x}})^2 + \frac{2g_0 \lambda^2}{\pi} (\partial_{\text{x}}^2 \phi_{\text{x}})^2 \right] \\ &= \frac{1}{2\pi} \int_{\text{x}} \left[\nu \text{K} (\partial_{\text{x}} \theta_{\text{x}})^2 + \frac{\nu}{\text{K}} (\partial_{\text{x}} \phi_{\text{x}})^2 + \frac{1}{\text{m}} (\partial_{\text{x}} \phi_{\text{x}}) (\partial_{\text{x}} \theta_{\text{x}})^2 + \frac{2g_0 \lambda^2}{\pi} (\partial_{\text{x}}^2 \phi_{\text{x}})^2 \right], \end{aligned} \quad (3.2.40)$$

where we introduced the fermionic Luttinger parameters

$$\nu = v_{\text{F}} \sqrt{1 + \frac{2g_0}{\pi v_{\text{F}}}}, \quad \text{and} \quad \text{K} = \sqrt{1 + \frac{2g_0}{\pi v_{\text{F}}}}^{-1}. \quad (3.2.41)$$

As for the bosons, there is a quadratic term, reflecting the elementary excitations, which are phonons with a linear dispersion, a Bogoliubov term that leads to a quadratic correction of the dispersion for larger momenta and a cubic interaction term that stems from the non-zero band curvature of the microscopic fermions. As for the bosons, the Bogoliubov term will play no role in our considerations since for an out of equilibrium setup, the band curvature is much more relevant and it is less irrelevant in the renormalization group sense than the Bogoliubov term. We can therefore write the interacting Luttinger model for fermions by dropping this term as

$$H_{\text{ILL}} = \frac{1}{2\pi} \int_{\text{x}} \left[\nu \text{K} (\partial_{\text{x}} \theta_{\text{x}})^2 + \frac{\nu}{\text{K}} (\partial_{\text{x}} \phi_{\text{x}})^2 + \frac{1}{\text{m}} (\partial_{\text{x}} \phi_{\text{x}}) (\partial_{\text{x}} \theta_{\text{x}})^2 \right]. \quad (3.2.42)$$

The difference to the bosonic model is only in the microscopic definitions of the Luttinger parameters and the corresponding operators but the Hamiltonian is exactly the same. In the next section, we will see that the Keldysh action of the interacting Luttinger model for fermions is as well exactly the same as for bosons and compute the fermionic response and correlation functions in the Keldysh framework.

3.2.2 Keldysh Path Integral for Fermionic Luttinger Liquids and Fermionic Correlation Functions

In order to study systems of interacting one-dimensional fermions, we derive the Keldysh path integral for the corresponding Luttinger Liquid theory, described by the Hamiltonian (3.2.42). Following the derivation of the Keldysh path integral formalism in chapter 1. Accordingly, the action on the (\pm) -contour is

$$\mathcal{S} = \int_{\mathbf{X}} \sum_{\alpha, \eta = \pm} [\bar{\psi}_{\alpha, \eta, \mathbf{X}} \alpha i \partial_t \psi_{\alpha, \eta, \mathbf{X}}] - \mathbf{H}_{\mathbf{F}}^+ + \mathbf{H}_{\mathbf{F}}^-, \quad (3.2.43)$$

where $\bar{\psi}_{\alpha, \eta, \mathbf{X}}, \psi_{\alpha, \eta, \mathbf{X}}$ are Grassmann fields on the (\pm) -contour. The index α labels the corresponding contour, $\alpha = \pm$ and the index $\eta = \pm$ labels right and left movers and $\mathbf{X} = (\mathbf{x}, t)$. $\mathbf{H}_{\mathbf{F}}^{\pm}$ is the Grassmann functional of the Hamiltonian (3.2.5) from the previous section. The representation of the fermionic Grassmann variables in terms of the Luttinger fields ϕ, θ is directly inferred from the representation in operator space (Eq. (3.2.27))

$$\psi_{\alpha, \eta, \mathbf{X}} = \frac{\xi_{\alpha, \eta}}{\sqrt{2\pi}} e^{i\eta k_{\mathbf{F}} \mathbf{x}} e^{-i(\eta \phi_{\alpha, \mathbf{X}} - \theta_{\alpha, \mathbf{X}})}. \quad (3.2.44)$$

Here, the variable $\xi_{\alpha, \eta}$ is a global contour dependent Grassmann variable, ensuring Grassmann commutation relations of the individual fermionic variables. The time derivative of the Grassmann fields is

$$\begin{aligned} \sum_{\eta = \pm} \bar{\psi}_{\alpha, \eta, \mathbf{X}} i \partial_t \psi_{\alpha, \eta, \mathbf{X}} &= \sum_{\eta = \pm} \rho_{\alpha, \eta, \mathbf{X}} (\eta \partial_t \phi_{\alpha, \mathbf{X}} - \partial_t \theta_{\alpha, \mathbf{X}}) \\ &= (\rho_{\alpha, +, \mathbf{X}} - \rho_{\alpha, -, \mathbf{X}}) \partial_t \phi_{\alpha, \mathbf{X}} - (\rho_{\alpha, +, \mathbf{X}} + \rho_{\alpha, -, \mathbf{X}}) \partial_t \theta_{\alpha, \mathbf{X}} \\ &= \frac{1}{\pi} (\partial_x \theta_{\alpha, \mathbf{X}} \partial_t \phi_{\alpha, \mathbf{X}} + \partial_x \phi_{\alpha, \mathbf{X}} \partial_t \theta_{\alpha, \mathbf{X}}), \end{aligned} \quad (3.2.45)$$

where we inserted the real field $\rho_{\alpha, \eta, \mathbf{X}} = \bar{\psi}_{\alpha, \eta, \mathbf{X}} \psi_{\alpha, \eta, \mathbf{X}}$ and applied the relations (3.2.29), (3.2.30) for real fields on the (\pm) -contour. In the same way, following the transformation rules in the previous section and extending them straightforward to Grassmann variables, we can substitute $\mathbf{H}_{\mathbf{F}}^{\alpha}$ by the corresponding version of the Luttinger Hamiltonian $\mathbf{H}_{\text{ILL}}^{\alpha}$ in Eq. (3.2.42). This leads to the action on the (\pm) -contour

$$\mathcal{S} = \sum_{\alpha = \pm} \alpha \left(\pi \int_{\mathbf{X}} (\partial_x \theta_{\alpha, \mathbf{X}} \partial_t \phi_{\alpha, \mathbf{X}} + \partial_x \phi_{\alpha, \mathbf{X}} \partial_t \theta_{\alpha, \mathbf{X}}) - \mathbf{H}_{\text{ILL}}^{\alpha} \right), \quad (3.2.46)$$

with

$$\mathbf{H}_{\text{ILL}}^{\alpha} = \frac{1}{2\pi} \int_{\mathbf{X}} \left[\nu K (\partial_x \theta_{\alpha, \mathbf{X}})^2 + \frac{\nu}{K} (\partial_x \phi_{\alpha, \mathbf{X}})^2 + \frac{1}{m} (\partial_x \phi_{\alpha, \mathbf{X}}) (\partial_x \theta_{\alpha, \mathbf{X}})^2 \right]. \quad (3.2.47)$$

As a result, after the Keldysh rotation, we obtain the identical Keldysh action for one-dimensional fermions as we did for one-dimensional bosons in Eq. (3.1.24) and all the corresponding transformations, i.e. the change to the phonon variables as given in Eqs. (3.1.28), (3.1.29) are equivalent.

In the remainder of this section, we will derive the expressions for fermionic real time Green's functions in the Luttinger-Keldysh framework. As we will perform all computations in the phonon representation, we start with relating the retarded, advanced and Keldysh Green's functions in the $\theta - \phi$ basis in terms of phonon Green's functions. The

corresponding transformation to the phonon basis is given in Eqs. (3.1.26) and (3.1.27) and in the momentum representation read

$$\phi_{\alpha, Q} = -\frac{i}{2} \left(\frac{2\pi K}{|q|} \right)^{\frac{1}{2}} \text{sgn}(q) (\bar{a}_{\alpha, Q} + a_{\alpha, -Q}) \quad (3.2.48)$$

$$\theta_{\alpha, Q} = \frac{i}{2} \left(\frac{2\pi}{K|q|} \right) (\bar{a}_{\alpha, Q} - a_{\alpha, -Q}), \quad (3.2.49)$$

where $Q = (q, \omega)$ is the combined momentum and frequency index and $\alpha = c, q$ is the Keldysh index. As we see from the definition of the fields ϕ and θ in Eqs. (3.2.29), (3.2.30), they are defined independently of the specific model parameters. On the other hand, the transformation to the phonon basis is a function of the Luttinger parameter K and therefore depends on the specific value of v_F and g_0 in the Hamiltonian. Therefore, the Green's functions in the $\theta - \phi$ basis are related to the fermionic observables independent of the model. In terms of phonon Green's functions they are

$$G_{\phi\phi}^{\alpha\beta}(Q) = -i \langle \phi_{\alpha, -Q} \phi_{\beta, Q} \rangle = \frac{\pi K}{2|q|} \left(G_Q^{\alpha\beta} + G_{-Q}^{\beta\alpha} + \Gamma_Q^{\alpha\beta} + \left(\Gamma_Q^{\alpha\beta} \right)^* \right), \quad (3.2.50)$$

$$G_{\theta\theta}^{\alpha\beta}(Q) = -i \langle \theta_{\alpha, -Q} \theta_{\beta, Q} \rangle = \frac{\pi}{2K|q|} \left(G_Q^{\alpha\beta} + G_{-Q}^{\beta\alpha} - \Gamma_Q^{\alpha\beta} - \left(\Gamma_Q^{\alpha\beta} \right)^* \right), \quad (3.2.51)$$

$$G_{\phi\theta}^{\alpha\beta}(Q) = -i \langle \phi_{\alpha, -Q} \theta_{\beta, Q} \rangle = -\frac{\pi}{2q} \left(G_Q^{\alpha\beta} - G_{-Q}^{\beta\alpha} + \Gamma_Q^{\alpha\beta} - \left(\Gamma_Q^{\alpha\beta} \right)^* \right), \quad (3.2.52)$$

$$G_{\theta\phi}^{\alpha\beta}(Q) = G_{\phi\theta}^{\beta\alpha}(-Q). \quad (3.2.53)$$

Here, we have introduced the normal and anomalous phonon Green's functions in frequency space

$$G_Q^{\alpha\beta} = -i \langle a_{\alpha, Q} \bar{a}_{\beta, Q} \rangle, \quad (3.2.54)$$

$$\Gamma_Q^{\alpha\beta} = -i \langle \bar{a}_{\alpha, -Q} \bar{a}_{\beta, Q} \rangle. \quad (3.2.55)$$

In order to determine fermionic Green's functions in terms of the phonon Green's functions above, we have to keep in mind the order of transformations. The transformation to the Luttinger basis has been performed in real space and on the (\pm) -contour. Although the mapping between Luttinger and fermionic variables is unique, it is not unitary and therefore does not commute with the Keldysh rotation and the Fourier transformation. We will therefore express the fermion Green's functions on the (\pm) contour and in real space and subsequently perform the transformation to Keldysh and momentum space in terms of the Luttinger variables.

The fermionic lesser, greater Green's functions for η -movers are

$$G_{\eta, X, X'}^< = -i \langle \bar{\psi}_{-, \eta, X'} \psi_{+, \eta, X} \rangle = \frac{e^{-i\eta k_F(x-x')}}{2\pi} \langle e^{i(\eta\phi_{+, X'} - \theta_{+, X'} - \eta\phi_{-, X} + \theta_{-, X})} \rangle \quad (3.2.56)$$

$$G_{\eta, X, X'}^> = -i \langle \psi_{-, \eta, X} \bar{\psi}_{+, \eta, X'} \rangle = \frac{e^{-i\eta k_F(x-x')}}{2\pi} \langle e^{i(\eta\phi_{-, X'} - \theta_{-, X'} - \eta\phi_{+, X} + \theta_{+, X})} \rangle. \quad (3.2.57)$$

Here, we again used the contour label (\pm) for fermionic Grassmann fields and two distinct spatio-temporal coordinates X, X' . In order to evaluate the expectation value of the exponential, we approximate its value by its first order cumulant expansion, which becomes exact for a quadratic action and it becomes a very good approximation for well-defined

quasi-particles even in the presence of interactions⁷. The expectation values of the exponentials are

$$G_{\eta,X,X'}^< = \frac{e^{-i\eta k_F(x-x')}}{2\pi} e^{-\frac{1}{2}\langle(\eta\phi_{+,X'}-\theta_{+,X'}-\eta\phi_{-,X}+\theta_{-,X})^2\rangle} = \frac{e^{-i\eta k_F(x-x')}}{2\pi} e^{-\frac{1}{2}\mathcal{G}_{\eta,X,X'}^<}. \quad (3.2.58)$$

In the Keldysh basis, the exponent $\mathcal{G}_{\eta,X,X'}^<$ can be evaluated and reads

$$\begin{aligned} 2\mathcal{G}_{\eta,X,X'}^< &= 2\langle(\eta\phi_{+,X'} - \theta_{+,X'} - \eta\phi_{-,X} + \theta_{-,X})^2\rangle \\ &= G_{\theta\theta,X',X'}^K + G_{\theta\theta,X,X}^K - 2G_{\theta\theta,X',X}^K + 2G_{\theta\theta,X,X'}^A - 2G_{\theta\theta,X,X'}^R \\ &\quad + G_{\phi\phi,X',X'}^K + G_{\phi\phi,X,X}^K - 2G_{\phi\phi,X',X}^K + 2G_{\phi\phi,X,X'}^A - 2G_{\phi\phi,X,X'}^R \\ &\quad + 2\eta(G_{\theta\phi,X,X'}^K + G_{\phi\theta,X,X'}^K + G_{\theta\phi,X,X'}^R + G_{\phi\theta,X,X'}^R - G_{\theta\phi,X,X'}^A - G_{\phi\theta,X,X'}^A). \end{aligned} \quad (3.2.59)$$

In a similar way, one can derive the expression for the fermionic greater Green's function. From now on, we will consider a translational invariant system, for which the Green's functions only depend on the difference $x - x'$. This is clearly the case for a homogeneous Luttinger Liquid as we consider in this thesis. On the other hand, systems out of equilibrium are no longer time translational invariant, so we cannot express the Green's functions only in terms of the relative time $t - t'$. However, for the purpose of describing out of equilibrium systems, it is very useful to introduce forward and relative time coordinates according to

$$\tau = \frac{t + t'}{2} \text{ and } \delta t = t - t'. \quad (3.2.60)$$

In doing so, the Green's functions can be expressed in terms of relative spatio-temporal coordinates and the absolute time,

$$G_{X,X'} = G_{\tau,\delta X}, \quad (3.2.61)$$

where $\delta X = X - X' = (x - x', t - t') = (\delta x, \delta t)$. We will from now on skip the δ and use x, t for the relative space and time coordinates and τ for the absolute time coordinate. In terms of the new coordinates, the exponent in the Keldysh basis (3.2.59) is rewritten according to

$$\begin{aligned} \mathcal{G}_{\eta,\tau,X}^< &= G_{\theta\theta,\tau,0}^K - G_{\theta\theta,\tau,X}^K + G_{\theta\theta,\tau,X}^A - G_{\theta\theta,\tau,X}^R \\ &\quad + G_{\phi\phi,\tau,0}^K - G_{\phi\phi,\tau,X}^K + G_{\phi\phi,\tau,X}^A - G_{\phi\phi,\tau,X}^R \\ &\quad + \eta(G_{\theta\phi,\tau,X}^K + G_{\phi\theta,\tau,X}^K + G_{\theta\phi,\tau,X}^R + G_{\phi\theta,\tau,X}^R - G_{\theta\phi,\tau,X}^A - G_{\phi\theta,\tau,X}^A). \end{aligned} \quad (3.2.62)$$

In the next step, we will express the exponent in terms of the Fourier transformed (with respect to the relative coordinates) Green's functions

$$\begin{aligned} \mathcal{G}_{\eta,\tau,X}^< &= \int_Q ((1 - \cos(qx) \cos(\omega t)) G_{\theta\theta,\tau,Q}^K - i \sin(\omega t) \cos(qx) (G_{\theta\theta,\tau,Q}^A - G_{\theta\theta,\tau,Q}^R)) \\ &\quad + \int_Q ((1 - \cos(qx) \cos(\omega t)) G_{\phi\phi,\tau,Q}^K - i \sin(\omega t) \cos(qx) (G_{\phi\phi,\tau,Q}^A - G_{\phi\phi,\tau,Q}^R)) \\ &\quad + 2i\eta \int_Q (\sin(\omega t) \sin(qx) G_{\theta\phi,\tau,Q}^K + \cos(\omega t) \sin(qx) (G_{\phi\theta,\tau,Q}^R + G_{\phi\theta,\tau,-Q}^A)). \end{aligned} \quad (3.2.63)$$

⁷Technically, the first order cumulant expansion is exact, if higher order Green's functions factorize. The correction term to the first order expansion is proportional to irreducible higher order correlation functions, which are typically negligibly small even for interacting Luttinger Liquids [122, 183, 74, 1, 80, 67].

Of major interest for our further analysis will be the fermionic lesser Green's function with non-zero absolute time but vanishing relative time. It is for instance necessary to determine the fermionic distribution function and the scaling behavior of equal-time correlation functions in real space. For zero relative time, the exponent reads

$$\begin{aligned} \mathcal{G}_{\eta,\tau,x}^< &= \int_Q ((1 - \cos(qx)) (G_{\theta\theta,\tau,Q}^K + G_{\phi\phi,\tau,Q}^K)) \\ &+ 2i\eta \int_Q \sin(qx) (G_{\phi\theta,\tau,Q}^R + G_{\phi\theta,\tau,-Q}^A). \end{aligned} \quad (3.2.64)$$

We will apply this transformation in the following sections in order to determine the fermionic correlations in a system, which has been initialized in a out of equilibrium state and will finish this section with a discussion of the fermionic equilibrium Green's function.

3.2.3 Equilibrium Fermion Green's Functions and $T = 0$ Scaling Behavior

We will now evaluate the Green's functions for interacting fermions in one-dimension for the case of thermal equilibrium. In this case, the bosonic excitations b_q^\dagger, b_q are distributed according to a Bose-Einstein distribution. Since the Hamiltonian doesn't contain any anomalous terms $\propto b_q^\dagger b_{-q}^\dagger$, their occupation is zero in equilibrium and the anomalous Green's functions $\Gamma = 0$. In the equilibrium case, the Green's functions do not depend on the forward time and we find (see Eq. (3.2.50))

$$\int_\omega G_{\phi\phi,Q}^K = G_{\phi\phi,q,t=0}^K = \frac{\pi K}{2|q|} (G_{q,t=0}^K + G_{-q,t=0}^K) = \frac{\pi K}{|q|} (2n_q + 1) e^{-\frac{|q|}{\Lambda}} \quad (3.2.65)$$

for the Keldysh Green's function, where n_q is the distribution function of the phonon excitations and

$$\int_\omega G_{\phi\theta,Q}^R = G_{\phi\theta,q,t=0}^R = -\frac{\pi}{2q} (G_{q,t=0}^R - G_{q,t=0}^A) = -\frac{\pi}{2q} e^{-\frac{|q|}{\Lambda}}. \quad (3.2.66)$$

The $\theta\theta$ -correlation function follows immediately by taking $K \rightarrow \frac{1}{K}$ in (3.2.65) and so

$$\begin{aligned} \mathcal{G}_{\eta,x}^< &= \pi \left(K + \frac{1}{K} \right) \int_q \frac{(1 - \cos(qx))}{|q|} (2n_q + 1) e^{-\frac{|q|}{\Lambda}} \\ &- i\eta\pi \int_q \frac{\sin(qx)}{q} e^{-\frac{|q|}{\Lambda}}. \end{aligned} \quad (3.2.67)$$

At zero temperature, $n_q = 0$ since the ground state of the system is excitation free. The integrals can be evaluated and yield

$$\mathcal{G}_{\eta,x}^< = \frac{1}{2} \left(K + \frac{1}{K} \right) \log(1 + x^2 \Lambda^2) - 2i\eta \arctan(\Lambda x). \quad (3.2.68)$$

After some calculations, this leaves us with the fermionic lesser Green's function

$$G_{x,t=0}^< = \frac{1}{2\pi} e^{-i\eta k_F x} e^{-\frac{1}{2}\mathcal{G}_{\eta,x}^<} = \frac{1}{2\pi} e^{-i\eta(k_F x - \arctan(\Lambda x))} (1 + x^2 \Lambda^2)^{-\frac{1+K^2}{4K}}. \quad (3.2.69)$$

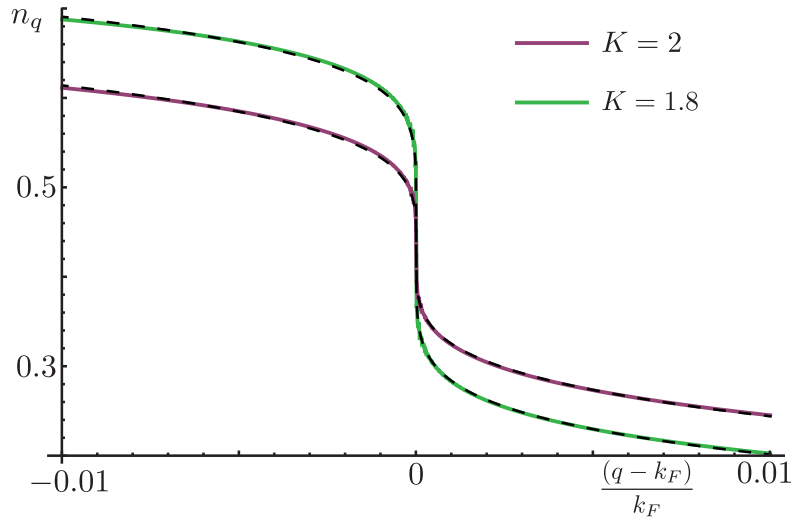


Figure 3.1: Fermionic density n_q^F in momentum space, obtained from Eq. (3.2.70), for two different Luttinger parameters $K_1 = 2, K_2 = 1.8$, corresponding to two different interaction strengths. Visible is the absence of a jump of the distribution function at the Fermi momentum $q = k_F$ and the algebraic divergence at the Fermi momentum. The dashed lines represent analytic functions $f_{1,2} = c_{1,2} - d_{1,2} \text{sgn}(q - k_F) |q - k_F|^{\frac{(K_{1,2}-1)^2}{2K_{1,2}}}$, where the parameters c, d are non-universal fit parameters.

This reveals the algebraic decay of the fermionic correlation function in real space, which for long distances is $\sim x^{-\frac{1+K^2}{2K}}$. For non-interacting fermions, at $K = 1$, one recovers the canonical scaling of the fermionic correlation function $\sim x^{-1}$, which corresponds to a one-dimensional density. The term $\sim \arctan(\Lambda x)$ is crucial as it implements the step function in the fermionic density in the momentum space representation, i.e. in

$$n_q^F = \int_x e^{iqx} G_{x,t=0}^< = \int_x \frac{1}{2\pi} e^{-i\eta((k_F - q)x - \arctan(\Lambda x))} (1 + x^2 \Lambda^2)^{-\frac{1+K^2}{4K}}. \quad (3.2.70)$$

Close to the Fermi momentum, this function scales as $n_q \sim |q - k_F|^{\frac{1+K^2}{2K} - 1} = |q - k_F|^{\frac{(K-1)^2}{2K}}$. Indicating the absence of a Fermi edge in interacting one-dimensional systems. In fact, the fermionic quasi-particle residue Z , which is the jump of the fermionic distribution function at the Fermi momentum is $Z = 0$ for $K \neq 1$, i.e. for interacting fermions in one dimension⁸. In Fig. 3.2.3, we show the distribution function $n_q = \langle \psi_q^\dagger \psi_q \rangle$ for the right movers for two different Luttinger parameters $K_1 = 2, K_2 = 1.8$

⁸This is in stark contrast to higher dimensional interacting fermions, where Fermi Liquid theory predicts $0 < Z < 1$ for interacting fermions. As Fermi Liquid theory relies on well-defined fermionic quasi-particles at $q = k_F$, this means that it is definitely not applicable in one dimension.

4 KINETIC THEORY FOR INTERACTING LUTTINGER LIQUIDS

In this chapter, we derive a closed set of equations for the kinetics and non-equilibrium dynamics of interacting Luttinger Liquids with cubic resonant interactions. In the presence of these interactions, the Luttinger phonons become dressed but still well defined quasi-particles, characterized by a lifetime much larger than the inverse energy. This enables the separation of forward time dynamics and relative time dynamics into slow and fast dynamics and justifies the so-called Wigner approximation, which can be seen as a "local-time approximation" for the relative dynamics. Applying field theoretical methods in the Keldysh framework, i.e. kinetic and Dyson-Schwinger equations, we derive a closed set of dynamic equations, describing the kinetics of normal and anomalous phonon densities, the phonon self-energy and vertex corrections for an arbitrary non-equilibrium initial state. In the limit of low phonon densities, the results from self-consistent Born approximation are recaptured, including Andreev's scaling solution for the quasi-particle lifetime in a thermal state. As an application, we compute the relaxation of an excited state to its thermal equilibrium. While the intermediate time dynamics displays exponentially fast relaxation, the last stages of thermalization are governed by algebraic laws. This can be traced back to the importance of energy and momentum conservation at the longest times, which gives rise to dynamical slow modes.

4.1 INTRODUCTION

The kinetics and non-equilibrium dynamics of low dimensional, interacting quantum systems is an outstanding and fascinating challenge in quantum many-body physics [33, 189]. On the one hand, it is strongly motivated by recent cold atom experiments performed on low entropy quantum wires under out-of-equilibrium conditions [111, 74, 122, 183, 197, 132, 172]. On the other hand, from a theoretical point of view, the study of non-equilibrium dynamics in integrable and non-integrable systems is currently a field of growing interest [39, 30, 37]. This is triggered by the question, whether and – if answered affirmatively – in which specific way a one-dimensional quantum system is able to thermalize [17].

An example of a one-dimensional integrable model is the linear Luttinger Liquid, which is the effective long-wavelength description of one-dimensional interacting quantum fluids, composed either of fermions or bosons [80, 67]. Due to integrability, even if prepared in a non-equilibrium state, this model will never thermalize, since the number of excitations

for each momentum mode q is a constant of motion [39]. However, as already pointed out by Andreev and Haldane [8, 80], there are non-zero corrections to the linear theory, which certainly break integrability in the Luttinger model. They are irrelevant in the sense of the renormalization group, and do not affect static observables. In contrast, they lead to a modification of dynamical, i.e. frequency resolved, correlation functions. These nonlinear corrections describe three-body scattering processes between phonons and are, due to their resonant nature, not straightforwardly approached theoretically.

Apart from a wealth of numerical studies [36, 150, 151, 60, 201, 32, 177, 156], based on matrix product state and Bethe ansatz calculations, several field theoretical approaches have been developed [176, 145, 162, 110, 173, 91, 168, 169]. A seminal early study was carried out by Andreev, who used a self-consistent Born approximation to determine the phonon self-energies, establishing a universal phonon absorption rate $\gamma_q \sim q^\eta$ with exponent $\eta = \frac{3}{2}$ for a finite temperature system [120, 198, 12]. A similar computation leads to an exponent $\eta = 2$ for the case of a zero temperature state [161], which has been verified by several numerical methods [150]. Recently, so-called nonlinear Luttinger Liquids have been introduced, which are designed to capture corrections to the linear Luttinger theory in the context of one dimensional fermions systems [93, 94, 162, 110]. These have been very successful in determining, for example, the power law divergences of the dynamic structure factor, or thermalization rates for near equilibrium systems [93]. Despite the large number of analytic and semi-analytic works [107, 103, 136, 158, 39, 40], only few approaches for far from equilibrium dynamics have been developed so far [137, 159, 194].

The purpose of this chapter is to provide a quantitative description of the kinetics of an interacting Luttinger Liquid. Strong motivation comes from a recent surge of experiments with interacting one-dimensional bosons and fermions in ultracold atom setups performed under out-of-equilibrium conditions [122, 74, 172, 132, 86]. Here a one-dimensional quantum fluid is prepared in a true non-equilibrium state, and the experiment subsequently witnesses the time evolution of the system. At the present stage, the systems' properties are still well described by linear Luttinger Liquid theory with, however, a time dependent, far from equilibrium distribution function [122, 74, 172, 183]. So far, there are numerous theoretical works which describe these systems in terms of non-interacting Luttinger liquids alone, where there is only dephasing dynamics and the evolution of the distribution function is absent [39, 107, 121, 1]. This describes well the prethermalized regime in the shorter time dynamics. However, current experiments are steadily pushed to larger observation times, where the thermalization crossover caused by the residual (RG irrelevant) interactions in the Luttinger liquid should occur. What is therefore lacking at present in the theoretical literature, is a kinetic theory for the time evolution of the distribution function in these systems, which is able to track such a crossover and the associated time scales. This is the aim of the present chapter.

On the technical side, achieving our goal amounts to obtaining theoretical control over the infrared divergences inherent to naive perturbation theory for the interacting Luttinger Liquid. While this issue was solved for the stationary equilibrium (or near equilibrium, in the sense of linear response) long time ago by Andreev and others [8, 176, 161], we focus here on getting this problem under control in the kinetic equation, initialized with a general Gaussian non-equilibrium distribution function.

In more detail, exploiting the resonant but subleading character of the interactions in a one-dimensional interacting quantum fluid, we apply non-equilibrium diagrammatic theory to solve for the non-equilibrium dynamics of an interacting Luttinger Liquid. We show that due to the resonant but subleading nature of the interactions, vertex corrections are moderate for many physical realizations and consequently the non-equilibrium dynamics and self-energy can be solved within self-consistent Born approximation. The self-consistency is however, crucial, and a perturbative Born approach leads to infrared divergences. The result is an effectively closed set of equations for the time-dependent phonon density and self-energy in the presence of resonant interactions. This approach, without considering the vertex correction and restricted to equilibrium systems, has been shown to work also for non-interacting one-dimensional dispersive fermions [10] and in the context of the Coulomb drag effect for sufficiently low temperatures [163].

As a major result of the RG irrelevant but resonant interactions, the excitations remain well-defined but dressed phonons, with a lifetime τ_q much larger than their typical coherent time-scale ϵ_q^{-1} . The dressed spectral function remains sharply peaked at the bare phonon energies ϵ_q with width τ_q^{-1} , such that the self-energy and distribution function of the phonons for frequencies sufficiently close to the on-shell frequency can be approximated by their on-shell value. This is referred to as the quasi-particle approximation. The long lifetime of the dressed phonons results in a further simplification, as it implies that the forward time evolution of the system is much slower than the relative time evolution. This decoupling leads to a "local time approximation", where an effectively stationary problem can be solved at each instant of time. We will quantify the validity of these approximations in terms of general but state dependent quantitative bounds below.

Our estimate of the vertex correction further supports the validity of the self-consistent Born approximation for the time evolution. More precisely, for zero temperature states, the vertex correction vanishes identically, reproducing previous results [63]. For the special case of a finite temperature state, the loop correction leads to a finite but small multiplicative renormalization of the vertex. This implies that for typical translation invariant low entropy initial states, the equations governing the time evolution of the phonon occupation and the self-energy are effectively closed. It does not rule out, however, the possibility of significant vertex renormalization in general.

The strength of this approach is the simplicity of the resulting final equations, which can directly be implemented and solved numerically, as we demonstrate by first explicit examples. This provides a useful tool with a broad spectrum of applicability, ranging from tracking the thermalization process of non-integrable, weakly interacting Bose and Fermi gases to the study of interacting open system dynamics [57, 177, 156, 155]. It is suited for an initial state of a general Gaussian form with arbitrary, non-zero phonon densities, including diagonal and off-diagonal occupations.

The structure of the kinetic equation and the equations for the self-energy and vertex correction reveal strong aspects of universal behavior. This concerns two key points: First, for a sufficiently strongly decreasing occupation they are independent of the short distance cutoff of the Luttinger liquid, and thus of microscopic details inherited from even shorter length scales. This property emerges via a "bootstrap" mechanism within the self-consistent Born approximation, as we elaborate on in the main text. Second, after a proper rescaling of time¹, all microscopic parameters are completely eliminated from the dynamic equations. Consequently and remarkably, the only microscopic information that enters the dynamics is the initial phonon density at $t = 0$.

At this point, we also mention three limitations of our approach, which however are not directly physically relevant for the ultracold atomic systems we are targeting. First, as already briefly mentioned above, our setting is restricted to initial quantum states with Gaussian, although in general far-from-equilibrium correlations. Such conditions have been discussed extensively in previous works [39, 137, 107, 122, 74, 172], mostly for the case of linear Luttinger Liquids generating the subsequent dynamics. However, should non-Gaussian initial conditions be accessible in future experiments, it would be possible to combine our techniques with those of Refs [76, 75] addressing precisely this issue. Second, our method is not suited to describe the asymptotic infrared behavior of a one-dimensional quantum fluid, where for the smallest momenta² it has been shown that the elementary excitations are fermions [162, 110, 168, 131, 169] with a strongly suppressed decay rate $\gamma \sim k^8$. Third, it doesn't work for frequencies (or temperatures) above the Luttinger cutoff, where the dominant interaction is given by scattering between Luttinger phonons and mobile electronic impurities [91, 92, 93, 94]. However, the range of validity of our approach coincides perfectly with cold atom experiments, which consider momenta $10^{-2}\Lambda < p < \Lambda$ and temperatures $k_B T < \hbar u \Lambda$, where u is the sound velocity and Λ the Luttinger cutoff. The Luttinger cutoff scale is given by the chemical potential for these experiments, $\Lambda \approx \sqrt{2gn_0}$ for weak interactions g , and n_0 the mean density. The infrared restriction of the

¹According to $t \rightarrow \frac{t}{v_0}$, where v_0 is the strength of the nonlinearity.

²For momenta $k \ll \sqrt{K}\Lambda$, where K is the Luttinger parameter and Λ the Luttinger cutoff.

momentum range results from typical trap sizes, with oscillator lengths roughly two orders of magnitude larger than $1/\Lambda$. This discards precision measurements of frequency resolved observables in these extreme infrared asymptotic regimes, and thus is not of foremost interest for our study.

The remainder of the chapter is organized as follows. In Sec. 4.2, we introduce and briefly discuss the action of the interacting Luttinger model in the phonon representation and in the Keldysh non-equilibrium framework. In Sec. 4.3, we derive the non-equilibrium fluctuation-dissipation relation (FDR) and determine the phonon self-energies in self-consistent Born approximation for an arbitrary phonon distribution. Furthermore, we discuss the necessary approximations and quantify their justification. Subsequently, taking advantage of Sec. 4.3, we determine the kinetic equation for the phonon density in self-consistent Born approximation in Sec. 4.4. In Sec. 4.5, we take into account non-zero off-diagonal (anomalous) phonon densities and show in which way the kinetic equation and the phonon self-energy are modified in their presence. Additionally, we derive a kinetic equation for the anomalous phonon densities. These results are applied in Sec. 4.6 to determine the relaxation of an excited, thermal state back to thermal equilibrium. Furthermore, the analytically obtained relaxation rate is compared to the numerical value, showing excellent agreement. Finally, in Sec. 4.7, we go beyond the self-consistent Born approximation and apply Dyson-Schwinger equations to take into account a non-zero vertex correction. We determine a closed set of equations for the kinetic equation, self-energy and vertex correction for arbitrary states, and discuss the effect of the latter.

4.2 MODEL

The action describing the interacting Luttinger model consists of two parts (we set $\hbar = 1$)

$$S = S_{\text{TL}} + S_{\text{Int}}. \quad (4.2.1)$$

Here, S_{TL} is the well-known quadratic Tomonaga-Luttinger (TL) action [196, 128, 80]

$$S_{\text{TL}} = \frac{1}{2\pi} \int_{\mathbf{x},t} \left[(\partial_{\mathbf{x}}\phi) (\partial_t\theta) - uK (\partial_{\mathbf{x}}\theta)^2 - \frac{u}{K} (\partial_{\mathbf{x}}\phi)^2 \right], \quad (4.2.2)$$

where $\int_{\mathbf{x},t} \equiv \int_{-\infty}^{\infty} dt dx$ is the integral over space and time and $\phi = \phi(\mathbf{x}, t)$ and $\theta = \theta(\mathbf{x}, t)$ are dimensionless, real fields. The non-linear part S_{Int} is cubic in the fields and reads [81]

$$S_{\text{Int}} = \frac{1}{2\pi} \int_{\mathbf{x},t} \left[\kappa_{\text{bc}} (\partial_{\mathbf{x}}\theta)^2 (\partial_{\mathbf{x}}\phi) + \kappa_{\text{qp}} (\partial_{\mathbf{x}}\phi)^3 \right]. \quad (4.2.3)$$

Starting from a microscopic derivation of the TL model as the effective long-wavelength description of interacting bosons or fermions in one dimension, the fields θ, ϕ represent local phase and density fluctuations [80, 67]. In this setting, we consider effective electron-electron (or boson-boson) interaction to be short ranged, i.e. of δ -function type [67]. The non-linearity corresponding to κ_{bc} as well is of microscopic origin and is referred to as band curvature. It originates from deviations from a perfectly linear dispersion of the microscopic particles. On the other hand, the term corresponding to κ_{qp} is generated in an effective long-wavelength description, where the fast modes have been integrated out already, and describes effective three-particle interactions.

The fields θ, ϕ are dimensionless, i.e. they have a canonical scaling dimension equal to zero. As a result, they do not scale when coarse graining to larger distances, i.e. when performing the rescaling

$$\mathbf{x} \rightarrow l\mathbf{x}, \quad t \rightarrow l^z t, \quad (4.2.4)$$

where $z = 1$ is the dynamical exponent and $l > 1$. In contrast

$$S_{\text{Int}} \rightarrow \frac{1}{2\pi l} S_{\text{Int}} \quad (4.2.5)$$

under the rescaling (4.2.4), such that the influence of S_{Int} vanishes on the longest wavelengths, i.e. it becomes irrelevant in the renormalization group (RG) sense. Consequently, the static equilibrium properties of the interacting Luttinger model (Eq. (4.2.1)) are well described by the quadratic part of the action alone and the partition function can be approximated by

$$Z = \int \mathcal{D}[\theta, \phi] e^{iS} \approx \int \mathcal{D}[\theta, \phi] e^{iS_{\text{TL}}}. \quad (4.2.6)$$

Here, $\int \mathcal{D}[\theta, \phi]$ stands for the functional integral over the fields θ, ϕ .

The Tomonaga-Luttinger action describes phonons with a dispersion $\epsilon_q = u|q|$ linear in the momentum $|q|$, propagating with the speed of sound u . In the absence of S_{Int} , these phonons are non-interacting and consequently the phonon density for a specific mode q is a conserved quantity. However, although the phonon interaction is irrelevant in the RG sense, it contains resonant processes where two phonons propagating in the same direction and the same speed of sound can interact with each other for an infinite time span. This leads to a non-trivial modification of time-dependent, dynamical observables compared to the case of non-interacting phonons. As pointed out in a seminal work by Andreev [8] (considering finite T) and more recent work [161, 150], the presence of S_{Int} leads to a finite phonon lifetime

$$\tau_q \sim |q|^{-\eta} \text{ with } \begin{cases} \eta = \frac{3}{2} & \text{for } T > 0 \\ \eta = 2 & \text{for } T = 0 \end{cases}, \quad (4.2.7)$$

which, in equilibrium, is visible only in dynamical, i.e. frequency dependent quantities such as the dynamical structure factor

$$S(q, \omega) = \int_{x,t} e^{i(\omega t - qx)} \langle (\partial_x \phi)_{x,t} (\partial_x \phi)_{0,0} \rangle, \quad (4.2.8)$$

with

$$\langle \dots \rangle = \frac{1}{Z} \int \mathcal{D}[\theta, \phi] \dots e^{iS}. \quad (4.2.9)$$

For dynamical quantities it is therefore important to take into account the full action, Eq. (4.2.1), instead of the reduced quadratic part only, as indicated in Eq. (4.2.6).

For a true non-equilibrium situation, the phonon distribution is not stationary, i.e. not a thermal or zero temperature distribution, but instead the phonon number n_q for a given momentum mode q becomes time-dependent. The redistribution of phonons between the different momentum modes with exact energy conservation is described by the resonant interactions in S_{Int} , and in a non-equilibrium situation the action can not be reasonably reduced to the quadratic Tomonaga-Luttinger action, for which the phonon density is a constant of motion.

Since we are interested in the non-equilibrium dynamics in the interacting TL model, we formulate the problem in a Keldysh path integral framework, which is able to treat both equilibrium and non-equilibrium dynamics on equal footing [106, 99, 101]. We will now shortly introduce the canonical Bogoliubov transformation, which switches from the basis

of real fields θ, ϕ to the basis of complex fields \bar{a}, a . Those correspond to creation and annihilation operators in an operator picture [67]. We close the model section by placing the action (4.2.1) on the Keldysh contour and briefly explaining the formalism.

4.2.1 Phonon Basis

In order to use a physically more appealing representation of the TL action, one commonly introduces a set of complex fields \bar{a}, a which represent the (bosonic) eigenmodes of the system, i.e. the discussed phonons. The corresponding Bogoliubov transformation is

$$\theta_{x,t} = \theta_0 + \frac{i}{2} \int_q \left(\frac{2\pi}{|q|K} \right)^{\frac{1}{2}} e^{-iqx} (\bar{a}_{q,t} - a_{-q,t}), \quad (4.2.10)$$

$$\phi_{x,t} = \phi_0 - \frac{i}{2} \int_q \left(\frac{2\pi K}{|q|} \right)^{\frac{1}{2}} \text{sgn}(q) e^{-iqx} (\bar{a}_{q,t} + a_{-q,t}), \quad (4.2.11)$$

with abbreviations $\phi_{x,t} = \phi(x, t)$ and $\int_q = \int_{-\infty}^{\infty} \frac{dq}{2\pi}$ and the Fourier transformed phonon fields

$$a_{q,t} = \int_x e^{-iqx} a_{x,t}. \quad (4.2.12)$$

The product $\bar{a}_{x,t} a_{x,t}$ represents a phonon density and, therefore, in the continuum limit, the fields $\bar{a}_{x,t}, a_{x,t}$ are not dimensionless, in contrast to $\phi_{x,t}, \theta_{x,t}$, but scale as $\bar{a}_{x,t} \sim \frac{1}{\sqrt{x}}$. The quadratic part of the action transforms into

$$S_{\text{TL}} = \frac{1}{2\pi} \int_{q,t} \bar{a}_{q,t} (i\partial_t - u|q|) a_{q,t}, \quad (4.2.13)$$

describing non-interacting phonons with a linear dispersion $\epsilon_q = u|q|$. The cubic part becomes

$$S_{\text{Int}} = \frac{1}{2\pi} \int_{q,p,t} v_{q,p,p+q} \sqrt{|qp(p+q)|} \\ \times \left(\bar{a}_{p+q,t} a_{q,t} a_{p,t} + \frac{a_{-q-p,t} a_{q,t} a_{p,t}}{3} + \text{h.c.} \right), \quad (4.2.14)$$

with the vertex function

$$v_{q,p,k} = \kappa_{bc} \sqrt{\frac{\pi}{2K}} \left(\frac{qp}{|qp|} + \frac{kp}{|kp|} + \frac{qk}{|qk|} \right) + \kappa_{qp} \sqrt{\frac{9K^3\pi}{2}}. \quad (4.2.15)$$

The interaction (4.2.14) describes cubic phonon scattering processes with total momentum conservation. However, not all of the processes contained in S_{Int} are resonant, i.e. exactly energy conserving in the sense that $\epsilon_{p+q} = \epsilon_q + \epsilon_p$. As explained by Andreev [8] and pointed out above, the resonant processes lead to a divergence of the self-energy (and the kinetic equation, as we see later) in perturbation theory and are therefore the only relevant terms from a dynamical perspective. The term in Eq. (4.2.14) describing the annihilation (creation) of three phonons can never be resonant. It will therefore play no role in our analysis and we will skip it from now on. For the residual terms, resonance requires $|p+q| = |p| + |q|$. For all momenta p, q fulfilling this condition, the vertex function

takes on the value

$$v_0 \equiv v_{1,1,1} = \sqrt{\frac{9\pi}{2K}} (\kappa_{bc} + K^2 \kappa_{qp}). \quad (4.2.16)$$

Consequently, instead of taking the full action S_{Int} , it is sufficient to consider the reduced but resonant phonon interaction

$$S_{\text{Res}} = \frac{v_0}{2\pi} \int'_{p,q,t} \sqrt{|pq(p+q)|} (\bar{a}_{p+q,t} a_{q,t} a_{p,t} + \text{h.c.}), \quad (4.2.17)$$

where the prime in $\int'_{p,q}$ indicates that the integral runs only over momenta q, p which have the same sign. Together the quadratic action and the resonant phonon interaction describe the dynamics of the interacting Luttinger model in the phonon basis,

$$S = S_{\text{TL}} + S_{\text{Res}}. \quad (4.2.18)$$

4.2.2 Keldysh Action

Non-equilibrium field theory is commonly performed in the Keldysh path integral framework, which is able to deal both with equilibrium and true non-equilibrium situations. To set up the Keldysh path integral, one first doubles the degrees of freedom in the theory by introducing plus and minus fields $a_{+,q,t}, a_{-,q,t}$, representing forward and backward time evolution on the Keldysh contour[99, 3]. In this representation, the partition function is determined via

$$Z = \int \mathcal{D}[a_+, a_-, \bar{a}_+, \bar{a}_-] e^{iS_+ - iS_-}, \quad (4.2.19)$$

where S_{\pm} is the phonon action (4.2.18) with the replacements $\{a_{p,t}, \bar{a}_{p,t}\} \rightarrow \{a_{\pm,p,t}, \bar{a}_{\pm,p,t}\}$. The \pm -representation contains redundancy, and a technically and physically more appealing representation is found by completing the transformation to the Keldysh representation, introducing classical and quantum fields according to

$$a_c = \frac{1}{\sqrt{2}} (a_+ + a_-), \quad a_q = \frac{1}{\sqrt{2}} (a_+ - a_-). \quad (4.2.20)$$

In the Keldysh representation, the quadratic action is

$$S^{(2)} = \frac{1}{2\pi} \int_{t,t',p} (\bar{a}_{p,t}^c, \bar{a}_{p,t}^q) \begin{pmatrix} 0 & D_{p,t,t'}^R \\ D_{p,t,t'}^A & D_{p,t,t'}^K \end{pmatrix} \begin{pmatrix} a_{p,t'}^c \\ a_{p,t'}^q \end{pmatrix}, \quad (4.2.21)$$

with the bare inverse retarded/advanced propagators

$$D_{p,t,t'}^R = \delta(t-t') (i\partial_{t'} - u|p| + i0^+), \quad (4.2.22)$$

$$D_{p,t,t'}^A = (D_{p,t,t'}^R)^\dagger = \delta(t-t') (i\partial_{t'} - u|p| - i0^+) \quad (4.2.23)$$

and the Keldysh component of the inverse propagator

$$D_{p,t,t'}^K = 2i0^+ F(p, t, t'). \quad (4.2.24)$$

Here, $F(p, t, t')$ is the distribution function of the excitations and 0^+ is the infinitesimal regularization for the quadratic theory [99]. In an equilibrium, i.e. time-translational invariant situation, $F(p, t, t') = F(p, t - t')$ and its Fourier transform is the bosonic distribution

$$F(p, \omega) = \coth\left(\frac{\omega}{2T}\right) = 2n_B(\omega) + 1 \quad (4.2.25)$$

with the Bose function $n_B(\omega) = \left(e^{\frac{\omega}{T}} - 1\right)^{-1}$. The resonant interactions in the Keldysh representation take on the form

$$\begin{aligned} S_{\text{Res}} = & \frac{v_0}{\sqrt{8\pi}} \int'_{p,k,t} \sqrt{|pk(k+p)|} \left[2\bar{a}_{k+p,t}^c a_{k,t}^c a_{p,t}^q \right. \\ & \left. + \bar{a}_{k+p,t}^q \left(a_{k,t}^c a_{p,t}^c + a_{k,t}^q a_{p,t}^q \right) + \text{h.c.} \right]. \end{aligned} \quad (4.2.26)$$

The bare response and correlation functions (retarded, advanced and Keldysh Green's functions) for the phonon degrees of freedom are obtained according to

$$\begin{aligned} G_{q,t,t'}^R &= -i\langle a_{q,t}^c \bar{a}_{q,t'}^q \rangle = (D^R)_{q,t,t'}^{-1} = -i\Theta(t-t') e^{-iu|q|(t-t')}, \\ G_{q,t,t'}^A &= -i\langle a_{q,t}^q \bar{a}_{q,t'}^c \rangle = (D^A)_{q,t,t'}^{-1} = i\Theta(t'-t) e^{-iu|q|(t-t')}, \\ G_{q,t,t'}^K &= -i\langle a_{q,t}^c \bar{a}_{q,t'}^c \rangle = -(G^R \circ D^K \circ G^A)_{q,t,t'} \\ &= -i(2n_B(u|q|) + 1) e^{-iu|q|(t-t')}. \end{aligned} \quad (4.2.27)$$

Here $\dots \circ \dots$ stands for the convolution in the non-diagonal elements, i.e. the time index, but means multiplication in momentum space.

In the presence of interactions, the Green's functions are modified by the emergence of non-zero self-energies $\Sigma^{R/A/K}$, which replaces the infinitesimal regularization. The corresponding formulas are

$$\begin{aligned} G_{q,t,t'}^R &= (D^R - \Sigma^R)_{q,t,t'}^{-1}, \\ G_{q,t,t'}^A &= (D^A - \Sigma^A)_{q,t,t'}^{-1}, \\ G_{q,t,t'}^K &= -(G^R \circ \Sigma^K \circ G^A)_{q,t,t'}, \end{aligned} \quad (4.2.28)$$

where the infinitesimal factor 0^+F has been overwritten by the finite Keldysh self-energy Σ^K . The distribution function F in the presence of interactions is determined by the formula

$$G_{q,t,t'}^K = (G^R \circ F - F \circ G^A)_{q,t,t'}. \quad (4.2.29)$$

This setting corresponds to the physical situation, in which a system is initialized at time $t = 0$ in a Gaussian density matrix ρ_0 (Gaussian in the bosonized language). It then evolves in time according to a Hamiltonian H , which constitutes the quadratic and cubic terms discussed in Eqs. (4.2.21) and (6.2.16). In the Keldysh setting, this dynamics is expressed in terms of the retarded and advanced quadratic and cubic parts of the action. The initial density matrix enters the action in terms of pure quantum vertices. In the present case, i.e. for purely Gaussian initial conditions, the initial density matrix is completely captured in terms of the distribution function F and Eq. (6.2.19). However, as has been pointed out recently, the bosonization procedure for interacting fermions or bosons out of equilibrium is in general not that simple, since initial conditions (even if quadratic in the microscopic

fermionic or bosonic picture) will, in principle, generate quantum vertices of arbitrary order [76, 75, 77, 78, 41], which have to be taken into account systematically for these cases. The aim of this work is to determine the self-energies $\Sigma^{\text{R/A/K}}$ and the distribution function $F(\mathbf{q}, t, t')$ for a system that is driven out of equilibrium and evolves in time, for instance relaxing to an equilibrium state and approaching a bosonic distribution.

This will be done in two parts. First, we show how one determines the self-energies $\Sigma^{\text{R/A/K}}$ from a given (non-) equilibrium distribution function $F(\mathbf{q}, t, t')$. To this end, we generalize Andreev's self-consistent Born approach to a non-thermal, non-equilibrium situation. Second, we use the kinetic equation approach to determine the time-evolution of the distribution function F in self-consistent Born approximation. Combining these two approaches allows us to determine the time-evolution of both the distribution function of the excitations and the self-energies, which play the role of finite lifetimes of the system's excitations.

4.3 SELF-ENERGIES

The presence of the cubic, resonant interactions S_{Res} modifies the phonon response and correlation functions according to Eqs. (4.2.28) by creating finite self-energies $\Sigma^{\text{R/A/K}}$. These self-energies are to leading order purely imaginary, leading to a finite decay rate of phonons or, in other words, to a finite phonon lifetime. We will now derive a method to determine these lifetimes for a non-equilibrium problem, where the distribution function $F(\mathbf{q}, t, t')$ is time dependent and varies on time scales which are larger than the individual phonon lifetimes. To this end, we first derive the non-equilibrium version of a fluctuation-dissipation relation for the two-point response and correlation functions.

4.3.1 Non-equilibrium Fluctuation-Dissipation Relation

Fluctuation-dissipation relations (FDR) relate the response (i.e. spectral) properties of the system encoded in $G^{\text{R/A}}$ to its correlations via the distribution function F . A particular example for such a relation is Eq. (4.2.29). Inverting this equation results in an FDR for the self-energies,

$$\begin{aligned}\Sigma_{\mathbf{q},t,t'}^{\text{K}} &= -((D^{\text{R}} - \Sigma^{\text{R}}) \circ F - F \circ (D^{\text{A}} - \Sigma^{\text{A}}))_{\mathbf{q},t,t'} \\ &= -i(\partial_t + \partial_{t'})F_{\mathbf{q},t,t'} + (\Sigma^{\text{R}} \circ F - F \circ \Sigma^{\text{A}})_{\mathbf{q},t,t'}.\end{aligned}\quad (4.3.1)$$

For a time-translational invariant system, the first term on the r.h.s. equals zero and due to the identity $\Sigma^{\text{A}} = (\Sigma^{\text{R}})^\dagger$, Eq. (4.3.1) reduces to the well-known relation in frequency space

$$\Sigma_{\mathbf{q},\omega}^{\text{K}} = -2i \text{Im}(\Sigma_{\mathbf{q},\omega}^{\text{R}}) F_{\mathbf{q},\omega}.\quad (4.3.2)$$

This is consistent with our initial regularization of the quadratic sector for the case $\Sigma^{\text{R}} = -i0^+$.

A useful representation for a two-time function $F(\mathbf{q}, t, t')$ is to choose Wigner coordinates in time, i.e. defining the forward time $\tau = \frac{t+t'}{2}$ and the relative time $\Delta_t = t - t'$ [99]. Then one defines $F(\mathbf{q}, \Delta_t, \tau) \equiv F(\mathbf{q}, \tau + \Delta_t/2, \tau - \Delta_t/2)$ and its Fourier transform

$$F(\mathbf{q}, \omega, \tau) = \int d\Delta_t e^{i\Delta_t\omega} F(\mathbf{q}, t, \tau).\quad (4.3.3)$$

Applying Wigner coordinates and the Wigner transformation (4.3.3) to the Keldysh self-energy in Eq. (4.3.2) leads to

$$\Sigma_{q,\omega,\tau}^K = -i\partial_\tau F_{q,\omega,\tau} + (\Sigma^R \circ F - F \circ \Sigma^A)_{q,\omega,\tau}. \quad (4.3.4)$$

Eq. (4.3.4) is an exact expression for the Keldysh self-energy in Wigner representation. A complication arises since the Wigner transform of a convolution is not the product of the corresponding Wigner transforms, in contrast to the ordinary Fourier transform. In fact, one finds

$$(\Sigma^R \circ F)_{q,\omega,\tau} = \Sigma_{q,\omega,\tau}^R e^{\frac{i}{2} \left(\overleftarrow{\partial}_\tau \overrightarrow{\partial}_\omega - \overleftarrow{\partial}_\omega \overrightarrow{\partial}_\tau \right)} F_{q,\omega,\tau}. \quad (4.3.5)$$

Without specific knowledge on the functional behavior of Σ^R and F , Eq. (4.3.5) is hard to evaluate explicitly. We will now briefly discuss a situation, with two particular approximations, which applies to the present model and for which the analytic evaluation of Eq. (4.3.5) is possible.

Wigner Approximation

For the case of scale separation in the forward and relative time, one can approximate the exponential in (4.3.5) by the leading order terms. The product $\partial_\tau \partial_\omega$ expresses the competition between relative time and forward time dynamics, it is small for slow forward time dynamics and fast relative dynamics[99, 164]. Comparing the zeroth order term with the first order term in an expansion of the exponential, we find the condition for approximating Eq. (4.3.5) by the zeroth order term to be

$$1 \gg \left| \frac{\partial_\omega \Sigma_{q,\omega,\tau}^R}{\Sigma_{q,\omega,\tau}^R} \right| \left| \frac{\partial_\tau F_{q,\omega,\tau}}{F_{q,\omega,\tau}} \right|. \quad (4.3.6)$$

If this condition is fulfilled, it allows for a separation into fast relative time dynamics and slow forward time dynamics. In general, it is a function of the Luttinger parameters u, K , the strength of the nonlinearity v_0 , as well as of the initial phonon distributions. Therefore, a general criterion for the applicability of the separation of time scales cannot be derived at this point. However, as has been shown in a different context[28], for equilibrium or near to equilibrium initial states, it is fulfilled for temperatures $k_B T < u\Lambda$ smaller than the Luttinger cutoff and therefore it will hold true for the situations we are considering here. We can thus apply the Wigner approximation to the FDR, resulting in

$$\Sigma_{q,\omega,\tau}^K = -i\partial_\tau F_{q,\omega,\tau} + 2i \operatorname{Im}(\Sigma_{q,\omega,\tau}) F_{q,\omega,\tau}. \quad (4.3.7)$$

The validity of the FDR in Wigner approximation is a very important result. It is commonly used as the starting point for deriving a kinetic equation for the distribution function in arbitrary dimensions. However, in the present case, we will further simplify the FDR by making use of the fact that we are dealing with resonant interactions in one dimension.

Quasi-particle Approximation and On-shell FDR

The major effect of the non-linearities in the action is the emergence of finite phonon lifetimes due to resonant phonon-phonon scattering processes. The resonant character of this interaction – the fact that for two phonons travelling in the same direction momentum and energy conservation is expressed by the identical δ -constraint – is the key property of

one-dimensional systems with linear dispersion. The resonant contributions dominate the self-energy and the kinetic equation, while the non-resonant processes give only subleading contributions to the lifetimes and the dispersion and have therefore already been eliminated on the basis of the action by using S_{Res} instead of S_{Int} in Eq. (4.2.18).

The retarded self-energy is decomposed according to

$$\Sigma_{\mathbf{q},\omega,\tau}^{\text{R}} = -i\sigma_{\mathbf{q},\tau}^{\text{R}} + \delta\Sigma_{\mathbf{q},\omega,\tau}^{\text{R}}, \quad (4.3.8)$$

where $\sigma_{\mathbf{q},\tau}^{\text{R}}$ is a positive, frequency independent function, which varies slowly in forward time τ . For resonant interactions $\delta\Sigma_{\mathbf{q},\omega,\tau}^{\text{R}} = 0$ and consequently, the self-energy is frequency independent and purely imaginary. Non-resonant contributions in the interaction lead to $\delta\Sigma^{\text{R}} \neq 0$, which however is generally strongly subleading compared to σ^{R} .

For the present model, the phonon interactions are RG-irrelevant and only their resonant character allows them to be of non-negligible influence. However, the effect of the interactions on the properties of the phonons will be small and subleading due to the RG-irrelevance. As a result, even in the presence of interactions, the phonons will have a lifetime $\tau_{\text{ph}}^{\text{q}} = -\text{Im}(\Sigma_{\mathbf{q}}^{\text{R}})^{-1}$ much larger than their associated coherent time-scale $\frac{1}{u|\mathbf{q}|}$, i.e. $\tau_{\text{ph}}^{\text{q}} \gg \frac{1}{u|\mathbf{q}|}$. Consequently, the phonons remain well defined quasi-particles with a spectral function $\mathcal{A}_{\mathbf{q},\omega,\tau} = i(G^{\text{R}} - G^{\text{A}})_{\mathbf{q},\omega,\tau}$ sharply peaked at the phonon energy $\omega = u|\mathbf{q}|$ ³. For well defined quasi-particles, the self-energies $\Sigma^{\text{R/A/K}}$ and the distribution function are evaluated on-shell, i.e. the frequencies are locked according to $\omega = u|\mathbf{q}|$, since frequencies $\omega \neq u|\mathbf{q}|$ do not contribute to the dynamics. For resonant interactions, on-shell evaluation is implied and

$$\delta\Sigma_{\mathbf{q},\omega,\tau}^{\text{R/A}} = 0, \quad (4.3.9)$$

as stated above. This is consistent with the result of Andreev's and later works for equilibrium and holds true for the non-equilibrium case as well. The corresponding decomposition for the Keldysh self-energy (with a convenient prefactor) reads

$$\Sigma_{\mathbf{q},\omega,\tau}^{\text{K}} = -2i\sigma_{\mathbf{q},\tau}^{\text{K}} + \delta\Sigma_{\mathbf{q},\omega,\tau}^{\text{K}} \quad \text{with} \quad \delta\Sigma_{\mathbf{q},\omega,\tau}^{\text{K}} = 0 \quad (4.3.10)$$

for resonant interactions. Inserting Eqs. (4.3.9), (4.3.10) in the non-equilibrium FDR (4.3.7) results in the on-shell, non-equilibrium FDR for resonant interactions

$$\sigma_{\mathbf{q},\tau}^{\text{K}} = \partial_{\tau}n_{\mathbf{q},\tau} + \sigma_{\mathbf{q},\tau}^{\text{R}}(2n_{\mathbf{q},\tau} + 1). \quad (4.3.11)$$

Here we have used the fact that for well defined quasi-particles, the on-shell distribution function $F_{\mathbf{q},\omega=u|\mathbf{q}|,\tau} = 2n_{\mathbf{q},\tau} + 1$ equals the time-dependent phonon density $n_{\mathbf{q},\tau}$ at momentum \mathbf{q} .

Eq. (4.3.11) is the final form of the non-equilibrium FDR that we will use to set up the kinetic equation in the following section and to determine the Keldysh self-energy σ^{K} for a system, for which the time-dependent phonon density $n_{\mathbf{q},\tau}$ is known. For the latter case, the only unknown quantity is the retarded self-energy σ^{R} and we can now set up the diagrammatic computation of σ^{R} in the Keldysh non-equilibrium framework.

³This underlies the functioning of the linear Luttinger-Liquid theory in equilibrium. In non-equilibrium situations, the RG-irrelevant nature of the interaction leads to a slowly varying density, and therefore the argument holds true even for this case

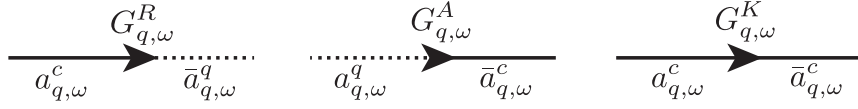


Figure 4.1: Green's functions in a diagrammatic representation. Full (dotted) lines represent classical (quantum) fields, while ingoing (outgoing) lines represent fields a (hermitian conjugate fields \bar{a}). The time index has been omitted

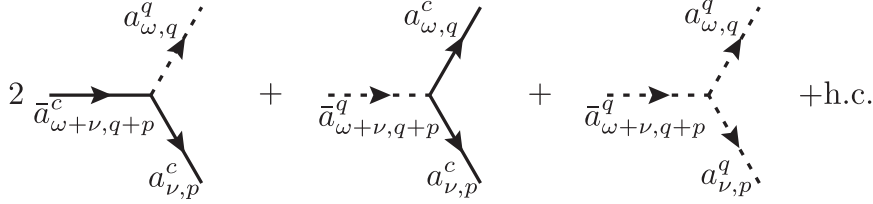


Figure 4.2: Diagrammatic representation of S_{Res} , see Eq. (6.2.16). In total, there exist six different vertices, three as depicted above and three corresponding hermitian conjugates. Each vertex has the prefactor $V(p, q) = \frac{v_0}{\sqrt{8\pi}} \sqrt{pq(p+q)}$.

4.3.2 Quasi-particle Lifetimes in Self-consistent Born Approximation

In this section, we perform the self-consistent Born approximation in a diagrammatic representation to obtain the self-energies $\sigma_{q,\tau}^R$. This amounts to an infinite resummation over a certain class of diagrams and cures the divergence of the self-energy occurring in the perturbative diagrammatic approach. In Sec. 4.7, we demonstrate that the self-energy can be determined exactly in a one-loop computation using Dyson-Schwinger equations and show that the deviation from the self-consistent Born approximation is negligible for many initial states.

In a diagrammatic approach, classical (quantum) fields are represented by a full (dotted) line, while ingoing lines represent fields a and outgoing lines their complex conjugate \bar{a} . This leads to a representation of Green's functions in terms of diagrams as indicated in Fig. 4.3.2, and vertices as depicted in Fig. 4.2. The retarded self-energy in self-consistent Born approximation can directly be derived by common diagrammatic rules and is depicted in Fig. 4.3. Inserting the Keldysh Green's function

$$G_{q,\omega}^K = G_{q,\omega}^R \Sigma_{q,\omega}^K G_{q,\omega}^A \quad (4.3.12)$$

and the on-shell self-energies $\Sigma_{q,\omega}^{R/A} = \mp i\sigma_q^R$, $\Sigma_{q,\omega}^K = -2i\sigma_q^K$, we can perform the frequency integration indicated in Fig. 4.3 and find for momenta $q > 0$

$$\begin{aligned} \sigma_q^R = v_0^2 & \left\{ \int_{0 < p < q} \frac{pq(q-p)\sigma_p^K}{\sigma_p^R (\sigma_p^R + \sigma_{q-p}^R)} - \int_{q < p} \frac{pq(p-q)\sigma_p^K}{\sigma_p^R (\sigma_p^R + \sigma_{p-q}^R)} \right. \\ & \left. + \int_{0 < p} \frac{pq(p+q)\sigma_p^K}{\sigma_p^R (\sigma_p^R + \sigma_{p+q}^R)} \right\}. \end{aligned} \quad (4.3.13)$$

Since the self-energies must be invariant under the transformation $p \rightarrow -p$, one can further

simplify Eq. (4.3.13), ending up with

$$\sigma_q^R = v_0^2 \int_{0 < p} \frac{\sigma_p^K}{\sigma_p^R} \left(\frac{qp(q-p)}{\sigma_p^R + \sigma_{q-p}^R} + \frac{qp(p+q)}{\sigma_p^R + \sigma_{p+q}^R} \right). \quad (4.3.14)$$

Finally, σ^K can be replaced using the FDR (4.3.11), which leads to

$$\sigma_q^R = v_0^2 \int_{0 < p} \left(\frac{\partial_\tau n_p}{\sigma_p^R} + 2n_p + 1 \right) \left(\frac{qp(q-p)}{\sigma_p^R + \sigma_{q-p}^R} + \frac{qp(p+q)}{\sigma_p^R + \sigma_{p+q}^R} \right). \quad (4.3.15)$$

For a given, time dependent distribution function $n_{q,\tau}$, $\sigma_{q,\tau}^R$ is the only unknown function in this equation and has to be determined self-consistently. For a general time-dependent function $n_{q,\tau}$ this has to be done by iterating Eq. (4.3.15) numerically until a self-consistent solution has been found. For the particular case for which $n_{q,\tau}$ shows scaling behavior in a sufficiently large momentum window, one can determine a scaling solution for the self-energy as well and extract the corresponding scaling exponent[8, 161]. We will now briefly discuss the latter case and determine possible scaling solutions for the self-energy, and close the section with a discussion on universal aspects of the scaling solution.

Scaling Solution for the Self-Energy

For the case when the density $n_{q,\tau}$ is a scaling function, i.e.

$$n_{q,\tau} = a_\tau |q|^{\eta_n}, \quad (4.3.16)$$

it is easy to show that also $\sigma_{q,\tau}^R$ will be a scaling function

$$\sigma_{q,\tau}^R = \gamma_\tau^R |q|^{\eta^R}, \quad (4.3.17)$$

where the exponent η^R and prefactor γ_τ^R solely depend on the scaling behavior of $n_{q,\tau}$, i.e. on η_n and a_τ . In order to show this, we introduce the rescaled self-energy $\tilde{\sigma}^R = \sigma^R/v_0$ and time $\tau = \tilde{\tau}/v_0$, leading to

$$\tilde{\sigma}_q^R = \int_{0 < p} \left(\frac{\partial_{\tilde{\tau}} n_p}{\tilde{\sigma}_p^R} + 2n_p + 1 \right) \left(\frac{qp(q-p)}{\tilde{\sigma}_p^R + \tilde{\sigma}_{q-p}^R} + \frac{qp(p+q)}{\tilde{\sigma}_p^R + \tilde{\sigma}_{p+q}^R} \right). \quad (4.3.18)$$

Next, we insert Eqs. (4.3.16), (4.3.17) into (6.3.10) and perform the transformation $p \rightarrow qx$, yielding

$$\begin{aligned} \tilde{\gamma}_\tau^R q^{\eta^R} &= \frac{1}{\tilde{\gamma}_\tau^R} q^{4-\eta^R} \int_{0 < x} \left[\left(\frac{x(1-x)}{x^{\eta^R} + |1-x|^{\eta^R}} + \frac{x(1+x)}{x^{\eta^R} + |1+x|^{\eta^R}} \right) \right. \\ &\quad \left. \times \left(1 + 2a_{\tilde{\tau}}(qx)^{\eta_n} + \frac{\partial_{\tilde{\tau}} a_{\tilde{\tau}}}{\tilde{\gamma}_\tau^R} (qx)^{\eta_n - \eta^R} \right) \right]. \end{aligned} \quad (4.3.19)$$

The exponent η^R is bounded from below and from above according to $1 < \eta^R \leq 2$. Here, $1 < \eta^R$ results from the fact that the interaction is RG irrelevant and the self-energy correction can only be subleading compared to the dispersion $\epsilon_q = u|q|$. The case $\eta^R = 2$, i.e. diffusive scaling of the lifetimes is only reached in the zero temperature situation,

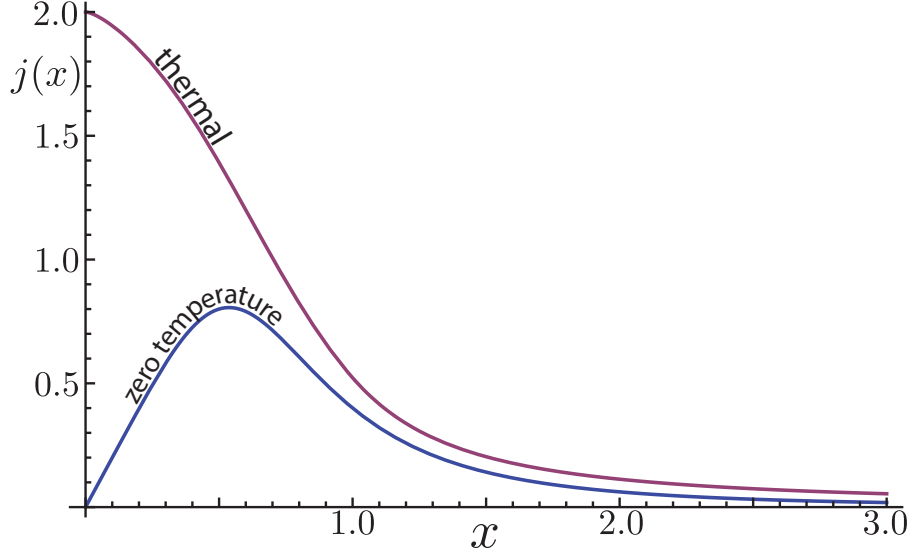


Figure 4.4: Integrand $j_{i_1, i_2}(x)$ in the self-energy integral $I_{i_1, i_2} = \int_x j_{i_1, i_2}(x)$ as a function of $x = p/q$, where q is the external momentum. The integrand $j(x)$ elucidates the contribution to σ_q^R from different momenta and shows clearly that the self-energy at momentum q is dominated by the behavior of σ_p^R for $p < q$.

bution stems from the time derivative in Eq. (4.3.19) and one finds

$$\eta^R = \frac{4 + \eta_m}{3}, \quad \tilde{\gamma}^R = \sqrt[3]{\dot{a}_\tau I_{\frac{4+\eta_m}{3}, \frac{2\eta_m-4}{3}}}. \quad (4.3.23)$$

The integral factor is defined as

$$I_{i_1, i_2} = \int_{0 < x} \left(\frac{x^{1+i_2}(1-x)}{x^{i_1} + |1-x|^{i_1}} + \frac{x^{1+i_2}(1+x)}{x^{i_1} + |1+x|^{i_1}} \right). \quad (4.3.24)$$

The results discussed above include the case of finite and zero temperature equilibrium. For the latter $n_q = 0$ and therefore $\eta^R = 2$, $\gamma_\tau^R = v_0 \sqrt{\frac{\pi}{4}}$, while for finite temperature $n_q \approx \frac{T}{u|q|}$ and $\partial_\tau n_q = 0$ and consequently $\eta^R = 3/2$, $\gamma_\tau^R = 0.789 v_0 \sqrt{\frac{2\pi T}{u}}$. These are the mentioned results obtained for the zero and finite temperature equilibrium cases[8, 161, 150].

Insensitivity of the Self-Energy to UV-behavior

The insensitivity of the above results to the behavior of the model in the ultraviolet (UV) regime and therefore the non-universal properties of the system is guaranteed by the structure of the vertex and the diagrams in Fig. 4.3. The self-energies σ_q^R are dominated by loop momenta $p < q$ below the external momentum q . Therefore the non-universal behavior in the UV does not enter the self-energies. This is emphasized in Fig. 4.4, where the integrand

$$j_{i_1, i_2}(x) = \frac{(1-x)x^{1+i_2}}{|1-x|^{i_1} + x^{i_1}} + \frac{(1+x)x^{1+i_2}}{(1+x)^{i_1} + x^{i_1}} \quad (4.3.25)$$

For the full Green's functions, we use the results from the previous section

$$G_{q,\omega,\tau}^{R/A} = 2\pi (\omega - u|q| \pm i\sigma_{q,\tau}^R)^{-1} \quad (4.4.2)$$

and the relation

$$G_{q,\omega,\tau}^K = G_{q,\omega,\tau}^R F_{q,\omega,\tau} - F_{q,\omega,\tau} G_{q,\omega,\tau}^A = \frac{-8\pi^2 i \sigma_{q,\tau}^R (2n_{q,\tau} + 1)}{(\omega - u|q|)^2 + (\sigma_{q,\tau}^R)^2}. \quad (4.4.3)$$

In Eq. (4.4.3), the first equality holds in Wigner approximation, while the second equality results from the quasi-particle approximation, both discussed in the previous section.

The frequency integration in the diagrammatic representation can be performed analytically and yields the kinetic equation (omitting time index)

$$\begin{aligned} \partial_\tau n_q &= 2v_0^2 \int_{0 < p < q} \frac{pq(q-p)}{\sigma_q^R + \sigma_p^R + \sigma_{q-p}^R} (n_p n_{q-p} - n_q (1 + n_p + n_{q-p})) \\ &\quad + 4v_0^2 \int_{0 < p} \frac{pq(q+p)}{\sigma_q^R + \sigma_p^R + \sigma_{q+p}^R} (n_{p+q} (n_q + n_p + 1) - n_q n_p). \end{aligned} \quad (4.4.4)$$

After transforming to dimensionless variables $\sigma^R = v_0 \tilde{\sigma}^R$, $\tau = \frac{\tilde{\tau}}{v_0}$, we finally arrive at

$$\begin{aligned} \partial_{\tilde{\tau}} n_q &= \int_{0 < p < q} \frac{2pq(q-p)}{\tilde{\sigma}_q^R + \tilde{\sigma}_p^R + \tilde{\sigma}_{q-p}^R} (n_p n_{q-p} - n_q (1 + n_p + n_{q-p})) \\ &\quad + \int_{0 < p} \frac{4pq(q+p)}{\tilde{\sigma}_q^R + \tilde{\sigma}_p^R + \tilde{\sigma}_{q+p}^R} (n_{p+q} (n_q + n_p + 1) - n_q n_p). \end{aligned} \quad (4.4.5)$$

This is the kinetic equation for the phonon density in self-consistent Born approximation.

Comparing this equation to Eq. (6.3.10), one finds that the rescaled self-energy $\tilde{\sigma}_q^R$ and therefore also the kinetic equation for a rescaled time $\tilde{\tau} = v_0 \tau$ only depend on the phonon distribution $n_{q,\tilde{\tau}}$ and is independent of all possible microscopic details that may enter u, K, v_0 in the model. As a result, the dynamics in the rescaled variables is very generic for an interacting Luttinger Liquid and only depends on the initial distribution function $n_{q,\tau=0}$ with which the system is initialized.

The typical time-scale for the kinetic equation in the original variables is $\tau_{\text{typ}} = \frac{1}{v_0}$, i.e. linear in the vertex v_0 . This is a non-perturbative effect resulting from the resonant interactions. Since two vertices enter the one-loop diagrams, one might naively (or in perturbation theory) expect that the typical time scale is given by the square of the non-linearity. However, this is normalized by the self-energies, which are proportional to v_0 and required to regularize the kinetic equation.

In the kinetic equation in (6.3.11), still the self-energies $\tilde{\sigma}^R$ occur. In principle, one could again replace them by a diagrammatic expression, which would give rise to an infinite hierarchy. However instead of doing so, we use an iterative process in which, for a given time τ , we determine self-consistently the self-energy $\sigma_{q,\tau}^R$. This result is then used to determine the r.h.s. of the kinetic equation, to subsequently compute the distribution function in the next time step $\tau + \delta\tau$. This procedure is illustrated in Fig. 4.6 and allows us to compute the non-equilibrium dynamics of an interacting Luttinger Liquid, which may be initialized in a non-thermal state.

We will now close this section by discussing two limiting cases where analytic results become available. First, the kinetic equation for small external momenta q , and second the kinetic equation for a phonon distribution $n_{q,\tau} = n_{q,T} + \delta n_{q,\tau}$ close to an equilibrium distribution $n_{q,T}$.

4.4.1 Kinetic Equation for Small External Momenta

For small external momenta, the kinetic equation (6.3.11) can be brought into an even simpler form, explicitly revealing the evolution of $n_{q,\tau}$ for small q . In this case, the first integral in (6.3.11) covers only a very small momentum region and is proportional to $q^{4-\eta^R}$, $1 < \eta^R \leq 2$. As a result, it is negligible compared to the second integral. On the other hand, in the second integral summations including q can be replaced according to $p+q \approx p$, $\sigma_q^R + \sigma_p^R \approx \sigma_p^R$. The kinetic equation then simplifies to

$$\partial_{\bar{\tau}} n_{q,\bar{\tau}} \stackrel{q \ll 1}{\approx} |q| \int_{0 < p} \frac{2p^2}{\sigma_{p,\bar{\tau}}^R} n_{p,\bar{\tau}} (1 + n_{p,\bar{\tau}}) = |q| \mathcal{I}_{\bar{\tau}}, \quad (4.4.6)$$

where $\mathcal{I}_{\bar{\tau}}$ is a time dependent but momentum independent functional. The phonon density becomes

$$n_{q,\bar{\tau}} \stackrel{q \ll 1}{\approx} n_{q,\bar{\tau}=0} + |q| \int_{0 < t < \bar{\tau}} \mathcal{I}_t \quad (4.4.7)$$

for sufficiently small momenta. Crucially, the change is linear in momentum q and for

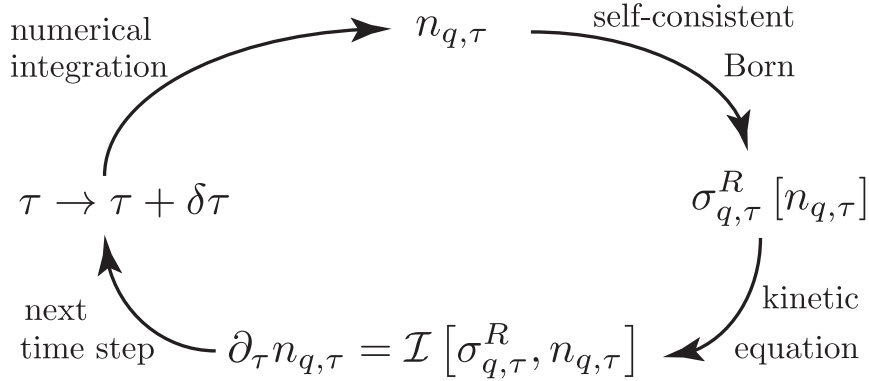


Figure 4.6: Schematic illustration of the iteration process to determine the time-dependent phonon density $n_{q,\tau}$. For a given time τ , the self-energy $\sigma_{q,\tau}^R$ is determined via the self-consistent Born approximation according to Eq. (6.3.10). Subsequently, the time-derivative of $n_{q,\tau}$ is computed via the kinetic equation (6.3.11). Using a Runge-Kutta solver for numerical differential equations, the density $n_{q,\tau+\delta\tau}$ can be computed and used as the starting point for the next iteration.

$q = 0$ the density is time independent, and for all times pinned to its initial value. This is an exact result, which can be traced back to particle number conservation in the underlying microscopic model [130].

4.4.2 Relaxation Close to Equilibrium

A stationary solution of the kinetic equation $\partial_\tau n_{\mathbf{q},\tau} = 0$ is given by the Bose distribution function

$$n_{\mathbf{q},\tau} = n_{\text{B}}(u|\mathbf{q}|, T) = \left(e^{u|\mathbf{q}|/T} - 1 \right)^{-1} \quad (4.4.8)$$

for arbitrary temperature T . Sometimes one is interested in the relaxation of the distribution function close to equilibrium

$$n_{\mathbf{q},\tau} = n_{\text{B}}(u|\mathbf{q}|, T) + \delta n_{\mathbf{q},\tau}, \quad (4.4.9)$$

where the variation $\delta n \ll n_{\text{B}}$. For small momenta $u|\mathbf{q}| \ll T$, $n_{\text{B}}(u|\mathbf{q}|, T) = \frac{T}{u|\mathbf{q}|}$ and we can expand the kinetic equation in the variation δn . The zeroth order part solves the kinetic equation, and the leading order contribution stems from the first order of the expansion. After eliminating negligible terms, it reads

$$\begin{aligned} \partial_\tau \delta n_{\mathbf{q}} = -\frac{2Tq^2 \delta n_{\mathbf{q}}}{u} & \left(\int_{0 < p < q} \frac{1}{\tilde{\sigma}_{\mathbf{q}}^{\text{R}} + \tilde{\sigma}_{\mathbf{p}}^{\text{R}} + \tilde{\sigma}_{\mathbf{q-p}}^{\text{R}}} \right. \\ & \left. + \int_{0 < p} \frac{2}{\tilde{\sigma}_{\mathbf{q}}^{\text{R}} + \tilde{\sigma}_{\mathbf{p}}^{\text{R}} + \tilde{\sigma}_{\mathbf{q+p}}^{\text{R}}} \right). \end{aligned} \quad (4.4.10)$$

For a distribution close to thermal equilibrium, the self-energy will take on the thermal form (4.3.22) and

$$\partial_\tau \delta n_{\mathbf{q}} \approx -\alpha_{\text{T}} \delta n_{\mathbf{q}} \sqrt{\frac{2\pi T}{u}} q^{\frac{3}{2}} = -\alpha_{\text{T}} \tilde{\sigma}_{\mathbf{q}}^{\text{R}} \delta n_{\mathbf{q}}, \quad (4.4.11)$$

where $\tilde{\sigma}_{\mathbf{q}}^{\text{R}}$ is the thermal self-energy and $\alpha_{\text{T}} \approx 1.1$ is a universal number. This result can also be seen as an expansion of Eq. (4.4.1) in $\delta n_{\mathbf{q}}$, which is

$$\partial_\tau \delta n_{\mathbf{q}} = -2\delta n_{\mathbf{q}} \tilde{\sigma}_{\mathbf{q}}^{\text{R}} + \frac{\partial}{\partial \delta n_{\mathbf{q}}} \left(\tilde{\sigma}_{\mathbf{q}}^{\text{K}} - (2n_{\text{B}} + 1) \tilde{\sigma}_{\mathbf{q}}^{\text{R}} \right) \Big|_{\delta n_{\mathbf{q}}=0} \delta n_{\mathbf{q}}. \quad (4.4.12)$$

The second term thus gives a correction to the simple factor of 2 in Eq. (4.4.11). We thus obtain a non-perturbative estimate for the relaxation time of the interacting Luttinger Liquid

$$\tau_{\mathbf{q}} = \frac{0.868}{v_0} \sqrt{\frac{u}{2\pi T}} q^{-\frac{3}{2}} \quad (4.4.13)$$

reflecting the very slow asymptotic approach to equilibrium of the long-wavelength modes. It is very similar to the lifetime of a single thermal phonon (cf. Eq. (4.3.22)), only modified by the prefactor $\alpha_{\text{T}} = 1.1$. This modification arises due to in-scattering processes of excitations $p \neq q$ scattering into the mode q . Since the main relaxation process is caused by out-scattering processes, the above result is quite intuitive and supports the statement that relative time dynamics $\sim \frac{1}{\epsilon_{\mathbf{q}}}$ are fast compared to forward time dynamics $\sim \tau_{\mathbf{q}}$.

4.5 KINETIC EQUATION AND DIAGRAMS IN PRESENCE OF ANOMALOUS DENSITIES

In this section, we consider the effect of non-zero anomalous (off-diagonal) phonon density, i.e. $\bar{a}_q \bar{a}_{-q} \neq 0$ on the diagonal kinetic equation and self-energy, and derive the kinetic equation for the anomalous density. Off-diagonal phonon densities can be populated due to external perturbations, as for instance density modulation due to a Bragg beam or a global interaction quench [40, 39], and their impact on the kinetics and non-equilibrium dynamics is therefore non-negligible. Summarizing the results of this section, due to the structure of the resonant interactions, the kinetic equation for the diagonal phonon density and the diagonal retarded/advanced self-energies are not modified in the presence of anomalous densities and remain unchanged compared to Eqs. (6.3.11) and (4.3.15). In contrast, the kinetic equation for the anomalous densities is fed by the normal occupations, cf. Eq. (4.5.25).

For a generic equilibrium situation and for certain realizations of systems brought out of equilibrium, the anomalous (off-diagonal) phonon density and consequently the corresponding response and correlation functions are zero, i.e.

$$\langle a_{q,t}^\alpha a_{-q,t'}^{\alpha'} \rangle = 0, \quad (4.5.1)$$

where $\alpha, \alpha' = c, q$ represent classical or quantum indices. However, when a system is driven out of equilibrium, it is possible to populate off-diagonal terms. A simple situation for which this is indeed the case is an interaction quench in a one dimensional quantum fluid, where the off-diagonal densities are non-zero after the quench and lead to non-equilibrium dynamics even in the absence of phonon-phonon scattering processes [39].

In order to deal with the situation of anomalous densities, we first have to modify the FDR accordingly. The Keldysh Green's function in the presence of off-diagonal terms, expressed in Nambu space, is

$$G_{q,t,t'}^K = \begin{pmatrix} g_{q,t,t'}^K & h_{q,t,t'}^K \\ -\left(h_{q,t,t'}^K\right)^* & g_{-q,t',t}^K \end{pmatrix} = -i \begin{pmatrix} \langle a_{q,t}^c \bar{a}_{q,t'}^c \rangle & \langle a_{q,t}^c a_{-q,t'}^c \rangle \\ \langle \bar{a}_{-q,t}^c \bar{a}_{q,t'}^c \rangle & \langle \bar{a}_{-q,t}^c a_{-q,t'}^c \rangle \end{pmatrix}. \quad (4.5.2)$$

For the quadratic theory in the absence of phonon scattering, i.e. $S = S_{TL}$ only, the Keldysh Green's function can be evaluated explicitly. In an operator representation, it reads

$$G_{q,t,t'}^K = -i \begin{pmatrix} \langle \{a_{q,t}, a_{q,t'}^\dagger\} \rangle & \langle \{a_{q,t}, a_{-q,t'}\} \rangle \\ \langle \{a_{-q,t}^\dagger, a_{q,t'}^\dagger\} \rangle & \langle \{a_{-q,t}^\dagger, a_{-q,t'}\} \rangle \end{pmatrix}, \quad (4.5.3)$$

with the anti-commutator $\{\cdot, \cdot\}$. In Wigner representation it is

$$G_{q,\omega,\tau}^K = -i \begin{pmatrix} \delta(\omega - \epsilon_q)(2n_q + 1) & \delta(\omega)2m_q e^{-i2\epsilon_q\tau} \\ \delta(\omega)2m_q^* e^{i2\epsilon_q\tau} & \delta(\omega + \epsilon_q)(2n_{-q} + 1) \end{pmatrix}, \quad (4.5.4)$$

where m_q is the anomalous phonon density ($m_q = |\langle a_q a_{-q} \rangle|$) in an operator representation in terms of annihilation operators a). In the quadratic theory, both the normal and the anomalous densities are constants of motion.

The Keldysh Green's function in (4.5.4) has two essential drawbacks. For the case of non-zero but slowly (compared to ϵ_q) varying anomalous density m_q , the off-diagonal terms of G^K are not slow but oscillate with the fastest scale in the problem, i.e. $t_{typ} = \frac{1}{2\epsilon_q}$.

The Wigner approximation is therefore not applicable for the off-diagonal terms of G^K . Furthermore, the Keldysh Green's function in frequency representation is peaked at three different frequencies, $\omega = (\epsilon_q, 0, -\epsilon_q)$. Both prevents an FDR in the form of Eq. (4.3.7) to exist in this representation.

In order to cure this problem, we switch to a rotating frame by introducing the fields $\alpha_{q,t} = a_{q,t}e^{i\epsilon_q t}$, $\bar{\alpha}_{q,t} = \bar{a}_{q,t}e^{-i\epsilon_q t}$, which modifies the quadratic action according to

$$S^{(2)} = \int_{t,p} (\bar{\alpha}_{p,t}^c, \bar{\alpha}_{p,t}^q) \begin{pmatrix} 0 & i\partial_t + i0^+ \\ i\partial_t - i0^+ & 2i0^+ \coth\left(\frac{\omega}{2T}\right) \end{pmatrix} \begin{pmatrix} \alpha_{p,t}^c \\ \alpha_{p,t}^q \end{pmatrix}. \quad (4.5.5)$$

The resonant phonon interaction is invariant under the transformation

$$S_{\text{Res}} = \frac{v_0}{\sqrt{2}} \int'_{p,k,t} \sqrt{|pk(k+p)|} \left[2\bar{\alpha}_{k+p,t}^c \alpha_{k,t}^c \alpha_{p,t}^q + \bar{\alpha}_{k+p,t}^q \left(\alpha_{k,t}^c \alpha_{p,t}^c + \alpha_{k,t}^q \alpha_{p,t}^q \right) + \text{h.c.} \right]. \quad (4.5.6)$$

since the phase $e^{it(\epsilon_{p+k} - \epsilon_k - \epsilon_p)} = 1$ in the case of resonance, i.e. for $|k+p| = |k| + |p|$. The corresponding correlation function in Nambu space and Wigner coordinates after the rotation is

$$\tilde{G}_{q,\omega,\tau}^K = -i\delta(\omega) \begin{pmatrix} 2n_q + 1 & 2m_q \\ 2m_q^* & 2n_{-q} + 1 \end{pmatrix}, \quad (4.5.7)$$

while the bare retarded Green's function reads

$$\tilde{G}_{q,\omega,\tau}^R = \begin{pmatrix} \frac{1}{\omega + i0^+} & 0 \\ 0 & \frac{1}{-\omega - i0^+} \end{pmatrix} = \sigma_z \frac{1}{\omega + i0^+}, \quad (4.5.8)$$

where σ_z is the Pauli matrix. Respecting the symplectic structure in bosonic Nambu space, the FDR in the presence of off-diagonal densities is

$$\tilde{G}_{q,\omega,\tau}^K = \left(\tilde{G}^R \circ \sigma_z \circ \tilde{F} - \tilde{F} \circ \sigma_z \circ \tilde{G}^A \right)_{q,\omega,\tau} = -i\delta(\omega) \tilde{F}_{q,\omega,\tau}. \quad (4.5.9)$$

Here \tilde{F} is the physical distribution function for the phonons, with the on-shell value

$$\tilde{F}_{q,\omega=0,\tau} = \begin{pmatrix} 2n_{q,\tau} + 1 & 2m_{q,\tau} \\ 2m_{q,\tau}^* & 2n_{-q,\tau} + 1 \end{pmatrix}. \quad (4.5.10)$$

Both the transformation to a rotating frame by switching from $\{a_q, \bar{a}_q\}$ to $\{\alpha_q, \bar{\alpha}_q\}$ as well as the symplectic factors σ_z in Eq. (4.5.9) are necessary modifications in order to obtain an FDR with a physically relevant distribution function \tilde{F} . The latter should consist of diagonal and anomalous densities that are slowly varying in time and reproduce the matrix structure of \tilde{G}^K .

Inversion of Eq. (4.5.9) yields the kinetic equation

$$i\partial_\tau F_{q,\omega,\tau} = \sigma_z \Sigma_{q,\omega,\tau}^R F_{q,\omega,\tau} - F_{q,\omega,\tau} \Sigma_{q,\omega,\tau}^A \sigma_z - \sigma_z \Sigma_{q,\omega,\tau}^K \sigma_z. \quad (4.5.11)$$

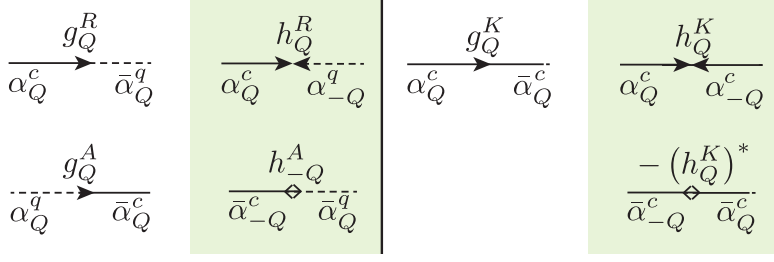


Figure 4.7: Diagrammatic representation of the diagonal and off-diagonal retarded/advanced and Keldysh Green's functions. In the presence of anomalous densities, the off-diagonal Keldysh components will be generally non-zero, $h^K \neq 0$. The retarded and advanced Green's functions only differ from zero if a finite off-diagonal self-energy is present, cf. Eq. (4.5.12).

In the absence of off-diagonal terms in both self-energies and the distribution function, this equation reduces to the ordinary kinetic equation discussed in the previous section. We will now set up the diagrammatic computation of the self-energies $\Sigma_{q,\omega,\tau}^{R/A/K}$ in order to derive the kinetic equation in the presence of anomalous phonon densities.

4.5.1 Diagrammatics for Off-diagonal Terms

In the presence of off-diagonal densities, one can no longer generally exclude non-zero off-diagonal self-energies and consequently non-zero off-diagonal Green's functions from the action. In this section we set up the diagrammatic computation of the self-energies in Nambu space. We obtain two key results, which crucially rely on the resonant character of the interaction. First, in the retarded/advanced sector, the off-diagonal self-energies are exactly zero even in the presence of anomalous densities. Second, we compute the off-diagonal self-energies in the Keldysh sector, which are different from zero.

The retarded Green's function in Nambu space is (we use a general index $Q = (q, \omega, \tau)$, $-Q = (-q, -\omega, \tau)$ for this paragraph)

$$\begin{aligned} G_Q^R &= \begin{pmatrix} g_Q^R & h_Q^R \\ h_{-Q}^A & g_{-Q}^A \end{pmatrix} = \begin{pmatrix} \omega - \Sigma_Q^R & -\Gamma_Q^R \\ -\Gamma_{-Q}^A & -\omega - \Sigma_{-Q}^A \end{pmatrix}^{-1} \\ &= \frac{1}{(\omega - \Sigma_Q^R)(\omega + \Sigma_{-Q}^A) + \Gamma_Q^R \Gamma_{-Q}^A} \begin{pmatrix} \Sigma_{-Q}^A + \omega & -\Gamma_Q^R \\ -\Gamma_{-Q}^A & \Sigma_Q^R - \omega \end{pmatrix}, \end{aligned} \quad (4.5.12)$$

with the off-diagonal self-energies Γ_Q^R and the Green's functions $g_Q^R = -i\langle \alpha_Q^c \bar{\alpha}_Q^q \rangle$, $g_Q^A = -i\langle \alpha_Q^q \bar{\alpha}_Q^c \rangle$, $h_Q^R = -i\langle \alpha_Q^q \alpha_{-Q}^c \rangle$ and $h_Q^A = -i\langle \bar{\alpha}_{-Q}^q \bar{\alpha}_Q^c \rangle$. The diagrammatic representation for the retarded and Keldysh Green's functions in Nambu space is depicted in Fig. 4.7.

With this at hand, we can set up diagrammatic rules in Nambu space, as we do in the following. To this end, we start from the most general diagram contributing to the retarded sector of the Green's function, which is shown in Fig. 4.8. Here we replaced the fields $\alpha_Q \rightarrow \alpha_{Q,1}$ and $\bar{\alpha}_Q \rightarrow \alpha_{Q,-1}$ in order to find a generalized representation of diagrams in Nambu space. Exploiting frequency and momentum conservation in the Green's functions (diagonal and off-diagonal ones) and the vertices, together with the resonance condition

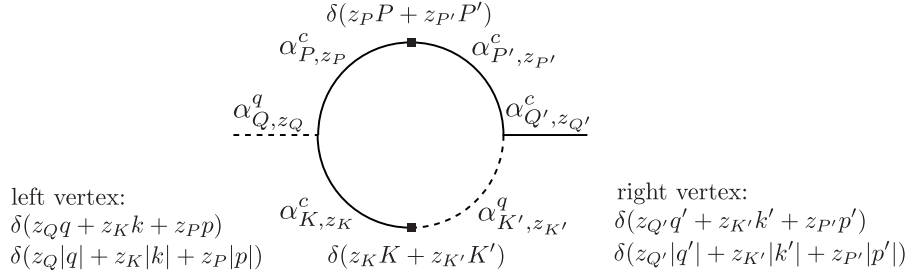


Figure 4.8: Diagrammatic representation of all possible one-loop diagrams contributing to the retarded sector of the self-energy. The additional index $z_{Q,P,K} = \pm 1$ represents ingoing lines ($\alpha_{Q,P,K}$ fields) for $z = 1$ and outgoing lines ($\bar{\alpha}_{Q,P,K}$ fields) for $z = -1$. The δ -constraints stem from the momentum/frequency conservation in the Green's function and the momentum/frequency conservation in the two vertices. Two additional constraints, one for each vertex, are caused by the resonance condition. This results in six crucial constraints discussed in the main text.

at each vertex, we end up with the following relations

$$z_Q Q = z_{Q'} Q', \quad (4.5.13)$$

$$z_P P = z_{P'} P', \quad (4.5.14)$$

$$z_K K = z_{K'} K', \quad (4.5.15)$$

$$z_Q Q = -z_K K - z_P P, \quad (4.5.16)$$

$$z_Q |q| + z_P |p| = -z_K |z_Q q + z_P p|, \quad (4.5.17)$$

$$z_K z_{K'} + z_Q z_{Q'} = 2z_P z_{P'}. \quad (4.5.18)$$

Eq. (4.5.18) is a result of the two independent resonance conditions in Fig. 4.8 and reduces the number of diagrams for the retarded self-energy significantly. As a result of Eq. (4.5.18), the product of all the corresponding z -factors must be identical. For the diagonal self-energy, where $z_Q z_{Q'} = -1$, this means that $z_P z_{P'} = z_K z_{K'} = -1$ and consequently only loops consisting of two diagonal Green's functions contribute to the diagonal self-energy. Consequently, the diagrammatic representation of the diagonal self-energy is still given by the loops shown in Fig. 4.3 even in the presence of off-diagonal Green's functions, i.e.

$$\begin{aligned}
-i\Sigma_Q^R &= \frac{v_0^2}{4\pi^2} \int_P |pq| (|q-p| g_P^K g_{Q-P}^R + |p+q| g_{Q+P}^K g_P^A \\
&\quad + |p+q| g_P^K g_{P+Q}^R). \quad (4.5.19)
\end{aligned}$$

In order to obtain the off-diagonal self-energy Γ_Q^R , one has to flip the sign of $z_{Q'} \rightarrow 1$, such that $z_Q z_{Q'} = z_P z_{P'} = z_K z_{K'} = 1$ in the corresponding loops. This means that the diagrams contain only off-diagonal terms. Γ_Q^R is then obtained by the diagrams in Fig. 4.3, but with all arrows from the right vertex flipped. We thus obtain

$$\begin{aligned}
-i\Gamma_Q^R &= \frac{v_0^2}{4\pi^2} \int_P |pq| (|q-p| h_P^K h_{Q-P}^R + |p+q| h_{Q+P}^K h_P^A \\
&\quad - |p+q| (h_P^K)^* h_{P+Q}^R). \quad (4.5.20)
\end{aligned}$$

The diagonal self-energy Σ^R diverges when the integral (4.5.19) is performed with the bare

$$\begin{aligned}
-\Gamma_q^K &= \text{Diagram 1} = -\frac{v_0^2}{4\pi^2} \int_P |pq(q-p)| h_{Q-P}^K (h_P^K)^* \\
&+ 2 \text{Diagram 2} = \frac{v_0^2}{2\pi^2} \int_P |pq(q+p)| h_{Q+P}^K h_P^K
\end{aligned}$$

Figure 4.9: Diagrammatic representation of the off-diagonal Keldysh self-energy Γ_q^K . Compared to the diagonal component, for the vertex of the left ingoing and outgoing lines have been replaced. The diagrams containing only retarded/advanced Green's functions, which contributed to σ_q^K , are absent because of the absence of off-diagonal retarded and advanced Green's functions.

Green's functions. This hints that a non-trivial self-energy is generated on the diagonal to regulate the integral, which can be computed in self-consistent Born approximation as explained in previous sections. On the other hand, for off-diagonal Green's functions $h^R = h^A = 0$ (e.g. for the bare off-diagonal values), the off-diagonal self-energy is zero, as visible from Eq. (4.5.20). Consequently, off-diagonal self-energies are not generated in the retarded sector even in self-consistent Born approximation and we have

$$\Gamma_Q^R = 0. \quad (4.5.21)$$

In the absence of off-diagonal self-energies in the retarded sector, we can directly apply the quasi-particle approximation discussed in the previous sections and evaluate the self-energies and distribution function on-shell. Consequently, the intermediate kinetic equation is

$$\partial_\tau F_{q,\omega=0,\tau} = -2\sigma_{q,\tau}^R F_{q,\omega=0,\tau} + i\sigma_z \Sigma_{q,\omega=0,\tau}^K \sigma_z \quad (4.5.22)$$

with the scalar, on-shell self-energy $\sigma_{q,\tau}^R$ as discussed in Sec. 4.3.2.

For the on-shell Keldysh self-energy,

$$\Sigma_{q,\omega=0,\tau}^K = -2i \begin{pmatrix} \sigma_{q,\tau}^K & \Gamma_{q,\tau}^K \\ \Gamma_{q,\tau}^K & \sigma_{q,\tau}^K \end{pmatrix} \quad (4.5.23)$$

the diagrammatic rules from the previous section do not have to be modified. This immediately yields the diagonal, on-shell Keldysh self-energy $\sigma_{q,\tau}^K$ according to Fig. 4.3.2. For the off-diagonal, on-shell Keldysh self-energy Γ_q^K the corresponding diagrams are obtained by reversing the arrows associated to the vertices on the right in Fig. 4.3.2, resulting in the diagrammatic representation of Γ_q^K shown in Fig. 4.9. The Keldysh Green's functions are obtained via the parametrization used in Eq. (4.5.9), which yields for the off-diagonal elements

$$h_{q,\omega,\tau}^K = \frac{16\pi^2 i \sigma_{q,\tau}^R m_{q,\tau}}{(\omega - u|q|)^2 + (\sigma_{q,\tau}^R)^2}. \quad (4.5.24)$$

Evaluation of the off-diagonal diagrams and insertion into the kinetic equation completes the set of equations for a system including anomalous phonon densities.

Finally, the off-diagonal retarded/advanced self-energies are exactly zero and the kinetic equation for the off-diagonal terms is

$$\begin{aligned} \partial_{\tilde{\tau}} m_q &= \int_{0 < p < q} \frac{2pq(q-p)}{\tilde{\sigma}_q^R + \tilde{\sigma}_p^R + \tilde{\sigma}_{q-p}^R} (m_p m_{q-p} - m_q (1 + n_p + n_{q-p})) \\ &+ \int_{0 < p} \frac{4pq(q+p)}{\tilde{\sigma}_q^R + \tilde{\sigma}_p^R + \tilde{\sigma}_{q+p}^R} (n_{p+q} m_q + m_p m_{p+q} - m_q n_p). \end{aligned} \quad (4.5.25)$$

Here, we have again used the transformed basis to eliminate the factor v_0^2 in front of the integrals. The time evolution for the off-diagonal terms depends on both the diagonal and off-diagonal densities, and the stationary solution of this equation is $m_q = 0$ due to the uncompensated spontaneous decay term in the first integral. Together with Eqs. (4.3.15) and (6.3.11), Eq. (4.5.25) represents the complete set of equations determining the time evolution of the phonon density and the self-energies of an interacting Luttinger Liquid for a system that has been initialized in an out-of-equilibrium state $n_q \neq n_B(u|q|)$, $m_q \neq 0$.

4.6 RELAXATION OF AN EXCITED THERMAL STATE

In this section, we will analyze the relaxation dynamics of a nearly thermal initial state and compare it to the analytical results from the previous sections. We consider an initial state with the densities

$$\begin{aligned} n_{q,\tau=0} &= n_B(T_i = 2u|q_0|) + \delta_q \\ &= \frac{1}{e^{0.5 \left| \frac{q}{q_0} \right|} - 1} + \alpha_1 e^{-\frac{(q-q_0)^2}{2\alpha_2^2}}, \end{aligned} \quad (4.6.1)$$

$$m_{q,\tau=0} = \delta m_{q,\tau=0} = 2\alpha_1 e^{-\frac{(q-q_0)^2}{2\alpha_2^2}}. \quad (4.6.2)$$

A state of this form can be created by perturbing a thermal state with initial temperature $T_i = 0.5u|q_0|$ in coupling the operator $\propto \partial_x \phi$ to a classical field with momentum q_0 , i.e. in a microscopic fermionic or bosonic model by a small density modulation with momentum q_0 [67]. For a specific simulation, we chose the parameters $\alpha_1 = 0.2$, $\alpha_2 = 4q_0$ and express momentum in units of q_0 .

The perturbation increases the energy

$$E(\tau) = \int_q u|q| n_{q,\tau} \quad (4.6.3)$$

of the system. As a result, the final state in the limit $\tau \rightarrow \infty$ will be a thermal state with increased temperature $T_f > T_i$. Since the kinetics is energy conserving, $E(\tau) = E(\tau = 0)$ for all $\tau > 0$, the temperature can be determined according to

$$E = \int_q \frac{u|q|}{e^{u|q|/T_f} - 1} = \frac{T_f^2 \pi^2}{6u} \quad (4.6.4)$$

from the system energy. In the present case, this leads to $T_f = 0.52u|q_0|$ and a final state of the system

$$\lim_{\tau \rightarrow \infty} n_{q,\tau} = n_B(T_f). \quad (4.6.5)$$

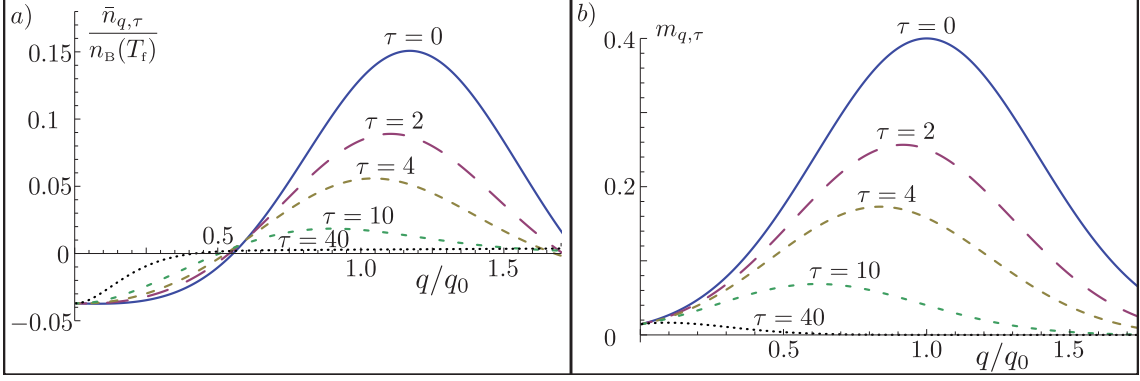


Figure 4.10: Time evolved phonon density $n_{q,\tau}$ after initializing the system in a state described by Eqs. (4.6.1), (4.6.2). The time τ is expressed in units of $\frac{1}{v_0 q_0}$. a) The deviation $\bar{n}_{q,\tau}$ of $n_{q,\tau}$ from the final thermal density $n_B(T_f)$ divided by $n_B(T_f)$. $\bar{n}_{q,\tau}$ decays to zero with a momentum dependent rate $\gamma_q \approx -1.1\sigma_q^R$. For smaller momenta, this rate decreases and finally becomes zero for $q \rightarrow 0$. b) Anomalous density $m_{q,\tau}$ for different times τ .

The quantity of interest is the deviation of the time-dependent phonon density from the final phonon density in the limit $\tau \rightarrow \infty$,

$$\delta n_{q,\tau} \equiv n_{q,\tau} - n_B(T_f). \quad (4.6.6)$$

In Fig. 4.10, we show $\delta n_{q,\tau}$ and $m_{q,\tau}$ for different time steps τ , and we see in which way both quantities decay to zero momentum as a function of time and momentum.

The evolution of this excited state to its new equilibrium proceeds in two different stages[126]: For short times, the set of excited modes is much more strongly occupied than all other modes, and the dominant effect is the decay of these modes into the continuum of non-excited ones. In this step, there is no back-action from the continuum, which acts as a bath for the excited states. As a consequence, the dynamics is described by the corresponding equilibrium linear response. According to Eq. (4.4.11), δn_q then follows the effective equation of motion

$$\partial_\tau \log(\delta n_{q,\tau}) = -1.1\sigma_q^R. \quad (4.6.7)$$

As a result, for short times $\delta n_{q,\tau}$ decays exponentially in time with a momentum dependent decay time $\tau_{\text{dec}}(q) = (1.1\sigma_q^R)^{-1}$.

In Fig. 4.11, we compare the numerical value of $\partial_\tau \log(\delta n_{q,\tau})$ with the analytical estimate $\partial_\tau \log(\delta n_{q,\tau}) \approx -1.1\sigma_{q,\tau}^R \approx 0.87\sqrt{\frac{2\pi T_f}{u}} q^{\frac{3}{2}}$ and find a good agreement in the momentum region where δn_q deviates from zero.

For larger times instead, many modes deviate only very weakly from the thermal occupation, but the system has still not found its equilibrium. In this case, back-action from the mode continuum can no longer be ignored. More precisely, due to energy and momentum conservation, this dynamics, which now is dominated by in- and out-scattering events on an equal footing, is very slow. It is no longer described by an equilibrium response theory, which is determined solely by the retarded self-energy. Instead the presence of dynamical slow modes is revealed, which are not captured by a simple exponential decay but have to be implemented as additional modes due to symmetries[129] and favor an algebraic decay in time, i.e. $\delta n_q(\tau) \sim \tau^{-\beta}$ with some exponent β . In Fig. 4.12, the two different stages of

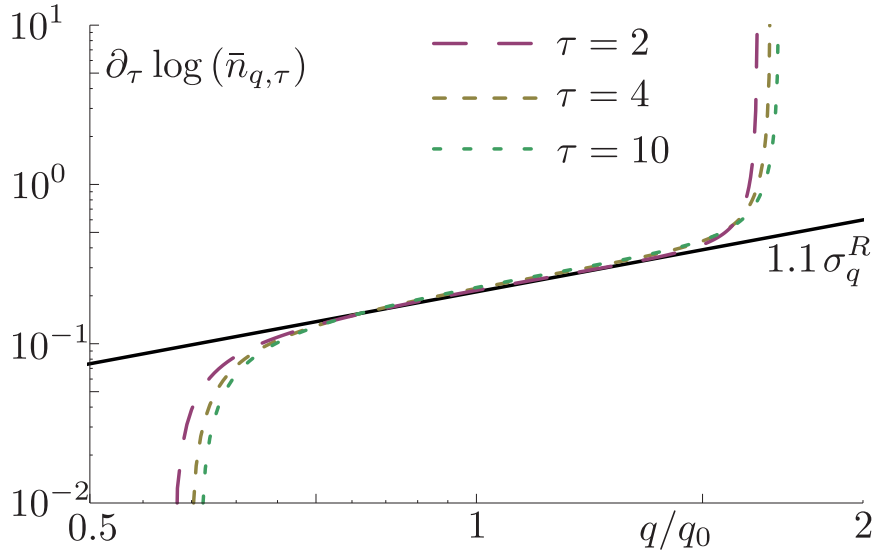


Figure 4.11: Comparison of the decay rate $\gamma_q = -\partial_\tau \log(\bar{n}_{q,\tau})$ as a function of momentum for different times τ with the analytically estimated decay factor $\gamma_q^A = 2.2\sigma_q^R$. The time is given in units of $\frac{1}{v_0 q_0^2}$. The exact decay coincides very well with the analytical prediction, only when $\bar{n}_{q,\tau} \approx 0$ becomes very small, the numerical error and therefore the relative deviation is significant.

the time evolution are visible in the numerical simulation of the quasi-particle occupation. The algebraic decay for long times, and the exponential decay for shorter times, are clearly distinguished. In order to estimate the algebraic exponent, we do not linearize the kinetic equation but instead take Eq. (6.3.11) and insert on the right hand side the solution for the phonon occupations $n_q(\tau) - n_B(T_f) \sim e^{-1.1\sigma_q^R \tau}$. Due to the scaling of the thermal self-energy $\sigma_q^R \sim q^{\frac{3}{2}}$, this yields the estimate $\beta = \frac{2}{3}$. In the numerical simulations presented in Fig. 4.12, we find for the algebraic exponent $\beta \approx 0.58$.

As mentioned already, this algebraic decay is a consequence of energy and momentum conservation in the dynamics, which leads to additional slow modes in the time evolution. The separation of the relaxation into two different time regimes, with first exponential decay according to bare phonon decay and then algebraic decay due to energy conservation, has already been found in a recent work on phenomenological grounds using an equilibrium formalism [126]. There energy conservation was implemented by hand, while being naturally incorporated in the formalism of this manuscript. The algebraic decay of the phonon occupations can be explained in terms of dynamical slow modes, resulting from conservation laws, i.e. symmetries, in the system. The analytical exponent $\beta = \frac{2}{3}$ would belong to a system with exact momentum and energy conservation, while the deviation of the numerical result $\beta \approx 0.58$ from the analytical one might be a result of subleading corrections that will vanish on even larger time scales[129].

4.7 DYSON-SCHWINGER EQUATIONS AND VERTEX CORRECTIONS

In this section we apply Dyson-Schwinger equations [6, 152] to the interacting Luttinger Liquid and determine the self-energy and three-point vertex as a function of the phonon

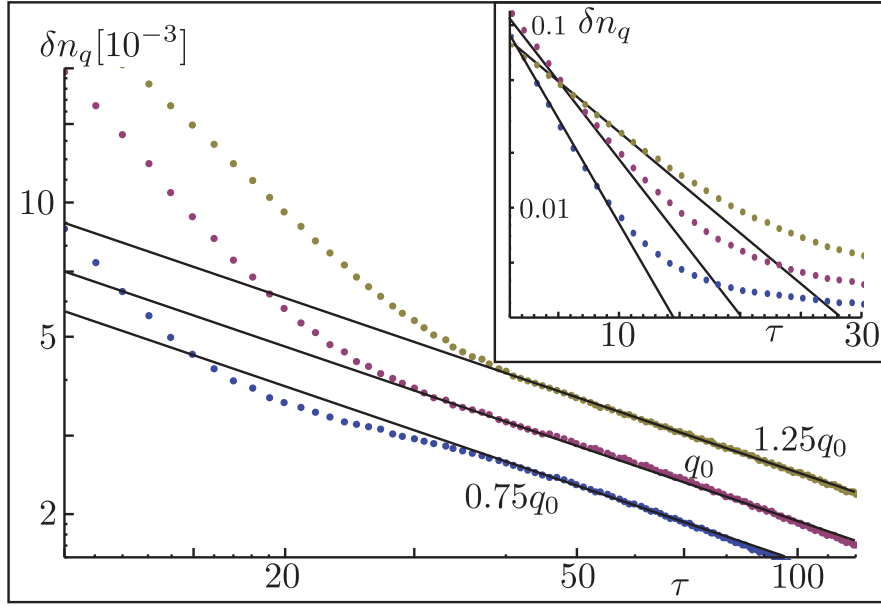


Figure 4.12: Decay of the deviation $\delta n_q(\tau)$ of the phonon density to its corresponding thermal value for fixed momenta $(q_1, q_2, q_3) = (0.75, 1, 1.25)q_0$. a) Log-Log plot of the deviation $\delta n_q(\tau)$ (blue dots: simulations; line: algebraic fit): For long times, the decay is described by a power law in time, i.e. $\delta n_q(\tau) \sim \tau^{-\beta}$ with an exponent $\beta \approx 0.58$. b) Semi-logarithmic plot of the deviation $\delta n_q(\tau)$: For short times, the decay is described by an exponential, $\delta n_q(\tau) \sim e^{-1.1\sigma_{q_0}^R \tau}$, where σ^R is the corresponding thermal self-energy (blue dots: numerical simulation; red line: exponential fit, obtained from the self-energy).

distribution. We show that the vertex correction is always real and will be exactly zero for a zero temperature state. More generally it leads to a modification $v_0 \rightarrow v_0(1 + \mathcal{I})$, where \mathcal{I} is a small ($1 \gg \mathcal{I}$) dimensionless function with weak momentum dependence, whose precise form is determined by the time-dependent phonon density. Based on these findings, we conjecture that also the corrections to the four-point and higher order vertices, which do not occur in the microscopic action, are small. As a result, the kinetic equation and the equation for the self-energies in self-consistent Born-approximation are modified according to the vertex correction, and we derive a coupled but closed set of equations.

In general, Dyson-Schwinger equations (DSE) represent an exact hierarchy for one-particle irreducible (1PI) correlation functions, generated by the effective action functional $\Gamma[a_\alpha, a_\beta]$ [6, 152, 204]. It relates the full vertices (e.g. the Green's function, which is the inverse two-point vertex) to their bare, microscopic counterparts, which form the microscopic action S . The hierarchy built up by the DSE is in general infinite and therefore lacking an exact solution. The main is then to find a physically reasonable truncation of the effective action, for which the main physical effects are captured and in which the DSE can be solved.

The effective action, as the generator of 1PI correlation functions, can be expanded according to [6, 152, 204]

$$\Gamma[a_\alpha, a_\beta] = \sum_{n=2}^{\infty} \frac{1}{n!} \Gamma_{\alpha_1, \dots, \alpha_n}^{(n)} a_{\alpha_1} \dots a_{\alpha_n}, \quad (4.7.1)$$

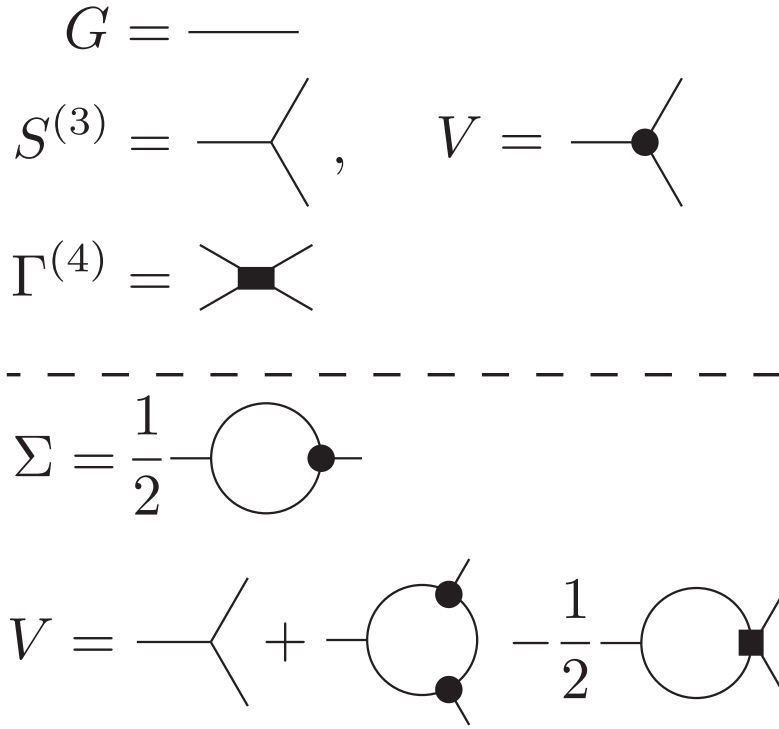


Figure 4.13: Schematic diagrammatic representation of the self-energy Σ and the full three-point vertex V in terms of the full Green's function G , bare three-point vertex \tilde{V} , and the full four-point vertex $\Gamma^{(4)}$.

where $\Gamma_{\alpha_1, \dots, \alpha_n}^{(n)}$ is the n -th order functional derivative of the effective action,

$$\Gamma_{a_1, \dots, a_n}^{(n)} = \left. \frac{\delta^n \Gamma}{\delta a_n \dots \delta a_1} \right|_{a_{a_i} = 0}, \quad (4.7.2)$$

i.e. the full n -point vertex function, and a_α are the fields with collective index $\alpha = (\omega, \mathbf{q}, \tau, c/q)$. The inverse Green's function and the full three-point vertex are the second and third order functional derivatives, respectively. In terms of formulas we have

$$G^{-1} = G_0^{-1} - \Sigma = \Gamma^{(2)} \quad \text{and} \quad V = \Gamma^{(3)}. \quad (4.7.3)$$

In the present case, the DSE relate the n -point vertex to the $n + 1$ point vertex of the theory. More specifically, we obtain for the full Green's function

$$(G^{-1})_{\alpha\beta} = (G_0^{-1})_{\alpha\beta} - \frac{i}{2} S_{\alpha\gamma\delta}^{(3)} G_{\gamma\mu} V_{\mu\beta\nu} G_{\nu\delta}, \quad (4.7.4)$$

and for the full three-point vertex

$$\begin{aligned} V_{\alpha\beta\gamma} = & S_{\alpha\beta\gamma}^{(3)} + i S_{\alpha\delta\nu}^{(3)} G_{\delta\mu} V_{\mu\beta\eta} G_{\eta\sigma} V_{\sigma\gamma\epsilon} G_{\epsilon\nu} \\ & - \frac{i}{2} S_{\alpha\delta\nu}^{(3)} G_{\delta\mu} \Gamma_{\mu\beta\gamma\eta}^{(4)} G_{\eta\nu}. \end{aligned} \quad (4.7.5)$$

Here, $S^{(3)}$ is the bare (microscopic) three-point vertex. A schematic diagrammatic repre-

sentation of Eqs. (4.7.3), (4.7.4) and (4.7.5) is depicted in Fig. 4.13.

We will show in the following that there are corrections to the bare three-point vertex, with the same scaling dimension as the bare three-point vertex itself. It is determined by a dimensionless function \mathcal{I} whose precise form is dictated by the time dependent phonon density $n_{q,\tau}$. This is in contrast to the two-point vertex, i.e. the inverse Green's function, where the correction due to the cubic vertex is subleading but introduces an imaginary part and therefore is of great qualitative importance. Here the correction is purely real, as the bare vertex itself, but on the other hand not subleading. It therefore can not be discarded directly without further discussion.

For the $\bar{a}_{Q+p}^q a_p^c a_Q^c$ term, the vertex correction $\delta V = V - S^{(3)}$ is illustrated in a diagrammatic representation in Fig. 4.14. It is equivalent to all other vertices that incorporate a single quantum and two classical fields. The lowest order contribution, incorporating only bare vertices, reads (for $q, p > 0$)

$$\begin{aligned} \delta V_{q,p,p+q}^{\text{ccq}} &= \frac{v_0^3}{\sqrt{8}} \sqrt{|qp(p+q)|} \int_{k>0} \left\{ \frac{k(q+k)(k-p)}{\sigma_{k+q}^R + \sigma_{k-p}^R} \left[\frac{n_{k-p} - n_k}{\sigma_k^R + \sigma_{k-p}^R} + \frac{n_{q+k} - n_k}{\sigma_k^R + \sigma_{k+q}^R} \right] \right. \\ &\quad \left. + \frac{k(p+k)(k-q)}{\sigma_{k+p}^R + \sigma_{k-q}^R} \left[\frac{n_{k-q} - n_k}{\sigma_{k-q}^R + \sigma_k^R} + \frac{n_{p+k} - n_k}{\sigma_{k+p}^R + \sigma_k^R} \right] \right\}. \end{aligned} \quad (4.7.6)$$

Here $\sigma_k^R = -\text{Im}(\Sigma_k^R) > 0$ are the on-shell self-energies obtained by the DSE in Fig. 4.13. The vertex correction due to cubic vertices is identical to zero for a zero temperature system ($n_k = 0$ for all momenta). This is an exact statement for the interacting Luttinger Liquid and can be seen on the level of the diagrams in Fig. 4.14. For $T = 0$, $G^K = G^R - G^A$ and the individual diagrams cancel each other⁴ due to the pole structure of G^R and G^A . For cubic vertices, in the absence of higher order terms and for a constant distribution function, the vertex correction is exactly zero, this has been shown to hold for arbitrary dimensions[63].

In order to find a compact expression for the vertex correction, we replace $\sigma^R \rightarrow v_0 \tilde{\sigma}^R$ and compare the integrand in Eq. (4.7.6) with the expression for the self-energy $\tilde{\sigma}^R$ in Eq. (6.3.10). We immediately see, that the vertex correction is linear in v_0 and the integral has scaling dimension zero⁵. In perturbation theory, this yields the vertex

$$\begin{aligned} V_{q,p,q+p}^{(1\text{st})} &= v_0 \sqrt{|pq(p+q)|} \left(1 + \mathcal{I}_0 \left(\frac{p}{q}, n \right) \right) \\ &= S_{q,p,p+q}^{(3)} \left(1 + \mathcal{I}_0 \left(\frac{p}{q}, n \right) \right). \end{aligned} \quad (4.7.7)$$

Here, $\mathcal{I}_0 \left(\frac{p}{q}, n \right)$ is a dimensionless function of the ratio p/q and the phonon density n , which is determined by the integral in Eq. (4.7.6). The scaling behavior of the one-loop vertex correction suggests the parametrization of the full vertex according to

$$V_{q,p,q+p} = v_0 \sqrt{|pq(p+q)|} \left(1 + \mathcal{I} \left(\frac{p}{q}, n \right) \right), \quad (4.7.8)$$

⁴Strictly speaking $G^K = \text{sgn}(\omega) (G^R - G^A)$, which however leaves the result invariant as can be seen from Eq. (4.7.6).

⁵This holds true for an arbitrary phonon density n_q since the dimensions cancel exactly, independent of the form of n_q .

where the functional \mathcal{I} encodes the full vertex correction. According to the DSE in Fig. 4.13, it is determined via

$$\mathcal{I}(x, n) = \frac{1}{\sqrt{8}} \int_{\tilde{k}>0} \left\{ \frac{\tilde{k}(1+\tilde{k})(\tilde{k}-x) \left(1 + \mathcal{I}\left(\frac{\tilde{k}}{|1-\tilde{k}|}, n\right)\right) \left(1 + \mathcal{I}\left(\frac{\tilde{k}}{x}, n\right)\right)}{\tilde{\sigma}_{\tilde{k}+1}^R + \tilde{\sigma}_{\tilde{k}-x}^R} \left[\frac{n_{\tilde{k}-x} - n_{\tilde{k}}}{\tilde{\sigma}_{\tilde{k}}^R + \tilde{\sigma}_{\tilde{k}-x}^R} + \frac{n_{1+\tilde{k}} - n_{\tilde{k}}}{\tilde{\sigma}_{\tilde{k}}^R + \tilde{\sigma}_{\tilde{k}+1}^R} \right] \right. \\ \left. + \frac{\tilde{k}(x+\tilde{k})(\tilde{k}-1) \left(1 + \mathcal{I}\left(\frac{x}{|\tilde{k}-x|}, n\right)\right) \left(1 + \mathcal{I}(\tilde{k}, n)\right)}{\tilde{\sigma}_{\tilde{k}+x}^R + \tilde{\sigma}_{\tilde{k}-1}^R} \left[\frac{n_{\tilde{k}-1} - n_{\tilde{k}}}{\tilde{\sigma}_{\tilde{k}-1}^R + \tilde{\sigma}_{\tilde{k}}^R} + \frac{n_{x+\tilde{k}} - n_{\tilde{k}}}{\tilde{\sigma}_{\tilde{k}+x}^R + \tilde{\sigma}_{\tilde{k}}^R} \right] \right\}. \quad (4.7.9)$$

where $\tilde{k} = \frac{k}{q}$ and the integral is dimensionless. In Eq. (4.7.9), we have already exploited the fact that the ingoing momenta of a vertex can be exchanged without modifying the vertex itself, and consequently the integral is invariant under $q \leftrightarrow p$. This is equivalent to $\mathcal{I}(x, n) = \mathcal{I}\left(\frac{1}{x}, n\right)$. The self-energy in the DSE approach is

$$\tilde{\sigma}_q^R = \int_{0 < p} \left(\frac{\partial_{\tilde{\tau}} n_p}{\tilde{\sigma}_p^R} + 2n_p + 1 \right) \left\{ \left[1 + \mathcal{I}\left(\frac{p}{|p-q|}\right) \right] \frac{qp(q-p)}{\tilde{\sigma}_p^R + \tilde{\sigma}_{q-p}^R} + \left[1 + \mathcal{I}\left(\frac{p}{q}\right) \right] \frac{qp(p+q)}{\tilde{\sigma}_p^R + \tilde{\sigma}_{p+q}^R} \right\}. \quad (4.7.10)$$

In the same way the kinetic equation can be modified to incorporate the vertex correction as well, and we find a set of coupled equations

$$\begin{pmatrix} \partial_{\tilde{\tau}} n \\ \tilde{\sigma}^R \\ \mathcal{I} \end{pmatrix} = \mathcal{F}(n, \tilde{\sigma}^R, \mathcal{I}). \quad (4.7.11)$$

They can be solved numerically according to the procedure described in Fig. 4.6. Including the vertex correction, the second step of the iteration additionally includes the self-consistent determination of \mathcal{I} .

We will now give an estimate of the order of the vertex correction for the case for which it is non-zero to estimate its impact on the dynamics and the kinetic equation. In the limit $T \rightarrow \infty$ the relevant phonon density is $n_q \approx \frac{T}{u|q|}$ and the self-energies have the thermal form $\tilde{\sigma}_q^R \propto \sqrt{\frac{T}{u}} q^{3/2}$. Consequently, the factor $\frac{T}{u}$ drops out and $\mathcal{I}(x, n)$ does no longer depend on temperature. In this case, $\mathcal{I}(0, n) \approx 0.012$, $\mathcal{I}(1, n) \approx 0.09$ and $\mathcal{I}(0, n) \leq \mathcal{I}(x, n) \leq \mathcal{I}(1, n)$. As can be seen in Fig. 4.15, the correction is small, with a weak momentum dependence. Consequently, the self-energy is only negligibly modified if instead of the full three-point vertex in Eq. (4.7.4), the bare value \tilde{V} is used. This is precisely the self-consistent Born approximation that we used to determine the self-energies and the kinetic equation for the interacting Luttinger Liquid.

4.8 CONCLUSION

In this chapter, we used non-equilibrium field theory, in particular kinetic and Dyson-Schwinger equations, to determine the kinetics and non-equilibrium dynamics of resonantly interacting Luttinger Liquids. Exploiting the fact that the interactions lead to dressed but still well defined phonons, which enables a separation of timescales into slow forward and fast relative dynamics, we applied the Wigner and quasi-particle approximation and derived a closed set of simple yet powerful equations for the normal and anomalous phonon

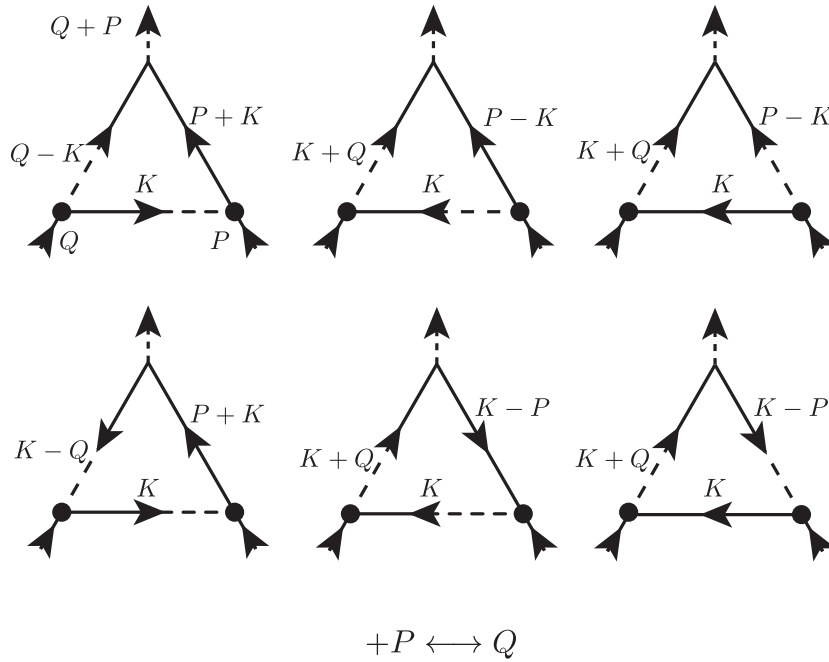


Figure 4.14: Diagrams contributing to the vertex correction of the three-point vertex $V_{q,p,p+q}$ illustrated for the particular example of an outgoing quantum field and two incoming classical fields, i.e. $\propto \bar{a}_{Q+P}^q a_Q^c a_P^c$. In total there are twelve distinct diagrams contributing to the vertex correction, six are depicted above and six further can be found by interchanging the ingoing momenta $P \leftrightarrow Q$.

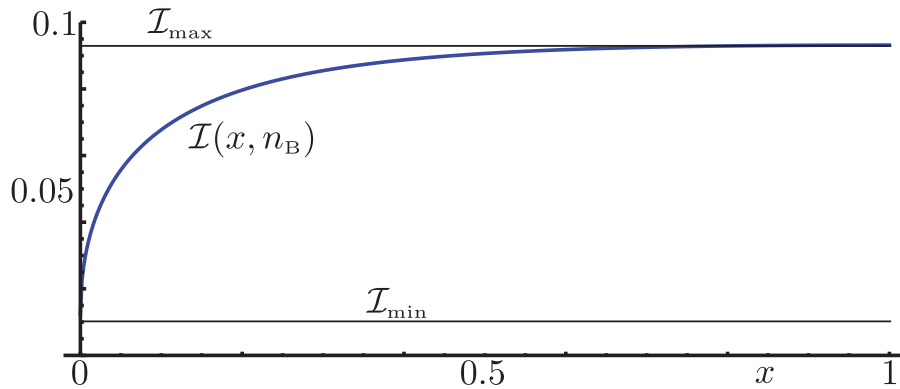


Figure 4.15: Vertex correction $\mathcal{I}(x, n_B(T))$ for an infinite temperature state. In the limit $T \rightarrow \infty$, the temperature drops out in Eq. (4.7.9), and the vertex correction becomes temperature independent. Due to the invariance of \mathcal{I} under $x \rightarrow \frac{1}{x}$, the plot is restricted to $0 \leq x \leq 1$. The dependence of \mathcal{I} on x is weak, especially for $x \approx 1$, where it takes its maximum $\mathcal{I}(x, n_B) \leq \mathcal{I}_{\max} \approx 0.093$.

density, the phonon self-energy and vertex correction. These equations determine the dynamics of an interacting Luttinger Liquid initialized in a Gaussian (non-) equilibrium state. The resulting equations show strong aspects of universality, on the one hand being independent of any UV-scale, in particular independent of the Luttinger cutoff. On the other hand, after a proper rescaling of the forward time, all microscopic parameters entering the Hamiltonian can be eliminated and the only microscopic information entering the dynamical equations is the initial phonon density. We further used our approach to analytically determine the relaxation rate of a thermally excited state. For this dynamics, we found an initial exponential decay corresponding to previous results computed from linear response theory [8, 161, 176, 150, 151]. However, for longer times, the decay of the excitations follows a power law in time, revealing the presence of dynamical slow modes due to energy conservation. These latter modes are not contained in a plain equilibrium linear response theory but have to be build in by hand on the basis of symmetry arguments and conservation laws[126, 129]. Here, the dynamics based on the kinetic equation approach reveals the presence of these modes due to the algebraic decay at long times without any further modification, which shows the strength of our approach in a simple yet nontrivial example.

The results of this work can be used in order to determine the kinetics and non-equilibrium dynamics of one-dimensional interacting quantum fluids prepared in a non-thermal initial state, which might occur as a consequence of a quantum quench or a sudden external perturbation. On the other hand, it paves the way to compute the dynamics of quantum fluids subject to drive and dissipation, and to determine the dynamics towards the steady state of an excited closed system. Of special interest and a strength of our approach is the treatment of long time dynamics in non-equilibrium systems, which are neither reachable by present numerical procedures nor by analytical approaches based on perturbation theory. Both examples belong to the uprising field of one-dimensional quantum fluids out-of-equilibrium and we leave their discussion open for future work.

5 THERMALIZATION AND PRETHERMALIZATION IN INTERACTING LUTTINGER LIQUIDS AFTER A QUANTUM QUENCH

The process of thermalization describes the dynamics of a physical system, which is initialized at $t = 0$ in a non-thermal state ρ_0 and evolves in time, until it reaches the stationary state of the dynamics, which is a thermal Gibbs ensemble. While equilibrium statistical mechanics (both quantum and classical) predict a stationary state, which is in thermal equilibrium, there is an active debate in the recent literature if an interacting quantum many-body system initialized in an arbitrary quantum state will actually thermalize. This question is triggered mainly by the fact that the time evolution of a quantum system is unitary, and for this reason reversible, which does not allow for a single fixed point in the dynamics in a strict mathematical sense. A solution to overcome this problem is the so-called eigenstate thermalization hypothesis (ETH) in combination with the statement of typicality of physical states. In a few words, when a system is initialized in a non-eigenstate of the system's Hamiltonian, the off-diagonal elements of the density matrix govern time dependent complex phases, which average out

$$\begin{aligned} \rho_t &= e^{-iHt} \rho_0 e^{iHt} = \sum_{l,m} \alpha_l \alpha_m^* e^{-iHt} |l\rangle \langle m| e^{iHt} \\ &= \sum_{l,m} \alpha_l \alpha_m^* e^{i(\omega_l - \omega_m)t} |l\rangle \langle m| \xrightarrow{t \rightarrow \infty} \sum_l |\alpha_l|^2 |l\rangle \langle l|, \end{aligned} \quad (5.0.1)$$

where the term on the right hand side is called the diagonal ensemble corresponding to the initial state. As a consequence, in the long time limit, physical observables are determined solely by the initial distribution of the eigenstates of the Hamiltonian $\sim |\alpha_l|^2$. If one now assumes a "typical" behavior for the relevant eigenstates, i.e. that for eigenstates in the relevant energy regime, which has been accessed by the initial state, the expectation value of local observables does not vary too strongly¹, the stationary state of the system can be

¹A more detailed and mathematically more strict definition of the terms "relevant eigenstates", "local observables" and "strong variation" can be found in the corresponding literature [166, 53, 184]. It is not the purpose of this thesis to review the arguments of the ETH and typicality with significant detail.

described in terms of a typical state of the relevant energy window

$$\rho_t \xrightarrow{t \rightarrow \infty} |l_t\rangle\langle l_t|, \quad (5.0.2)$$

where $|l_t\rangle$ is a typical eigenstate, reflecting the initial states average energy. This is the eigenstate thermalization hypothesis. As a consequence, systems, for which typicality and therefore ETH are applicable, will reach a thermal state in their long time dynamics after being initialized in a non-thermal state at $t = 0$.

However, there are many exceptions, for which the above arguments are not applicable and which will not thermalize to a Gibbs ensemble. A broad class of such systems are so-called integrable systems, which have an infinite number of constants of motion and for which the initial distribution of eigenstates is crucial in order to describe the long time dynamics. These states evolve to a stationary state, which properly takes into account all constants of motion and is referred to as generalized Gibbs ensemble. Examples for integrable systems are quadratic Hamiltonians², the Lieb-Liniger model for bosons (Eq. (3.1.6)) and the Luttinger model for interacting fermions with a linear dispersion (Eq. (3.2.6)). While it is evident, that an integrability breaking term added to an integrable Hamiltonian will finally lead to thermalization of the system in the long time limit, it is not clear, whether or not the dynamical fixed point of the integrable model plays an important role in the non-equilibrium dynamics of the non-integrable model. In the recent literature, however, there is consensus that a non-thermal fixed point of an integrable theory serves as a metastable fixed point for the transient dynamics of the corresponding non-integrable theory and therefore determines the short time dynamics. Whether this is the case and in which way the short time dynamics is determined by the corresponding integrable fixed point is however not systematically investigated and an open topic of current research.

In this chapter, we will study precisely this question by performing an interaction quench (to be precise, a quench of the microscopic interactions) in the interacting Luttinger model (3.1.24). In this quench scenario, the system is initialized in an eigenstate ρ_0 of the interacting Luttinger model H_i at $t = 0$. Suddenly, the interaction strength is changed and the system evolves in time according to a different Hamiltonian $H_f \neq H_i$, for which the initial state ρ_0 is no longer an eigenstate. As the interacting Luttinger model is not integrable, its dynamical fixed point is a thermal Gibbs ensemble, with a temperature β , which is determined by the energy injected by the quench. On the other hand, the non-interacting Luttinger model is integrable and does not thermalize but evolves to a generalized Gibbs ensemble, for which the constants of motion, i.e. the phonon occupancies, depend on the initial state. The interaction quench in a non-interacting Luttinger model has been studied by Cazalilla and others only recently [39, 95, 96] and the corresponding stationary state features algebraic correlation functions in space (as known for the ground state of the Luttinger model) but with a new non-equilibrium exponent and an algebraically decaying quasi-particle residue $Z(t) \sim t^{-\gamma_{\text{neq}}}$.

For the interacting Luttinger model, we find that for long distances, thermalization takes place in two steps. First, a light cone of quasi-particles spreads into the left and right direction with velocity u , such that at distances $x = 2ut$ the system reaches an intermediate, metastable state, which is described by the non-interacting Luttinger theory. However, due to the interaction of the excited quasi-particles, there is a second, thermal regime, spreading in space as $x = \lambda t^\alpha$, with $\alpha < 1$ and λ some constant, which is due to the interactions. The intermediate regime $\lambda t^\alpha < x < 2ut$ is described by the steady state of the integrable theory and due to its metastability, we refer to this state as prethermal and the effect of reaching an intermediate, metastable state as prethermalization. As $\alpha < 1$, there exists a minimal distance for prethermalization, defined by the time t_{min} , for which $\lambda t_{\text{min}}^\alpha = 2ut_{\text{min}} = x_{\text{min}}$. Below this distance, the prethermal regime does not occur, since the redistribution of energy is faster than the formation of quasi-particles³.

²Quadratic in terms of creation and annihilation operators for the elementary excitations.

³This does not contradict with Lieb-Robinson bounds for this system, as Lieb-Robinson bounds feature non-universal corrections on short distances as well and only obtain their typical form in the asymptotic limit.

In order to study the prethermalization and thermalization of fermions after an interaction quench, we consider the fermionic Luttinger model with non-zero band curvature. At $t = 0$, the microscopic fermion-fermion interaction is ramped suddenly from some initial value g_i to some final value g_f and subsequently the time evolution of the system is computed using the kinetic equation approach, which we have derived in the previous section. With this approach, we can then finally determine the time evolution of fermionic correlation functions and the fermionic momentum distribution.

The chapter is organized as follows, in the first section, we determine the initial state after the quench in the Luttinger basis. In the subsequent section, we discuss the prethermal state by considering the time evolution of the non-interacting Luttinger model. Finally, in the last section, we determine the time evolution of the system after the quench for the interacting Luttinger model and discuss the corresponding fermionic properties.

5.1 FERMIONIC INTERACTION QUENCH AND INITIAL STATE AFTER THE QUENCH

We consider a model of spin polarized, interacting fermions with non-zero band curvature as described by the Hamiltonian (3.2.5), i.e.

$$H_F = \int_x \sum_{\eta=\pm} \psi_{\eta,x}^\dagger \left(i\eta v_F \partial_x - \frac{\partial_x^2}{2m^*} \right) \psi_{\eta,x} + \int_{x,x'} g(x-x') \rho(x) \rho(x'). \quad (5.1.1)$$

This model is integrable in the limit of vanishing band curvature, $m \rightarrow \infty$ and can be exactly mapped to a quadratic Luttinger Liquid model, as described in Sec. 3.2. For $m < \infty$, the model is non-integrable and can be mapped to an interacting Luttinger Liquid [93, 110, 94], described by the Hamiltonian (3.2.42),

$$H_{\text{ILL}} = \frac{1}{2\pi} \int_x \left[uK (\partial_x \theta_x)^2 + \frac{u}{K} (\partial_x \phi_x)^2 + \frac{1}{m} (\partial_x \phi_x) (\partial_x \theta_x)^2 \right], \quad (5.1.2)$$

where the Luttinger parameters u, K are determined from the microscopic parameters according to

$$u = v_F \sqrt{1 + \frac{2g_0}{\pi v_F}}, \quad \text{and} \quad K = \sqrt{1 + \frac{2g_0}{\pi v_F}}^{-1}. \quad (5.1.3)$$

Here, g_0 is the effective zero momentum interaction potential⁴. In an interaction quench at $t = 0$, the interaction g_0 is suddenly ramped from some initial value $g_{0,i}$ to some final value g_0 (for convenience, we attribute an extra label for the final value of the parameters after the quench). In the Hamiltonian (5.1.2), this corresponds to a sudden change of the parameters $(u_i, K_i) \rightarrow (u, K)$ at $t = 0$, while the cubic nonlinearity $\sim \frac{1}{m}$ is left unchanged. We consider the system to be at equilibrium for times $t < 0$ and therefore its density matrix is

$$\rho_{t<0} = \frac{1}{Z} e^{-\beta H_i}, \quad (5.1.4)$$

where H_i is the initial Hamiltonian of the interacting Luttinger Liquid, i.e. the Hamiltonian in Eq. (5.1.2) with the initial set of parameters (u_i, K_i) .

⁴For a detailed derivation, see Sec. 3.2.

The nonlinearity in the Hamiltonian can be decomposed into resonant, i.e. energy conserving, scattering processes and non-resonant, i.e. virtual, scattering processes. The virtual processes are irrelevant and neither modify the spectrum of the system nor have an impact on the ground state but lead to subleading correction in the phonon self-energies⁵. On the other hand, the resonant nonlinearities commute with the quadratic part of the Hamiltonian, which is evident from the fact that they describe energy conserving collisions. The reason for non-trivial dynamics in this set-up is that the Hamiltonian, on the many-body level, features a highly degenerate spectrum and the collisions lead to a dynamics within the fixed-energy subspace. Therefore, the initial state is determined by the initial values of the quadratic Hamiltonian alone and we write

$$\rho_{t<0} = \frac{1}{Z} e^{-\beta H_i^{(2)}}. \quad (5.1.5)$$

Here,

$$H^{(2)} = \frac{1}{2\pi} \int_x \left[uK (\partial_x \theta_x)^2 + \frac{u}{K} (\partial_x \phi_x)^2 \right] \quad (5.1.6)$$

is the quadratic Luttinger Liquid Hamiltonian. In order to determine the initial state at $t = 0$, we have to express the state $\rho_{t<0}$ in terms of the eigenmodes of the Hamiltonian $H_{t>0}$. The transformation from the parameter independent fields ϕ, θ to the eigenmodes depends on the Luttinger parameter K and reads (see Eqs. (3.1.26), (3.1.27))

$$\phi_q = -\frac{i}{2} \left(\frac{2\pi K}{|q|} \right)^{\frac{1}{2}} \text{sgn}(q) \left(a_q^\dagger + a_{-q} \right), \quad (5.1.7)$$

$$\theta_q = \frac{i}{2} \left(\frac{2\pi}{|q|K} \right)^{\frac{1}{2}} \left(a_q^\dagger - a_q \right). \quad (5.1.8)$$

Since the Luttinger parameter K is quenched $K_i \rightarrow K$ at $t = 0$, the transformation into the eigenbasis (Eqs. (5.1.7), (5.1.8)) is changed accordingly. We label the creation and annihilation operators of the initial eigenbasis before the quench with b_q^\dagger, b_q . They are defined in terms of the Luttinger fields

$$\phi_q = -\frac{i}{2} \left(\frac{2\pi K_i}{|q|} \right)^{\frac{1}{2}} \text{sgn}(q) \left(b_q^\dagger + b_{-q} \right), \quad (5.1.9)$$

$$\theta_q = \frac{i}{2} \left(\frac{2\pi}{|q|K_i} \right)^{\frac{1}{2}} \left(b_q^\dagger - b_q \right). \quad (5.1.10)$$

Inverting the transformation (5.1.7), (5.1.8), in terms of Luttinger fields, the phonon modes after the quench are

$$a_q^\dagger = -i \left(\frac{|q|K}{2\pi} \right)^{\frac{1}{2}} \left(\theta_q - \frac{\text{sgn}(q)}{K} \phi_q \right), \quad (5.1.11)$$

$$a_q = i \left(\frac{|q|K}{2\pi} \right)^{\frac{1}{2}} \left(\theta_{-q} - \frac{\text{sgn}(q)}{K} \phi_{-q} \right). \quad (5.1.12)$$

Combining the two transformations, the phonon modes after the quench can be expressed

⁵See Sec. 4 for more details on resonant interactions.

in terms of the phonon modes before the quench,

$$a_q^\dagger = \frac{1}{2} \left(\sqrt{\frac{K}{K_i}} (b_q^\dagger - b_{-q}) + \sqrt{\frac{K_i}{K}} (b_q^\dagger + b_{-q}) \right). \quad (5.1.13)$$

If the Luttinger parameter is not changed by the quench, i.e. for $K = K_i$, the operators before the quench are identical to the operators after the quench, as the eigenbasis of the Hamiltonian is unchanged in this case. In terms of the phonon occupation before the quench, the phonon occupation after the quench is

$$\begin{aligned} a_q^\dagger a_q &= \frac{K}{4K_i} \left[(b_q^\dagger - b_{-q}) + \frac{K_i}{K} (b_q^\dagger + b_{-q}) \right] \left[(b_q - b_{-q}^\dagger) + \frac{K_i}{K} (b_q + b_{-q}^\dagger) \right] \\ &= \frac{1}{4} \left[\left(\frac{K}{K_i} + \frac{K_i}{K} + 2 \right) b_q^\dagger b_q + \left(\frac{K}{K_i} + \frac{K_i}{K} - 2 \right) b_{-q} b_{-q}^\dagger + \left(\frac{K_i}{K} - \frac{K}{K_i} \right) (b_q^\dagger b_{-q}^\dagger + b_q b_{-q}) \right] \\ &= \frac{1}{2} \left[\frac{K^2 + K_i^2}{KK_i} b_q^\dagger b_q + \frac{(K - K_i)^2}{2KK_i} + \frac{K_i^2 - K^2}{2KK_i} (b_q^\dagger b_{-q}^\dagger + b_q b_{-q}) \right]. \end{aligned} \quad (5.1.14)$$

The anomalous phonon density after the quench is determined the same way and is

$$\begin{aligned} a_q^\dagger a_{-q}^\dagger &= \frac{K}{4K_i} \left[(b_q^\dagger - b_{-q}) + \frac{K_i}{K} (b_q^\dagger + b_{-q}) \right] \left[(b_{-q}^\dagger - b_q) + \frac{K_i}{K} (b_{-q}^\dagger + b_q) \right] \\ &= \frac{K_i^2 - K^2}{4KK_i} (2b_q^\dagger b_q + 1) + \frac{(K + K_i)^2}{4KK_i} b_q^\dagger b_{-q}^\dagger + \frac{(K - K_i)^2}{4KK_i} b_q b_{-q}. \end{aligned} \quad (5.1.15)$$

For $K \neq K_i$, the quench mixes anomalous and normal occupations of the phonons. Therefore, for a system that is in equilibrium before the quench, after the quench, there will be non-zero off-diagonal occupations and the system is clearly brought out of equilibrium.

At $t = 0$, the initial state is

$$\rho_{t < 0} = \frac{1}{Z} \exp \left(-\frac{\beta}{2\pi} \int_x \left[uK (\partial_x \theta_x)^2 + \frac{u}{K} (\partial_x \phi_x)^2 \right] \right) = \frac{1}{Z} \exp \left(-\beta u_i \int_q |q| b_q^\dagger b_q \right) \quad (5.1.16)$$

and the initial occupations in the post-quench basis are

$$\langle a_q^\dagger a_q \rangle = \left[\frac{K^2 + K_i^2}{2KK_i} n_B(\beta u_i |q|) + \frac{(K - K_i)^2}{4KK_i} \right] e^{-\frac{|q|}{\Lambda}}, \quad (5.1.17)$$

$$\langle a_q^\dagger a_{-q}^\dagger \rangle = \frac{K_i^2 - K^2}{4KK_i} (2n_B(\beta u_i |q|) + 1) e^{-\frac{|q|}{\Lambda}}. \quad (5.1.18)$$

Here, we used the Bose-Einstein distribution function

$$n_B(\epsilon) = (e^\epsilon - 1)^{-1} \quad (5.1.19)$$

which describes the thermal distribution of the initial phonons and implemented the phonon cutoff Λ in the distribution function. The energy injected into the system by the quench can be computed as the difference between the initial energy and the final energy. The initial energy is

$$E_i = \int_q u_i |q| n_B(\beta |q| u_i) = u_i \frac{\pi^2}{3\beta^2 u_i^2} = \frac{\pi^2 K_i}{3\beta^2 v_F}, \quad (5.1.20)$$

where we used the definition of the Luttinger variables in Eq. (3.2.41). The final energy is

$$\begin{aligned} E &= \int_{\mathbf{q}} u|\mathbf{q}| \left[\frac{K^2 + K_i^2}{2KK_i} n_{\text{B}}(\beta u_i |\mathbf{q}|) + \frac{(K - K_i)^2}{4KK_i} \right] e^{-\frac{|\mathbf{q}|}{\Lambda}} = \frac{\pi^2 u}{3\beta^2 u_i^2} \frac{K^2 + K_i^2}{2KK_i} + \frac{(K - K_i)^2}{2KK_i} u \Lambda^2 \\ &= \frac{\pi^2 K_i}{3\beta^2 v_{\text{F}}} \frac{1}{2} \left(1 + \frac{K_i^2}{K^2} \right) + \frac{1}{2} \left(\frac{K_i}{K} - 1 \right)^2 \frac{K_i u_i^2 \Lambda^2}{v_{\text{F}}}. \end{aligned} \quad (5.1.21)$$

This amounts to an energy difference

$$\Delta E = E - E_i = \frac{\pi^2 K_i}{3\beta^2 v_{\text{F}}} \frac{1}{2} \left(\frac{K_i^2}{K^2} - 1 \right) + \frac{1}{2} \left(\frac{K_i}{K} - 1 \right)^2 \frac{K_i u_i^2 \Lambda^2}{v_{\text{F}}}. \quad (5.1.22)$$

By definition, the Luttinger cutoff must be much larger than the thermal energy $u_i \Lambda \gg \frac{1}{\beta}$, such that the major energy difference results from the second term in Eq. (5.1.22), which is always positive and describes the uniform population of the phonon modes due to the quench, especially the high energy modes with energies $u|\mathbf{q}| \gg \frac{1}{\beta}$. As one can infer from Eq. (5.1.17),

$$\langle a_{\mathbf{q}}^\dagger a_{\mathbf{q}} \rangle > n_{\text{B}}(\beta u_i |\mathbf{q}|) e^{-\frac{|\mathbf{q}|}{\Lambda}} = \langle b_{\mathbf{q}}^\dagger b_{\mathbf{q}} \rangle \quad (5.1.23)$$

for all kinds of initial and final values of K_i, K . Furthermore, under the transformation $K \leftrightarrow K_i$ the normal phonon occupation remains unchanged and the anomalous occupation obtains a relative minus sign, which can be gauged away by $a_{\mathbf{q}}^\dagger \rightarrow e^{i\frac{\pi}{2}} a_{\mathbf{q}}^\dagger$. In this section, we have determined the initial state after the quench in the Keldysh framework, which has been determined for the first time in Ref. [39] but in a slightly different formalism. The form of the initial state does not depend on the presence of the band curvature term, i.e. it remains unchanged in the presence of phonon scattering. Starting from this initial state, we will in the following sections discuss the time evolution of the post-quench system both in the absence and in the presence of band curvature (i.e. phonon scattering) systematically.

5.2 QUENCH IN THE QUADRATIC THEORY

In this section, we discuss an interaction quench in a system of one-dimensional interacting fermions in the absence of band curvature. As this system is integrable and the Hamiltonian is only quadratic, the time-evolution after the quench can be solved exactly. This has been done for the first time by Cazalilla [39] and we review his main results in the framework of the Keldysh path integral. Although the formalism presented here is much more appealing than the operator based methods in the literature, we will not discuss any new results in this section. However, the dynamics discussed for the non-interacting Luttinger Liquid will be relevant as well for the interacting version and many of the formulas presented here in a simpler context will be very useful in the next section, where the interaction quench in an interacting Luttinger Liquid will be discussed.

As we have seen in the previous section, the initial state after the quench in the fermionic interaction does not depend on whether the fermionic band curvature is absent or not. However, the time evolution strongly depends on the presence of the band curvature term, as it breaks integrability and leads to the relaxation of the system towards a thermal equilibrium state.

After quenching the system and preparing it in the above discussed initial state at $t = 0$, we compute the time evolution of the Green's functions under the evolution of the Hamiltonian

$$H^{(2)} = \frac{1}{2\pi} \int_{\mathbf{x}} \left[uK (\partial_{\mathbf{x}}\theta_{\mathbf{x}})^2 + \frac{u}{K} (\partial_{\mathbf{x}}\phi_{\mathbf{x}})^2 \right] = \int_{\mathbf{q}} u|q|b_{\mathbf{q}}^{\dagger}b_{\mathbf{q}}. \quad (5.2.1)$$

This problem has been analyzed by Cazalilla et al. in detail [39] and we will just give a short review here in our formalism.

In the quadratic framework, the retarded and advanced Green's functions do not depend on the distribution function and one can determine them directly in the operator formalism. We apply Wigner coordinates, such that in the Keldysh framework the Green's function read

$$G_{\mathbf{p},\tau,t}^{\mathbf{R}} = -i\langle a_{\mathbf{c},\mathbf{p},\tau+\frac{t}{2}}\bar{a}_{\mathbf{q},\mathbf{p},\tau-\frac{t}{2}} \rangle = -i\theta(t)e^{-iu|p|t}, \quad (5.2.2)$$

$$G_{\mathbf{p},\tau,t}^{\mathbf{A}} = -i\langle a_{\mathbf{q},\mathbf{p},\tau+\frac{t}{2}}\bar{a}_{\mathbf{c},\mathbf{p},\tau-\frac{t}{2}} \rangle = i\theta(-t)e^{-iu|p|t}, \quad (5.2.3)$$

$$\Gamma_{\mathbf{p},\tau,t}^{\mathbf{R}} = \Gamma_{\mathbf{p},\tau,-t}^{\mathbf{A}} = -i\langle \bar{a}_{\mathbf{c},-\mathbf{p},\tau+\frac{t}{2}}\bar{a}_{\mathbf{q},\mathbf{p},\tau-\frac{t}{2}} \rangle = 0. \quad (5.2.4)$$

The last equation is a consequence of the fact that the Hamiltonian does not mix positive and negative momenta as it does not contain any off-diagonal parts in the eigenbasis.

The correlation functions after the quench are determined in the operator formalism as well

$$G_{\mathbf{p},\tau,t}^{\mathbf{K}} = -i\langle a_{\mathbf{c},\mathbf{p},\tau+\frac{t}{2}}\bar{a}_{\mathbf{c},\mathbf{p},\tau-\frac{t}{2}} \rangle = -i\langle \{a_{\mathbf{p},\tau+\frac{t}{2}}, a_{\mathbf{p},\tau-\frac{t}{2}}^{\dagger}\} \rangle = -i(2n_{\mathbf{q}} + 1)e^{-iu|q|t}, \quad (5.2.5)$$

$$\Gamma_{\mathbf{p},\tau,t}^{\mathbf{K}} = -i\langle \bar{a}_{\mathbf{c},-\mathbf{p},\tau+\frac{t}{2}}\bar{a}_{\mathbf{c},\mathbf{p},\tau-\frac{t}{2}} \rangle = -i\langle \{a_{-\mathbf{p},\tau+\frac{t}{2}}^{\dagger}, a_{\mathbf{p},\tau-\frac{t}{2}}^{\dagger}\} \rangle = 2m_{\mathbf{q}}e^{-i2u|q|\tau}. \quad (5.2.6)$$

Here, we have introduced the normal phonon density $n_{\mathbf{q}} = \langle a_{\mathbf{q}}^{\dagger}a_{\mathbf{q}} \rangle$ and the anomalous phonon density $m_{\mathbf{q}} = \langle a_{\mathbf{q}}^{\dagger}a_{-\mathbf{q}}^{\dagger} \rangle$.

The translation table from phonon Green's functions to Luttinger Green's functions in terms of the Luttinger fields θ, ϕ is shown in Eqs. (3.2.50)-(3.2.52) and yields

$$G_{\phi\phi,\mathbf{p},\tau,t}^{\mathbf{R}} = \frac{\pi K}{2|p|} (G_{\mathbf{p},\tau,t}^{\mathbf{R}} + G_{\mathbf{p},\tau,-t}^{\mathbf{A}}) = \theta(t) \frac{\pi K \sin(u|p|t)}{|p|} e^{-\frac{|p|t}{\Lambda}}, \quad (5.2.7)$$

$$G_{\theta\theta,\mathbf{p},\tau,t}^{\mathbf{R}} = \theta(t) \frac{\pi \sin(u|p|t)}{K|p|} e^{-\frac{|p|t}{\Lambda}}, \quad (5.2.8)$$

$$G_{\theta\phi,\mathbf{p},\tau,t}^{\mathbf{R}} = -\frac{\pi}{2p} (G_{\mathbf{p},\tau,t}^{\mathbf{R}} - G_{\mathbf{p},\tau,-t}^{\mathbf{A}}) = i\theta(t) \frac{\pi \cos(u|p|t)}{p} e^{-\frac{|p|t}{\Lambda}}, \quad (5.2.9)$$

$$\begin{aligned} G_{\phi\phi,\mathbf{p},\tau,t}^{\mathbf{K}} &= \frac{\pi K}{2|p|} \left(G_{\mathbf{p},\tau,t}^{\mathbf{K}} + G_{\mathbf{p},\tau,-t}^{\mathbf{K}} + \Gamma_{\mathbf{p},\tau,t}^{\mathbf{K}} - (\Gamma_{\mathbf{p},\tau,t}^{\mathbf{K}})^* \right) \\ &= -i \frac{\pi K}{|p|} [\cos(u|p|t) (2n_{\mathbf{p}} + 1) + 2 \cos(2u|p|\tau) m_{\mathbf{p}}] e^{-\frac{|p|t}{\Lambda}}, \end{aligned} \quad (5.2.10)$$

$$G_{\theta\theta,\mathbf{p},\tau,t}^{\mathbf{K}} = -i \frac{\pi}{K|p|} [\cos(u|p|t) (2n_{\mathbf{p}} + 1) - 2 \cos(2u|p|\tau) m_{\mathbf{p}}] e^{-\frac{|p|t}{\Lambda}}, \quad (5.2.11)$$

$$G_{\theta\phi,\mathbf{p},\tau,t}^{\mathbf{K}} = \frac{\pi}{p} [\sin(u|p|t) (2n_{\mathbf{p}} + 1) + 2 \sin(2u|p|\tau) m_{\mathbf{p}}] e^{-\frac{|p|t}{\Lambda}}. \quad (5.2.12)$$

The information about the quench is encoded in the non-zero values of $n_{\mathbf{p}}$ and $m_{\mathbf{p}}$, which will modify the fermionic Green's functions. Since neither $n_{\mathbf{p}}$ nor $m_{\mathbf{p}}$ enter the

retarded/advanced Luttinger Green's functions, their effect on the fermionic Green's functions will be the same as if the system was in the ground state of the Hamiltonian. However, the fermionic spectral properties (encoded in the fermionic retarded/advanced Green's functions) will be modified by the quench, as has been shown in Refs. [107, 103]. The reason for the latter is that the fermionic greater and lesser Green's functions are implicit functionals on both, the phonon spectrum and the phonon occupation.

In order to determine the fermionic lesser Green's function, we have to compute the exponent $\mathcal{G}_{\eta,\tau,X}^<$ of (see Eq. (3.2.58))

$$\mathbf{G}_{\eta,\tau,X}^< = \frac{e^{-i\eta\mathbf{k}_F\mathbf{x}}}{2\pi} e^{-\frac{i}{2}\mathcal{G}_{\eta,\tau,X}^<}. \quad (5.2.13)$$

Here, $\eta = \pm$ labels right/left moving fermions, τ the forward time and $X = (x, t)$ is the relative space and time coordinate. The exponent has been formally determined in the previous section and in terms of Luttinger Green's functions is

$$\begin{aligned} \mathcal{G}_{\eta,\tau,X}^< &= \mathbf{G}_{\theta\theta,\tau,0}^K - \mathbf{G}_{\theta\theta,\tau,X}^K + \mathbf{G}_{\theta\theta,\tau,X}^A - \mathbf{G}_{\theta\theta,\tau,X}^R \\ &+ \mathbf{G}_{\phi\phi,\tau,0}^K - \mathbf{G}_{\phi\phi,\tau,X}^K + \mathbf{G}_{\phi\phi,\tau,X}^A - \mathbf{G}_{\phi\phi,\tau,X}^R \\ &+ \eta \left(\mathbf{G}_{\theta\phi,\tau,X}^K + \mathbf{G}_{\phi\theta,\tau,X}^K + \mathbf{G}_{\theta\phi,\tau,X}^R + \mathbf{G}_{\phi\theta,\tau,X}^R - \mathbf{G}_{\theta\phi,\tau,X}^A - \mathbf{G}_{\phi\theta,\tau,X}^A \right). \end{aligned} \quad (5.2.14)$$

With the above formulas, it evaluates to

$$\begin{aligned} \mathcal{G}_{\eta,\tau,X}^< &= \left(K + \frac{1}{K} \right) \int_{\mathbf{p}} \left[\frac{\pi e^{-\frac{|p|}{\Lambda}}}{|p|} \left[\sin(u|p|t) \cos(px) - i \left((2n_p + 1 - 2 \cos(2u|p|\tau)) m_p \right) \right. \right. \\ &\quad \left. \left. - \cos(px) \left(\cos(u|p|t) (2n_p + 1) - 2 \cos(2u|p|\tau) m_p \right) \right] \right] \\ &+ 2\eta \int_{\mathbf{p}} \left[\frac{\pi e^{-\frac{|p|}{\Lambda}} \sin(|p|x)}{|p|} \left[\cos(u|p|t) + i \left(\sin(u|p|t) (2n_p + 1) + 2 \sin(2u|p|\tau) m_p \right) \right] \right] \\ &= \left(\frac{K^2+1}{2K} - \eta \right) \arctan[\Lambda(ut-x)] + \left(\frac{K^2+1}{2K} + \eta \right) \arctan[\Lambda(tu+x)] \\ &- i \frac{K^2+1}{4K} (2n+1) \left[\log \left[1 + \Lambda^2(x-ut)^2 \right] + \log \left[1 + \Lambda^2(x+ut)^2 \right] \right] \\ &- i \frac{K^2-1}{2K} m \left[\log \left(\frac{1+\Lambda^2(x-2u\tau)^2}{1+4u^2\tau^2\Lambda^2} \right) + \log \left(\frac{1+\Lambda^2(x+2u\tau)^2}{1+4u^2\tau^2\Lambda^2} \right) \right] \\ &+ \frac{i\eta}{2} \left\{ (2n+1) \log \left(\frac{1+\Lambda^2(x-ut)^2}{1+\Lambda^2(x+ut)^2} \right) + 2m \log \left(\frac{1+\Lambda^2(x-2u\tau)^2}{1+\Lambda^2(x+2u\tau)^2} \right) \right\}. \end{aligned} \quad (5.2.16)$$

While the first equality is correct for a distribution function, which is an arbitrary function of momentum, the second equality holds for the specific case, for which the distribution function is constant in momentum space, i.e. $n_p = n$, $m_p = m$ for all momenta p . In the case of a zero relative time, i.e. for fermionic Green's functions that depend only on the forward time and the relative distance, the formulas simplify and we obtain

$$\mathcal{G}_{\eta,\tau,x}^< = i \int_{\mathbf{p}} \left[\frac{\pi e^{-\frac{|p|}{\Lambda}}}{|p|} \left(\cos(px) - 1 \right) \left(\frac{K^2+1}{K} (2n_p + 1) + 2 \frac{K^2-1}{K} \cos(2u|p|\tau) m_p \right) \right] \quad (5.2.17)$$

$$\begin{aligned} &+ 2\eta \int_{\mathbf{p}} \left[\frac{\pi e^{-\frac{|p|}{\Lambda}}}{|p|} \left[\sin(|p|x) + 2i \sin(|p|x) \sin(2u|p|\tau) m_p \right] \right] \\ &= 2\eta \arctan[\Lambda x] - i \frac{K^2+1}{2K} (2n+1) \log \left[1 + \Lambda^2 x^2 \right] + i\eta m \log \left(\frac{1+\Lambda^2(x-2u\tau)^2}{1+\Lambda^2(x+2u\tau)^2} \right) \\ &- i \frac{K^2-1}{2K} m \left[\log \left(\frac{1+\Lambda^2(x-2u\tau)^2}{1+4u^2\tau^2\Lambda^2} \right) + \log \left(\frac{1+\Lambda^2(x+2u\tau)^2}{1+4u^2\tau^2\Lambda^2} \right) \right]. \end{aligned} \quad (5.2.18)$$

The equal time exponent $\mathcal{G}_{\eta,\tau,x}$ is only a function of the forward time and the relative distance. For the quench scenario from a zero temperature initial state, the occupancies are according to (5.1.17)

$$2n + 1 = \frac{K^2 + K_i^2}{2KK_i}, \quad (5.2.19)$$

$$2m = \frac{K_i^2 - K^2}{2KK_i}. \quad (5.2.20)$$

We can now analyze the above equation and distinguish three relevant regimes.

First, for distances larger than $2u\tau$, i.e. for distances $|x| \gg 2u\tau$, which have not been reached by the light cone, we can expand the exponent, reading

$$\begin{aligned} \mathcal{G}_{\eta,\tau,x}^{\leq} \stackrel{|x| \gg 2u\tau}{=} & 2\eta \arctan[\Lambda x] - i \left(\frac{K^2+1}{2K} (2n+1) + \frac{K^2-1}{2K} 2m \right) \log [1 + \Lambda^2 x^2] \\ & + i 2m \frac{K^2-1}{2K} \log [1 + 4\tau^2 u^2 \Lambda^2] \\ = & 2\eta \arctan[\Lambda x] - i \frac{K_i^2+1}{2K_i} \log [1 + \Lambda^2 x^2] + i 2m \frac{K^2-1}{2K} \log [1 + 4\tau^2 u^2 \Lambda^2] \\ = & \mathcal{G}_{\eta,\tau=0,x}^{\leq} + i 2m \frac{K^2-1}{2K} \log [1 + 4\tau^2 u^2 \Lambda^2], \end{aligned} \quad (5.2.21)$$

where $\mathcal{G}_{\eta,\tau=0,x}^{\leq}$ is the initial, zero temperature exponent before the quench. As a consequence, the fermionic Green's function after the quench can be written as

$$G_{\eta,\tau,x}^{\leq} \stackrel{|x| \gg 2u\tau}{=} G_{\eta,\tau=0,x}^{\leq} \left(\sqrt{1 + 4u^2 \tau^2 \Lambda^2} \right)^{m \frac{K^2-1}{K}} = G_{\eta,\tau=0,x}^{\leq} Z(\tau), \quad (5.2.22)$$

where $G_{\eta,0,x}^{\leq}$ is the initial fermion Green's function and $Z(\tau)$ is a spatially independent, global amplitude, which decays algebraically in time with an exponent $\eta_\tau = m \frac{K^2-1}{K} = \frac{K^2-1}{2K} \frac{K_i^2-K^2}{2KK_i}$. For the initial fermionic Green's function we are dealing with in this regime, we have $Z(0) = 1$.

Second, for distances smaller than $2u\tau$, i.e. for $|x| \ll 2u\tau$, the light cone has past this distance, i.e. the phonons had time to equilibrate, and the exponent takes the form

$$\begin{aligned} \mathcal{G}_{\eta,\tau,x}^{\leq} \stackrel{|x| \ll 2u\tau}{=} & 2\eta \arctan[\Lambda x] - i \left(\frac{K^2+1}{2K} (2n+1) \right) \log [1 + \Lambda^2 x^2] \\ = & 2\eta \arctan[\Lambda x] - i \left[\frac{K_i^2+1}{2K_i} - 2m \frac{K^2-1}{2K} \right] \log [1 + \Lambda^2 x^2] \\ = & \mathcal{G}_{i,\eta,x}^{\leq} + i 2m \frac{K^2-1}{2K} \log [1 + x^2 \Lambda^2]. \end{aligned} \quad (5.2.23)$$

Therefore, the fermion Green's function is stationary and can be written as

$$G_{\eta,\tau,x}^{\leq} \stackrel{|x| \ll 2u\tau}{=} G_{\eta,0,x}^{\leq} \left(\sqrt{1 + x^2 \Lambda^2} \right)^{m \frac{K^2-1}{K}} = G_{\eta,0,x}^{\leq} Z\left(\frac{x}{2u}\right), \quad (5.2.24)$$

where the amplitude Z is now no longer time- but spatially dependent. This is the stationary fermionic Green's function in the limit $\tau \rightarrow \infty$.

Directly at the light cone, for $x = \pm 2u\tau$, the fermionic correlations strongly depend on the form of the interactions and whether we consider right or left movers. As an example, we consider a quench from weak to strong repulsive interactions. For this case, right movers have strongly increased correlations at the positive light cone $x = 2u\tau$ and reduced

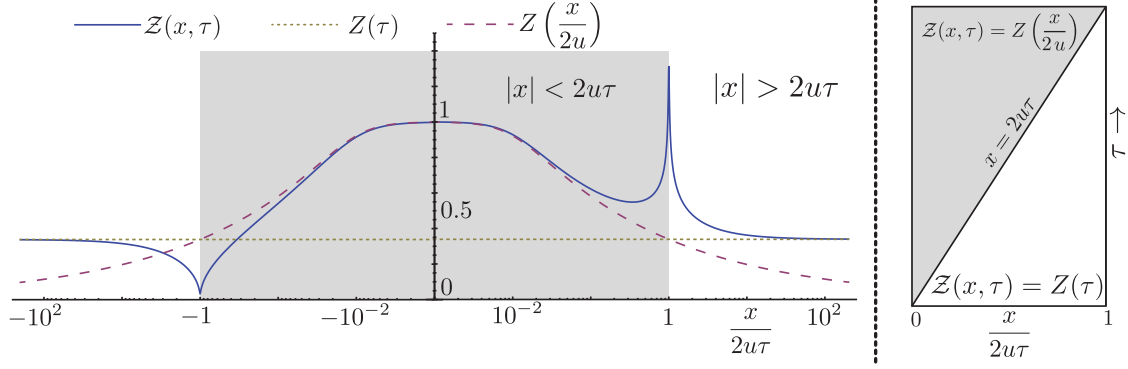


Figure 5.1: Left: Time and space dependent amplitude function $\mathcal{Z}(\eta x, \tau) = \frac{G_{\eta, \tau, x}^<}{G_{\eta, 0, x}^<}$ for a quench from $K_i = 1$ (non-interacting fermions) to $K = 1.4$ (repulsive interactions) for a fixed time τ . $\mathcal{Z}(x, \tau)$ for right movers is shown in blue. For comparison, we also plotted the long time and long distance limits $Z(\tau) = \mathcal{Z}(x, \tau)|_{x \gg 2u\tau}$ (yellow) and $Z(\frac{x}{2u}) = \mathcal{Z}(x, \tau)|_{x \ll 2u\tau}$ (red). Exactly at the light cone, for $|x| = 2u\tau$, the correlations are strongly increased for positive x and decreased for negative x , as we considered right moving fermions. Right: Illustration of the different regimes for the amplitude function $\mathcal{Z}(x, \tau)$ in the spatio-temporal coordinate system.

correlations at the negative light cone $x = -2u\tau$, as illustrated in Fig. 5.1. The form of the exponent in Eq. (5.2.23) suggests a factorization of the form

$$G_{\eta, \tau, x}^< = G_{\eta, 0, x}^< \mathcal{Z}(\eta x, \tau), \quad (5.2.25)$$

where the function $\mathcal{Z}(\eta x, \tau)$ becomes a universal scaling function in the limit $\Lambda \rightarrow \infty$,

$$\mathcal{Z}(\eta x, \tau) \stackrel{\Lambda \rightarrow \infty}{=} \mathcal{Z}\left(\frac{\eta x}{2u\tau}\right). \quad (5.2.26)$$

The universal function \mathcal{Z} is shown in Fig. 5.1 for a quench from $K_i = 1$ to $K = 1.4$ (for right movers, as $\eta = +$). For $x \gg 2u\tau$, it reduces to $Z(\tau)$, whereas for $x \ll 2u\tau$ it equals $Z(\frac{x}{2u})$.

For the fermionic momentum distribution function, this means that for momenta $q < \frac{1}{2u\tau}$, the momentum distribution is essentially described by the initial distribution

$$n_p(\tau) = \int_x e^{-ipx} G_{\eta, \tau, x}^< \stackrel{p < (2u\tau)^{-1}}{=} Z(\tau) \int_x e^{-ipx} G_{\eta, 0, x}^< = Z(\tau) n_p(\tau = 0). \quad (5.2.27)$$

On the other hand, for momenta larger $q > \frac{1}{2u\tau}$, the integral is essentially determined by the region, which has already reached a steady state behavior and

$$n_p(\tau) \stackrel{p > (2u\tau)^{-1}}{=} \int_x e^{-ipx} G_{\eta, 0, x}^< Z\left(\frac{x}{2u}\right) = n_p(\tau \rightarrow \infty). \quad (5.2.28)$$

As a consequence of Eq. (5.2.28), the steady state (for $\tau \rightarrow \infty$) scaling behavior of the fermionic momentum distribution close to the Fermi momentum is

$$n_p \sim |p - k_F|^{\frac{K_i^2 + 1}{2K_i} - m \frac{K^2 - 1}{K} - 1} = |p - k_F|^{\frac{K^2 + 1}{2K} - \frac{K_i^2 + K^2}{2KK_i} - 1}. \quad (5.2.29)$$

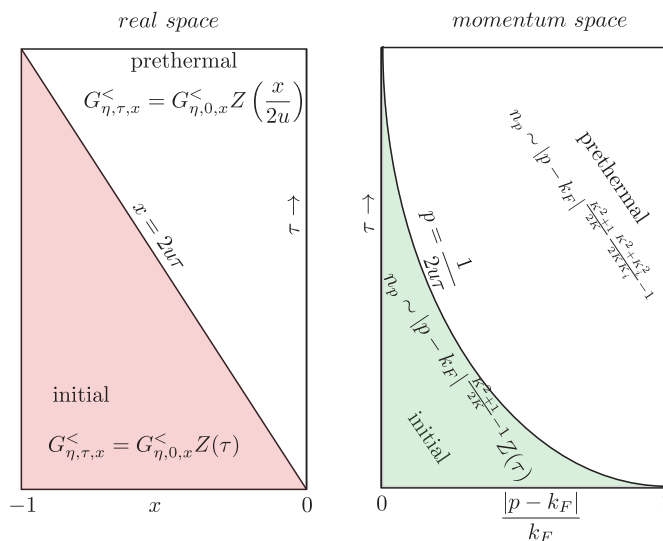


Figure 5.2: Illustration of the prethermalization process in the non-interacting Luttinger model. On the left, the spreading of correlations $\sim 2u\tau$ in real space, leading to two distinct regions with significantly varying correlation functions. On the right, spreading of prethermalization in momentum space $\sim \frac{1}{2u\tau}$ with the different scaling behavior of the fermionic distribution function in the corresponding regimes.

This is in contrast to the ground state scaling behavior of the fermionic momentum distribution, which is $\sim \frac{K^2+1}{2K} - 1$ and depends only on the Hamiltonian but not on the initial state. For a quench from a non-interacting fermionic model, $Z(\tau)$ in Eq. (5.2.27) coincides exactly with the quasi-particle residue, i.e. the jump of the fermionic distribution at the Fermi momentum. After a quench to an interacting fermion model, this residue vanishes algebraically in time due to Eq. (5.2.27).

Let us finish the section, with an illustration of the time-evolution of correlation functions and the spreading of the prethermal region after the quench in Fig. 5.2.

5.3 QUENCH IN THE NON-LINEAR THEORY

In order to study thermalization and prethermalization in general one-dimensional quantum fluids, we analyze the post-quench dynamics of an interacting Luttinger Liquid, microscopically realized with interacting fermions with non-zero band curvature. In the absence of band curvature, the system is integrable and evolves towards a non-thermal fixed point, which we have analyzed in the previous section. In the presence of phonon-phonon interactions, the system will thermalize after the quench in the limit $\tau \rightarrow 0$, and the stationary state can be described by a thermal ensemble. The temperature of the stationary state of the system can be determined from the energy injected by the quench at $\tau = 0$. As we will see, similar to the quench in the integrable model, the relaxation process after the quench can be decomposed into different spatio-temporal regimes. Two of these regimes are familiar from the previous section. On the largest distances, the fermionic correlations are governed by the initial fermion correlations, modified by a time dependent, global amplitude. On intermediate distances, we will recover the prethermal state, which was the fixed point of the integrable theory. Finally, starting from the shortest distances, a thermalized region spreads in space, reaching large distances in a power law in time $x_{\text{thermal}} \sim \tau^\alpha$ with $\alpha < 1$. This behavior will be visible in the fermion correlation functions in real space

and the fermionic momentum distribution, as we will discuss. A spreading of the thermal region with an exponent $\alpha > 1$ is forbidden by the Lieb-Robinson bounds for this model, which predicts, according to the RG-relevant contributions of the Hamiltonian, information propagation with the light cone $x_{\text{Info}} = 2u\tau$.

5.3.1 Keldysh Action and Structure of the Correlation Functions

The Keldysh action of the interacting Luttinger model has been derived in Sec. 3.2 and reads (3.1.24)

$$\begin{aligned} \mathcal{S} = & \frac{1}{\pi} \int_X -(\theta_{c,X}, \phi_{c,X}) \begin{pmatrix} uK\partial_x^2 & \partial_x\partial_t \\ \partial_x\partial_t & \frac{u}{K}\partial_x^2 \end{pmatrix} \begin{pmatrix} \theta_{q,X} \\ \phi_{q,X} \end{pmatrix} \\ & + \frac{v}{\sqrt{8\pi}} \int_X \left[2(\partial_x\theta_{c,X})(\partial_x\phi_{q,X})(\partial_x\theta_{q,X}) + (\partial_x\phi_{q,X}) \left((\partial_x\theta_{q,X})^2 + (\partial_x\theta_{c,X})^2 \right) \right]. \end{aligned} \quad (5.3.1)$$

In the phonon representation, it transforms to

$$\begin{aligned} \mathcal{S} = & \frac{1}{2\pi} \int_{t,t',p} (\bar{a}_{p,t}^c, \bar{a}_{p,t}^q, a_{-p,t}^q) \begin{pmatrix} 0 & D_{p,t,t'}^R & 0 \\ D_{p,t,t'}^A & D_{p,t,t'}^K & \Delta_{p,t,t'}^K \\ 0 & (\Delta_{p,t,t'}^K)^\dagger & D_{-p,t',t}^K \end{pmatrix} \begin{pmatrix} a_{p,t'}^c \\ a_{p,t'}^q \\ \bar{a}_{p,t'}^q \end{pmatrix} \\ & + \frac{v_0}{\sqrt{8\pi}} \int'_{p,k,t} \sqrt{|pk(k+p)|} \left[2\bar{a}_{k+p,t}^c a_{k,t}^c a_{p,t}^q + \bar{a}_{k+p,t}^q (a_{k,t}^c a_{p,t}^c + a_{k,t}^q a_{p,t}^q) + \text{h.c.} \right]. \end{aligned} \quad (5.3.2)$$

The integral \int' only takes into account resonant processes and the bare inverse Green's functions

$$D_{p,t,t'}^R = \delta(t-t') (i\partial_{t'} - u|p| + i0^+), \quad (5.3.3)$$

$$D_{p,t,t'}^A = (D_{p,t,t'}^R)^\dagger = \delta(t-t') (i\partial_{t'} - u|p| - i0^+), \quad (5.3.4)$$

$$D_{p,t,t'}^K = 2i0^+ (2n_{p, \frac{t+t'}{2}} + 1). \quad (5.3.5)$$

have been defined in Eqs. (4.2.22)-(6.2.19). In the action (5.3.2), we included off-diagonal Keldysh components in the Green's function

$$\Delta_{p,t,t'}^K = 4i0^+ m_{p, \frac{t+t'}{2}}, \quad (5.3.6)$$

as off-diagonal modes become occupied by the quench. For a thermal or zero temperature initial state, the off-diagonal occupations are zero and the action (5.3.2) reduces to a diagonal form in Nambu space. In the retarded/advanced sector on the other hand, we did not take into account off-diagonal terms. The reason is that in the bare theory, determined by the Hamiltonian in its eigenbasis, off-diagonal terms are absent. Furthermore, the resonant interactions describe only scattering of phonons, which are propagating in the same direction and therefore momenta q and $-q$ never couple. As a consequence, the operators $a_{q,t}^\dagger$ and $a_{-q,t'}^\dagger$ commute for all possible times t, t' and the off-diagonal retarded Green's functions

$$\Gamma_{q,t,t'}^R = -i\theta(t-t') \langle [a_{q,t}^\dagger, a_{-q,t'}^\dagger] \rangle = 0 \quad (5.3.7)$$

are always exactly zero.

The effect of the phonon-phonon scattering is the creation of a finite self-energy $\sigma_{p,\tau}^R$ and an associated non-trivial time evolution of the phonon densities $n_{p,\tau}, m_{p,\tau}$. The time evolution of the phonon densities will be solved by the kinetic equation approach, derived in the previous chapter 4 with the initial conditions dictated by the quench (compare to Sec. 5.1). In order to determine the fermion Green's functions, we apply the first order cumulant expansion in Eq. (3.2.56)

$$G_{\eta,X,X'}^< = \frac{e^{-i\eta k_F(x-x')}}{2\pi} \langle e^{i(\eta\phi_{+,X'} - \theta_{+,X'} - \eta\phi_{-,X} + \theta_{-,X})} \rangle = \frac{e^{-i\eta k_F(x-x')}}{2\pi} e^{-\frac{1}{2}\mathcal{G}_{\eta,X,X'}^<}. \quad (5.3.8)$$

This is exact for a quadratic theory, i.e. for factorizing higher order correlation functions. The phonon scattering term induces a non-trivial dynamics of the phonon occupation but still is a subleading, renormalization group (RG) irrelevant term and the induced higher order correlation functions will deviate only in an RG irrelevant way from perfectly factorizing correlation functions for this reason. Therefore, the cumulant expansion is well justified in this setting as the only non-negligible effect of the non-linearity is the time-evolution of the distribution function and the emergence of a finite phonon lifetime (i.e. self-energy)⁶. The exponent $\mathcal{G}_{\eta,\tau,X}^<$ is therefore defined in the same way as in the previous section, i.e. in Eq. (5.2.14). What is required for the fermionic Green's functions are the Luttinger Green's functions in the presence of interactions. In the Wigner representation, they can be determined straightforwardly from the formulas of the previous sections, reading

$$G_{\phi\phi,p,\tau,t}^R = \theta(t) \frac{\pi K \sin(u|p|t)}{|p|} e^{-\sigma_\tau^R t} e^{-\frac{|p|}{\Lambda}}, \quad (5.3.9)$$

$$G_{\theta\theta,p,\tau,t}^R = \theta(t) \frac{\pi \sin(u|p|t)}{K|p|} e^{-\sigma_\tau^R t} e^{-\frac{|p|}{\Lambda}}, \quad (5.3.10)$$

$$G_{\theta\phi,p,\tau,t}^R = i\theta(t) \frac{\pi \cos(u|p|t)}{p} e^{-\sigma_\tau^R t} e^{-\frac{|p|}{\Lambda}}, \quad (5.3.11)$$

$$G_{\phi\phi,p,\tau,t}^K = -i \frac{\pi K}{|p|} [\cos(u|p|t) e^{-\sigma_\tau^R t} (2n_{p,\tau} + 1) + 2 \cos(2u|p|\tau) m_{p,\tau} e^{-\sigma_\tau^R t}] e^{-\frac{|p|}{\Lambda}}, \quad (5.3.12)$$

$$G_{\theta\theta,p,\tau,t}^K = -i \frac{\pi}{K|p|} [\cos(u|p|t) e^{-\sigma_\tau^R t} (2n_{p,\tau} + 1) - 2 \cos(2u|p|\tau) m_{p,\tau} e^{-\sigma_\tau^R t}] e^{-\frac{|p|}{\Lambda}}, \quad (5.3.13)$$

$$G_{\theta\phi,p,\tau,t}^K = \frac{\pi}{p} [\sin(u|p|t) e^{-\sigma_\tau^R t} (2n_{p,\tau} + 1) + 2 \sin(2u|p|\tau) m_{p,\tau} e^{-\sigma_\tau^R t}] e^{-\frac{|p|}{\Lambda}}. \quad (5.3.14)$$

Compared to the previous section and the non-interacting Luttinger model, there is now an additional forward time dependence in the phonon densities $n_{p,\tau}, m_{p,\tau}$, where $m_{p,\tau} = \langle a_{p,\tau}^\dagger a_{-p,\tau}^\dagger \rangle e^{2i\tau u|p|}$ is the anomalous density for which the dynamical phase has been gauged away. It is taken into account separately by the cosine and sine prefactor. One should note, that in any case, the self-energy appears as a damping factor, which is proportional to the relative time difference, even for the off-diagonal terms $\sim m_{p,\tau}$ as it describes the decay of a single annihilation or creation operator but not the decay of the phonon density operator. The latter is taken fully into account in the time evolution of $m_{p,\tau}$ by the kinetic equation.

For zero relative time $t = 0$, i.e. for fermionic equal time Green's functions, the self-energy is not visible in any of the above Green's functions and the exponent $\mathcal{G}_{\eta,\tau,X}^<$ is determined

⁶A further argument, why the cumulant expansion is justified, is simple power counting. This works well in equilibrium where the non-linearities are always present as well and there influence is obviously negligible. In a non-equilibrium setting, the scaling introduced by the distribution is different compared to equilibrium but the subleading nature of higher order expansions remains.

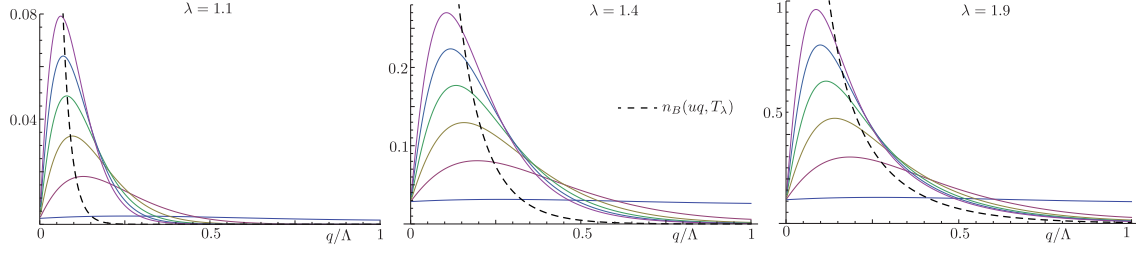


Figure 5.3: Stroboscopic plot of the time evolution of the diagonal distribution function after three different quench scenarios. The initial distribution is a flat line in momentum space, $n_{q,\tau=0} = n_\lambda = \frac{(\lambda-1)^2}{4\lambda}$. From left to right, the initial densities are $n_\lambda = (0.0022, 0.028, 0.106)$. The dashed line represents the final phonon distribution $n_{q,\tau \rightarrow \infty} = n_B(u|q, T_\lambda)$. The corresponding temperatures are $T_\lambda/u = (0.035, 0.124, 0.24)$. One can identify a crossover scale q_τ^c for each curve, at which the slope $\partial_q n_{q,\tau}$ changes its sign from positive to negative. For momenta $q < q_\tau^c$, the momentum distribution increases linearly in momentum $n_{q,\tau} \sim |q|Z_0\tau$ and time. On the other hand, for momenta $q > q_\tau^c$, the distribution follows a Bose-Einstein distribution $n_{q,\tau} = n_B(u|q, T_\lambda + \delta T_\lambda)$.

as in the previous section

$$\begin{aligned} \mathcal{G}_{\eta,\tau,x}^< &= i \int_{\mathbf{p}} \left[\frac{\pi e^{-\frac{|p|}{\Lambda}}}{|p|} \left[(\cos(\mathbf{p}\mathbf{x}) - 1) \left(\frac{K^2+1}{K} (2n_{\mathbf{p},\tau} + 1) + 2\frac{K^2-1}{K} \cos(2u|p|\tau)m_{\mathbf{p},\tau} \right) \right] \right. \\ &\quad \left. + 2\eta \arctan[\Lambda\mathbf{x}] + 4i\eta \int_{\mathbf{p}} \left[\frac{\pi e^{-\frac{|p|}{\Lambda}}}{|p|} \sin(|\mathbf{p}\mathbf{x}|) \sin(2u|p|\tau)m_{\mathbf{p},\tau} \right] \right]. \end{aligned} \quad (5.3.15)$$

Except for the time dependent densities $n_{q,\tau}, m_{q,\tau}$, all parameters in the above expression are determined by the Hamiltonian and the initial state. Furthermore, $n_{q,\tau=0}, m_{q,\tau=0}$ are determined by the initial state as well. The time evolution of the phonon densities is solved numerically with the kinetic equation approach from the previous chapter and discussed in the following section.

5.3.2 Dynamics of the Phonon Densities

To compute the equal time fermion correlation function, the time dependent phonon densities are required and we determine them with the help of the kinetic equation approach derived and extensively discussed in the previous chapter (see chapter 4). In terms of the rescaled time variable $\tilde{\tau} = v_0\tau$, the kinetic equation for the diagonal densities is (6.3.11)

$$\begin{aligned} \partial_{\tilde{\tau}} n_q &= \int_{0 < p < q} \frac{2pq(q-p)}{\tilde{\sigma}_q^R + \tilde{\sigma}_p^R + \tilde{\sigma}_{q-p}^R} (n_p n_{q-p} - n_q (1 + n_p + n_{q-p})) \\ &\quad + \int_{0 < p} \frac{4pq(q+p)}{\tilde{\sigma}_q^R + \tilde{\sigma}_p^R + \tilde{\sigma}_{q+p}^R} (n_{p+q} (n_q + n_p + 1) - n_q n_p), \end{aligned} \quad (5.3.16)$$

whereas for the off-diagonal densities it is (4.5.25)

$$\begin{aligned}\partial_{\tilde{\tau}}m_q &= \int_{0 < p < q} \frac{2pq(q-p)}{\tilde{\sigma}_q^R + \tilde{\sigma}_p^R + \tilde{\sigma}_{q-p}^R} (m_p m_{q-p} - m_q (1 + n_p + n_{q-p})) \\ &+ \int_{0 < p} \frac{4pq(q+p)}{\tilde{\sigma}_q^R + \tilde{\sigma}_p^R + \tilde{\sigma}_{q+p}^R} (n_{p+q} m_q + m_p m_{p+q} - m_q n_p).\end{aligned}\quad (5.3.17)$$

The rescaled retarded self-energies are determined according to Eq. (6.3.10)

$$\tilde{\sigma}_q^R = \int_{0 < p} \left(\frac{\partial_{\tilde{\tau}} n_p}{\tilde{\sigma}_p^R} + 2n_p + 1 \right) \left(\frac{qp(q-p)}{\tilde{\sigma}_p^R + \tilde{\sigma}_{q-p}^R} + \frac{qp(p+q)}{\tilde{\sigma}_p^R + \tilde{\sigma}_{p+q}^R} \right).\quad (5.3.18)$$

In the rescaled time variable $\tilde{\tau}$, Eqs. (5.3.16)-(5.3.18) do not explicitly depend on any system variables but only on the initial densities $n_{q,\tau=0} \equiv n$ and $m_{q,\tau=0} \equiv m$. Both of the initial densities depend, according to Eqs. (5.2.19), (5.2.20), only on the ratio $\lambda = \frac{K}{K_i}$ and we can express the non-equilibrium quench dynamics solely in terms of the quench parameter λ ,

$$2n + 1 = \frac{\lambda^2 + 1}{2\lambda}, \quad 2m = \frac{1 - \lambda^2}{2\lambda}.\quad (5.3.19)$$

The time evolution of the diagonal distribution function $n_{q,\tau}$, determined by the kinetic equation (5.3.16), is plotted in Fig. 5.3 for certain quench parameters λ , it has the corresponding initial value $n_{q,\tau=0} = n_\lambda = \frac{(1-\lambda)^2}{4\lambda}$ and the final value $n_{q,\tau \rightarrow \infty} = n_B(u|q|, T_\lambda) = \left(e^{\frac{u|q|}{T_\lambda}} - 1 \right)^{-1}$, where u is the velocity of sound and T_λ is the quench dependent temperature. Since the dynamics is exactly energy conserving, we can determine the final temperature T_λ by equating the initial and final energy density of the system. The energy density is defined as

$$E_\tau = \int_q u|q| n_{q,\tau}.\quad (5.3.20)$$

The quench populates the low energy modes and therefore induces an energy increase according to

$$E_0 = un_\lambda \int_q |q| e^{-\frac{|q|}{\Lambda}} = un_\lambda \Lambda^2.\quad (5.3.21)$$

The regularization of this energy proportional to the cut-off stems from the fact that also the microscopic interaction (which is quenched) has to be cut-off at some short-distance scale. Here, we chose this scale to equal the Luttinger cut-off for simplicity. The final thermal energy in the limit of infinite time after the quench is

$$E_\infty = u \int_q |q| \left(e^{\frac{u|q|}{T_\lambda}} - 1 \right)^{-1} = \frac{T_\lambda^2 \pi^2}{3u}.\quad (5.3.22)$$

This yields a quench dependent temperature⁷

$$T_\lambda = \frac{u\Lambda}{\pi} \sqrt{3n_\lambda} = \frac{u\Lambda}{2\pi} |1 - \lambda| \sqrt{\frac{3}{\lambda}}. \quad (5.3.23)$$

The final temperature depends on the quench parameter λ as well as on the Luttinger cutoff Λ . This is not surprising, as the energy injected by the quench is a non-universal number and depends on the microscopic details of the model. However, the dynamics of the distribution function approach this non-universal temperature in a generic way and therefore the non-equilibrium dynamics, as well as the equilibrium dynamics in a Luttinger Liquid have a high degree of universality⁸.

We will now discuss the structure of the relaxation dynamics in the interacting Luttinger model. For $q = 0$, both the diagonal and the off-diagonal densities are locked to their initial value $n_{q=0,\tau} = n_{q=0,\tau=0} = n_\lambda$ and $m_{q=0,\tau} = m_\lambda$ this can be seen from the kinetic equations (Eqs. (5.3.16), (5.3.17)), which in the limit $q \rightarrow 0$ scale as $\sim |q|$ and therefore vanish exactly for $q = 0$. On the other hand, the values of $n_{q=0}, m_{q=0}$ are associated with the global particle number and since the dynamics conserve the total particle number exactly, i.e. preserve $U(1)$ -symmetry, the densities at $q = 0$ are pinned to their respective initial values.

For small momenta $q < q_0$, the kinetic equation is approximately linear in the momentum q , and has the form (see Eq. (4.4.7))

$$n_{q,\tilde{\tau}} \stackrel{q \leq q^c}{=} n_{q,\tilde{\tau}=0} + |q| \int_{0 < t < \tilde{\tau}} \mathcal{I}_t \approx n_{q,\tilde{\tau}=0} + |q| \mathcal{I}_0 \tau, \quad (5.3.24)$$

where in the last step, we assumed a very weak time dependence in the function \mathcal{I}_t . It is defined as

$$\mathcal{I}_t = \int_{0 < p} \frac{2p^2}{\tilde{\sigma}_{p,t}^R} n_{p,t} (1 + n_{p,t}) \stackrel{t=0}{=} \frac{4\Lambda}{\sqrt{\pi(2n_\lambda+1)}} n_\lambda (1 + n_\lambda) = \Lambda \frac{(\lambda^2-1)^2}{4\lambda^2} \sqrt{\frac{2\lambda}{\pi(\lambda^2+1)}}. \quad (5.3.25)$$

The cutoff dependence in this function can be seen as a dependence of the speed of the time evolution on the energy of the system. A larger energy ($\sim \Lambda^2$) leads to a faster non-equilibrium time evolution, consistent with Eq. (5.3.25).

As we see from Fig. 5.3, the distribution function indeed is linear in momentum for sufficiently small momenta $q < q_\tau^c$. For larger momenta, the distribution function is approximately thermal

$$n_{q,\tau} \stackrel{q > q_\tau^c}{=} n_B(u|q|, T_\lambda + \delta T_\tau), \quad (5.3.26)$$

where δT_τ indicates the deviation of the associated temperature of the momentum modes at time τ from the final temperature T_λ . The momentum scale q_τ^c , which determines the crossover from a linear scaling of the distribution to a thermal scaling, does itself depend on time. For momenta $q < q^c$, smaller than this crossover, the modes are essentially populated by scattering of phonons from modes with larger momenta $q > q^c$ into modes with lower momenta. On the other hand, for $q > q^c$, the phonon density has already obtained a quasi-thermal form and the dynamics is close to a situation of detailed balance between in and out scattering processes. For these momenta, the relaxation dynamics become very slow and are dominated by dynamical slow modes (cf. Sec. 4.6 and the end of this section). The crossover momentum scale q_τ^c indicates the progress of thermalization in the system as for momenta $q > q_\tau^c$, i.e. for distances $x < \frac{1}{q_\tau^c}$ the system has the

⁷The integral over the thermal distribution does not have to be regularized by the cutoff, as by definition $T \ll u\Lambda$.

⁸In the same way, the temperature in an equilibrium Luttinger Liquid is, of course, not a universal number and depends on the details of the system-bath coupling.

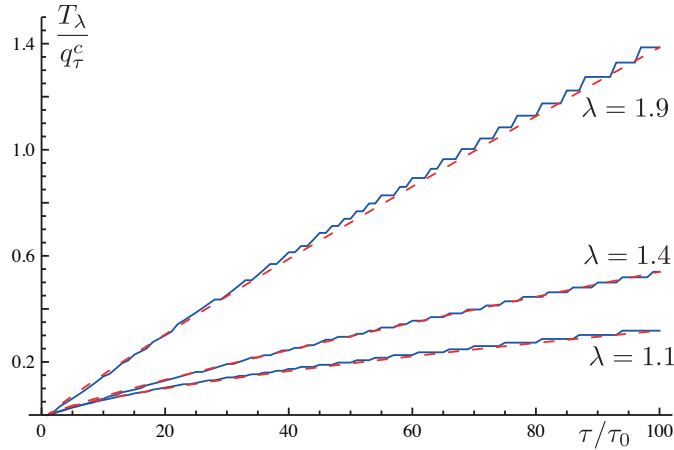


Figure 5.4: Time evolution of the inverse of the crossover momentum scale $\frac{T_\lambda}{q_\tau^c}$ for the three different quench scenarios $\lambda = (1.1, 1.4, 1.9)$, normalized with the corresponding final temperature T_λ . The bumps result from the discretization in momentum space and appear for very large times τ_0 . The inverse crossover scale evolves according to a power law in time, $\frac{T_\lambda}{q_\tau^c} \sim \tau^{-\eta_\lambda}$, where the exponent depends non-trivially on the quench parameter. Numerical values are $\eta_{1.1} = 0.7$, $\eta_{1.4} = 0.85$ and $\eta_{1.9} = 0.92$. The exponent is lower than one (which is the corresponding exponent for the phonon propagation) but approaches one in the limit $\lambda \rightarrow \infty$. Since the crossover scale indicates the spreading of thermalization in the system, an exponent $\eta_\lambda < 1$ allows for a finite prethermalized region in the dynamical phase diagram, as the thermal region spreads slower than the propagation of phonons and therefore the prethermal region.

properties of a thermalized system with a relaxing temperature $T_\tau = T_\lambda + \delta T_\tau$. The time dependence of the crossover scale is non-trivial and depends on the quench parameter λ . In Fig. 5.4, the time dependent crossover scale is shown for different quench parameters. It follows a power law in time $q_\tau^c \sim \tau^{-\eta_\lambda}$, with an exponent η_λ that depends on the quench parameter. The numerical determination of η_λ shows that $\eta_\lambda < 1$ for all λ , and that it increases with increasing λ . As a consequence, the spatial coordinate associated with the crossover scale and thermalization $x_{\text{thermal}} = \frac{1}{q_\tau^c} \sim \tau^{\eta_\lambda}$ increases slower than ballistically. As a consequence, it spreads slower than the ballistically expanding prethermal region $x_{\text{pretherm}} = 2u\tau$ and on large scales, the thermalization process takes place in three steps, as discussed at the beginning of the section.

The off-diagonal densities $m_{q,\tau}$ evolve in time according to Eq. (5.3.17) and decay to zero in the limit $\tau \rightarrow 0$, which corresponds to their thermal value. The time evolution of the off-diagonal densities is shown in Fig. 5.5. In order to estimate the momentum scale, above which the off-diagonal densities are negligible, one can define the momentum q_τ^h , at which the off-diagonal distribution has reached half of its initial value $m_{q_\tau^h,\tau} = \frac{1}{2}m_\lambda$. As it turns out from the numerical evaluation, $q_\tau^h = \alpha_q q_\tau^c$, where $\alpha_q = \mathcal{O}(1)$. This is consistent with the statement that for momenta $q > q_\tau^c$, the system has reached a quasi-thermal state.

5.3.3 Momentum Dependent Thermalization and Emergence of Dynamical Slow Modes

The phonon distribution function for momenta larger than the crossover momentum $q > q_\tau^c$ is quasi-thermal, i.e. described by a Bose distribution $n_{q,\tau} = n_B(u|q|, T_\lambda + \delta T_\tau)$, which

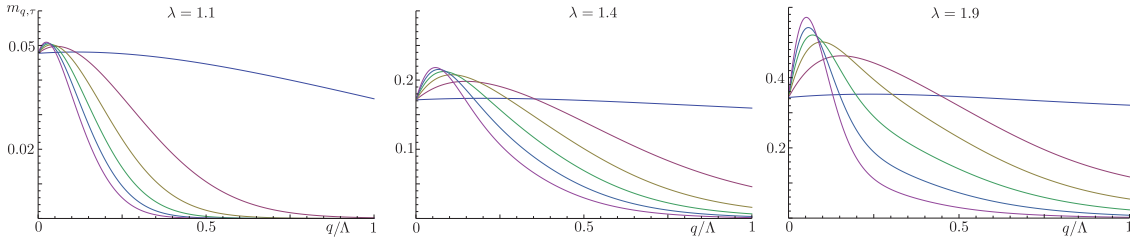


Figure 5.5: Time evolution of the off-diagonal distribution $m_{q,\tau}$ for different quench scenarios. The off-diagonal densities start from the initial value $m_{q,\tau=0} = m_\lambda = \frac{\lambda^2-1}{4\lambda}$ and decay to zero in the limit $\tau \rightarrow \infty$. For momenta larger than the crossover scale $q > q_\tau^c$, the off-diagonal distribution is almost zero, while for momenta lower than the crossover scale, it can be approximated by the initial value.

deviates from the final distribution function $n_{q,\tau \rightarrow \infty} = n_B(u|q|, T_\lambda)$ by a time dependent temperature δT_τ , which decays to zero in the limit $\tau \rightarrow \infty$. For $\tau < \infty$, there is still additional energy stored in the momentum modes $q > q_\tau^c$, which has to be transported to the infrared regime. However, since the system is already quasi-thermal, i.e. detailed balance between in- and out-scattering processes is almost exactly fulfilled, energy transport to the low momentum modes becomes algebraically slow.

This is the same mechanism as discussed in Sec. 4.6, which leads to an algebraic decay of excitations close to thermal equilibrium with an exponent $\alpha = 0.58$. From an analytic approach to this model, one expects an exponent $\alpha = 0.5$ at zero temperature and $\alpha = 2/3$ for finite temperature for the dynamical slow modes. However, as pointed out in Ref. [129], there might be subleading algebraic corrections, which are very hard to separate, even for very long simulation times. Furthermore, the quench scenario is neither describing a zero temperature state, nor is the energy in the system large enough to consider it a large temperature state and therefore the scaling is expected to lie between these two cases.

Here, we find the same exponent in the decay of the temperature $\delta T_\tau = \Delta \tau^{-0.58}$, as it stems from the same mechanism of energy transport over large distances. It results from the global energy conservation of the system and the corresponding presence of dynamical slow modes. In Fig. 5.6, we show the effective, time dependent temperature of the different momentum modes

$$T_{q,\tau} \equiv u|q| \left[\log \left(\frac{1}{n_{q,\tau}} + 1 \right) \right]^{-1}. \quad (5.3.27)$$

During the time evolution, the different modes align and obtain the same temperature, i.e. $T_{q,\tau} = T_{p,\tau}$ for $p, q > q_\tau^c$, which, however, is not yet the final temperature of the system. The difference of the time dependent effective temperature to the final temperature decays algebraically in time with the same exponent as we found for the dynamical slow modes.

We can again see this as a thermalization processes in two subsequent steps. First, for a given region in momentum space $q - \Delta < q < q + \Delta$, in and out scattering processes of phonons are not balanced, since the system is described by a non-equilibrium distribution function. Fast scattering processes lead to a local equilibration of the system such that in the interval $p \in [q - \Delta, q + \Delta]$ all modes are described by the same effective temperature $T_{\Delta,\tau}$. Locally, detailed balance has been achieved but the temperature of this momentum region is still too large, i.e. the energy density in this momentum region is larger than in the infrared. Since detailed balance (i.e. thermalization) has been achieved locally, the energy in this momentum region has to be transported over large distances, which visualizes the presence of the dynamical, macroscopic slow modes and an algebraically slow relaxation.

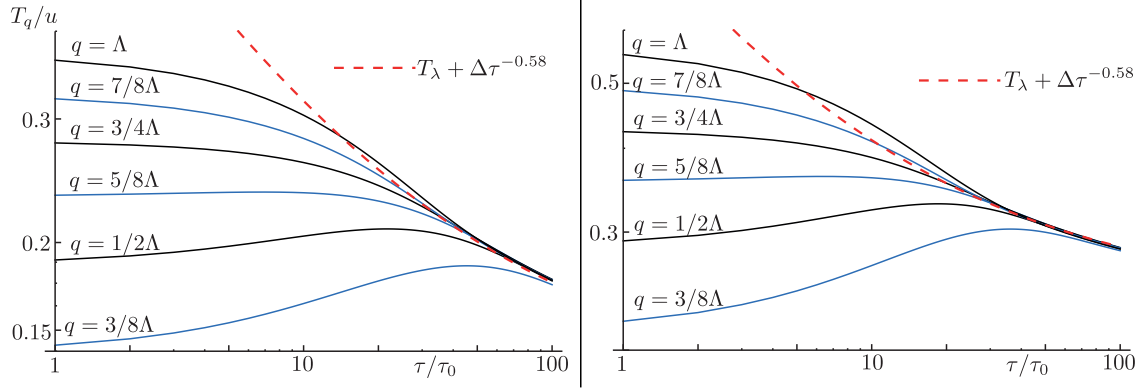


Figure 5.6: Momentum dependent temperature of the different momentum modes $T_{q,\tau}$, as defined in Eq. (5.3.27), after two different quenches. First, for smaller times one observes an alignment of the temperature for modes with different momenta, indicating local detailed balance, i.e. local thermalization of the modes. For larger times, the collective effective temperature decreases algebraically in time, resulting from slow energy transport over large distances, i.e. from the large momentum modes to the infrared. Since detailed balance is achieved locally, energy transport is only possible via macroscopic, dynamical slow modes. These yield the exponent $\alpha = 0.58$, as found for the late time decay of excitations in Sec. 4.6.

5.3.4 Pinning of the Zero Momentum Modes due to Global Particle Number and Current Conservation

In the previous section, we discussed the pinning of the zero momentum phonon densities $n_{q=0,\tau}, m_{q=0,\tau}$ to their corresponding initial value. This result is a consequence of the conservation of the global particle number and current density in the present system. According to Eqs. (3.2.29) and (3.2.30), the local density and current operators are

$$\hat{n}_x = \rho_{+,x} + \rho_{-,x} = -\frac{1}{\pi} \partial_x \phi_x, \quad (5.3.28)$$

$$\hat{j}_x = \rho_{+,x} - \rho_{-,x} = \frac{1}{\pi} \partial_x \theta_x. \quad (5.3.29)$$

The corresponding momentum dependent operators are

$$\hat{n}_q = \int_x e^{iqx} \hat{n}_x, \quad (5.3.30)$$

$$\hat{j}_q = \int_x e^{iqx} \hat{j}_x. \quad (5.3.31)$$

For a given momentum q , the fluctuations in the density and current operator are

$$\delta n_q = \langle \hat{n}_{-q} \hat{n}_q \rangle = \int_{x,x'} e^{iq(x-x')} \langle \hat{n}_x \hat{n}_{x'} \rangle = \int_{x,x'} e^{iq(x-x')} \langle \hat{n}_{x-x'} \hat{n}_0 \rangle = \int_x e^{iqx} \langle \hat{n}_x \hat{N} \rangle, \quad (5.3.32)$$

$$\delta j_q = \langle \hat{j}_{-q} \hat{j}_q \rangle = \int_{x,x'} e^{iq(x-x')} \langle \hat{j}_x \hat{j}_{x'} \rangle = \int_{x,x'} e^{iq(x-x')} \langle \hat{j}_{x-x'} \hat{j}_0 \rangle = \int_x e^{iqx} \langle \hat{j}_x \hat{J} \rangle, \quad (5.3.33)$$

where \hat{N}, \hat{J} are the global number and current operator. Consequently, $\lim_{q \rightarrow 0} \delta \hat{n}_q = \langle \hat{N}^2 \rangle$ and $\lim_{q \rightarrow 0} \delta \hat{j}_q = \langle \hat{J}^2 \rangle$. Since dynamics in the present system conserves both the particle number (due to $U(1)$ -invariance and the current (due to translational invariance) exactly, the fluctuations of the global particle number and the global current are time independent.

In terms of phonon fields in the Keldysh representation, the density and current fluctuations are

$$\begin{aligned} \delta n_{q,\tau} &= \langle n_{c,-q,\tau} n_{c,q,\tau} \rangle = -\frac{q^2}{\pi} \langle \phi_{c,-q,\tau} \phi_{c,q,\tau} \rangle = \frac{|q|K}{\pi} (G_{q,\tau,0}^K + \Gamma_{q,\tau,0}^K) \\ &= \frac{|q|K}{\pi} (2n_{q,\tau} + 1 + 2 \cos(u|q|\tau) m_{q,\tau}), \end{aligned} \quad (5.3.34)$$

$$\begin{aligned} \delta j_{q,\tau} &= \langle j_{c,-q,\tau} j_{c,q,\tau} \rangle = -\frac{q^2}{\pi^2} \langle \theta_{c,-q,\tau} \theta_{c,q,\tau} \rangle = \frac{|q|}{K\pi} (G_{q,\tau,0}^K - \Gamma_{q,\tau,0}^K) \\ &= \frac{|q|}{K\pi} (2n_{q,\tau} + 1 - 2 \cos(u|q|\tau) m_{q,\tau}). \end{aligned} \quad (5.3.35)$$

For the initial state after the quench, the diagonal and off-diagonal occupations are finite at $q = 0$, leading to

$$\lim_{q \rightarrow 0} \delta j_{q,\tau} = \lim_{q \rightarrow 0} \delta n_{q,\tau} = 0 \quad (5.3.36)$$

for all times $\tau \geq 0$. On the other hand, for a thermal state, $n_q = (e^{u|q|/T} - 1)^{-1} \stackrel{q \rightarrow 0}{=} \frac{T}{u|q|}$ and

$$\lim_{q \rightarrow 0} \delta n_q = \frac{2TK}{u\pi} \quad \text{and} \quad \lim_{q \rightarrow 0} \delta j_q = \frac{2T}{uK\pi}. \quad (5.3.37)$$

As the fluctuations $\delta n_{q,\tau}, \delta j_{q,\tau}$ are smooth functions of q and τ , starting with an initial state which has no $1/|q|$ divergence in the momentum distribution, $\delta n_{q,\tau} \xrightarrow{q \rightarrow 0} 0$ for any finite $\tau < \infty$. The same is true for the current fluctuations. As a result, a thermal state, which shows the characteristic $1/|q|$ divergence can only be built up by shifting weight continuously from larger to slower momenta and the phonon distribution for $q \rightarrow 0$ is continuously connected to the initial value at $q = 0$. In a derivative expansion of the initial density, this means $n_{q,\tau} = n_{0,\tau} + |q| \partial_q n_{q,\tau}|_{q=0} + \mathcal{O}(q^2) = n_{0,0} + |q| \partial_q n_{q,\tau}|_{q=0}$. This is exactly the structure that we found for $n_{q,\tau}$ in the limit $q \rightarrow 0$ in Eq. (5.3.24), which is based on the structure of the cubic vertex. Here, we derived the same structure simply based on the observation that the time evolution conserves current and density fluctuations.

5.3.5 Fermion Correlations 1: Analytical Results

Based on the observations in the previous sections, we can perform some approximations on the fermionic Green's function, which will allow us to determine the structural form of the Green's function in the different spatio-temporal regimes. The central result of these approximations will be the following factorized form of the fermionic Green's function.

The exponent $\mathcal{G}_{\eta,\tau,x}^<$ consists of contributions from the diagonal densities, the off-diagonal densities and of density independent contributions. We begin with the contributions from the off-diagonal densities, which are summarized in the integral

$$\mathcal{I}_{m,\tau} = 2i \int_{\mathbf{p}} \frac{\pi e^{-\frac{|p|}{\Lambda}} m_{\mathbf{p},\tau}}{|p|} \left[\frac{K^2 - 1}{K} (\cos(\mathbf{p}x) - 1) \cos(2u|p|\tau) + 2\eta \sin(|p|x) \sin(2u|p|\tau) \right]. \quad (5.3.38)$$

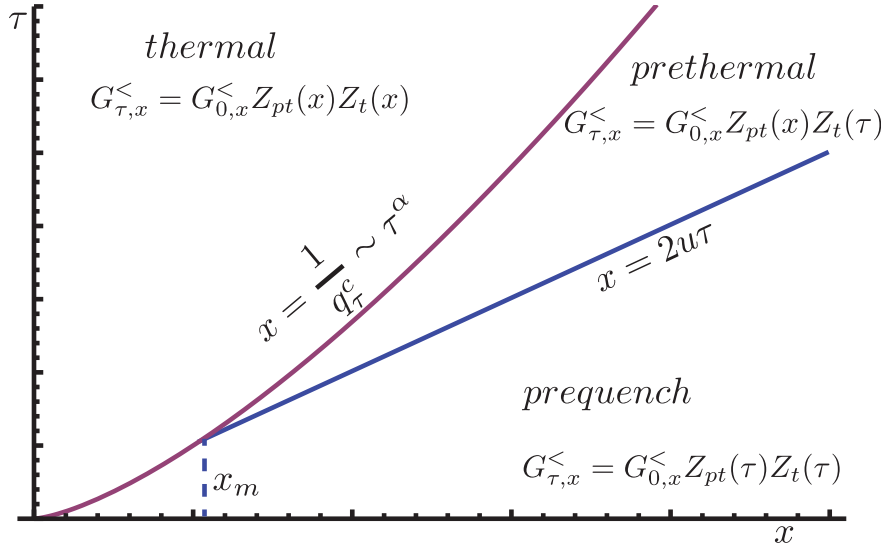


Figure 5.7: Illustration of the spatio-temporal regimes for the interacting Luttinger Liquid after the quench. For $|x| > \max\{2u\tau, \frac{1}{q_\tau^c}\}$, the fermionic correlations are determined by the initial Green's function, modified by a global, time dependent amplitude. The spatial behavior of the Green's function is therefore determined by the prequench Green's function. For $|x| > \frac{1}{q_\tau^c}$, the system has locally thermalized, indicated by a thermal Green's function for an effective temperature $T_\tau > T_\lambda$, which is decaying in time towards the final temperature $T_\lambda = T_{\tau \rightarrow \infty}$. The system is locally in equilibrium in this regime and the only dynamics is energy transport to larger distances, resulting in a decreasing effective temperature. For distances $\frac{1}{q_\tau^c} < x < 2u\tau$, the light cone of single phonons has reached these distances but only a few phonon scattering processes have happened such that the fermionic Green's function is described by the prethermal Green's function of the non-interacting theory modified with a global time dependent amplitude. This regime is determined by the dynamical fixed point of the non-interacting theory and is a prethermal plateau. As collisions become faster on smaller and smaller distances, there is a minimal distance x_m for prethermalization.

At a time $\tau > 0$, the off-diagonal density is hardly modified for momenta $q < q_\tau^c$ but decays rapidly to zero for momenta $q > q_\tau^c$. This can be implemented in $\mathcal{I}_{m,\tau}$ easily, by replacing $m_{p,\tau}$ by the bare value $m_{p,0} = m_\lambda$ and the cutoff Λ by the crossover momentum q_τ^c . As a result

$$\begin{aligned} \mathcal{I}_{m,\tau} &\approx 2im_\lambda \int_p \left[\frac{\pi e^{-\frac{|p|}{q_\tau^c}}}{|p|} \left[\frac{K^2-1}{K} (\cos(px) - 1) \cos(2u|p|\tau) + 2\eta \sin(|p|x) \sin(2u|p|\tau) \right] \right] \\ &= -2im_\lambda \left[\frac{K^2-1}{4K} \left(\log \left(\frac{1 + (q_\tau^c)^2(x - 2u\tau)^2}{1 + 4(q_\tau^c)^2 u^2 \tau^2} \right) + \log \left(\frac{1 + (q_\tau^c)^2(x + 2u\tau)^2}{1 + 4(q_\tau^c)^2 u^2 \tau^2} \right) \right) \right. \\ &\quad \left. + \frac{\eta}{2} \log \left(\frac{1 + (q_\tau^c)^2(x - 2u\tau)^2}{1 + (q_\tau^c)^2(x + 2u\tau)^2} \right) \right] \end{aligned} \quad (5.3.39)$$

$$\approx -i2\theta(x^2 - 4u^2\tau^2) m_\lambda \frac{K^2-1}{2K} \log \left[\frac{1 + (q_\tau^c)^2 x^2}{1 + 4(q_\tau^c)^2 u^2 \tau^2} \right]. \quad (5.3.40)$$

The last step is obviously exact for $|x| \gg 2u\tau$ and $|x| \ll 2u\tau$ and interpolates smoothly between these cases.

The second integral contribution to the exponent $\mathcal{G}_{\eta,\tau,x}^<$ contains the diagonal phonon distribution and is

$$\begin{aligned}\mathcal{I}_{n,\tau} &= i\frac{K^2+1}{K} \int_{\text{p}} \frac{\pi e^{-\frac{|p|}{\Lambda}} (\cos(px)-1)}{|p|} (2n_{\text{p},\tau} + 1) \\ &= -i\frac{K^2+1}{2K} (2n_{\lambda} + 1) \log[1 + \Lambda^2 x^2] + \delta\mathcal{I}_{n,\tau},\end{aligned}\quad (5.3.41)$$

with

$$\delta\mathcal{I}_{n,\tau} = 2i\frac{K^2+1}{K} \int_{\text{p}} \frac{\pi e^{-\frac{|p|}{\Lambda}} (\cos(px)-1)}{|p|} (n_{\text{p},\tau} - n_{\lambda}). \quad (5.3.42)$$

For momenta lower than the crossover momentum $q < q_{\tau}^c$, the difference of the initial distribution and the actual distribution can, according to Eq. (5.3.24), be written as

$$n_{q,\tau} - n_{\lambda} \stackrel{q < q_{\tau}^c}{=} |q| \mathcal{J}_{\tau}, \quad \text{with } \mathcal{J}_{\tau} = \int_{0 < t < \tau} \mathcal{I}_t \quad (5.3.43)$$

and \mathcal{I}_t as defined in Eq. (5.3.25). Replacing the cutoff again by the crossover momentum $\Lambda \leftrightarrow q_{\tau}^c$ and writing

$$\begin{aligned}\delta\mathcal{I}_{n,\tau} &= 2i\frac{K^2+1}{K} \left\{ \int_{\text{p}} \frac{\pi e^{-\frac{|p|}{q_{\tau}^c}} (\cos(px)-1)}{|p|} (n_{\text{p},\tau} - n_{\lambda}) + \int_{q_{\tau}^c < \text{p}} \frac{\pi e^{-\frac{|p|}{q_{\tau}^c}} (\cos(px)-1)}{p^2} \frac{\text{T}}{u} \right\} \\ &= -2i\frac{K^2+1}{K} \left\{ \mathcal{J}_{\tau} q_{\tau}^c \frac{(q_{\tau}^c)^2 x^2}{1 + (q_{\tau}^c)^2 x^2} + \frac{\text{T}_{\tau}}{u q_{\tau}^c} ((q_{\tau}^c |x| - 1) e^{-q_{\tau}^c x} + 1) \right\},\end{aligned}\quad (5.3.44)$$

where T_{τ} is again the effective temperature in the large momentum region. As at the crossover momentum, $\mathcal{J}_{\tau} q_{\tau}^c \approx \frac{\text{T}_{\tau}}{u q_{\tau}^c}$, we can further simplify the above expression, reading

$$\delta\mathcal{I}_{n,\tau} = -2i\frac{K^2+1}{K} \frac{\text{T}_{\tau}}{u q_{\tau}^c} \left[\frac{1 + 2(q_{\tau}^c)^2 x^2}{1 + (q_{\tau}^c)^2 x^2} + (q_{\tau}^c |x| - 1) e^{-q_{\tau}^c x} \right]. \quad (5.3.45)$$

With these results, we can write the exponent of the fermion correlation function

$$\begin{aligned}\mathcal{G}_{\eta,\tau,x}^< &= -i\frac{K^2+1}{2K} (2n_{\lambda} + 1) \log[1 + x^2 \Lambda^2] - i2\frac{K^2+1}{K} \frac{\text{T}_{\tau}}{u q_{\tau}^c} \left[\frac{1 + 2(q_{\tau}^c)^2 x^2}{1 + (q_{\tau}^c)^2 x^2} + (q_{\tau}^c |x| - 1) e^{-q_{\tau}^c x} \right] \\ &\quad + 2\eta \arctan[\Lambda x] - i2m_{\lambda} \theta(x^2 - 4u^2 \tau^2) \frac{K^2-1}{2K} \left[\log \left[\frac{1 + \Lambda^2 x^2}{1 + 4u^2 \tau^2 \Lambda^2} \right] \right].\end{aligned}\quad (5.3.46)$$

Comparing this expression with the exponent in the quench scenario for the linear theory, we can identify the parts that are independent of the temperature as the exponent for non-interacting theory, where there was only prethermalization. As a consequence, we write

$$\mathcal{G}_{\eta,\tau,x}^< = \tilde{\mathcal{G}}_{\eta,\tau,x}^< - i2\frac{K^2+1}{K} \frac{\text{T}_{\tau}}{u q_{\tau}^c} \left[\frac{1 + 2(q_{\tau}^c)^2 x^2}{1 + (q_{\tau}^c)^2 x^2} + (q_{\tau}^c |x| - 1) e^{-q_{\tau}^c x} \right], \quad (5.3.47)$$

where $\tilde{\mathcal{G}}_{\eta,\tau,x}^<$ is the exponent for the quench dynamics in the non-interacting theory. This implies for the fermionic Green's function

$$G_{\eta,\tau,x}^< = \tilde{G}_{\eta,\tau,x}^< e^{-\frac{K^2+1}{K} \frac{\text{T}_{\tau}}{u q_{\tau}^c} \left[\frac{1 + 2(q_{\tau}^c)^2 x^2}{1 + (q_{\tau}^c)^2 x^2} + (q_{\tau}^c |x| - 1) e^{-q_{\tau}^c x} \right]}. \quad (5.3.48)$$

Here, $\tilde{G}_{\eta,\tau,x}^<$ is the fermionic Green's function for the linear Luttinger model after the quench, which has been discussed extensively in Sec. 5.2. In the simplified picture presented here, the interactions lead only to a modification of the fermionic Green's function in terms of a multiplicative factor. We will analyze this factor now.

Eq. (5.3.48) allows for a distinction of two additional regimes in the dynamics of the interacting fermions after the interaction quench. First, for length scales much larger than the inverse crossover scale $x \gg \frac{1}{q_\tau^c}$, the system has not yet experienced a major influence of the phonon scattering and, since $xq_\tau^c \gg 1$,

$$G_{\eta,\tau,x}^< \stackrel{xq_\tau^c \gg 1}{=} \tilde{G}_{\eta,\tau,x}^< e^{-\frac{K^2+1}{K} \frac{2T_\tau}{uq_\tau^c}}. \quad (5.3.49)$$

The fermion Green's function in the non-thermalized regime is therefore modified by a global, time dependent amplitude, which grows in time. While the temperature decreases according to $T_\tau = T_\lambda + \Delta\tau^{-0.58}$, where T_λ is the final temperature and $\eta_D = 0.58$ is the exponent corresponding to the dynamical slow modes. On the other hand, the time dependence of $q_\tau^c \sim \tau^{-\eta_\lambda}$ depends on the quench parameter λ (see Fig. 5.4) and has to be determined for the individual realization. One should note, that the form of the fermion correlation function in Eq. (5.3.49) implies that the correlation function still decays algebraically in time and the system shows in this respect the typical feature of a zero temperature Luttinger Liquid.

For distances shorter than the inverse crossover scale $xq_\tau^c \ll 1$, the system already shows a thermal form of correlation functions

$$G_{\eta,\tau,x}^< \stackrel{xq_\tau^c \ll 1}{=} \tilde{G}_{\eta,\tau,x}^< e^{-\frac{K^2+1}{K} \frac{T_\tau|x|}{u}}, \quad (5.3.50)$$

featuring exponential decay in space, as it is known for a finite temperature Luttinger Liquid. However, the exponential decay is space time dependent as well, as T_τ is decaying in time towards its final value. This is caused by the energy redistribution on large length scales, as discussed in Fig. 5.6.

According to the previous discussion, we can separate the non-equilibrium dynamics after the quench into three different regimes. This results in a double factorization of the fermionic Green's functions according to

$$G_{\eta,\tau,x}^< = G_{\eta,\tau=0,x}^< Z_{\text{pt}}(s_1) Z_t(s_2). \quad (5.3.51)$$

The factor Z_{pt} is the prethermalization factor, which is determined by the linear theory and Z_t is the thermalization factor, which is introduced by the non-linearity and the values of s_1 and s_2 depend on the spatio-temporal regime. In the post-quench regime, s_1, s_2 are functions of the forward time τ , in the prethermal regime, s_1 is a function of position, while s_2 remains a function of the forward time and in the thermal regime both s_1 and s_2 depend on the distance x . We will now discuss the different regimes.

For $|x| > \max\{2u\tau, \frac{1}{q_\tau^c}\}$, the fermion Green's function is

$$G_{\eta,\tau,x}^< = \tilde{G}_{\eta,\tau,x}^< e^{-\frac{K^2+1}{K} \frac{2T_\tau}{uq_\tau^c}} = G_{\eta,0,x}^< Z_{\text{pt}}(2u\tau) Z_t\left(\frac{2}{q_\tau^c}\right), \quad (5.3.52)$$

where $\tilde{G}_{\eta,\tau,x}^<$ is the Green's function after the quench for a non-interacting Luttinger Liquid and $G_{\eta,0,x}^<$ is the initial Green's function before the quench. According to Eq. (5.2.22), the prethermal prefactor Z_{pt} is

$$Z_{\text{pt}}(s_1) = \left(\sqrt{1 + \Lambda^2 s_1^2} \right)^{\frac{K^2-1}{2K} \frac{1-\lambda^2}{2\lambda}} \quad (5.3.53)$$

and depends on the quench parameter λ and the Luttinger parameter after the quench. The thermal prefactor Z_t is defined as

$$Z_t(s) = e^{-\frac{K^2+1}{K} \frac{T_\tau}{u} s}. \quad (5.3.54)$$

In this spatio-temporal regime, the Green's functions have the scaling behavior of the initial Green's function in real space and are modified by a global, time dependent prefactor. While $Z(2u\tau)$ decays algebraically in time, $Z(2/q_\tau^c)$ decays according to a stretched exponential $\sim e^{-\tau^{\eta\lambda}}$ (see Fig. 5.4), reflecting the ongoing thermalization process. Initially $Z_{\text{pt}}(0) = Z_t(0) = 1$ and the non-interacting Luttinger Liquid is included in the form (5.3.52) as $q_\tau^c \rightarrow \infty$ in this case.

For $|x| < \frac{1}{q_\tau^c}$ on the other hand, we find

$$G_{\eta,\tau,x}^< = G_{\eta,0,x}^< Z_{\text{pt}}(x) Z_t(x). \quad (5.3.55)$$

In this regime, the algebraic decay of the correlation function in real space, resulting from the initial Green's function and the prethermal factor $Z_{\text{pt}}(x)$ is overwritten by the dominating exponential decay in real space due to the thermal factor $Z_t(x)$. Only for length scales larger than the effective temperature T_τ in the exponent, remnants of the initial zero temperature state are visible. As thermalization is proceeding to larger regions and energy is redistributed to the largest wavelengths, the temperature T_τ and therefore the exponential prefactor is decaying towards $T_\tau \rightarrow T_\lambda$. The fermionic correlations are already thermal but correspond to an larger effective temperature in this regime.

Finally, for $\frac{1}{q_\tau^c} < |x| < 2u\tau$ the correlation function can be written as

$$G_{\eta,\tau,x}^< = G_{\eta,0,x}^< Z_{\text{pt}}(x) Z_t\left(\frac{2}{q_\tau^c}\right). \quad (5.3.56)$$

Here, the real space behavior is determined by the prethermal Green's function $G_{\eta,0,x}^< Z_{\text{pt}}(x)$ and modified by the global, time-dependent exponential $Z_t\left(\frac{2}{q_\tau^c}\right)$. In this regime, fermionic properties are determined by the prethermal state of the system, i.e. by the dynamical fixed point of the non-interacting theory. The existence of this region is guaranteed by the RG irrelevant nature of the interactions, which let the thermalization spread sub-ballistically. However, as $q_\tau^c \sim \tau^{-\alpha}$, with $\alpha < 1$, there will exist a minimal length scale x_m , for which $\frac{1}{q_\tau^c} = x_m = 2u\tau$ and below which the prethermal region does not exist. The spatio-temporal dynamical phase diagram after the quench is illustrated in Fig. 5.7, showing the three different regimes that we discussed in this section.

5.3.6 Fermion Correlations 2: Numerical Results

In this section, we validate the analytical results from the previous section by simulating a quench from initially non-interacting fermions, i.e. from $K_i = 1$, to attractively interacting fermions with $K = 0.65$. The Luttinger parameter for this quench is $\lambda = K = 0.65$. As we have discussed the time evolution of the phonon modes already in Sec. 5.3.2, in this section the focus will be solely on the fermionic equal time correlation functions in real space $G_{+,\tau,x}^<$. We choose $v_0/u = 0.1$ and express time in units of $\tilde{\tau}u$. In Fig. 5.8, the real space correlation function is plotted as a function of distance x for increasing times τ , reflecting the behavior of the correlation function discussed in the previous section and justifying the approximations made.

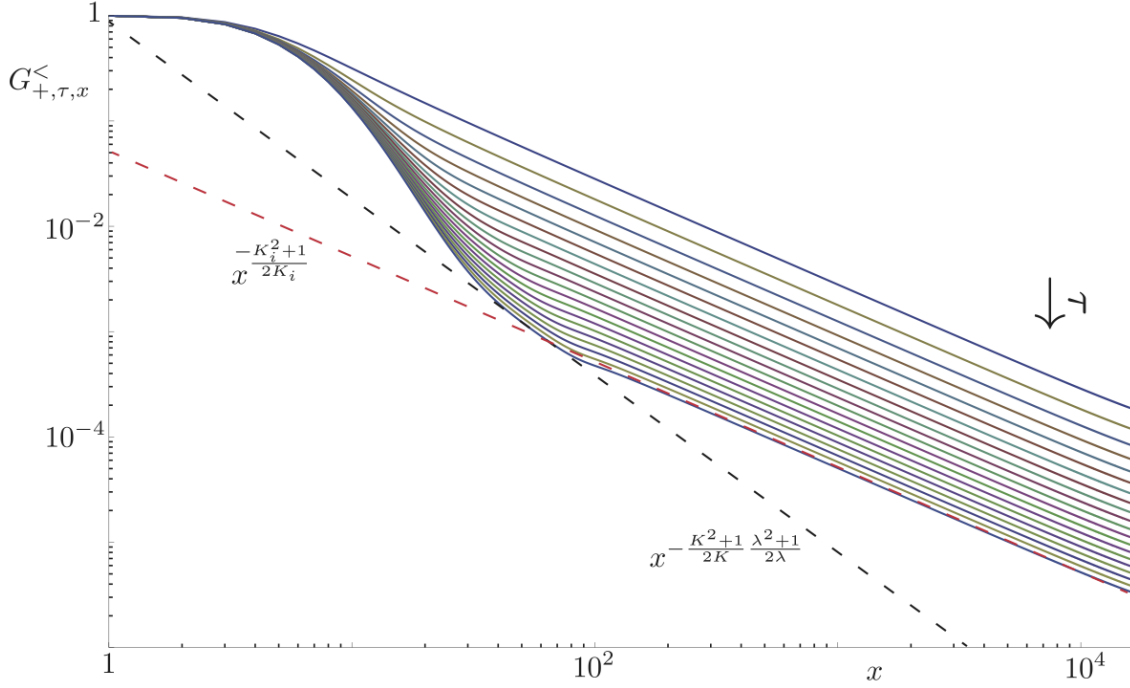


Figure 5.8: Fermionic lesser Green's function $G_{+, \tau, x}^<$ for different times τ after a quench with parameter $\lambda = 0.65$. The final Luttinger parameter $K = 0.65$ and $v_0/u = 0.1$. For initial times $\tau = 0$, the Green's function is determined by the initial value of the Luttinger parameter, i.e. $G_{+, 0, x}^< \sim x^{-\frac{K_i^2+1}{2K_i}}$. For short distances, the exponential decay of the Green's function in space is emerging, associated with thermalization on short distances. On intermediate distances, one observes the emergence of an algebraic region $G_{+, \tau, x}^< \sim x^{-\frac{K^2+1}{2K} \frac{\lambda^2+1}{2\lambda}}$, corresponding to the prethermalized region. The overall amplitude for the algebraic regimes is $Z_t(\tau) \sim e^{-T_\tau/q_\tau^c}$, i.e. a stretched exponential in time.

The time dependent momentum distribution of the fermionic particles can, as for the real space Green's function, be decomposed into three different regimes. For the smallest momenta $|q - k_F| < q_\tau^< = \min\{\frac{1}{2u\tau}, q_\tau^c\}$, the momentum space behavior is determined by the form of the Green's function for the largest distances $|x| > \max\{2u\tau, \frac{1}{q_\tau^c}\}$ and has therefore at the Fermi momentum the same scaling behavior as for the initial momentum distribution, modified by a time-dependent prefactor,

$$n_{q, \tau}^F \stackrel{q < q_\tau^<}{\sim} n_{q, 0}^F Z_{\text{pt}}(\tau) Z_t \left(\frac{2}{q_\tau^c} \right). \quad (5.3.57)$$

For the largest momenta, $|q - k_F| > q_\tau^c$, the distribution equals the thermal distribution, but for a time-dependent effective temperature T_τ , corresponding to the Fourier transform of the Green's function for small distances (5.3.55),

$$n_{q, \tau}^F \stackrel{q > q_\tau^c}{\sim} \frac{u T_\tau}{T_\tau^2 + u^2 |q - k_F|^2} |q - k_F|^{\frac{(K-1)^2}{2K}}. \quad (5.3.58)$$

For momenta corresponding to the prethermal regime $\frac{1}{2u\tau} < |q - k_F| < q_\tau^c$, the momentum

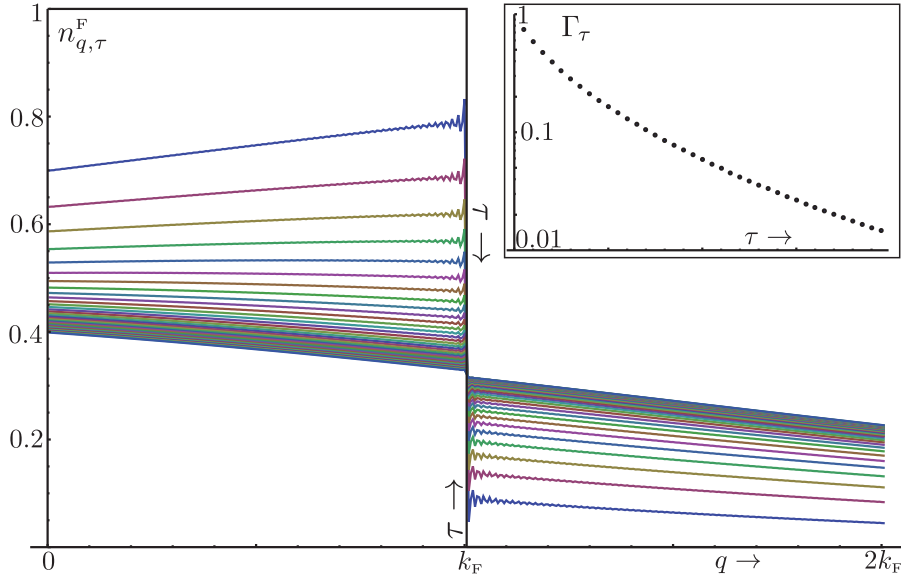


Figure 5.9: Stroboscopic plot of the fermionic momentum distribution $n_{q,\tau}^F$ for a quench from $K = 1$ (non-interacting) to $K = 0.65$. The initial distribution is a perfect Heaviside $n_{q,\tau=0}^F = \Theta(k_F - q)$, while the final distribution ($\tau \rightarrow \infty$) belongs to thermal Fermions. The time dependent residue $\Gamma_\tau = \lim_{q \rightarrow 0} |n_{k_F - q}^F - n_{k_F + q}^F|$ decays as a stretched exponential, as expected from the long distance behavior of the spatial Green's function.

distribution has the prethermal scaling but with a time dependent exponential prefactor,

$$n_{q,\tau}^F \sim |q - k_F|^{\frac{K^2+1}{2K} \frac{1+\lambda^2}{2\lambda} - 1} Z_t \left(\frac{2}{q_\tau^c} \right). \quad (5.3.59)$$

The time-dependent momentum distribution $n_{q,\tau}^F$ after a quench from $K_i = 1$ to $K = 0.65$, is shown in Fig. 5.9. The initial state corresponds to non-interacting fermions, for which at $\tau = 0$ attractive interactions are switched on. As a consequence of the previous analysis, the discontinuity of the initial momentum distribution at $q = k_F$ survives for all times $\tau < \infty$ but is damped out by a time dependent factor $Z_{\text{pt}}(\tau)Z_t(\frac{2}{q_\tau^c})$, which is faster than algebraic but a stretched exponential. For $\tau \rightarrow \infty$, the non-equilibrium regimes shrink to zero and the distribution function obtains its final, thermal form. The step at the Fermi momentum $\Gamma_\tau \equiv \lim_{\delta \rightarrow 0} |n_{\delta,\tau}^F - n_{-\delta,\tau}^F|$ is plotted in the inset of Fig. 5.9 and shows the predicted stretched exponential behavior.

5.4 CONCLUSION

In this chapter, we have analyzed the non-equilibrium time evolution of interacting, dispersive fermions in one dimension after an interaction quench. The main observables were the time dependent phonon densities, the fermionic real space Green's function and the fermionic momentum distribution. As the major result for the fermionic observables, we showed that the non-equilibrium dynamics at time τ can be separated into three different regimes: a region dominated by the prequench or initial state, which is located on the largest distances and has not experienced phonon scattering or dephasing effects yet. In

this regime, the fermionic correlations show the scaling behavior corresponding to the initial state, but are damped out exponentially in time.

On the other hand, on short distances, multiple phonon scattering processes have been establishing a local thermal equilibrium, including local detailed balance, which features exponentially decaying fermionic correlations corresponding to a Luttinger Liquid at a finite temperature. However, since the energy density in this region is larger than in the infrared, there is still energy transfer from the large momentum modes to the small momentum modes, resulting in a decreasing effective temperature. As local detailed balance does not allow for a fast energy redistribution, the energy transport over large distances relies on dynamical slow modes, witnessed by the algebraic decay of the effective temperature with the same exponent as found for the relaxation dynamics in Sec. 4.6. Therefore, even though the system has reached a local thermal equilibrium for small distances, the equilibration process is still observable.

On intermediate length scales, where collisions have not yet established equilibration but to which propagating phonons have transported information about the quench, the fermionic observables are governed by the dynamical fixed point of the non-interacting theory, i.e. by a prethermal behavior, which is characterized by an algebraic decay of correlations with a non-equilibrium exponent and a global exponentially decaying prefactor in time.

In this chapter, we have for the first time investigated the thermalization dynamics of interacting Luttinger Liquids and computed the corresponding observables. We have further addressed and answered the question, in which way the non-interacting dynamical fixed point, i.e. the prethermal state corresponding to the quadratic Luttinger theory, plays a role in this dynamics and can be used to gain information on the system without computing the complete thermalization dynamics explicitly. This information is consistent with recent experiments performed with one-dimensional interacting bosons, which have observed the emergence of a prethermal state and only on larger time scales the onset of thermalization [1, 121, 172, 74].

6 HEATING DYNAMICS OF OPEN, INTERACTING LUTTINGER LIQUIDS

We establish a new non-equilibrium scaling regime in the short time evolution of one-dimensional interacting open quantum systems subject to a generic heating mechanism. This dynamical regime is characterized by uncompensated phonon production and a superdiffusive, universal scaling of quasi-particle lifetimes with momentum $\sim q^{-5/3}$, distinct from finite and zero temperature cases. It is separated from a high momentum regime by a time dependent scale fading out as $q_0(t) \sim t^{-4/5}$. In the latter region we observe thermalization to an effective time-dependent equilibrium with linearly increasing temperature. By mapping out the dynamical phase diagram and computing the dynamical structure factor within an open system Keldysh functional integral approach, we show how these predictions can be explored in cold atom experiments by means of Bragg spectroscopy.

6.1 INTRODUCTION

Universality – the insensitivity of long wavelength macroscopic observables to the microscopic details of a given physical system – is a powerful concept in equilibrium many-body physics. Particularly low dimensional systems show a strong degree of universality, which is reflected in the low-energy description of both bosonic and fermionic one-dimensional systems in terms of Luttinger liquids [80, 67], where microscopic physics enters only via the value of two independent parameters governing the non-interacting Luttinger Hamiltonian. Static equilibrium properties are accurately described in terms of the correlation functions for this free Hamiltonian. In contrast, as recognized in seminal early work by Andreev, dynamic, finite frequency equilibrium observables, such as the dynamic structure factor, are governed by non-linear effects [8]. In particular, Andreev predicted a universal, superdiffusive scaling of the particle lifetime with momentum $\sim q^{-3/2}$ for finite temperatures (see also [176, 145, 124]). This result has been related to the famous Kardar-Parisi-Zhang equation [102] recently [198, 120], and put into a domain of validity for ultracold gases in [12]. Moreover, the zero temperature quantum limit has been shown to exhibit a different universal, diffusive scaling $\sim q^{-2}$ [150, 161, 36].

Given the strong notion of universality in equilibrium in one spatial dimension, a key question is whether and in which precise sense this leverages over to non-equilibrium conditions. This is particularly pressing in the light of recent experiments preparing and

probing the nature of low entropy quantum wires [74, 122, 197, 132]. From this, but also from a fundamental theoretical perspective, it is highly desirable to identify universal yet directly observable aspects of many-body dynamics, where the notion of insensitivity not only refers to the microscopic details, but also extends to the initial conditions. Beautiful examples of dynamical universality have been identified in the dynamics of closed, Hamiltonian systems in [17, 30, 136, 137, 103, 194, 90, 85, 129].

In this work, we address a natural situation in the context of open quantum systems: The many-body dynamics of bosons prepared in their ground state, and exposed to a weak, number conserving heating mechanism, as ubiquitous in experiments with ultracold atomic systems. Specifically, we focus on the short time domain of such a system – which ultimately reaches the infinite temperature state – where it is well described by a non-linear Luttinger liquid. This setting may be viewed as a continuous counterpart of a quantum quench [33], where energy is injected softly but permanently, instead of suddenly. We develop the theoretical framework and a first physical picture of universal aspects in this interacting quantum dynamics. In particular, we find that the specific nature of the interactions leads to a remarkably simple structure characterized by a decoupling of the forward or “ageing” time evolution, and the frequency resolved dynamic properties. The latter have to be treated fully non-perturbatively, while former is captured by a quantum kinetic equation in the self-consistent Born approximation, featuring the non-perturbatively evaluated self-energies at each time step. On this basis we obtain the following key results. (i) Low momentum non-equilibrium scaling – We demonstrate the robust presence of a window of momenta q , which is dominated by phonon production and governed by quasi-particle lifetimes which are neither thermal $\sim q^{-3/2}$, nor zero temperature $\sim q^{-2}$, but rather are dictated by a new non-equilibrium super-diffusive scaling law $\sim q^{-5/3}$ in between the known cases. The existence of this regime is granted for low temperature initial states by a combination of particle number conservation and systematic derivative expansion of the gapless problem.

(ii) High momentum effective thermalization – The phonon production regime is separated from a scattering dominated region, where we observe thermalization into a quasi-equilibrium with a time-dependent, increasing temperature (see also [177] for a numerical investigation). The crossover momentum scale between both regimes itself satisfies a scaling law $q_0(t) \sim t^{-4/5} \rightarrow 0$. It thus ultimately erases the non-equilibrium momentum window in favor of a time-dependent equilibrium state, but delimits the speed of low-frequency thermalization in a power-law fashion. We determine a dynamical phase diagram in Fig. 6.4.1. The large extent of the genuine non-equilibrium regime is promising for exploring these results in experiments, and we show that Bragg spectroscopy is a suitable tool for probing both the universal forward time and the frequency resolved dynamics.

This article is structured as follows. In Sec. 6.2, we introduce the underlying microscopic model, the one-dimensional Bose-Hubbard model (BHM) subject to permanent but number conserving heating. We also specify its low energy representation, the heated interacting Luttinger Liquid in a Keldysh path integral framework. In Sec. 6.3, we discuss the theoretical approach to address the non-equilibrium dynamics in the present system, based on diagrammatic methods, and derive the kinetic equation and self-energy for the elementary phononic excitations of the Luttinger model. Subsequently, we discuss the results obtained within this approach in Sec. 6.4, with a focus on the scaling solution for the self-energies and the time-dependent phonon density. We conclude in Sec. 6.5.

6.2 MODEL

We consider the dynamics of bosonic atoms in a one-dimensional optical lattice, as described by the quantum master equation ($\hbar = 1$)

$$\partial_t \rho = -i[H, \rho] + \gamma_E \sum_i [2\hat{n}_i \rho \hat{n}_i - \{\hat{n}_i^2, \rho\}], \quad (6.2.1)$$

where $H = \sum_i [-J(b_i^\dagger b_{i+1} + \text{h.c.}) + \frac{U}{2} \hat{n}_i(\hat{n}_i - 1)]$ is the Bose-Hubbard Hamiltonian with creation (annihilation) operators b_i^\dagger (b_i) and $\hat{n}_i = b_i^\dagger b_i$. J, U are the hopping and interaction constants, respectively. The dissipative dynamics, generated by hermitian Lindblad operators \hat{n}_i , is the leading, generic contribution due to spontaneous emission from the lattice drive laser [154] with a microscopic heating rate γ_E . This is equivalent to a locally fluctuating chemical potential and it leads to dephasing and to a linear increase of the system's energy, $\langle H \rangle(t) \sim \gamma_E t$ [154]. We will be interested in a regime of low filling $\rho_0 = \langle \hat{n}_i \rangle \ll 1$, weak interaction and heating, $U, \gamma_E \ll J$, and an initial state of the system close to the (superfluid) ground state of the Hamiltonian.

6.2.1 Master Equation in the Luttinger Description

For the description of the long wavelength, low frequency dynamics we can work in the continuum limit $b_i \rightarrow b(\mathbf{x})$, and introduce a standard Luttinger liquid representation of the field operators [80, 67],

$$b(\mathbf{x}) \approx \sqrt{\rho(\mathbf{x})} e^{i\theta(\mathbf{x})} \quad (6.2.2)$$

$$\rho(\mathbf{x}) \approx \rho_0 + \partial_x \phi(\mathbf{x}) / \pi. \quad (6.2.3)$$

The smooth component of density fluctuations $\phi(\mathbf{x})$ and the phase fluctuations $\theta(\mathbf{x})$ are conjugate variables, $[\partial_x \phi(\mathbf{x}), \theta(\mathbf{x}')] = i\pi \delta(\mathbf{x} - \mathbf{x}')$. The resulting continuum master equation, valid on length scales larger than $x_c \approx 1/(\sqrt{\rho_0 U m})$ ¹, thus reads

$$\begin{aligned} \partial_t \rho &= -i[H, \rho] + \frac{2\gamma_H}{K\pi} \int_x [2\partial_x \phi \rho \partial_x \phi - \{(\partial_x \phi)^2, \rho\}], \\ H &= \frac{1}{2\pi} \int_x [\nu K (\partial_x \theta)^2 - \frac{\nu}{K} (\partial_x \phi)^2 + \kappa_c (\partial_x \phi) (\partial_x \theta)^2], \end{aligned} \quad (6.2.4)$$

with an effective heating rate γ_H ². At weak coupling, the Luttinger parameters are $\nu = \sqrt{\frac{\rho_0 U}{m}}$, $K = \frac{\pi}{2} \sqrt{\frac{\rho_0}{U m}}$. We keep the leading non-linearity resulting from the expansion of the quantum pressure term in the effective low energy Hamiltonian ($\kappa_c = 1/m$)³. The non-linearities are irrelevant for the description of any static correlation function of the Luttinger liquid, but indispensable for capturing quantitatively dynamic correlation functions [8] as well as the forward time dynamics addressed below. The heating term becomes quadratic in the Luttinger representation, and crucially preserves the gapless, collective nature of the Hamiltonian problem.

The above heating mechanism may seem rather specific to optical lattices. However, the linear increase in system energy is ubiquitously observed, also in experiments in the spatial continuum [172]. This effect is captured by the continuum heating term in Eq. (6.2.4), and we may thus view it as the leading order in a generic model for heating in the long wavelength limit⁴. The key property of the heating term exploited here is its particle number conserving nature. This guarantees the existence of a hydrodynamic linear sound

¹The effective mass $m^{-1} = \partial_q^2 \epsilon_q$ in the lattice evaluates to $m = (4Ja^2)^{-1}$, a being the lattice constant.

²The effective heating rate is defined as $\gamma_H = \gamma_E \left(\sum_{q < \Lambda} 2\nu q^2 \right)^{-1}$.

³A term $\sim (\partial_x \phi)^3$, not present in the microscopic theory, only slightly modifies prefactors, but not the scaling laws, while a contribution $\sim (\partial_x \theta)^3$ is ruled out by the $\theta \rightarrow -\theta$ symmetry of the Hamiltonian.

⁴While the present heating mechanism corresponds to a fluctuating chemical potential, i.e. to the class of Langevin equations with additive noise, it is also possible to imagine mechanisms with multiplicative noise, such as fluctuating interaction parameters. However, while these would correspond to a completely different universality class, typically featuring an exponential energy increase, which is not relevant for optical lattice experiments, where the energy increase is linear in time.

mode as long as the system is in its low entropy ordered phase, where the Luttinger description is appropriate. This sharp mode in turn underlies the universality established here, as argued below. It is in stark contrast to an open system with particle number exchange, where the low frequency dynamics is diffusive to leading order. Clearly, the permanent heating ultimately leads to a breakdown of the Luttinger description, and the corresponding time scale is determined below. Our analysis concentrates on the preceding short-time behavior, and is complementary to the late time asymptotics studied in [156, 155, 32].

A further comment on the heating is in order at this point. As one can see from Eq. (6.2.4), the effect of the heating term is becoming stronger for shorter wavelengths. Without an appropriate cutoff, this leads to an immediate breakdown of the Luttinger description, since high momentum modes become very strongly populated. However, as has been shown in Ref. [154], the population of higher bands due to spontaneous emission is suppressed exponentially strongly, such that there exists a very natural cutoff, which on a microscopic scale is set by the inverse lattice spacing. We have verified with explicit numerical simulations, that the exact value at which the heating is cut off does not modify the dynamics of the system as long as the rate with which energy is pumped into the system is kept fixed. The non-universal properties in the heating dynamics depend on numerical value of this heating rate (and therefore implicitly on the way in which the heating cutoff is implemented). However, we want to stress that the universal results, which we focus on in this work, are independent of the heating rate and the cutoff and are in this sense indeed universal.

In order to prepare for a detailed theoretical analysis, we perform a canonical Bogoliubov transformation of both quadratic and cubic terms. That is, we expand the hermitian field operators into physically more transparent phononic creation and annihilation operators a_q^\dagger, a_q according to

$$\theta(x) = \theta_0 + i \int_q \left(\frac{\pi}{2|q|K} \right)^{1/2} e^{-iqx} \left(a_q^\dagger - a_{-q} \right), \quad (6.2.5)$$

$$\phi(x) = \phi_0 - i \int_q \left(\frac{\pi K}{2|q|} \right)^{1/2} \text{sgn}(q) e^{-iqx} \left(a_q^\dagger + a_{-q} \right). \quad (6.2.6)$$

The master equation in the phonon basis is

$$\begin{aligned} \partial_t \rho &= -i [H_{\text{ph}}, \rho] + \sum_q 2\gamma_H |q| \left[\left(a_q^\dagger + a_{-q} \right) \rho \left(a_q + a_{-q}^\dagger \right) \right. \\ &\quad \left. - \frac{1}{2} \left\{ \left(a_q + a_{-q}^\dagger \right) \left(a_q^\dagger + a_{-q} \right), \rho \right\} \right] \end{aligned} \quad (6.2.7)$$

with the phonon Hamiltonian

$$H_{\text{ph}} = \sum_q \nu |q| a_q^\dagger a_q + H_{\text{ph}}^{(3)}. \quad (6.2.8)$$

Here, $H_{\text{ph}}^{(3)}$ contains cubic phonon scattering processes, resulting from the cubic part of the Hamiltonian in Eq. (6.2.4).

Dynamics from the Quadratic Part

The quadratic part of the master equation (6.2.7) describes the heating of linear dispersing phonon modes, which leads to a linear increase of the phonon occupation in time. This is most easily seen by evaluating the time evolution of quadratic operators by neglecting the

cubic part of the Hamiltonian. Using the adjoint equation of the master equation (6.2.7), one derives the Heisenberg equations of motion for the operators

$$\partial_t \hat{n}_q = \gamma_H |q| \Rightarrow \hat{n}_q(t) = \hat{n}_q(0) + \gamma_H |q| t, \quad (6.2.9)$$

with $\hat{n}_q = a_q^\dagger a_q$. For the anomalous operator $\hat{m}_q := a_q^\dagger a_{-q}^\dagger$, one finds

$$\begin{aligned} \partial_t \hat{m}_q &= -\gamma_H |q| - 2i\nu |q| \hat{m}_q \\ \Rightarrow \hat{m}_q(t) &= i \frac{\gamma_H}{2\nu} \left(e^{-2i\nu |q| t} - 1 \right) + e^{-2i\nu |q| t} \hat{m}_q(0). \end{aligned} \quad (6.2.10)$$

The linear increase of the phonon number in time, with a momentum dependent rate $\Gamma_q = \gamma_H |q|$, in turn leads to a linear increase of the system energy in time, consistent with previous results [154]. In contrast, $|\hat{m}_q(t)|$ is bounded to a very small value and therefore of negligible influence on the dynamics as we briefly discuss later.

At this point, two further comments are in order.

(i) UV cutoff – In order not to pump an infinite amount of energy into the system, the heating has to be cut-off at some ultraviolet (UV) momentum q_h . This is an artifact of taking the continuum limit of the heating Liouvillian in the main text without accounting for the finite width of the lowest Bloch band, for which \mathcal{L} is defined. A similar problem occurs for correlation functions in the Luttinger Liquid theory, which are commonly regularized introducing an exponential cutoff $e^{-|p|\alpha}$ for the creation and annihilation operators [67]. However, the precise form of the cutoff does not modify the results of our analysis, as long as q_h is sufficiently large to not cause discontinuities in the time evolution, and we therefore set $q_h = \Lambda$, with Λ the cutoff of the Luttinger theory. For a given heating rate, the microscopic heating rate $\gamma_E = \partial_\tau E(\tau)$ must be independent of the cutoff and determines the effective heating rate γ_H implicitly via $\gamma_E = \gamma_H \sum_{q < q_h} 2\nu q^2$.

(ii) Adequacy of the Luttinger representation – The main physical ingredient of the Luttinger representation of the bosonic field operators Eq. (6.2.2) is the fact that the density fluctuations $\delta\rho(x) = \partial_x \phi(x)$ are gapless, which is due to the collective nature of one-dimensional systems. Intuitively, this collective nature should be preserved in an exactly number conserving system such as the one considered here. Indeed, formally the dissipative term in the master equation with hermitian Lindblad operators $\rho(x) = \rho_0 + \partial_x \phi(x)$ is invariant under a constant shift $\rho(x) \rightarrow \rho(x) - \rho_0$, which together with the familiar form of the Hamiltonian demonstrates the gapless, collective nature of the master equation. This underlies the existence of a sharp collective, coherent phonon mode with dynamical exponent $z = 1$ and subleading dissipative corrections. This should be contrasted with a number non-conserving system, where a finite density results from a balance of loss and pumping terms, as e.g. described by non-hermitian Lindblad operators such as $b(x), b^\dagger(x)$. The dissipative term in a corresponding master equation does not exhibit the above shift invariance, and so its gapless nature is not obvious. In fact, in such a situation no coherent mode exists at long wavelength. Instead, the leading dynamics is dissipative, with a dissipative dynamical exponent governed by the Kardar-Parisi-Zhang universality class [4]. This circumstance would completely invalidate the approach taken here.

Resonant Three-Phonon Scattering

Applying the transformation (6.2.5), (6.2.6) to the cubic part of the Hamiltonian (6.2.4), leads to the cubic phonon scattering term

$$\begin{aligned} H_{\text{ph}}^{(3)} &= \int_{q,p} \left\{ \frac{1}{3} V_{q,p,-p-q} a_q a_p a_{-q-p} \right. \\ &\quad \left. + V_{q,p,p+q} a_{p+q}^\dagger a_q a_p + \text{h.c.} \right\} \end{aligned} \quad (6.2.11)$$

with the permutation invariant vertex

$$\begin{aligned} V(\mathbf{k}, \mathbf{q}, \mathbf{p}) &= \sqrt{|\mathbf{p} \cdot \mathbf{k} \cdot \mathbf{q}|} v(\mathbf{k}, \mathbf{q}, \mathbf{p}), \\ v(\mathbf{k}, \mathbf{q}, \mathbf{p}) &= \sqrt{\frac{\kappa_c^2 \pi}{2K}} \left\{ \frac{qk}{|qk|} + \frac{pk}{|pk|} + \frac{pq}{|pq|} \right\}. \end{aligned} \quad (6.2.12)$$

While momentum conservation is guaranteed by the Hamiltonian (6.2.11), not all of the processes are also energy conserving with respect to $H^{(2)}$. For instance a process in which three phonons are destroyed or created ($a_q a_p a_{-p-q}$ or its hermitean conjugate) violate energy conservation since there is a positive energy associated to each phonon. In contrast, the process $a_{p+q}^\dagger a_p a_q$ can be energy conserving. Since the dispersion is linear ($\epsilon_q = u|q|$), the process is resonant if

$$|p + q| = |p| + |q|. \quad (6.2.13)$$

Due to the RG-irrelevant nature of the interaction, only those processes can become relevant for the dynamics, which describe phonons interacting with each other for arbitrary long time without dephasing. These are exactly the resonant processes and we will from now on only consider these [8, 161]. For the case of resonant scattering, the function $v(p + q, q, p)$ takes a constant value

$$v_0 := v(1, 1, 1) = 3\kappa_c \sqrt{\frac{\pi}{2K}}. \quad (6.2.14)$$

Since κ_c is only roughly determined by microscopic parameters $\kappa_c \approx \frac{\hbar^2}{m}$, the full interaction strength v_0 has to be determined by numerics or inferred from experimental data. The corresponding Hamiltonian is

$$H_{\text{res}} = v_0 \int'_{\mathbf{q}, \mathbf{p}} \sqrt{|q p (p + q)|} \left(a_{p+q}^\dagger a_q a_p + \text{h.c.} \right). \quad (6.2.15)$$

Here, \int' indicates that the integral runs only over momenta for which the integrand describes resonant scattering.

6.2.2 Keldysh Action

The scale invariant, gapless nature of the continuum master equation (6.2.4) rules out a perturbative treatment of the non-linearities, which could be performed on the level of the master equation [109, 52, 125]. It is therefore advantageous to map the master equation into a fully equivalent Keldysh functional integral [50, 181], which opens up the problem to non-perturbative techniques from many-body physics.

In a Keldysh path integral framework [3, 99], the partition function is defined as the functional integral $\mathcal{Z} = \int \mathcal{D}[\bar{a}_q^c, a_q^c, \bar{a}_q^q, a_q^q] e^{i\mathcal{S}}$. The microscopic action \mathcal{S} is a functional of the complex classical and quantum fields $\bar{a}_q^{c/q}, a_q^{c/q}$, which can be derived directly from the markovian master equation (6.2.7) according to the translation table described in Refs. [50, 182]. The Keldysh action $\mathcal{S} = \mathcal{S}_H + \mathcal{S}_D$ is composed of the Hamiltonian contribution \mathcal{S}_H and the dissipative part \mathcal{S}_D , which reflects the Liouvillian. The Hamiltonian parts of the

action, including the nonlinearities, read [29]

$$\begin{aligned} \mathcal{S}_H = & \frac{1}{2\pi} \int_{t,t',p} (\bar{a}_{p,t}^c, \bar{a}_{p,t}^q) \begin{pmatrix} 0 & D_{p,t,t'}^R \\ D_{p,t,t'}^A & D_{p,t,t'}^K \end{pmatrix} \begin{pmatrix} a_{p,t'}^c \\ a_{p,t'}^q \end{pmatrix} \\ & + \frac{v_0}{\sqrt{8\pi}} \int'_{p,k,t} \sqrt{|pk(k+p)|} \left[2\bar{a}_{k+p,t}^c a_{k,t}^c a_{p,t}^q \right. \\ & \left. + \bar{a}_{k+p,t}^q \left(a_{k,t}^c a_{p,t}^c + a_{k,t}^q a_{p,t}^q \right) + \text{h.c.} \right], \end{aligned} \quad (6.2.16)$$

with the bare inverse retarded/advanced propagator

$$D_{p,t,t'}^R = \delta(t-t') (i\partial_{t'} - u|p| + i0^+), \quad (6.2.17)$$

$$D_{p,t,t'}^A = (D_{p,t,t'}^R)^\dagger = \delta(t-t') (i\partial_{t'} - u|p| - i0^+) \quad (6.2.18)$$

and the Keldysh component of the inverse propagator

$$D_{p,t,t'}^K = 2i0^+ F(p, t, t'). \quad (6.2.19)$$

The dissipative action, determined by the Liouvillian is

$$\mathcal{S}_D = i \int_{p,t} \gamma_H |p| (\bar{a}_p^q, a_{-p}^q) \begin{pmatrix} 1 & 1 \\ 1 & 1 \end{pmatrix} \begin{pmatrix} a_p^q \\ \bar{a}_{-p}^q \end{pmatrix} \quad (6.2.20)$$

and modifies only the quantum-quantum part of the action. It describes permanent phonon production with a momentum dependent rate $\gamma_H |q|$ in the diagonal phonon channel, as already derived on an operator level in Eq. (6.2.9). Clearly, this cannot be compensated by the non-linearities, which can redistribute energy between the phonon modes but not counteract the energy pump. Therefore a time-independent fluctuation dissipation relation in this system can only be established at $t \rightarrow \infty$ – when an infinite temperature steady state is reached.

The off-diagonal phonon production, represented by the $\bar{a}_p^q a_{-p}^q + \text{h.c.}$ terms is however affected by the quadratic Hamiltonian (c.f. Eq. (6.2.10)). The off-diagonal density is not continuously pumped by the heating but instead shows oscillatory behavior with a maximum $|\langle a_p^\dagger a_{-p}^\dagger \rangle|_{\text{max}} = \frac{\gamma_H^d}{\nu} \ll 1$, due to the interplay of quadratic unitary and dissipative dynamics. Due to the dominant resonant scattering, there is no scattering from the normal phonon mode into the anomalous phonon mode, which would require a resonant scattering vertex that is cubic in creation operators. However, such a cubic vertex is unable to fulfill energy and momentum conservation (for a detailed discussion of the technical details see [29]). As a result, the kinetic equation for the diagonal elements can be solved independently of the off-diagonal elements. Furthermore the occupation of the off-diagonal correlator remains small even in the presence of interactions, as shown in Eq. (6.2.10). Therefore, we neglect the latter and project the dissipation onto diagonal terms. The corresponding dissipative action is

$$\mathcal{S}_D = i\gamma_H \int_{p,t} |p| \bar{a}_p^q a_p^q. \quad (6.2.21)$$

In this section, we have derived the Keldysh action for the low energy dynamics of interacting lattice bosons subject to dephasing. The dephasing is caused by spontaneous emission processes of the bosonic atoms. The action $\mathcal{S} = \mathcal{S}_H + \mathcal{S}_D$ consists of a Hamiltonian part \mathcal{S}_H , describing an interacting Luttinger Liquid with resonant phonon scattering

processes, and a dissipative part \mathcal{S}_D representing the dephasing, which leads to a permanent production of phonons in the system. Here, we have justified and already implemented two approximations, namely the resonant approximation, taking only energy conserving phonon scattering processes into account and leading to the Hamiltonian action (6.2.16), and the "diagonal" approximation, which neglects the off-diagonal phonon density and results in the dissipative part (6.2.21). Both of them will be used in the next section to derive the quantum kinetic equation and phonon self-energy for the present system.

6.3 PHONON GREEN'S FUNCTIONS

We are interested in the full phononic single-particle Green's functions, i.e. the retarded Green's function

$$G_{p,t,t'}^R = (D^R - \Sigma^R)_{p,t,t'}^{-1} \quad (6.3.1)$$

and the Keldysh Green's function

$$G_{p,t,t'}^K = (G^R \circ F - F \circ G^A)_{p,t,t'}. \quad (6.3.2)$$

Here, Σ^R is the retarded self-energy generated by the resonant phonon interaction and $F_{q,t,t'}$ is the non-equilibrium phonon distribution function depending on the interplay of dissipation and interaction.

6.3.1 Non-equilibrium Fluctuation-Dissipation Relation

For an out-of-equilibrium situation with explicitly broken time translational invariance, it is useful to introduce Wigner coordinates. Accordingly, a two time function $F_{q,t,t'}$ is expressed in terms of relative time $\Delta_t = t - t'$ and forward time $\tau = \frac{t+t'}{2}$. The Wigner transform of $F_{q,t,t'}$ is defined as

$$F_{q,\omega,\tau} = \int d\Delta_t e^{i\omega\Delta_t} F_{q,\tau+\Delta_t/2,\tau-\Delta_t/2}. \quad (6.3.3)$$

In Wigner coordinates, the non-equilibrium fluctuation-dissipation relation (FDR)

$$\partial_\tau F_{q,\omega,\tau} = i\Sigma_{q,\omega,\tau}^K - i(\Sigma^R \circ F - F \circ \Sigma^A)_{q,\omega,\tau} \quad (6.3.4)$$

yields the time-evolution of the distribution function in terms of the Keldysh self-energy Σ^K and the retarded/advanced self-energies $\Sigma^{R/A}$. In the present case, the Keldysh self-energy (fluctuation contribution)

$$\Sigma_{q,\omega,\tau}^K = -i\gamma_H|q| + \tilde{\Sigma}_{q,\omega,\tau}^K \quad (6.3.5)$$

consists of a term $\tilde{\Sigma}^K$ generated solely by the phonon scattering and a term $\gamma_H|q|$ stemming from the dephasing. The latter drives the system away from equilibrium: It generates a permanent time evolution, which cannot be compensated by the dissipation contribution (term in brackets in Eq. (6.3.4)) generated entirely by conservative Hamiltonian contribution to the dynamics.

In the following, we will use two distinct approximations in order to simplify this equation and solve for the phonon Green's functions. We will justify these approximations at the end of the section.

First, we exploit the fact, that the forward time evolution and the frequency dynamics decouple due to the subleading nature of the interactions. This justifies the Wigner approximation in time and simplifies Eq. (6.3.4) significantly. In Wigner approximation, the time evolution can be solved first, and independently of the frequency dynamics, yielding a time-dependent single particle distribution function. In a second step, for each instant in time the impact of the non-linearities on the frequency dynamics can be studied in a quasi-stationary state. This can be seen as a "local time approximation" in some analogy to a local density approximation in space. Technically speaking, in Wigner approximation, the Wigner transform of a convolution is identical to the product of the Wigner transforms. Second, due to the RG irrelevant interactions, the phonons become dressed, yet still well-defined quasi-particles. This is expressed by the fact that the phonon spectral function

$$\mathcal{A}_{\mathbf{q},\omega,\tau} = i(G^{\text{R}} - G^{\text{A}})_{\mathbf{q},\omega,\tau} \quad (6.3.6)$$

is sharply peaked at the bare phonon energy $\omega = \epsilon_{\mathbf{q}}$ with a typical width $\gamma_{\mathbf{q}} \ll \epsilon_{\mathbf{q}}$ much smaller than the energy. Consequently, all the quasi-particle weight is located at $\omega = \epsilon_{\mathbf{q}}$ and the self-energy and distribution function can be evaluated on-shell. The on-shell self-energies can be parametrized as

$$\Sigma_{\mathbf{q},\omega=\epsilon_{\mathbf{q}},\tau}^{\text{R}} = -i\sigma_{\mathbf{q},\tau}^{\text{R}}, \quad \tilde{\Sigma}_{\mathbf{q},\omega=\epsilon_{\mathbf{q}},\tau}^{\text{K}} = -2i\sigma_{\mathbf{q},\tau}^{\text{K}}. \quad (6.3.7)$$

Here, $\sigma^{\text{R/K}}$ are positive and real functions of momentum and forward time [29]. The on-shell distribution function for well-defined quasi-particles

$$F_{\mathbf{q},\omega=\epsilon_{\mathbf{q}},\tau} = 2n_{\mathbf{q},\tau} + 1 \quad (6.3.8)$$

is simply the phonon density [99].

Utilizing both Wigner and quasi-particle approximations, the FDR, Eq. (6.3.4), simplifies to

$$\partial_{\tau} n_{\mathbf{q},\tau} = \frac{\gamma_{\text{H}}|\mathbf{q}|}{2} + \sigma_{\mathbf{q},\tau}^{\text{K}} - \sigma_{\mathbf{q},\tau}^{\text{R}} (2n_{\mathbf{q},\tau} + 1). \quad (6.3.9)$$

This is the on-shell non-equilibrium FDR for an open interacting Luttinger Liquid, driven by spontaneous emission processes of the microscopic particles. Due to the first term on the r.h.s. of the FDR, the system is driven away from a thermal equilibrium state and is unable to thermalize to a stationary finite temperature state.

6.3.2 Self-Energies and Kinetic Equation

The on-shell self-energy $\sigma_{\mathbf{q},\tau}^{\text{R}}$ and the kinetic equation for Luttinger Liquids with resonant interactions have been derived in a previous work for an isolated system [29]. Here modifications arise due to openness of the system, expressed by the presence of the factor $\propto \gamma_{\text{H}}|\mathbf{q}|$ in Eq. (6.3.9).

We consider a zero temperature initial state with $n_{\mathbf{q},\tau=0} = 0$. For this case, the vertex correction is exactly zero at $\tau = 0$ [29] and the self-consistent Born approximation becomes is justified at sufficiently short times. For this situation, the self-consistency equation, obtained by non-equilibrium diagrammatics, for the retarded self-energy is

$$\tilde{\sigma}_{\mathbf{q}}^{\text{R}} = \int_{0 < \tau < \text{p}} \left(\frac{\partial_{\tau} n_{\text{p}}}{\tilde{\sigma}_{\text{p}}^{\text{R}}} + 2n_{\text{p}} + 1 \right) \left(\frac{\text{qp}(\mathbf{q}-\text{p})}{\tilde{\sigma}_{\text{p}}^{\text{R}} + \tilde{\sigma}_{\mathbf{q}-\text{p}}^{\text{R}}} + \frac{\text{qp}(\text{p}+\mathbf{q})}{\tilde{\sigma}_{\text{p}}^{\text{R}} + \tilde{\sigma}_{\text{p}+\mathbf{q}}^{\text{R}}} \right). \quad (6.3.10)$$

Here, we have omitted the forward time index and performed the rescaling $\tilde{\tau} = v_0\tau$, $\tilde{\sigma}^R = \sigma^R/v_0$ in order to make this equation independent of microscopic variables. For a given phonon density n_p and its time derivative $\partial_{\tilde{\tau}}n_p$, it can be solved self-consistently either by using numerics or by a scaling ansatz. The latter is applicable only for the special case for which the phonon density itself is a scaling solution, as we discuss below. In order to obtain the time dependent phonon density a kinetic equation approach is used.

The kinetic equation for the phonon density is again derived via the diagrammatic approach, outlined in Ref. [29]. In terms of the rescaled time $\tilde{\tau}$ and self-energy $\tilde{\sigma}^R$ it reads

$$\begin{aligned} \partial_{\tilde{\tau}}n_q = & \frac{\gamma_H|q|}{2v_0} \\ & + \int_{0 < p < q} \frac{2pq(q-p)(n_p n_{q-p} - n_q(1+n_p+n_{q-p}))}{\tilde{\sigma}_q^R + \tilde{\sigma}_p^R + \tilde{\sigma}_{q-p}^R} \\ & + \int_{0 < p} \frac{4pq(q+p)(n_{p+q}(n_q+n_p+1) - n_q n_p)}{\tilde{\sigma}_q^R + \tilde{\sigma}_p^R + \tilde{\sigma}_{q+p}^R}. \end{aligned} \quad (6.3.11)$$

The kinetic equation determines the time evolution of the phonon density in the system $n_{q,\tau}$. Together with Eq. (6.3.10) it forms a closed set of equations for the non-equilibrium dynamics of the driven, interacting Luttinger Liquid. Both can be solved iteratively according to the scheme depicted in Fig. 6.3.2.

A specific but relevant case is the kinetic equation for small momenta $q \ll 1$. For this condition fulfilled, it simplifies to

$$\partial_{\tilde{\tau}}n_q \stackrel{q \ll 1}{=} |q| \left(\frac{\gamma_H}{2} + \mathcal{I}_{\tilde{\tau}} \right), \quad (6.3.12)$$

where

$$\mathcal{I}_{\tilde{\tau}} = \int_{0 < p} \frac{2p^2(n_{p,\tilde{\tau}}+1)n_{p,\tilde{\tau}}}{\tilde{\sigma}_{p,\tilde{\tau}}^R} \quad (6.3.13)$$

is a time dependent but momentum independent function. Consequently, the change of n_q is linear in the momentum q for small momenta.

One should note, that except for the initial phonon distribution $n_{q,\tau=0}$ and the heating term $\propto \gamma_H$, no additional microscopic information enters the dynamics expressed in the kinetic equation (6.3.11) and self-energy equation (6.3.10). In particular, both equations are insensitive to an UV cutoff for the Luttinger Liquid $\sim \sqrt{U\rho_0 m}$ for sufficiently strongly decaying distribution $n_{p,\tilde{\tau}}$, which is provided, e.g., for zero or finite temperature initial states. Consequently, the dynamics induced by the heating is universal, in the sense that it only depends on the energy pump into the system $\propto \gamma_H$ and the initial state. We will now close this section with a discussion of the validity of the above made approximations, namely the Wigner and the quasi-particle approximation.

6.3.3 Validity

In the previous sections, we have used two essential approximations, namely the Wigner approximation and the quasi-particle approximation, in order to obtain analytical results for the self-energy and kinetic equation of the phonons. Although these are quite standard approximations in the kinetic theory of interacting particles, they have to be justified properly. In this section, we will show that both approximations are valid in the present case and give a proper bound for their applicability.

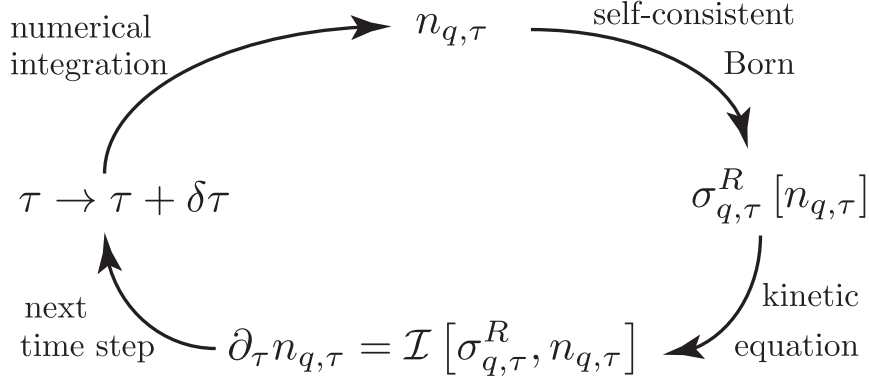


Figure 6.1: Schematic illustration of the iteration process to determine the time-dependent phonon density $n_{q,\tau}$. For a given time τ , the self-energy $\sigma_{q,\tau}^R$ is determined via the self-consistent Born approximation according to Eq. (6.3.10). Subsequently the time derivative of $n_{q,\tau}$ is computed via the kinetic equation (6.3.11). Using a Runge-Kutta solver for numerical differential equations, the density $n_{q,\tau+\delta\tau}$ is computed and used as the starting point for the next iteration.

Wigner Approximation

We applied the Wigner approximation in order to simplify the Wigner transform of the convolution in the FDR (6.3.4) and approximate it by the lowest order contribution. As a consequence, the Wigner transform of the product in (6.3.4) equals the product of the individual Wigner transformed functions, i.e.

$$\begin{aligned}
 (\Sigma^R \circ F)_{q,\omega,\tau} &= \Sigma_{q,\omega,\tau}^R e^{\frac{i}{2}(\overleftarrow{\partial}_\tau \overrightarrow{\partial}_\omega - \overleftarrow{\partial}_\omega \overrightarrow{\partial}_\tau)} F_{q,\omega,\tau} \\
 &\approx \Sigma_{q,\omega,\tau}^R F_{q,\omega,\tau}.
 \end{aligned} \tag{6.3.14}$$

As one can see, in the Wigner approximation, all the terms beyond zeroth order in the expansion of the exponential are neglected. This is justified, if the contribution of these terms, which contains derivatives of the self-energy and the distribution function, is negligibly small. We will now show that the time scale for the breakdown of the Wigner approximation lies on the order of the time scale where the Luttinger liquid description breaks down, and thus never poses an additional restriction to our approach.

The condition for which the Wigner approximation in Eq. (6.3.14) is justified reads

$$1 \gg \underbrace{\left| \frac{\partial_\omega \Sigma_{q,\omega,\tau}^R}{\Sigma_{q,\omega,\tau}^R} \right|}_{t_{\Delta t}} \underbrace{\left| \frac{\partial_\tau n_{q,\tau}}{n_{q,\tau} + \frac{1}{2}} \right|}_{1/t_\tau}, \tag{6.3.15}$$

which is equivalent to requesting the first order term of the expansion of the exponential to be already much smaller than the zeroth order term. Physically, this means that the characteristic time scale of the forward dynamics t_τ is much larger than for the relative dynamics. The characteristic time scale for the relative dynamics is determined by the Hamiltonian time evolution, i.e. is set by the inverse quasi-particle energy, while the characteristic forward time scale is set by the dissipation on the r.h.s of Eq. (6.3.15), which

is generated by the subleading interactions. As we show now, the criterion (6.3.15) is fulfilled for sufficiently small $\gamma_H \tau$, with heating rate γ_H and forward time τ . To demonstrate this, we use the result for the phonon lifetimes from the subsequent section and evaluate it on shell (i.e. for $\omega = \nu|q|$) to find $t_{\Delta_t} = \left| \frac{\partial \omega \Sigma_{q,\omega,\tau}^R}{\Sigma_{q,\omega,\tau}^R} \right| = \frac{1}{\nu} \left| \frac{\partial_q \sigma_{q,\tau}^R}{\sigma_{q,\tau}^R} \right| = \frac{\eta_R}{\epsilon_q}$ with $\eta_R = \mathcal{O}(1)$ as seen below. To estimate the time-scale of the forward evolution, we use the decay integrals in (6.3.11) and evaluate them in the thermalized regime (this sets a lower bound: in the low momentum regime, the occupation is much lower than a corresponding thermal occupation, leading to a slower decay compared to the thermal regime, and the Wigner approximation is valid for even longer times) to get

$$\frac{1}{t_\tau} = c_0 \frac{v_0^2}{\nu^2} T(\tau) q^2, \quad (6.3.16)$$

with $c_0 = \mathcal{O}(1)$. The increase in total energy is only caused by the heating term and is linear in $\gamma_H \tau$. As a consequence, we find $T(\tau) = T_0 \gamma_H \tau$ with $T_0 = \mathcal{O}(\frac{1}{10})$ typically. Evaluating (6.3.15) at the UV cutoff momentum again in a conservative way, $q = \Lambda$ (with $\Lambda \approx \nu/v_0$, v_0 defined in Eq. (6.2.14)) yields

$$\tau \ll \frac{1}{c_0 \eta_R} \frac{\nu^2}{T_0 v_0 \gamma_H}. \quad (6.3.17)$$

Comparing this to the criterion for the validity of the Luttinger Liquid description $T(\tau) \ll \nu \Lambda$, which we can rearrange to

$$\tau \ll \frac{\nu^2}{T_0 v_0 \gamma_H}, \quad (6.3.18)$$

shows that the Wigner approximation is justified for times τ , for which the Luttinger description is applicable.

Quasi-particle Approximation

In the quasi-particle approximation, the elementary excitations (in the present case the phonons) are dressed but well defined quasi-particles in the sense that their spectral weight is essentially located at a specific frequency $\omega = \epsilon_q$, the quasi-particle energy. Consequently, physical quantities like the self-energy and the distribution function can be evaluated on-shell (at $\omega = \epsilon_q$). As already stated above, this requires $\epsilon_q \gg \left| \text{Im} \left(\Sigma_{q,\omega=\epsilon_q,\tau}^R \right) \right|$. In other words, the imaginary part of the self-energy must be much smaller than the quasi-particle energy. For the present case, the on-shell self-energy is purely imaginary and the above condition transforms into

$$\epsilon_q \gg \sigma_{q,\tau}^R. \quad (6.3.19)$$

From the time-dependent phonon density $n_{q,\tau}$, we determine below the self-energy $\sigma_{q,\tau}^R$ according to Eq. (6.3.10). Indeed $\sigma_{q,\tau}^R \ll \epsilon_q$ for all times and momenta considered. Furthermore

$$\frac{\sigma_{q,\tau}^R}{\epsilon_q} \xrightarrow{q \rightarrow 0} 0 \quad (6.3.20)$$

for all times is guaranteed by the subleading nature of the interactions. Thus, obedience of the quasi-particle criterion is justified a posteriori. For the specific case of an equilibrium state (for $T \geq 0$), the quasi-particle approximation breaks down exactly at the UV cutoff $q = \Lambda$.

6.4 TIME-EVOLUTION AND NON-EQUILIBRIUM SCALING

In this section, we discuss the non-equilibrium dynamics of a heated interacting Luttinger Liquid obtained by solving Eqs. (6.3.11) and (6.3.10) numerically as described in the previous section. The main results are the time evolution of the phonon density $n_{q,\tau}$ and a scaling solution for the quasi-particle lifetimes $t_q \sim q^{\eta_R}$ with a new non-equilibrium exponent $\eta_R = \frac{5}{3}$. The latter is observable in the low momentum regime for momenta $q < q_0(\tau)$, where $q_0(\tau)$ is a time-dependent momentum scale that separates the non-equilibrium low momentum regime from a quasi-thermal large momentum regime and fades out as $q_0(\tau) \sim \tau^{-\frac{4}{5}}$.

6.4.1 Time-dependent Phonon Density

The time evolution of the phonon occupation obtained numerically is plotted for different times in Fig. 6.4.1. We clearly identify a (time dependent) crossover scale $q_0(\tau)$, which we find analytically to scale to zero as $q_0(\tau) \sim \tau^{-4/5}$, consistent with numerics. The crossover scale separates a non-equilibrium low momentum regime $n_q(\tau) \sim |q|$ from a scattering dominated thermalized high momentum region $n_q \sim 1/|q|$.

In the latter regime, the integral and dephasing contributions scale $\sim q^2, |q|$ respectively. As a consequence of this scaling, for sufficiently large momenta, the collision term yields the dominant contribution to the dynamics compared to the heating term. The dominant relaxational dynamics for the distribution function then approaches the Bose distribution function $n_B(c|q|/T(t))$, which is the dynamical fixed point for the collisional term in Eq. (6.3.11) alone, and where there is an approximate detailed balance between phonon emission and absorption. Indeed, the occupation number is fitted well with a thermal distribution $n_q = n_B(c|q|, T(t)) \approx T(t)/c|q|$ in this regime. In a stochastic wavefunction interpretation of the underlying master equation, in this regime multiple thermalizing collisions happen in between two subsequent spontaneous emission events. While the individual heating processes continuously create additional phonons, the system finds the time to relax to a local equilibrium in between two subsequent heating events. Consequently, in the large momentum regime, the heating is described by a time dependent temperature. Such a behavior has been observed numerically in [177].

In contrast to this, the low momentum regime is strongly non-thermal; this fact underlies the new scaling law for the particle decay width established below. Here we encounter a strongly overweighing phonon production both due to heating and phonon scattering. Two structural properties ensure the linear rise with no offset, $n_q(\tau) \sim |q|$. First, both terms in Eq. (6.3.11) contribute $\sim |q|$ for $|q| \rightarrow 0$ as emphasized in the discussion of the low momentum version of the kinetic equation (6.3.12). This dependence is guaranteed by the form of both dephasing term and scattering vertex, which in turn are dictated by the collective nature of the system, or technically by the systematic derivative expansion of the low frequency action to leading order.

Second, the value of $n_{q=0}(\tau)$ at zero momentum is pinned to its initial value for all times. This is a key structural property of the problem, related to particle number conservation: The static structure factor at zero momentum is related to the particle number variance via $S_\tau(q=0) = (\langle \hat{N}^2(\tau) \rangle - \langle \hat{N}(\tau) \rangle^2)/L = S_{\tau=0}(q=0)$, where $\hat{N}(\tau)$ is the total particle number operator in the Heisenberg picture and L the system length, cf. [130]. The last

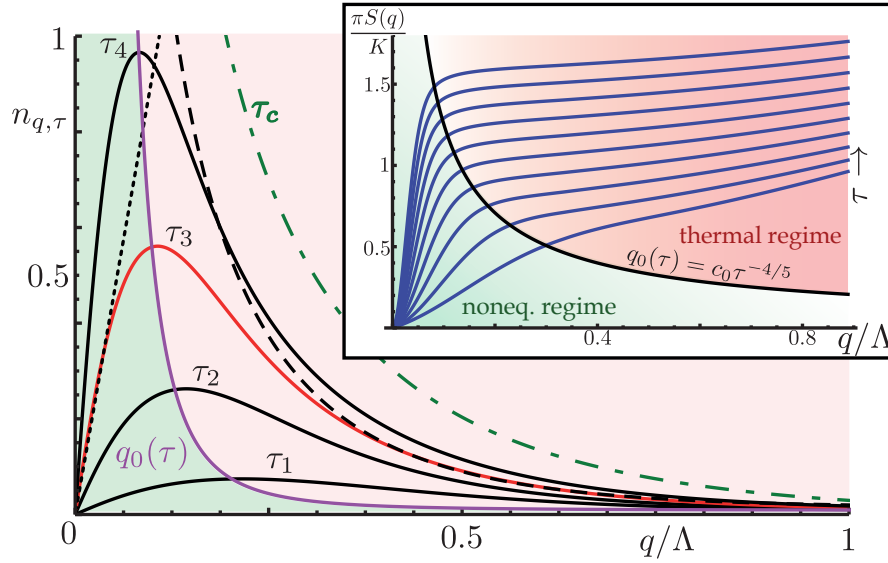


Figure 6.2: Dynamics of the phonon occupation $n_q(\tau)$ in a sequence of times $(\tau_1, \tau_2, \tau_3, \tau_4) = (1, 2, 3, 4) \cdot \frac{10}{v_0 \Lambda^2}$ as a function of q/Λ , with heating rate $\gamma_H = 0.06 v_0 \Lambda$. ($\Lambda = 1/x_c$ is the high momentum cutoff delimiting the validity of the Luttinger liquid description. For weak interactions $\Lambda \approx \sqrt{\rho_0 m \bar{U}}$.) Non-equilibrium ($n_q \sim |q|$) and time-dependent thermalized ($n_q \sim n_B(\nu|q|)$) regimes are indicated by the dotted (dashed) line for τ_3 ($T(\tau_3) = 0.38\nu\Lambda$), and separated by the crossover scale $q_0(\tau)$. The dash-dotted line shows $n_B(T(\tau_c))$, where $T(\tau_c) \approx \nu\Lambda$, at which the Luttinger description breaks down. Inset: Dynamical phase diagram mapped out by the experimentally accessible static structure factor, which is a direct measure of the phonon distribution (see text).

equality then holds in a particle number conserving system as the present one. Since in addition $n_q(\tau) \sim S_\tau(q)$ in the Luttinger model, cf. Eq. (6.4.8), this ensures a permanent “pinning” of the phonon occupation at zero momentum. For zero temperature initial states, these two facts guarantee the existence of a linear phonon occupation regime described above. Remarkably, this mechanism leads to very slow, algebraic thermalization of the low momenta: Establishment of the $1/c|q|$ Rayleigh-Jeans divergence can only be achieved due to the scaling of the crossover momentum $q_0(t) \rightarrow 0$, but not via a direct filling of the low momentum modes. We conjecture that this is generic for the thermalization of one-dimensional quantum systems in phases with superfluid order, comprising the setting of a quantum quench.

6.4.2 Quasi-particle Lifetime Scaling and Dynamical Phase Diagram

We now address the frequency dynamics at each time step. In particular, we are interested in the scaling behavior of the phonon quasi-particle lifetimes, which results from the overlap of the coherent phonon mode with the many-body continuum. This is achieved within the Keldysh framework, where the distribution function is not fixed a priori to its equilibrium shape, but is replaced by the dynamically determined non-equilibrium distribution. The quasi-particle lifetimes t_q are defined via

$$t_{q,\tau} = - \left(\text{Im} \Sigma_{q,\omega=\epsilon_{q,\tau}}^R \right)^{-1} = (\sigma_{q,\tau}^R)^{-1}. \quad (6.4.1)$$

As we have seen in the previous subsection, the phonon density can be described by a scaling ansatz in the two different regimes $q \ll q_0$ and $q \gg q_0$. For small momenta, $n_{q,\tau} = |q|f_\tau$, where f is a positive function of the forward time, while for large momenta $n_{q,\tau} = \frac{T_\tau}{\nu|q|}$ with an effective time-dependent temperature T_τ . From the form of the self-energy equation (6.3.10), we infer directly that if the first factor under the integral can be written as a scaling form

$$\left((\tilde{\sigma}_p^R)^{-1} \partial_{\tilde{\tau}} n_p + 2n_p + 1 \right) = a_\tau p^{\eta_n} \quad (6.4.2)$$

with a positive (time-dependent) prefactor a_τ , the self-energy itself will be a scaling function (see Ref. [29] for a detailed analysis of possible scaling forms). In the above mentioned momentum regimes, Eq. (6.4.2) is expected to hold since the phonon occupation n_p has a scaling form, which directly translates to a scaling of the left hand side of Eq. (6.4.2). Consequently, we parametrize $\tilde{\sigma}_q^R = \gamma_\tau |q|^{\eta_R}$.

The scaling equation for the retarded self-energy reads

$$\begin{aligned} \sigma_q^R &= \gamma_\tau |q|^{\eta_R} = \frac{a_\tau |q|^{4+\eta_n-\eta_R}}{\gamma_\tau} I_\eta, \\ I_\eta &= \int_0^\infty \frac{dx}{2\pi} \left(\frac{|x|^{\eta_n+1}(1-x)}{|x-1|^{\eta_R} + |x|^{\eta_R}} + (x \rightarrow -x) \right), \end{aligned} \quad (6.4.3)$$

with a dimensionless integral whose value depends parametrically on the scaling exponents but otherwise is a pure number. It leads to the scaling relation for the phonon lifetime and occupation exponents η_R, η_n

$$\eta_R = 2 + \frac{\eta_n}{2}, \quad (6.4.4)$$

which is a key result of this work. η_n is determined by the solution of the generalized kinetic equation discussed previously.

Below the crossover scale q_0 , the phonon density scales linear in momentum $n_q \sim |q|$. Since $\tilde{\sigma}_q^R \sim |q|^{\eta_R}$ with $\eta_R > 1$, this means that $\frac{\partial_{\tilde{\tau}} n_q}{\tilde{\sigma}_q^R (2n_q+1)} \xrightarrow{q \rightarrow 0} \infty$ and Eq. (6.4.2) is dominated by the first term in brackets. Consequently $\eta_n = 1 - \eta_R$, which implies a super-diffusive behavior $\eta_R = 5/3$ with no equilibrium counterpart.

In contrast, above the scale, $n_q \sim |q|^{-1}$ and $\frac{\partial_{\tilde{\tau}} n_q}{\tilde{\sigma}_q^R (2n_q+1)} \xrightarrow{q \rightarrow \infty} 0$ and Eq. (6.4.2) is dominated by the phonon density $(2n_q + 1) \sim |q|^{-1}$ (or $\sim |q|^0 = 1$, for very large momenta). This leads to $\eta_n = -1$ and as a consequence $\eta_R = \frac{3}{2}$, as it is known for the finite temperature equilibrium case. In contrast, for the largest momenta $\eta_n = 0$ and $\eta_R = 2$, implying the zero temperature diffusive behavior [150, 161].

Following the above discussion, we identify the crossover momentum q_0 between non-equilibrium and effective equilibrium scaling to be determined by the condition

$$\frac{\partial_{\tilde{\tau}} n_{q_0}}{2n_{q_0} + 1} = \tilde{\sigma}_{q_0}^R. \quad (6.4.5)$$

The scaling behavior of this equation in momentum and time yields

$$q_0(\tau) \sim (\tau \gamma_\tau)^{-\frac{1}{\eta_R}}. \quad (6.4.6)$$

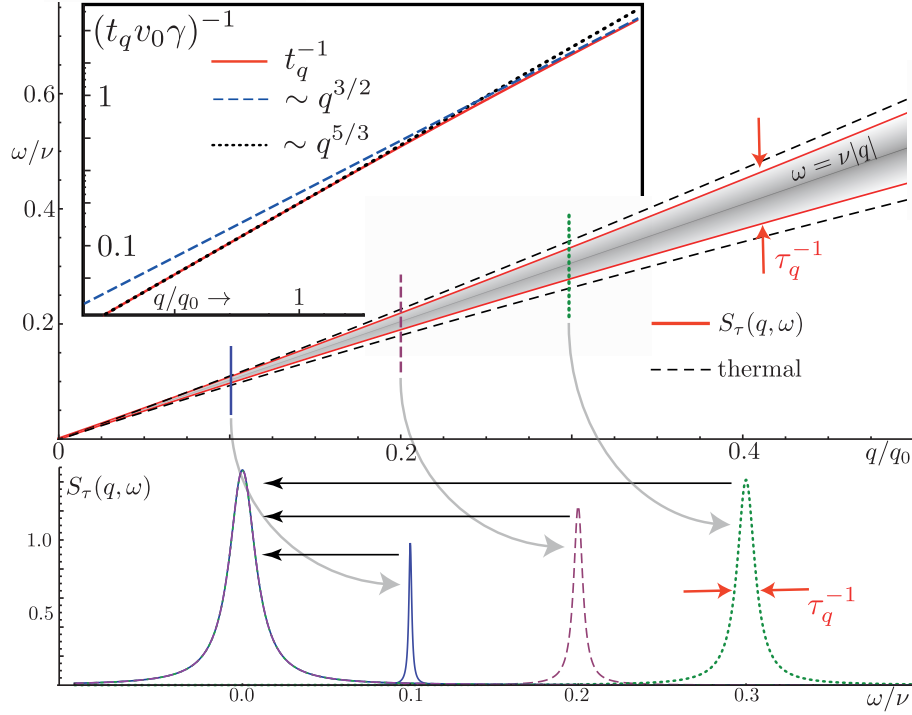


Figure 6.3: Dynamical structure factor (DSF). Upper panel: The DSF reveals the universal scaling behavior of the phonon lifetimes and allows us to discriminate the new non-equilibrium scaling from equilibrium thermal scaling, both of which are clearly separated. Inset: Log-Log comparison of t_q from $n_q(\tau)$ with the analytically predicted scaling solutions. For small momenta (in units of the crossover scale q_0), one clearly identifies the non-equilibrium scaling behavior and only for momenta $q \gg q_0$ the thermal scaling sets in. Lower panel: DSF for fixed momenta $q = (0.1, 0.2, 0.3)$. The plots collapse on top of each other after rescalings $\omega \rightarrow |q|^{-5/3}(\omega - \nu|q|)$ and $S \rightarrow |q|^{-1/3}S$, which demonstrates the scaling $t_q \sim |q|^{-5/3}$.

Approaching the crossover from the low momentum regime yields (remember $n_{q,\tau} = f_\tau |q|$ for small momenta) $\eta_R = 5/3$, $\gamma_\tau \sim \left(\frac{f_\tau}{\tau}\right)^{1/3}$. Using the numerical result $f_\tau \sim \tau^2$, Eq. (6.4.6) can be solved semi-analytically and yields $q_0(\tau) \sim \tau^{-4/5}$. This agrees perfectly with our numerical result for the crossover scale $q_0 \sim \tau^{-0.808}$. The semi-analytical analysis in this way demonstrates, that the low momentum regime is responsible for the observed scaling of q_0 .

6.4.3 Experimental Detection

We demonstrate that Bragg spectroscopy gives immediate access to all the characteristics of the universal heating dynamics. It enables a direct probe of the density-density correlations in ultracold atomic gases [185, 187, 189, 22]. More precisely, in a stationary state, the Bragg signal is directly proportional to the Fourier transform of two-point density-density correlations, or dynamical structure factor (DSF) $S(\omega, q) = \int dt dx e^{i(qx - \omega t)} \langle \{\hat{n}(t, x), \hat{n}(0, 0)\} \rangle$. In the Keldysh formalism and long wavelength limit, this translates into $S_\tau(\omega, q) =$

$-\langle \rho_c(\tau, -\omega, -q) \rho_c(\tau, \omega, q) \rangle$, for which we obtain the explicit expression

$$S_\tau(\omega, q) = \frac{(2n_q(\tau)+1)|q|K}{\pi\Sigma_q^R} \left(\tilde{f}\left(\frac{\omega-\epsilon_q}{\Sigma_q^R}\right) + (\omega \rightarrow -\omega) \right), \quad (6.4.7)$$

where $\tilde{f}(x) = 1/(1+x^2)$ is the dimensionless Lorentzian. As per the above discussion, time enters only parametrically, giving a snapshot, effectively stationary DSF. The different scaling regimes of the quasi-particle lifetimes are clearly identified in Fig. 6.3 (a).

The time-dependent crossover scale $q_0(\tau)$ obtains most directly from the equal-time DSF, or static structure factor,

$$S_\tau^s(q) = \int \frac{d\omega}{2\pi} S_\tau(\omega, q) = \frac{|q|K}{\pi} (2n_q(\tau) + 1), \quad (6.4.8)$$

which is plotted in Fig. 6.4.1. In particular, it provides direct access to the phonon occupation number, and thus to the scaling of the crossover scale $q_0(\tau)$ and the peak height.

6.4.4 Modifications for $T > 0$

The computations and results presented in the previous sections have been obtained for a system initialized in the $T = 0$ ground state. Here, we discuss how an initial finite temperature ($T > 0$) state modifies these results, corroborating that the new scaling regime remains observable in an experimentally accessible window of parameters $T_{\text{in}} \ll q_0(\tau)$. This analysis is relevant and necessary since experiments are never carried out for systems with zero initial but usually very small temperatures. For the Luttinger description to be applicable, the initial temperature must be much lower than the Luttinger ultraviolet cutoff, i.e. $T \ll \nu\Lambda$, $k_B = 1$, which we consider in the following.

In order to obtain the time-dependent phonon occupation for the case of an initial $T > 0$ state, we numerically solve the kinetic equation, Eq. (6.3.11), with an initial phonon distribution function

$$n_q(\tau = 0) = n_B(\nu|q|) = \left(e^{\frac{\nu|q|}{T}} - 1 \right)^{-1}. \quad (6.4.9)$$

However, for a finite temperature distribution, the vertex correction is generally non-zero and has to be implemented in the kinetic equation and self-energy according to the procedure described in Ref. [29]. As a result, the numerical computation becomes more involved but still feasible. From the time evolved phonon occupation, we then determine the static structure factor $S_\tau^s(q)$ (Fig. 6.4.4) and the scaling of the quasi-particle lifetimes t_q (Fig. 6.4.4) as a function of time and momentum.

Our analysis of the phonon occupation dynamics for $T = 0$ showed that dynamics is mainly governed by a fast energy redistribution for the high energy modes and a comparably slow evolution in the low frequency sector. This results from the structure of the particle number conserving vertex and the pinning of $n_{q=0}(\tau) = n_{q=0}(\tau = 0)$ to its initial value. For a $T > 0$ initial state, the situation does not change and the initial temperature has only little influence on the dynamics of n_q . The latter is dominated by the effect that drives the system away from equilibrium, i.e. the constant heating. We therefore decompose n_q into an initial part and another one which builds up in time according to

$$n_q(\tau) = n_q(\tau = 0) + \delta n_q(\tau). \quad (6.4.10)$$

From our numerical simulations, we find that $\delta n_q(\tau)$ is almost independent of the initial temperature and for $T > 0$ qualitatively equivalent to the $T = 0$ scenario. While our

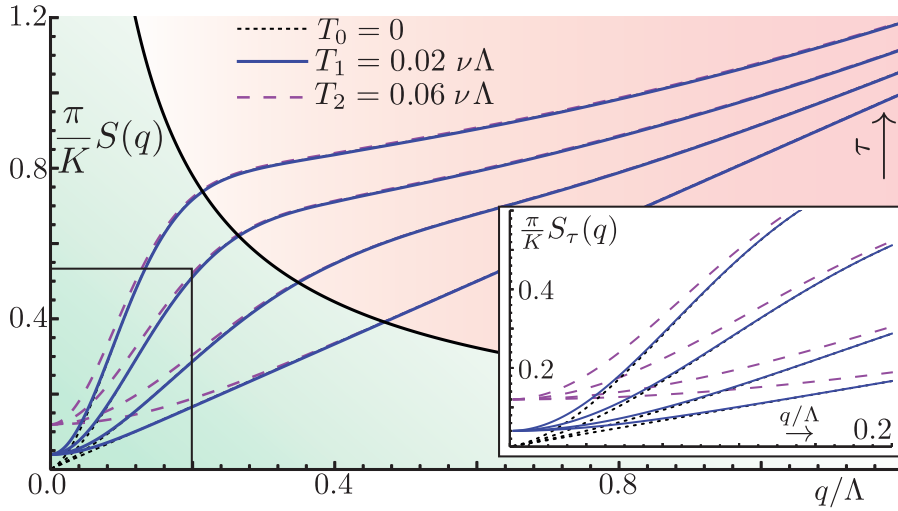


Figure 6.4: Comparison of the time evolved static structure factor $S_\tau^s(q)$ for different initial temperatures T at different times τ . The black dotted (blue solid, red dashed) lines corresponds to an initial temperature $T = 0$ ($T = 0.02\nu\Lambda$, $T = 0.06\nu\Lambda$). The different lines correspond to increasing times $(\tau_0, \tau_1, \tau_2, \tau_3) = (0, 1, 2, 3)\frac{4}{\nu_0\Lambda^2}$. As for the zero temperature case, $S_\tau^s(q = 0)$ is pinned to its initial value $S_{\tau=0}^s(q = 0) = \frac{KT}{\pi}$ due to particle number conserving dynamics. For $0 < q < q_0$, the characteristic $S^s(q) \sim q^2$ scaling in the non-equilibrium regime is clearly visible and the $T > 0$ curves approach the one for $T = 0$. For larger momenta, the finite temperature curves lie on top of the $T = 0$ ones. Inset: Zoom into the low momentum region.

results are obtained for the full simulation of the kinetic equation, we will use the above finding to explain the results.

To determine the static structure factor, we employ Eq. (6.4.8), leading to

$$S_\tau^s(q) = \frac{|q|K}{\pi} (2n_q(\tau = 0) + 2\delta n_q(\tau) + 1) \quad (6.4.11)$$

$$\stackrel{\nu|q| \ll T}{\approx} \frac{2TK}{\nu\pi} + \frac{|q|K}{\pi} (2\delta n_q(\tau) + 1).$$

Compared to the $T = 0$ case, this leads to a non-zero structure factor for $q = 0$, $S_\tau^s(q = 0) = \frac{2TK}{\nu\pi}$. For $q > 0$, we find a q^2 scaling of the structure factor in the non-equilibrium regime as in the zero temperature case. For larger momenta $\nu|q| > T$, $n_q(\tau = 0)$ vanishes and the finite and zero temperature structure factor are identical. In particular, the two different momentum regimes can still be characterized by the $T = 0$ scaling properties of $S^s(q)$, see Fig. 6.4.4.

In view of the scaling of the quasi-particle lifetimes t_q , and thereby the dynamic structure factor, our analysis fully confirms and corroborates the following expected scenario, cf. Fig. 6.4.4. Most importantly, an additional scaling regime for momenta much smaller than the temperature $\nu|q| \ll T$ occurs. In this regime, lifetimes scale with the thermal exponent $t_q \sim q^{-3/2}$. For momenta in the range $\frac{T}{\nu} < |q| < q_0$, a momentum region showing non-equilibrium scaling $t_q \sim q^{-5/3}$ is found, while for $|q| > q_0$, again thermal scaling behavior emerges. For $\frac{T}{\nu} \ll q_0$, the non-equilibrium scaling regime is sufficiently large to be resolved numerically and analytically. Such a situation is presented in Fig. 6.4.4. For this specific example $\frac{\nu q_0}{T} \approx 12$, while the non-equilibrium scaling regime has a momentum

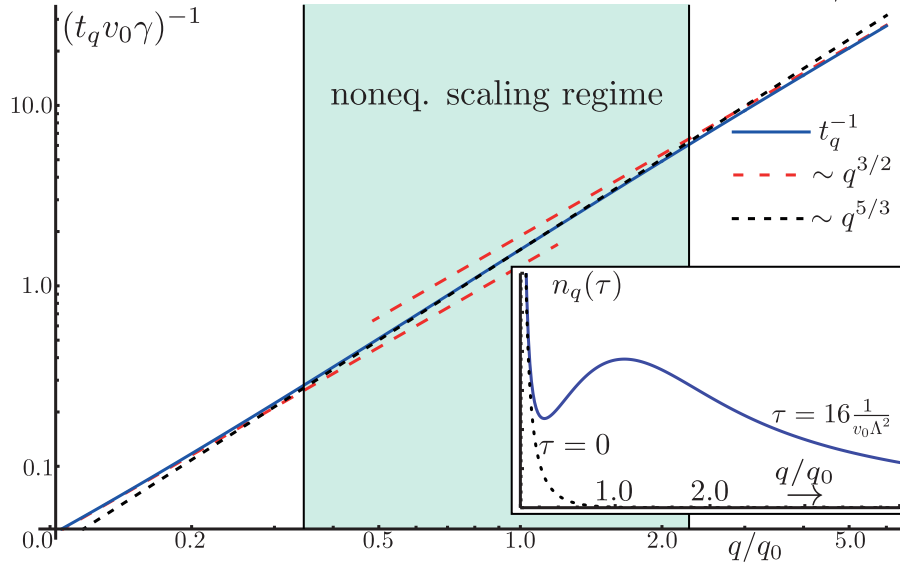


Figure 6.5: Scaling behavior of the inverse quasi-particle lifetime t_q^{-1} for system dynamics initialized at a finite temperature $T = 0.02\nu\Lambda$ and evaluated at time $\tau = \frac{16}{v_0\Lambda^2}$. Due to the initial finite temperature, we identify three scaling regimes. For momenta smaller than the initial temperature $q < q_T = \frac{2T}{\nu}$, the $\frac{1}{q}$ divergence of the phonon-distribution dictates a thermal $t_q \sim q^{-3/2}$ scaling behavior. For momenta $q_T < q < q_0$ in between the temperature and the non-equilibrium crossover scale q_0 , the non-equilibrium scaling $t_q \sim q^{-5/3}$ can be identified, while for $q_0 < q$ the system obeys thermal scaling again. As a result, for $q_T \ll q_0$, one will be able to find a sufficiently large scaling regime with the non-equilibrium scaling behavior. Inset: Corresponding phonon distribution $n_q(\tau)$ for times $\tau = 0$ (black dotted) and $\tau = \frac{16}{v_0\Lambda^2}$ (blue solid) in units of the crossover momentum.

window ranging from $q_{\min} \approx 0.35q/q_0$ to $q_{\max} \approx 2q/q_0$, i.e. $\frac{q_{\max}}{q_{\min}} \approx 5.7$. The initial temperatures used here are in reach for current experiments [132, 183], holding the promise to resolve the discussed non-equilibrium scaling regime in the lab. We finally note that while the different scaling regimes may not be very clearly visible in Fig. 6.4.4, using the data collapse procedure described in Fig. 6.3 will allow to clearly discriminate the different scaling regimes.

6.5 CONCLUSIONS

We have identified a new universal non-equilibrium scaling regime in the heating dynamics of interacting Luttinger liquids. Its existence is granted by the defining property of a Luttinger liquid, the presence of a sharp phonon mode, which prevails in the number conserving, permanently forward evolving open system. This triggers the hope that large classes of one-dimensional systems subject to non-equilibrium drive could exhibit similarly strong notions of universality as their equilibrium counterparts. Both extending the theoretical concepts familiar from closed systems, and exploring the status of universality in low dimensional driven open quantum systems, represent fascinating challenges for future research.

BIBLIOGRAPHY

- [1] K. Agarwal, E. G. Dalla Torre, B. Rauer, T. Langen, J. Schmiedmayer, and E. Demler. Chiral Prethermalization in supersonically split condensates. *Phys. Rev. Lett.*, 113:190401, 2014.
- [2] A. Altland and F. Haake. Quantum Chaos and Effective Thermalization. *Phys. Rev. Lett.*, 108:073601, Feb 2012.
- [3] A. Altland and B. Simons. *Condensed Matter Field Theory*. Cambridge University Press, 2010.
- [4] E. Altman, L. M. Sieberer, L. Chen, S. Diehl, and J. Toner. Two-dimensional superfluidity of exciton-polaritons requires strong anisotropy. *Phys. Rev. X*, 5:011017, 2015.
- [5] D. J. Amit, H. Gutfreund, and H. Sompolinsky. Storing Infinite Numbers of Patterns in a Spin-Glass Model of Neural Networks. *Phys. Rev. Lett.*, 55:1530–1533, Sep 1985.
- [6] D. J. Amit and V. Martin-Mayor. *Field Theory, the Renormalization Group, and Critical Phenomena*. World Scientific, Singapore, third edition, 2005.
- [7] J. Andreasen, A. A. Asatryan, L. C. Botten, M. A. Byrne, H. Cao, L. Ge, L. Labonté, P. Sebbah, A. D. Stone, H. E. Türeci, and C. Vanneste. Modes of random lasers. *Adv. Opt. Photon.*, 3(1):88–127, Mar 2011.
- [8] A. F. Andreev. The hydrodynamics of two- and one-dimensional liquids. *Sov. Physics JETP*, 51:1038, 1980.
- [9] L. Angelani, C. Conti, G. Ruocco, and F. Zamponi. Glassy Behavior of Light. *Phys. Rev. Lett.*, 96:065702, Feb 2006.
- [10] D. N. Aristov. Luttinger liquids with curvature: Density correlations and Coulomb drag effect. *Phys. Rev. B*, 76:085327, 2007.
- [11] V. I. Arnold. *Mathematical Methods of Classical Mechanics*. Springer, New York, 1989.
- [12] M. Arzamasovs, F. Bovo, and D. M. Gangardt. Kinetics of mobile impurities and correlation functions in one-dimensional superfluids at finite temperature. *Phys. Rev. Lett.*, 112(170602):170602, 2014.
- [13] V. Bapst, L. Foini, F. Krzakala, G. Semerjian, and F. Zamponi. The Quantum Adiabatic Algorithm applied to random optimization problems: the quantum spin glass perspective. *Physics Reports*, 523(3):127 – 205, 2013.

- [14] Th. Barthel and U. Schollwöck. Dephasing and the Steady State in Quantum Many-Particle Systems. *Phys. Rev. Lett.*, 100:100601, 2008.
- [15] K. Baumann, C. Guerlin, F. Brennecke, and T. Esslinger. The Dicke Quantum Phase Transition with a Superfluid Gas in an Optical Cavity. *Nature*, 464:1301, 2010.
- [16] K. Baumann, R. Mottl, F. Brennecke, and T. Esslinger. Exploring Symmetry Breaking at the Dicke Quantum Phase Transition. *Phys. Rev. Lett.*, 107:140402, Sep 2011.
- [17] J. Berges, Sz. Borsányi, and C. Wetterich. Prethermalization. *Phys. Rev. Lett.*, 93:142002, Sep 2004.
- [18] B. Bertini, F. H. L. Essler, S. Groha, and N. J. Robinson. Prethermalization and thermalization in models with weak integrability breaking. *arXiv:1506.02994*, 2015.
- [19] M. J. Bhaseen, J. Mayoh, B. D. Simons, and J. Keeling. Dynamics of nonequilibrium Dicke models. *Phys. Rev. A*, 85:013817, Jan 2012.
- [20] K. Binder and A. P. Young. Spin glasses: Experimental facts, theoretical concepts, and open questions. *Rev. Mod. Phys.*, 58:801–976, Oct 1986.
- [21] G. Biroli, C. Kollath, and A. M. Läuchli. Effect of Rare Fluctuations on the Thermalization of Isolated Quantum Systems. *Phys. Rev. Lett.*, 105:250401, 2010.
- [22] U. Bissbort, S. Götze, Y. Li, J. Heinze, J. S. Krauser, M. Weinberg, C. Becker, K. Sengstock, and W. Hofstetter. Detecting the Amplitude Mode of Strongly Interacting Lattice Bosons by Bragg Scattering. *Phys. Rev. Lett.*, 106:205303, 2011.
- [23] Adam T. Black, Hilton W. Chan, and Vladan Vuletić. Observation of Collective Friction Forces due to Spatial Self-Organization of Atoms: From Rayleigh to Bragg Scattering. *Phys. Rev. Lett.*, 91:203001, Nov 2003.
- [24] L. Boltzmann. Über die Eigenschaften Monocyklischer und andere damit verwandter Systeme. *Crelles Journal*, 98:68–94, 1884.
- [25] D. Braun, F. Haake, and W. T. Strunz. Universality of Decoherence. *Phys. Rev. Lett.*, 86:2913, 2001.
- [26] F. Brennecke, T. Donner, S. Ritter, T. Bourdel, M. Köhl, and T. Esslinger. Cavity QED with a Bose-Einstein condensate. *Nature*, 450(268-271), 2007.
- [27] H.-P. Breuer and F. Petruccione. *The Theory of Open Quantum Systems*. Oxford University Press, USA, 2002.
- [28] M. Buchhold and S. Diehl. Non-Equilibrium Universality in the Heating Dynamics of Interacting Luttinger Liquids. *arXiv:1404.3740*, 2014.
- [29] M. Buchhold and S. Diehl. Kinetic Theory for Interacting Luttinger Liquids. *arXiv:1501.01027*, 2015.
- [30] A. A. Burkov, M. D. Lukin, and E. Demler. Decoherence Dynamics in Low-Dimensional Cold Atom Interferometers. *Phys. Rev. Lett.*, 98:200404, May 2007.
- [31] J. Eisert C. Gogolin. Equilibration, thermalisation, and the emergence of statistical mechanics in closed quantum systems. *arXiv:1503.07538*, 2015.
- [32] Z. Cai and Th. Barthel. Algebraic versus Exponential Decoherence in Dissipative Many-Particle Systems. *Phys. Rev. Lett.*, 111:150403, Oct 2013.
- [33] P. Calabrese and J. Cardy. Time Dependence of Correlation Functions Following a Quantum Quench. *Phys. Rev. Lett.*, 96:136801, Apr 2006.
- [34] H. J. Carmichael. *Statistical Methods in Quantum Optics 1: Master Equations and Fokker-Planck Equations*. Springer Verlag, Berlin, 1999.

- [35] H. J. Carmichael, C. W. Gardiner, and D. F. Walls. Higher order corrections to the Dicke superradiant phase transition. *Phys. Lett. A*, 46:47, 1973.
- [36] J.-S. Caux and P. Calabrese. Dynamical density-density correlations in the one-dimensional Bose gas. *Phys. Rev. A*, 74:031605, 2006.
- [37] J.-S. Caux and F. H. L. Essler. Time evolution of local observables after quenching to an integrable model. *Phys. Rev. Lett.*, 110:257203, 2013.
- [38] A. L. Cavalieri, N. Müller, Th. Uphues, V. S. Yakovlev, A. Baltuška, B. Horvath, B. Schmidt, L. Blümel, R. Holzwarth, S. Hendel, M. Drescher, U. Kleineberg, P. M. Echenique, R. Kienberger, F. Krausz, and U. Heinzmann. Attosecond spectroscopy in condensed matter. *Nature*, 449:1029–1032, 2007.
- [39] M. A. Cazalilla. The Luttinger model following a sudden interaction switch-on. *Phys. Rev. Lett.*, 97:156403, 2006.
- [40] M. A. Cazalilla, R. Citro, T. Giamarchi, E. Orignac, and M. Rigol. One dimensional Bosons: From Condensed Matter Systems to Ultracold Gases. *Rev. Mod. Phys.*, 83:1405–1466, 2011.
- [41] I. Chernii, I. P. Levkivskiy, and E. V. Sukhorukov. Fermi-edge singularity in chiral one-dimensional systems far from equilibrium. *Phys. Rev. B*, 90:245123, 2014.
- [42] M. J. Collett and C. W. Gardiner. Squeezing of intracavity and traveling-wave light fields produced in parametric amplification. *Phys. Rev. A*, 30:1386–1391, Sep 1984.
- [43] D. G. Comer. Effect of antiresonant atom-field interactions on phase transitions in the Dicke model. *Phys. Rev. A*, 9:418–421, Jan 1974.
- [44] L. F. Cugliandolo, D. R. Grempel, G. Lozano, and H. Lozza. Effects of dissipation on disordered quantum spin models. *Phys. Rev. B*, 70:024422, Jul 2004.
- [45] L. F. Cugliandolo, D. R. Grempel, G. Lozano, H. Lozza, and C. A. da Silva Santos. Dissipative effects on quantum glassy systems. *Phys. Rev. B*, 66:014444, Jul 2002.
- [46] L. F. Cugliandolo and G. Lozano. Real-time nonequilibrium dynamics of quantum glassy systems. *Phys. Rev. B*, 59:915–942, Jan 1999.
- [47] E. G. Dalla Torre, E. Demler, T. Giamarchi, and E. Altman. Quantum critical states and phase transitions in the presence of non equilibrium noise. *Nature Physics*, 85:806, 2010.
- [48] E. G. Dalla Torre, E. Demler, T. Giamarchi, and E. Altman. Dynamics and universality in noise-driven dissipative systems. *Phys. Rev. B*, 85:184302, May 2012.
- [49] E. G. Dalla Torre, S. Diehl, M. D. Lukin, S. Sachdev, and P. Strack. Keldysh approach for nonequilibrium phase transitions in quantum optics: Beyond the Dicke model in optical cavities. *Phys. Rev. A*, 87:023831, Feb 2013.
- [50] E. G. Dalla Torre, S. Diehl, M. D. Lukin, S. Sachdev, and P. Strack. Keldysh approach for nonequilibrium phase transitions in quantum optics: Beyond the Dicke model in optical cavities. *Phys. Rev. A*, 87:023831, Feb 2013.
- [51] E. G. Dalla Torre, J. Otterbach, E. Demler, V. Vuletic, and M. D. Lukin. Dissipative Preparation of Spin Squeezed Atomic Ensembles in a Steady State. *Phys. Rev. Lett.*, 110:120402, Mar 2013.
- [52] P. Degenfeld-Schonburg and M. J. Hartmann. Self-Consistent Projection Operator Approach to Quantum Many-Body Systems. *Phys. Rev. B*, 89:245108, 2014.
- [53] J. M. Deutsch. Quantum statistical mechanics in a closed system. *Phys. Rev. A*, 43:2046–2049, 1991.

- [54] S. Diehl, A. Tomadin, A. Micheli, R. Fazio, and P. Zoller. Dynamical Phase Transitions and Instabilities in Open Atomic Many-Body Systems. *Phys. Rev. Lett.*, 105:015702, Jul 2010.
- [55] F. Dimer, B. Estienne, A. S. Parkins, and H. J. Carmichael. Proposed realization of the Dicke-model quantum phase transition in an optical cavity QED system. *Phys. Rev. A*, 75:013804, Jan 2007.
- [56] P. Domokos and H. Ritsch. Collective Cooling and Self-Organization of Atoms in a Cavity. *Phys. Rev. Lett.*, 89:253003, Dec 2002.
- [57] M. Eckstein, M. Kollar, and P. Werner. Dynamical phase transition in correlated fermionic lattice systems. *Phys. Rev. Lett.*, 103:056403, 2009.
- [58] C. Emary and T. Brandes. Chaos and the quantum phase transition in the Dicke model. *Phys. Rev. E*, 67:066203, Jun 2003.
- [59] C. Emary and T. Brandes. Quantum Chaos Triggered by Precursors of a Quantum Phase Transition: The Dicke Model. *Phys. Rev. Lett.*, 90:044101, Jan 2003.
- [60] F. H. L. Essler. Threshold Singularities in the One Dimensional Hubbard Model. *Phys. Rev. B*, 81:205120, 2010.
- [61] F. H. L. Essler, S. Kehrein, S. R. Manmana, and N. J. Robinson. Quench dynamics in a model with tuneable integrability breaking Quench dynamics in a model with tuneable integrability breaking. *Phys. Rev. B*, 89:165104, 2014.
- [62] M. P. A. Fisher, P. B. Weichman, G. Grinstein, and D. S. Fisher. Boson localization and the superfluid-insulator transition. *Phys. Rev. B*, 40:546–570, Jul 1989.
- [63] D. Forster, D. R. Nelson, and M. J. Stephen. Large-distance and long-time properties of a randomly stirred fluid. *Phys. Rev. A*, 16:732–749, Aug 1977.
- [64] G. Gallavotti. *Statistical Mechanics: A Short Treatise*. Springer Verlag, Berlin, 1999.
- [65] C. W. Gardiner and M. J. Collett. Input and output in damped quantum systems: Quantum stochastic differential equations and the master equation. *Phys. Rev. A*, 31:3761–3774, Jun 1985.
- [66] C. W. Gardiner and P. Zoller. *Quantum Noise*. Springer Verlag, Berlin, 1999.
- [67] T. Giamarchi. *Quantum Physics in One Dimension*. International Series of Monographs on Physics. Oxford University Press, Oxford, 2004.
- [68] J. W. Gibbs. On the Equilibrium of Heterogeneous Substances. *Transactions of the Connecticut Academy of Arts and Sciences*, 3:108–248, 343–524, 1874-1878.
- [69] I. Gierz, M. Mitrano, H. Bromberger, C. Cacho, R. Chapman, E. Springate, S. Link, U. Starke, B. Sachs, M. Eckstein, T. O. Wehling, M. I. Katsnelson, A. Lichtenstein, and A. Cavalleri. Phonon-Pump Extreme-Ultraviolet-Photoemission Probe in Graphene: Anomalous Heating of Dirac Carriers by Lattice Deformation. *Phys. Rev. Lett.*, 114:125503, 2015.
- [70] S. Goldstein, J. L. Lebowitz, R. Tumulka, and N. Zangh'i. Canonical Typicality. *Phys. Rev. Lett.*, 96:050403, 2006.
- [71] S. Gopalakrishnan, B. L. Lev, and P. M. Goldbart. Emergent superfluid crystals, frustration, and topologically defected states in multimode cavity QED. *Nature Physics*, 5:845–850, 2009.
- [72] S. Gopalakrishnan, B. L. Lev, and P. M. Goldbart. Atom-light crystallization of Bose-Einstein condensates in multimode cavities: Nonequilibrium classical and quantum phase transitions, emergent lattices, supersolidity, and frustration. *Phys. Rev. A*, 82:043612, Oct 2010.

- [73] S. Gopalakrishnan, B. L. Lev, and P. M. Goldbart. Frustration and Glassiness in Spin Models with Cavity-Mediated Interactions. *Phys. Rev. Lett.*, 107:277201, Dec 2011.
- [74] M. Gring, M. Kuhnert, T. Langen, T. Kitagawa, B. Rauer, M. Schreitl, I. Mazets, D. Adu Smith, E. Demler, and J. Schmiedmayer. Relaxation and Prethermalization in an Isolated Quantum System. *Science*, 337(6100):1318–1322, 2012.
- [75] D. B. Gutman, Y. Gefen, and A. D. Mirlin. Bosonization of one dimensional fermions out of equilibrium. *Phys. Rev. B*, 81:085436, 2010.
- [76] D. B. Gutman, Y. Gefen, and A. D. Mirlin. Bosonization out of equilibrium. *EPL*, 90(37003), 2010.
- [77] D. B. Gutman, Y. Gefen, and A. D. Mirlin. Non-equilibrium 1D many-body problems and asymptotic properties of Toeplitz determinants. *J. Phys. A: Math. Theor.*, 44:165003, 2011.
- [78] D. B. Gutman, Y. Gefen, and A. D. Mirlin. Cold bosons in the Landauer setup. *Phys. Rev. B*, 85:125102, 2012.
- [79] H. Habibian, A. Winter, S. Paganelli, H. Rieger, and G.a Morigi. Bose-Glass Phases of Ultracold Atoms due to Cavity Backaction. *Phys. Rev. Lett.*, 110:075304, Feb 2013.
- [80] F. D. M. Haldane. Effective Harmonic-Fluid Approach to Low-Energy Properties of One-Dimensional Quantum Fluids. *Phys. Rev. Lett.*, 47:1840–1843, Dec 1981.
- [81] F. D. M. Haldane. 'Luttinger liquid theory' of one-dimensional quantum fluids. I. Properties of the Luttinger model and their extension to the general 1D interacting spinless Fermi gas. *J. Phys. Condens. Matter*, 14:2585, 1981.
- [82] R. Haussmann, M. Punk, and W. Zwerger. Spectral functions and rf response of ultracold fermionic atoms. *Phys. Rev. A*, 80:063612, Dec 2009.
- [83] R. Heidenreich, R. Seiler, and D. A. Uhlenbrock. The Luttinger model. *J. Stat. Phys.*, 22:27, 1980.
- [84] Klaus Hepp and Elliott H Lieb. On the superradiant phase transition for molecules in a quantized radiation field: the Dicke maser model. *Annals of Physics*, 76(2):360 – 404, 1973.
- [85] M. Heyl, A. Polkovnikov, and S. Kehrein. Dynamical Quantum Phase Transitions in the Transverse-Field Ising Model. *Phys. Rev. Lett.*, 110:135704, Mar 2013.
- [86] S. Hild, T. Fukuhara, P. Schauß, J. Zeiher, M. Knap, E. Demler, I. Bloch, and C. Gross. Far-from-equilibrium spin transport in Heisenberg quantum magnets. *Phys. Rev. Lett.*, 113:147205, 2014.
- [87] S. Hofferberth, I. Lesanovsky, B. Fischer, T. Schumm, and J. Schmiedmayer. Non-equilibrium coherence dynamics in one-dimensional Bose gases. *Nature*, 449:324–327, 2007.
- [88] P. C. Hohenberg and B. I. Halperin. Theory of dynamic critical phenomena. *Rev. Mod. Phys.*, 49:435–479, Jul 1977.
- [89] K. Huang. *Statistical Mechanics*. WILEY-VCH Verlag, 1987.
- [90] S. D. Huber and E. Altman. Universal Dephasing of Many-Body Rabi Oscillations of Atoms in One-Dimensional Traps. *Phys. Rev. Lett.*, 103:160402, Oct 2009.
- [91] A. Imambekov and L. I. Glazman. Exact exponents of edge singularities in dynamic correlation functions of 1D Bose gas. *Phys. Rev. Lett.*, 100:206805, 2008.

- [92] A. Imambekov and L. I. Glazman. Phenomenology of One-Dimensional Quantum Liquids Beyond the Low-Energy Limit. *Phys. Rev. Lett.*, 102:126405, 2009.
- [93] A. Imambekov and L. I. Glazman. Universal theory of nonlinear Luttinger Liquids. *Science*, 323:228, 2009.
- [94] A. Imambekov, T. L. Schmidt, and L. I. Glazman. One-Dimensional Quantum Liquids: Beyond the Luttinger Liquid Paradigm. *Rev. Mod. Phys.*, 84:1253, 2012.
- [95] A. Iucci and M. A. Cazalilla. Quantum quench dynamics of the Luttinger model. *Phys. Rev. A*, 80:063619, 2009.
- [96] A. Iucci and M. A. Cazalilla. Quantum quench dynamics of the sine-Gordon model in some solvable limits. *New J. Phys.*, 12:055019, 2010.
- [97] S. Ji, C. Ates, and I. Lesanovsky. Two-dimensional Rydberg Gases and the Quantum Hard-Squares Model. *Phys. Rev. Lett.*, 107:060406, Aug 2011.
- [98] L. P. Kadanoff and G. Baym. *Quantum Statistical Mechanics*. New York: Benjamin, 1962.
- [99] A. Kamenev. *Field Theory of Non-Equilibrium Systems*. Cambridge University Press, 2011.
- [100] A. Kamenev and A. Levchenko. Keldysh technique and non-linear sigma-model: basic principles and applications. *Advances in Physics*, 58:197, 2009.
- [101] A. Kamenev and A. Levchenko. Keldysh technique and non-linear σ -model: basic principles and applications. *Adv. Phys.*, 58(3):197–319, 2009.
- [102] M. Kardar, G. Parisi, and Y.-Z. Zhang. Dynamic Scaling of Growing Interfaces. *Phys. Rev. Lett.*, 56:889–892, 1986.
- [103] C. Karrasch, J. Rentrop, D. Schuricht, and V. Meden. Luttinger-liquid universality in the time evolution after an interaction quench. *Phys. Rev. Lett.*, 109:126406, Sep 2012.
- [104] C. Kasztelan, S. Trotzky, Y-A. Chen, I. Bloch, I. P. McCulloch, U. Schollwöck, and G. Orso. Landau-Zener sweeps and sudden quenches in coupled Bose-Hubbard chains. *Phys. Rev. Lett.*, 106:155302, 2011.
- [105] J. Keeling, M. J. Bhaseen, and B. D. Simons. Collective Dynamics of Bose-Einstein Condensates in Optical Cavities. *Phys. Rev. Lett.*, 105:043001, Jul 2010.
- [106] L. V. Keldysh. Diagram Technique for Nonequilibrium Processes. *Zh. Eksp. Teor. Fiz.*, 47:1515, 1964.
- [107] D. M. Kennes and V. Meden. Luttinger liquid properties of the steady state after a quantum quench. *Phys. Rev. B*, 88:165131, Oct 2013.
- [108] M. P. Kennett, C. Chamon, and J. Ye. Aging dynamics of quantum spin glasses of rotors. *Phys. Rev. B*, 64:224408, Nov 2001.
- [109] E. M. Kessler. Generalized Schrieffer-Wolff formalism for dissipative systems. *Phys. Rev. A*, 86:012126, Jul 2012.
- [110] M. Khodas, M. Pustilnik, A. Kamenev, and L. I. Glazman. Fermi-Luttinger liquid: Spectral function of interacting one-dimensional fermions. *Phys. Rev. B*, 76:155402, 2007.
- [111] T. Kinoshita, T. Wenger, and D. S. Weiss. A quantum Newton’s cradle. *Nature*, 440:900, 2006.
- [112] J. Klaers, J. Schmitt, F. Vewinger, and M. Weitz. Bose-Einstein condensation of photons in an optical microcavity. *Nature*, 468:545–548, 2010.

- [113] W. Kohn. Theory of the Insulating State. *Phys. Rev.*, 133:A171, 1964.
- [114] A. J. Kollár, A. T. Papageorge, K. Baumann, M. A. Armen, and B. L. Lev. An adjustable-length cavity and Bose-Einstein condensate apparatus for multimode cavity QED. *New J. Phys.*, 17:043012, 2015.
- [115] M. Kollar, F. A. Wolf, and M. Eckstein. Generalized Gibbs ensemble prediction of prethermalization plateaus and their relation to nonthermal steady states in integrable systems. *Phys. Rev. B*, 84:054304, 2011.
- [116] O. V. Konstantinov and V. I. Perel'. A Diagram Technique for Evaluating Transport Quantities. *Zh. Eksp. Teor. Fiz.*, 39:197, 1960.
- [117] V. E. Korepin, N. M. Bogoliubov, and A. G. Izergin. *Quantum Inverse Scattering Method and Correlation Functions*. Cambridge University Press, 1997.
- [118] A. Kossakowski. On quantum statistical mechanics of non-Hamiltonian systems. *Rep. Math. Phys.*, 3:247, 1972.
- [119] N. S. Krylov. *Works of the Foundation of Statistical Physics*. Princeton University Press, Princeton, 1979.
- [120] M. Kulkarni and A. Lamacraft. Finite-temperature dynamical structure factor of the one-dimensional Bose gas: From the Gross-Pitaevskii equation to the Kardar-Parisi-Zhang universality class of dynamical critical phenomena. *Phys. Rev. A*, 88:021603, Aug 2013.
- [121] T. Langen, S. Erne, R. Geiger, B. Rauer, T. Schweigler, M. Kuhnert, W. Rohringer, I. E. Mazets, T. Gasenzer, and J. Schmiedmayer. Experimental Observation of a Generalized Gibbs Ensemble. [arXiv:14117185](https://arxiv.org/abs/1411.7185), 2014.
- [122] T. Langen, R. Geiger, M. Kuhnert, B. Rauer, and J. Schmiedmayer. Local emergence of thermal correlations in an isolated quantum many-body system. *Nat. Phys.*, 9:640–643, 2013.
- [123] W. Lechner, S. J. M. Habraken, N. Kiesel, M. Aspelmeyer, and P. Zoller. Cavity Optomechanics of Levitated Nanodumbbells: Nonequilibrium Phases and Self-Assembly. *Phys. Rev. Lett.*, 110:143604, Apr 2013.
- [124] Stefano Lepri, Roberto Livi, and Antonio Politi. Universality of anomalous one-dimensional heat conductivity. *Phys. Rev. E*, 68:067102, Dec 2003.
- [125] A. C. Y. Li, F. Petruccione, and J. Koch. Perturbative approach to Markovian open quantum systems. [arXiv: 1311.3227](https://arxiv.org/abs/1311.3227), 2013.
- [126] J. Lin, K. A. Matveev, and M. Pustilnik. Thermalization of acoustic excitations in a strongly interacting one-dimensional quantum liquid. *Phys. Rev. Lett.*, 110:016401, 2013.
- [127] G. Lindblad. On the generators of quantum dynamical semigroups. *Commun. Math. Phys.*, 48:119, 1976.
- [128] J. M. Luttinger. An Exactly Soluble Model of a Many-Fermion System. *Journal of Mathematical Physics*, 4:1154, 1963.
- [129] J. Lux, J. Müller, A. Mitra, and A. Rosch. Hydrodynamic long-time tails after a quantum quench. *Phys. Rev. A*, 89:053608, 2014.
- [130] G. D. Mahan. *Many-Particle Physics*. Plenum Press, New York, 2nd edition, 1990.
- [131] K. A. Matveev and A. Furusaki. Decay of fermionic quasiparticles in one-dimensional quantum liquids. *Phys. Rev. Lett.*, 111:256401, 2013.

- [132] F. Meinert, M. J. Mark, E. Kirilov, K. Lauber, P. Weinmann, A. J. Daley, and H.-C. Nägerl. Quantum Quench in an Atomic One-Dimensional Ising Chain. *Phys. Rev. Lett.*, 111:053003, Jul 2013.
- [133] I. B. Mekhov, C. Maschler, and H. Ritsch. Probing quantum phases of ultracold atoms in optical lattices by transmission spectra in cavity QED. *Nature Physics*, 3:319–323, 2007.
- [134] J. Miller and D. A. Huse. Zero-temperature critical behavior of the infinite-range quantum Ising spin glass. *Phys. Rev. Lett.*, 70:3147–3150, May 1993.
- [135] E. Miranda and V. Dobrosavljević. Disorder-Driven Non-Fermi Liquid Behavior of Correlated Electrons. *Rep. Prog. Phys.*, 68:2337, 2005.
- [136] A. Mitra and T. Giamarchi. Mode-Coupling-Induced Dissipative and Thermal Effects at Long Times after a Quantum Quench. *Phys. Rev. Lett.*, 107:150602, Oct 2011.
- [137] A. Mitra and T. Giamarchi. Thermalization and dissipation in out-of-equilibrium quantum systems: A perturbative renormalization group approach. *Phys. Rev. B*, 85:075117, Feb 2012.
- [138] A. Mitra, S. Takei, Y. B. Kim, and A. J. Millis. Nonequilibrium Quantum Criticality in Open Electronic Systems. *Phys. Rev. Lett.*, 97:236808, Dec 2006.
- [139] M. Moeckel and S. Kehrein. Interaction Quench in the Hubbard Model. *Phys. Rev. Lett.*, 100:175702, 2008.
- [140] R. Mottl, F. Brennecke, K. Baumann, R. Landig, T. Donner, and T. Esslinger. Roton-type mode softening in a quantum gas with cavity mediated long-range interactions. *Science*, 336:1570–3, 2012.
- [141] M. Müller, P. Strack, and S. Sachdev. Quantum charge glasses of itinerant fermions with cavity-mediated long-range interactions. *Phys. Rev. A*, 86:023604, Aug 2012.
- [142] G. Mussardo. Infinite-Time Average of Local Fields in an Integrable Quantum Field Theory After a Quantum Quench. *Phys. Rev. Lett.*, 111(100401), 2013.
- [143] D. Nagy, G. Kónya, G. Szirmai, and P. Domokos. Dicke-Model Phase Transition in the Quantum Motion of a Bose-Einstein Condensate in an Optical Cavity. *Phys. Rev. Lett.*, 104:130401, Apr 2010.
- [144] D. Nagy, G. Szirmai, and P. Domokos. Critical exponent of a quantum-noise-driven phase transition: The open-system Dicke model. *Phys. Rev. A*, 84:043637, Oct 2011.
- [145] O. Narayan and S. Ramaswamy. Anomalous Heat Conduction in One-Dimensional Momentum-Conserving Systems. *Phys. Rev. Lett.*, 89:200601, Oct 2002.
- [146] J. W. Negele and H. Orland. *Quantum Many-particle Systems*. Perseus Books, 1998, Revised Edition.
- [147] N. Nessi and A. Iucci. Glass-like Behavior in a System of One-Dimensional Fermions after a Quantum Quench. *arXiv:1503.02507*, 2015.
- [148] B. Olmos, I. Lesanovsky, and J. P. Garrahan. Facilitated Spin Models of Dissipative Quantum Glasses. *Phys. Rev. Lett.*, 109:020403, Jul 2012.
- [149] B. Öztop, M. Bordyuh, O. E. Müstecaplıoğlu, and H. E. Türeci. Excitations of optically driven atomic condensate in a cavity: theory of photodetection measurements. *New Journal of Physics*, 14:085011, 2012.
- [150] R. G. Pereira, J. Sirker, J.-S. Caux, R. Hagemans, J. M. Maillet, S. R. White, and I. Affleck. Dynamical Spin Structure Factor for the Anisotropic Spin-1/2 Heisenberg Chain. *Phys. Rev. Lett.*, 96:257202, Jun 2006.

- [151] R. G. Pereira, S. R. White, and I. Affleck. Exact edge singularities and dynamical correlations in spin-1/2 chains. *Phys. Rev. Lett.*, 100:027206, 2008.
- [152] M. E. Peskin and D. V. Schroeder. *An Introduction to Quantum Field Theory*. Westview Press, 1995.
- [153] T. Peyronel, O. Firstenberg, Q. Y. Liang, S. Hofferberth, A. V. Gorshkov, T. Pohl, M. D. Lukin, and V. Vuletic. Quantum nonlinear optics with single photons enabled by strongly interacting atoms. *Nature*, 488:57, 2012.
- [154] H. Pichler, A. J. Daley, and P. Zoller. Nonequilibrium dynamics of bosonic atoms in optical lattices: Decoherence of many-body states due to spontaneous emission. *Phys. Rev. A*, 82:063605, Dec 2010.
- [155] D. Poletti, P. Barmettler, A. Georges, and C. Kollath. Emergence of Glasslike Dynamics for Dissipative and Strongly Interacting Bosons. *Phys. Rev. Lett.*, 111:195301, Nov 2013.
- [156] D. Poletti, J.-S. Bernier, A. Georges, and C. Kollath. Interaction-Induced Impeding of Decoherence and Anomalous Diffusion. *Phys. Rev. Lett.*, 109:045302, Jul 2012.
- [157] A. Polkovnikov, K. Sengupta, A. Silva, and M. Vengalattore. Colloquium: Nonequilibrium dynamics of closed interacting quantum systems. *Rev. Mod. Phys.*, 83:863, 2011.
- [158] I. V. Protopopov, D. B. Gutman, and A. D. Mirlin. Relaxation in Luttinger liquids: Bose-Fermi duality. *Phys. Rev. B*, 90:125113, 2014.
- [159] I. V. Protopopov, D. B. Gutman, M. Oldenburg, and A. D. Mirlin. Dissipationless kinetics of one dimensional interacting fermions. *Phys. Rev. B*, 89:161104, 2014.
- [160] T. Pruttivarasin, M. Ramm, I. Talukdar, A. Kreuter, and H. Haefner. Trapped ions in optical lattices for probing oscillator chain models. *New Journal of Physics*, 13:075012, 2011.
- [161] M. Punk and W. Zwerger. Collective mode damping and viscosity in a 1D unitary Fermi gas. *New J. Phys.*, 8:168, 2006.
- [162] M. Pustilnik, M. Khodas, A. Kamenev, and L. I. Glazman. Dynamic response of one-dimensional interacting fermions. *Phys. Rev. Lett.*, 96:196405, 2006.
- [163] M. Pustilnik, E. G. Mishchenko, L. I. Glazman, and A. V. Andreev. Coulomb drag by small momentum transfer between quantum wires. *Phys. Rev. Lett.*, 91:126805, 2003.
- [164] J. Rammer and H. Smith. Quantum field-theoretical methods in transport theory of metals. *Rev. Mod. Phys.*, 58:323, 1986.
- [165] N. Read, S. Sachdev, and J. Ye. Landau theory of quantum spin glasses of rotors and Ising spins. *Phys. Rev. B*, 52:384–410, Jul 1995.
- [166] M. Rigol, V. Dunjko, and M. Olshanii. Thermalization and its mechanism for generic isolated quantum systems. *Nature*, 452:854–858, 2008.
- [167] M. Rigol, V. Dunjko, V. Yurovsky, and M. Olshanii. Relaxation in a Completely Integrable Many-Body Quantum System: An Ab Initio Study of the Dynamics of the Highly Excited States of Lattice Hard-Core Bosons. *Phys. Rev. Lett.*, 98:050405, 2007.
- [168] Z. Ristivojevic and K. A. Matveev. Relaxation of weakly interacting electrons in one dimension. *Phys. Rev. B*, 87:165108, 2013.
- [169] Z. Ristivojevic and K. A. Matveev. Decay of Bogoliubov quasiparticles in a nonideal one-dimensional Bose gas. *Phys. Rev. B*, 89:180507(R), 2014.

- [170] H. Ritsch, P. Domokos, F. Brennecke, and T. Esslinger. Cold atoms in cavity-generated dynamical optical potentials. *Rev. Mod. Phys.*, 85:553–601, Apr 2013.
- [171] S. Ritter, A. Öttl, T. Donner, T. Bourdel, M. Köhl, and T. Esslinger. Observing the Formation of Long-range Order during Bose-Einstein Condensation. *Phys. Rev. Lett.*, 98:090402, 2007.
- [172] W. Rohringer, D. Fischer, F. Steiner, I. E. Mazets, J. Schmiedmayer, and M. Trupke. Scaling of phonons and shortcuts to adiabaticity in a one-dimensional quantum system. arXiv: 1312.5948, 2013.
- [173] A. Rozhkov. Fermionic Quasiparticle Representation of Tomonaga-Luttinger Hamiltonian. *Eur. Phys. J. B*, 47:193, 2005.
- [174] S. Sachdev. Quantum phase transitions. Cambridge University Press, 2nd edition, 2011.
- [175] L. E. Sadler, J. M. Higbie, S. R. Leslie, M. Vengalattore, and D. M. Stamper-Kurn. Spontaneous symmetry breaking in a quenched ferromagnetic spinor Bose-Einstein condensate. *Nature*, 443:312–315, 2006.
- [176] K. V. Samokhin. Lifetime of excitations in a clean Luttinger liquid. *J. Phys. Condens. Matter*, 10:L533, 1998.
- [177] J. Schachenmayer, L. Pollet, M. Troyer, and A. J. Daley. Spontaneous emissions and thermalization of cold bosons in optical lattices. *Phys. Rev. A*, 89:011601, 2014.
- [178] J. Schwinger. The special canonical group. *PNAS*, 46:1401, 1960.
- [179] J. Schwinger. Brownian Motion of a Quantum Oscillator. *J. Math. Phys.*, 2:407, 1961.
- [180] S. Sevinçli, N. Henkel, C. Ates, and T. Pohl. Nonlocal Nonlinear Optics in Cold Rydberg Gases. *Phys. Rev. Lett.*, 107:153001, Oct 2011.
- [181] L. M. Sieberer, S. D. Huber, E. Altman, and S. Diehl. Dynamical Critical Phenomena in Driven-Dissipative Systems. *Phys. Rev. Lett.*, 110:195301, May 2013.
- [182] L. M. Sieberer, S. D. Huber, E. Altman, and S. Diehl. Non-equilibrium Functional Renormalization for Driven-Dissipative Bose-Einstein Condensation. *Phys. Rev. D*, 89:134310, 2014.
- [183] A. D. Smith, M. Gring, T. Langen, M. Kuhnert, B. Rauer, R. Geiger, T. Kitagawa, I. Mazets, Demler E., and J. Schmiedmayer. Prethermalization revealed by the relaxation dynamics of full distribution functions. *New J. Phys.*, 15:075011, 2013.
- [184] M. Srednicki. Chaos and quantum thermalization. *Phys. Rev. E*, 50:888–901, 1994.
- [185] D. M. Stamper-Kurn, A. P. Chikkatur, A. Görlitz, S. Inouye, S. Gupta, D. E. Pritchard, and W. Ketterle. Excitation of Phonons in a Bose-Einstein Condensate by Light Scattering. *Phys. Rev. Lett.*, 83:2876–2879, Oct 1999.
- [186] M. Stark and M. Kollar. Kinetic description of thermalization dynamics in weakly interacting quantum systems. arXiv:1308.1610, 2013.
- [187] J. Stenger, S. Inouye, A. P. Chikkatur, D. M. Stamper-Kurn, D. E. Pritchard, and W. Ketterle. Bragg Spectroscopy of a Bose-Einstein Condensate. *Phys. Rev. Lett.*, 82:4569–4573, Jun 1999.
- [188] J T Stewart, J P Gaebler, and D S Jin. Using photoemission spectroscopy to probe a strongly interacting Fermi gas. *Nature*, 454(7205):744–7, August 2008.
- [189] T. Stöferle, H. Moritz, C. Schori, M. Köhl, and T. Esslinger. Transition from a Strongly Interacting 1D Superfluid to a Mott Insulator. *Phys. Rev. Lett.*, 92:130403, Mar 2004.

- [190] P. Strack and S. Sachdev. Dicke Quantum Spin Glass of Atoms and Photons. *Phys. Rev. Lett.*, 107:277202, Dec 2011.
- [191] P. Strack and V. Vitelli. Soft quantum vibrations of PT-symmetric nonlinear ion chain. *Phys. Rev. A*, 88:053408, 2013.
- [192] W. T. Strunz and F. Haake. Decoherence scenarios from micro- to macroscopic superpositions. *Phys. Rev. A*, 67:022102, 2003.
- [193] H. Tasaki. From Quantum Dynamics to the Canonical Distribution: General Picture and a Rigorous Example. *Phys. Rev. Lett.*, 80:1373–1376, 1998.
- [194] M. Tavora and A. Mitra. Quench dynamics of one-dimensional bosons. *Phys. Rev. B*, 88:115144, 2013.
- [195] M. Tavora, A. Rosch, and A. Mitra. Quench dynamics of interacting one-dimensional bosons is a disordered potential. *Phys. Rev. Lett.*, 113:010601, 2014.
- [196] S. Tomonaga. Remarks on Bloch’s Method of Sound Waves applied to Many-Fermion Problems. *Progress of Theoretical Physics*, 5:544, 1950.
- [197] S. Trotzky, Y-A. Chen, A. Fleisch, I. P. McCulloch, U. Schollwöck, J. Eisert, and I. Bloch. Probing the relaxation towards equilibrium in an isolated strongly correlated one-dimensional Bose gas. *Nat. Phys.*, 8:325–330, Jul 2013.
- [198] H. van Beijeren. Exact Results for Anomalous Transport in One-Dimensional Hamiltonian Systems. *Phys. Rev. Lett.*, 108:180601, 2012.
- [199] J. von Neumann. Beweis des Ergodensatzes und des H-Theorems in der neuen Mechanik. *Zeitschrift für Physik*, 57:30, 1929.
- [200] Y. K. Wang and F. T. Hioe. Phase Transition in the Dicke Model of Superradiance. *Phys. Rev. A*, 7:831–836, Mar 1973.
- [201] B. Wouters, J. De Nardis, M. Brockmann, D. Fioretto, M. Rigol, and J.-S. Caux. Quenching the Anisotropic Heisenberg Chain: Exact Solution and Generalized Gibbs Ensemble Predictions. *Phys. Rev. Lett.*, 113:117202, 2014.
- [202] M. Wouters and I. Carusotto. Absence of long-range coherence in the parametric emission of photonic wires. *Phys. Rev. B*, 74:245316, Dec 2006.
- [203] J. Ye, S. Sachdev, and N. Read. Solvable spin glass of quantum rotors. *Phys. Rev. Lett.*, 70:4011–4014, Jun 1993.
- [204] J. Zinn-Justin. *Quantum Field Theory and Critical Phenomena*. World Scientific, Singapore, fourth edition, 2005.